nature

www.nature.com/nature

Vol 446 | Issue no. 7131 | 1 March 2007

Trial and failure

Only the most promising AIDS gels should reach large-scale trials.

Last month saw the failure of a clinical trial of a cellulose sulphate vaginal gel as a protective measure against HIV infection (see page 12). The result was a disappointment for microbicide researchers, and a setback for millions of women in Africa and elsewhere who could benefit from such a product. The international trial, organized by CONRAD, a reproductive-health research group based in Virginia, ended when the gel in question was found not only to be ineffective, but actually to increase the risk of HIV infection.

This is the third large-scale clinical trial of a microbicidal gel for AIDS protection to fail. Naturally, it leaves researchers asking where the approach will go from here. Some counsel patience: the development of new therapies is always an arduous and unpredictable process, they argue.

The concept of microbicide gels — one of the few interventions that might allow women to protect themselves from HIV infection — has been heavily promoted by activists, particularly in the United States. Buoyed by success in raising awareness and funds, these activists want to see the product pipeline filled with as many reasonable candidates as possible.

But a continued pattern of well-publicized trial failure carries risks. This has been amply demonstrated by the history of AIDS vaccine research, where failed trials of products that hadn't even done well in animal models did little to further the development of a working vaccine. And when different groups push their favourite products into trials without taking a hard, rational look at which are most likely to succeed, the whole enterprise suffers. Multiple failures lead to a loss of public confidence. Even if donors continue funding the work, it becomes difficult to recruit volunteers for clinical trials if people think the product is doomed to failure — or worse, that it might even harm their health.

The microbicide field therefore requires a mechanism to help it make rational choices about the best candidates to move through trials. The field is already good at exchanging information. As part of this process, leaders and funders of microbicide clinical trials meet twice a year and are considering doing so more often. But they are not in the business of filtering late-stage trial candidates.

Participants need to explore ways of doing just that, however. Researchers, activists and funders of microbicide work should construct a consultative body that will have the confidence of the community, and help it reach a consensus on issues such as how best to test for efficacy and safety in animals, and how to use the results from such tests to move the best microbicide candidates into large human studies.

Ideally, this should be part of a wider discussion on how to test and roll out interventions to prevent AIDS. Several groups have recommended that researchers convene a cross-community forum to discuss issues related to all the concepts now in trials: prophylaxis with oral antiretroviral drugs; barrier methods initiated by women; treatment of HIV-infected patients who have non-infected partners; vaccines; microbicides; and male circumcision and herpes suppression, which both got a boost from positive trial results last week.

Such a discussion could also help researchers address common problems, such as how best to accommodate the high pregnancy rates in trial populations (which tend to disrupt trials, as pregnant women withdraw from them), and the fact that when counselling is provided in trials of new interventions, the rate of HIV infection plummets, potentially obscuring the effect of the intervention. Researchers also have a common interest in working out how to ensure that interventions that prove to be successful end up being used where they are most badly needed.

Researchers are supportive of such cross-community discussion. At the XVI International AIDS Conference in Toronto last August, for example, a group of about 50 researchers and activists known as the Global HIV Prevention Working Group laid out its own blueprint of challenges for AIDS prevention. On 23 February, the Forum for Collaborative HIV Research released a report that echoed the working group's findings. And a panel of the US Institute of Medicine will report later in the year on the challenges facing clinical trials of interventions to prevent HIV. There is broad and diverse agreement on the urgent need for cross-disciplinary dialogue on these questions. But all the talk must lead to active and careful coordination of AIDS prevention research, to confront the pandemic. ■

Solid foundations

In praise of those physicists who are unobtrusively revolutionizing everyday life.

The perception of physics in the minds of the public is one of esoteric exploration, elucidating the fundamentals of space, time and energy — even the nature of reality itself. And much effort is indeed devoted to articulating and exploring these deep concepts, whose grip on the public's imagination is both undeniable and entirely appropriate. But such investigations do not form the stock-in-trade for the vast majority of physicists, who have chosen instead to focus their efforts on understanding the physical properties of solid matter. Should we conclude that they have little to boast about? Or even suggest that solid-state physics is fundamentally rather mundane?

Far from it. Much of the research that underpins modern technologies — from cars to computers, televisions to telecommunications — has its roots in the physics of the solid state. Occasional debates over whether one should have confidence in science more generally have already been fundamentally won by these self-same developments.

The impact of solid-state physics on society is hard to overstate.

But it would be disingenuous to imply that the attraction of research in solid-state physics is primarily driven by a desire to benefit humanity materially. Such a motivation is undoubtedly present within the community, but for most physicists studying the solid state, the central appeal is similar to that driving their more exotically inclined brethren: intellectual richness and the excitement of the imagination. And a very large element of surprise.

Consider two very different examples, both of which continue to feature frequently in these pages. Just over twenty years ago, the solid-state physics community was shaken by the discovery of high-temperature superconductivity — the unanticipated realization of zero-resistance electrical transport in a family of complex copper oxides, at temperatures too high to be accommodated by the theoretical framework that already existed for explaining such phenomena. (As it happens, the classical Bardeen–Cooper–Schrieffer (BCS) theory of conventional superconductivity is itself celebrating its 50th anniversary this year.) Of course, this stimulated much anticipation about how such materials might find serious practical application — still largely wishful thinking, unfortunately, although not altogether beyond the realms of possibility. But what continues to drive interest in these fascinating materials is the fact that their properties have yet to be understood.

More recently, this same community has born witness to another unexpected development: the discovery of unusual electronic and mechanical properties in graphene — individual crystalline layers of carbon only one atom thick. The surprise in this case is that these layers, when stacked up to form their parent material, graphite, constitute a well-known and much-studied material system that, from a solid-state physics perspective, arguably does fit the description of mundane. This system, too, has potential for practical application, but let's not get ahead of ourselves — the true cause for compelling interest is that graphene provides a powerful test-bed on which to explore the validity of some of the core concepts of solid-state physics. So far, these theoretical foundations are standing up to scrutiny pretty well, but there may well be further surprises to come. Several papers in this issue highlight some of the richness of graphene and of solid-state research in other areas (see pages 36, 52–70 and www.nature.com/conferences/aps/index.html).

The next few years can be expected to bring outstanding, high-profile science as the Large Hadron Collider at CERN, the European particle-physics laboratory near Geneva, starts to explore the landscape of particles and forces at energies never before attained in a laboratory. Who knows what other surprises may be in store (see page 16) as astronomers and physicists probe the nature of the vacuum in other ways? The results will be of no obvious use to anyone, and yet they represent exactly the sort of fundamental exploration that fascinates much of humanity. At the much lower energies found in any university lab, meanwhile, solid-state physicists will carry on unobtrusively changing our lives. ■

Not saving the whale

Japan's professed interest in whale research rings rather hollow.

As the world's biggest consumer of whale meat, Japan has a special interest in whale conservation. While fighting tenaciously to protect its whaling industry, it publicly supports the need for conservation. In a statement released last June, for example, it called on the International Whaling Commission (IWC) to "protect endangered and depleted species, while allowing the sustainable utilization of abundant species under a controlled, transparent and science-based management regime".

Japan has placed considerable emphasis on research into whaling. It spends about ¥830 million (US$7 million) each year to establish whether there are enough whales to support whaling (and in the case of the minke, at least, it finds that there are). And it works hard to get support in the IWC, sometimes from member nations that have no obvious interest in whaling. Two weeks ago, many of these countries sent representatives to a meeting in Tokyo — boycotted by the Western nations most strongly opposed to whaling — at which Japan reaffirmed its commitment to the goal of sustainable whaling.

When it comes to events on the high seas, however, Japan's actions leave much to be desired. Lately, for example, there have been repeated cases of western grey whales (*Eschrichtius robustus*) being caught in Japanese fishing nets. Only about 120 of these whales, which migrate along the Pacific coasts of Asia, are thought to survive, although a much larger, sustainable population of eastern grey whales lives off the west coast of North America. The World Conservation Union (IUCN) estimates that the population of reproductive female western grey whales totals only about 30 animals. But four females have been trapped in Japanese fishing nets and accidentally killed in the past two years.

Japan has expressed concern over this issue. Its fisheries agency says it has been asking fishermen to report sightings of the whales, and to release them when trapped, instead of keeping them and selling their meat, as permitted under the law. The agency claims that its effort has worked so far, with no meat from grey whales being sold on the market.

"When it comes to events on the high seas, however, Japan's actions leave much to be desired."

However, the agency's efforts have not actually prevented the deaths, even though much could be done to that end, including supporting better research into the whales' migration and breeding habits, and the development and use of fishing nets that can release trapped animals. One might expect the Institute of Cetacean Research (ICR), which heads Japan's research whaling programme, to take charge of this effort. But it says that responsibility rests with other research institutes and with the fisheries agency. The overall result has been inaction.

The ICR is often characterized by its critics as little more than a cover for Japan's whaling industry. If it is to claim a real role in whale conservation, it could start by responding more energetically to the clear and present danger to the grey whale. ■

RESEARCH HIGHLIGHTS

STRUCTURAL BIOLOGY

Hitching a ride

Nature Struct. Mol. Biol. doi:10.1038/nsmb1212 (2007)

A glimpse into the molecular machinery of the flu virus suggests how it smuggles one of its key enzymes into the infected cell's nucleus, where the enzyme helps the virus to replicate.

Scientists are particularly interested in this enzyme, RNA polymerase, because it is a potential drug target and because mutations in it could help avian flu adapt to humans. Its structure has been hard to study because the enzyme is difficult to make in a suitable form.

Darren Hart and Stephen Cusack of the European Molecular Biology Laboratory in Grenoble, France, and their colleagues used a new method to identify a small, soluble fragment of one of the polymerase's subunits. They found that it has a grappling-hook-like structure and showed that the subunit slings this across a host protein, which then ferries it into the nucleus.

CLIMATE SCIENCE

Clouds on the horizon

Geophys. Res. Lett. **34,** L04701 (2007)

A trend in satellite data suggesting that Earth's cloud cover has decreased by 4% over the past 20 years is an artefact of the observations, say Amato Evan at the University of Wisconsin-Madison and his colleagues. This adds new uncertainty to the role that clouds have played in recent climate change.

The International Satellite Cloud Climatology Project collects data from different satellites to build global cloud maps. Satellites tend to perceive zones viewed obliquely as being more cloudy, because they are looking through a thicker swath of atmosphere. The launch of additional satellites during the project's lifetime has reduced this effect because each satellite now scans a smaller patch of sky. Evan's team says that this explains the apparent drop in cloudiness.

A flash of NO_x

Geophys. Res. Lett. **34,** L03816 (2007)

Nitrogen oxide production by lightning has been measured directly for the first time. The experiments were performed on lightning triggered by shooting a rocket trailing a copper wire towards a thunder cloud.

Lightning is a major source of nitrogen oxides (NO_x) in the atmosphere, and pinning down its contribution is important in assessing man-made levels of the pollutant gases.

Mahbubur Rahman of Uppsala University in Sweden and his colleagues diverted a portion of the triggered lightning through a sealed chamber on the ground. They found that the flash produced up to 3×10^{20} NO_x molecules per metre for every coulomb of charge it carried. This is roughly consistent with estimates based on data from aircraft flying through thunderstorms.

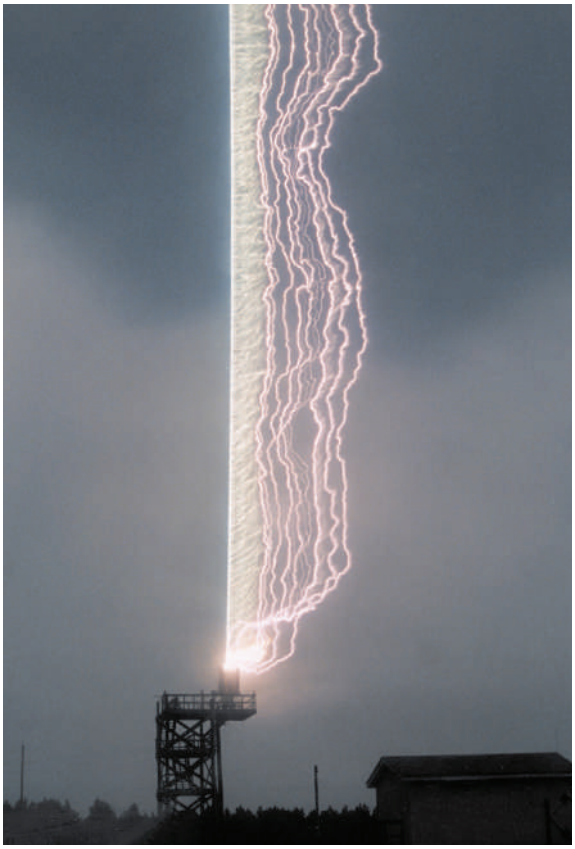

V. A. RAKOV

EVOLUTION

All right for snakes

Biol. Lett. doi:10.1098/rsbl.2007.0600 (2007)

A study of snail-eating snakes in southeast Asia has shown a remarkable feeding adaptation: many snakes of the subfamily Pareatinae have more teeth on the right side of their jaw than on the left, to match the fact that their snail prey tend to be coiled in a right-handed, or clockwise, way.

This observation was made by Masaki Hoso of Kyoto University, Japan, and his colleagues, who also confirmed the advantage it confers. In feeding experiments (pictured), one such snake, *Pareas iwasakii*, extracted and ate right-handed snails faster than left-handed ones. The diversity of left-handed snails in southeast Asia, which is higher than elsewhere in the world, may result from this evolutionary pressure.

ROYAL SOC.

FUEL CELLS

Hot chemistry

Anal. Chem. doi:10.1021/ac062189o (2007)

Researchers trying to understand the chemistry occurring inside solid-oxide fuel cells have a problem: the devices operate at temperatures that few chemical probes can tolerate. Infrared spectroscopy, for example, is thwarted by the brightness of thermal radiation emitted by a hot fuel cell.

Robert Walker of the University of Maryland, College Park, and his colleagues now show that it is possible to obtain real-time information using another technique, known as Raman spectroscopy. They tracked how carbon deposits grow and disappear from fuel-cell electrodes fed with butane or carbon monoxide, and identified intermediates formed during fuel-cell operation.

MATERIALS CHEMISTRY

Switchable shapes

Science **315,** 1116–1119 (2007)

Polymer sheets can be programmed to bend and wrinkle into prescribed structures, report Eran Sharon and his co-workers at

the Hebrew University of Jerusalem. They made flat discs of a soft gel that, when warmed gently, curved into domes, saddles and even sombrero shapes. Such switchable shape control in a soft material could have applications ranging from optics to biomedicine.

The sheets change shape because the gel — a web of crosslinked polymers — shrinks at temperatures above 33 °C by an amount determined by the local polymer density. When the density varies across the disc, the sheet buckles to relieve the pressure of uneven shrinkage. The researchers worked out what shrinkage patterns would produce the structures they wanted, then used an automated mixing system to produce gels with the right properties.

NEUROSCIENCE

Whiff of duality

Nature Neurosci. doi:10.1038/nn1856 (2007)

A faint odour can be captured more strongly by a powerful sniff, and researchers may have discovered why.

Minghong Ma from the University of Pennsylvania in Philadelphia and her colleagues have shown that up to half of mammalian olfactory sensory neurons respond to mechanical stimulation through air-pressure changes, as well as to specific smells.

The responses seem to share the same cellular pathway, with increased air pressure raising the firing rate of neurons that have been weakly stimulated by odorants. This mechanism may also help to synchronize the firing of neurons in the olfactory bulb with breathing.

CHEMICAL BIOLOGY

It's unnatural

Nature Methods doi:10.1038/nmeth1016 (2007)

Researchers in the United States have devised a reliable way of getting mammalian cells to integrate unnatural amino acids into their proteins. This will allow the design of proteins that act as biological probes containing, for example, amino acids that fluoresce.

During protein synthesis, enzymes called aminoacyl-tRNA synthetases hitch naturally occurring amino acids to transfer RNAs, which string them together in the order specified by the genetic code. Peter Schultz from the Scripps Research Institute in La Jolla, California, and his colleagues mutated a tRNA, and its corresponding aminoacyl-tRNA synthetase, so that the tRNA would insert an unnatural amino acid into a protein in response to a code normally reserved for a 'stop' signal. Similar methods have been successful in yeast and bacteria.

PHYSICS

Spinning up a whirl

Phys. Rev. Lett. **98,** 087205 (2007)

Simulations of a 'spin wave' generator make the idea that future computing devices might use these magnetic phenomena more plausible. Spin waves propagate as oscillations in the orientation of the magnetic moments of atoms in a magnetic medium. Harnessing their wave-like behaviour could lead to new paradigms for logic devices.

Sang-Koog Kim at Seoul National University in South Korea and his colleagues present a computer model of a 150-nanometre disc shooting spin waves into a magnetic wire.

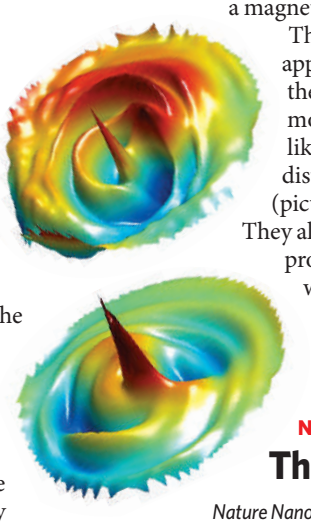

A.M. PHYS. SOC.

They predict that briefly applying an external field to the disc when the magnetic moments are in a whirlpool-like arrangement will create disturbances in their orientation (pictured) that spill into the wire. They also model how spin waves propagate in the wire, and how wires with different magnetic properties could filter out specific frequencies of spin wave.

NANOTECHNOLOGY

Thin blue line

Nature Nanotechnol. doi:10.1038/nnano.2007.35 (2007)

A multitalented polymer nanowire has been unveiled by Gareth Redmond of the Tyndall National Institute in Cork, Ireland, and his co-workers. The nanowire has two properties that, together, turn it into a miniature laser: the polymer emits blue light, and the wire's cylindrical shape provides the 'optical cavity' required in lasers to amplify emission.

The researchers made the wires by melting a polymer called poly(9,9-dioctylfluorene) into a block of material riddled with holes. When that material was dissolved, the team was left with polymer wires that had diameters up to 400 nanometres and flat ends.

Such wires, which lase when light is shone on them, could form components in data-processing or sensing devices.

JOURNAL CLUB

Timothy M. Swager
Massachusetts Institute of Technology, Cambridge, USA

A chemist predicts a bright future for sensors based on carbon nanotubes.

I am struck by the parallels between the development of polymer-based chemical sensors and those made from carbon nanotubes.

About ten years ago, I started to develop sensors from conjugated organic polymers, which took advantage of the materials' optical properties, rather than the electrical properties that had been exploited in devices until that time. This work led to fluorescent sensors, which are now being used in Iraq to detect explosives.

As with polymers, early work on nanotube sensors focused on detecting changes in a tube's electrical conduction when it binds to a molecule of interest. But electrical responses are sensitive to stray electric fields, which create interference in the signal.

Now, researchers working with nanotubes are also moving towards optical methods. A demonstration of a biosensor for glucose (P. W. Barone and M. S. Strano *Angew. Chem. Int. Edn* **45,** 8138–8141; 2006) sets the stage.

To make the sensor, the team first attached glucose groups to nanotubes. They then mixed these nanotubes with a large molecule, known as concanavalin A, which can bind to four glucose molecules at once. The glucose-decked nanotubes end up caught in clumps around the concanavalin A, which attenuates their emission. This system is sensitive to glucose because any glucose in solution loosens the nanotube clusters, and so boosts fluorescence.

A significant advantage of nanotubes is that they emit near infrared light, a longer wavelength than that accessible with polymers. And it just happens that human tissue is almost transparent in this spectral region. As a result, sensors based on these materials might be used for *in vivo* clinical diagnostics.

NEWS

Death toll in Iraq: survey team takes on its critics

C. AZIZ/REUTERS

It's not often that George W. Bush takes time out to attack a scientific paper on the day that it's released. But then few papers attract as much attention as the one that claimed that more than half a million people, or 2.5% of the population, had died in Iraq as a result of the 2003 invasion. Published last October in the run-up to the US mid-term elections, the interview-based survey attracted huge press interest and controversy.

The media spotlight has moved on, but interest within the scientific community has not. The paper has been dissected online, graduate classes have been devoted to it and critiques have appeared in the literature with more in press. So far, the discussion has created more heat than light. Many of the criticisms that dogged the study are unresolved. For example, *Nature* has discovered that different authors give conflicting accounts of exactly how the survey was carried out. And although many researchers say the questions hanging over the study are not substantial enough for it to be dismissed, a vocal minority disagrees.

The controversy creates extra interest in the authors' decision, made last week, to release the raw data behind the study. Critics and supporters will finally have access to information that may settle disputes.

"Some researchers fear that the Iraqi interviewers might have inflated their results for political reasons."

On paper, the study seems simple enough. Eight interviewers questioned more than 1,800 households throughout Iraq. After comparing the mortality rate before and after the invasion, and extrapolating to the total population, they concluded that the conflict had caused 390,000–940,000 excess deaths (G. Burnham, R. Lafta, S. Doocy and L. Roberts *Lancet* **368,** 1421–1428; 2006). This estimate was much higher than those based on media reports or Iraqi government data, which put the death toll at tens of thousands, and the authors, based at Johns Hopkins University in Baltimore, Maryland, and Al Mustansiriya University in Baghdad, have found their methods under intense scrutiny.

Much of the debate has centred on exactly how the survey was run, and finding out exactly what happened in Iraq has not been straightforward. The Johns Hopkins team, which dealt with enquiries from other scientists and the media, was not able to go to the country to supervise the interviews. And accounts of the method given by the US researchers and the Iraqi team do not always match up.

Several researchers, including Madelyn Hicks, a psychiatrist at King's College London, recently published criticisms of the study's methodology in *The Lancet* (**369,** 101–105; 2007). One key question is whether the interviews could have been done in the time stated. The October paper implied that the interviewers worked as two teams of four, each conducting 40 interviews a day — a very high number given the need to obtain consent and the sensitive nature of the questions.

The US authors subsequently said that each team split into two pairs, a workload that is "doable", says Paul Spiegel, an epidemiologist at the United Nations High Commission for Refugees in Geneva, who carried out similar surveys in Kosovo and Ethiopia. After being asked by *Nature* whether even this system allowed enough time, author Les Roberts of Johns Hopkins said that the four individuals in a team often worked independently. But an Iraqi researcher involved in the data collection, who asked not to be named because he fears that press attention could make him the target of attacks, told *Nature* this never happened. Roberts later said that he had been referring to the procedure used in a 2004 mortality survey carried out in Iraq with the same team (L. Roberts *et al. Lancet* **364,** 1857–1864; 2004).

Other arguments focus on the potential for 'main-street bias', first proposed by Michael Spagat, an expert in conflict studies at Royal Holloway, University of London. In each survey area, the interviewers selected a starting point by randomly choosing a residential street that crossed the main business street. Spagat says this method would have left out residential streets that didn't cross the main road and, as attacks such as car bombs usually take place in busy areas, introduced a bias towards areas likely to have suffered high casualties.

The Iraqi interviewer told *Nature* that in bigger towns or neighbourhoods, rather than taking the main street, the team picked a business street at random and chose a residential street leading off that, so that peripheral parts of the area would be included. But again, details are unclear. Roberts and Gilbert Burnham, also at Johns Hopkins, say local people were asked to identify pockets of homes away from the centre; the Iraqi interviewer says the team never worked with locals on this issue.

Many epidemiologists say such discrepancies are understandable given that Roberts and Burnham could not directly oversee the survey, and do not justify accusations that the process was flawed. For those who disagree, access to the raw data is essential. Although previously reluctant to release them, Roberts and Burnham now say they are removing information that could be used to identify interviewers or respondents and will release the data within the next month to people with appropriate "technical competence".

One researcher keen to see the numbers is Spagat. The 2004 survey used GPS coordinates instead of the main-street system to identify streets to sample, and when Spagat used the limited data available so far to compare the two studies for the period immediately following the invasion, he found that the 2006 study turned up twice as many violent deaths, suggesting that main-street bias may be present.

Baghdad, February 2007: Iraqi civilians are still in danger from car bombs in their neighbourhoods.

Roberts and others question Spagat's methods. But the issue could be checked using the raw data. If main-street bias exists, says Spagat, then death rates will fall as the interviews move away from the main street.

The raw data may also help address a fear that some researchers are expressing off the record: that the Iraqi interviewers might have inflated their results for political reasons. That could show up in unusual patterns within the data.

Roberts and Burnham say they have complete confidence in the Iraqi interviewers, after working with them directly for the 2004 study. And supporters say that criticisms should not detract from the fact that the Iraqi team managed to produce a survey under extremely difficult circumstances. Security threats forced the team to change travel plans and at one point to consider cancelling the survey altogether. Since its completion, one interviewer has been killed and another has left Baghdad, although it is not known whether either case is linked to their involvement in the survey. Either way, the continuing violence in the country is enough for the remaining interviewers to say that they are not willing to repeat the exercise. ■

Jim Giles

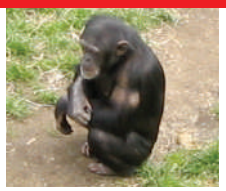

CHIMPS MAKE SPEARS TO CATCH DINNER
Wooden weapons are a first in animal kingdom.
www.nature.com/news

Q&A: Ronald Plasterk

Molecular geneticist Ronald Plasterk is one of the Netherlands' most highly cited researchers, publishing regularly in top journals in fashionable research fields such as regulation of gene expression by inhibitory RNAs. A lifelong member of the centre-left Labour party, he was last month named minister of research and universities in the country's new coalition government. He talked to **Alison Abbott** about how he ended up in this position.

How long have you been active in politics?
I was a member of the local council in Leiden in my student days, but then I went to do postdocs at the California Institute of Technology and the MRC Laboratory of Molecular Biology in Cambridge, UK. I started my family when I returned to the Netherlands, so I was only active in a marginal way. But in the past ten years or so I've been writing a weekly newspaper column and a commentary on TV, whose themes can be political. I also co-authored the Labour party's election platform.

What will being research minister mean for your research?
I hate to say it, but it will mean the end of research for me. At a meeting only a few weeks ago I was exchanging scientific views with Nobel prizewinners — you can't step out of this level of research for four years and then hope to go back. It's not yet clear whether I will be able to retain my professorship.

How do you feel about that?
I feel like Alice, stepping through the mirror into another, slightly unreal, world. I feel a little disconnected right now, but the people in my lab will not suffer. They will be taken care of by others in the institute.

What are the key issues for science in the Netherlands?
Europe is losing ground — compared with the United States, for example, from which we have a lot to learn in terms of meritocracy and researcher mobility. Holland is not so bad actually, but it could be, and needs to be, better. The academic system must become less hierarchical. The number of women in top science jobs is embarrassingly low, among the worst in Europe.

How can scientific quality be improved?
Ask yourself why so many top physicists, including three Nobel prizewinners, ended up in Leiden 100 years ago? Or at the Cavendish laboratories in Cambridge? There is no blueprint for quality — top scientists will go where they can work best. We just need to provide sufficient funding to allow centres of excellence to emerge from within the community. And there is in fact more money for research foreseen in the government plan. ■

Ronald Plasterk believes that his political appointment spells the end of his research career.

R. CREMERS/HOLLANDSE HOOGTE

Meet the human metabolome

Imagine that at a routine medical check-up your doctor takes a urine sample, then reports a few days later that your risk of type 2 diabetes is normal, but there are hints that your arteries are furring up.

A similar scenario has been promised for the past 20 years by those working in genomics and proteomics, but has not yet materialized. Now, however, an increasing number of researchers are claiming that metabolomics — the study of all the body's metabolites — will finally come up with the goods.

Supporters of this burgeoning branch of molecular medicine are gung-ho about their chances of success. "In retrospect, we wonder why we spent millions on the genome," says Bruce German, who studies lipid metabolism at the University of California, Davis. With the knowledge we have today, he reckons, scientists should have gone straight for the metabolome. But can it deliver?

"In retrospect, we wonder why we spent millions on the genome."

Metabolomics is the study of the raw materials and products of the body's biochemical reactions, molecules that are smaller than most proteins, DNA and other macromolecules. The aim is to be able to take urine, blood or some other body fluid, scan it in a machine and find a profile of tens or hundreds of chemicals that can predict whether an individual is on the road to a disease, say, or likely to experience side-effects from a particular drug.

Researchers are already trying to flag impending disease by measuring levels of gene expression or proteins, but supporters of metabolomics say they should be able to do it better. Small changes in the activity of a gene or protein (which may have an unknown impact on the workings of a cell) often create a much larger change in metabolite levels. The approach has already proved its worth: cholesterol and glucose have long been chemical canaries for heart disease and diabetes.

Data fingerprinting

But realizing this vision isn't straightforward. One of the first tasks is to create a catalogue of compounds in the human body, and this is proving hard to define. David Wishart at the University of Alberta, Edmonton, and his colleagues have taken an initial step forward by producing something they rather grandly call the first draft of the human metabolome[1]. They searched the published literature for known human metabolites, and have collected around 2,500 of them into a public database (www.hmdb.ca) along with other information such as known links to disease. The researchers also used nuclear magnetic resonance and mass spectroscopy to produce characteristic 'fingerprints' for more than 400 compounds, and have added these to the database.

It's the most comprehensive collection of metabolite data to be made publicly available. But others in the field point out that Wishart's catalogue is far from complete because the number and nature of compounds in the human metabolome will vary depending on which body fluid is looked at and the method used for the analysis. There is also no clear division between compounds produced by the human body, those produced by our gut bacteria and fleeting products generated by food or drugs swallowed that day.

"The notion that this is a first draft of the human metabolome is nonsense," says Jeremy Nicholson of Imperial College London, one of the pioneers of the field. "I agree that it covers a helluva lot of important metabolites, but it's a very arbitrary guess at what might be useful and what might not."

An added complication is that one person's profile of metabolites is likely to be dramatically different from another's, and each may fluctuate markedly depending on the time of day, what they last ate and other aspects of their lifestyle. To get a handle on this variation, Nicholson has studied tens of thousands of urine samples from many ethnic groups around the world and found that each group is remarkably different. A separate study showed that the metabolic profile of meat eaters is very different from that of vegetarians[2]. This means that a person's metabolome might need to be measured many times during their lives in order to be able to pick out changes that might signal disease. Also, any one metabolite will have to be assessed relative to the pattern of many others.

PHOTOTAKE INC./PHOTOLIBRARY.COM

Hopes are high that in future a urine sample might reveal our health profile from our metabolites.

Whatever the total metabolite tally, researchers will have to prove that particular concentrations and combinations can reveal something about drugs or disease. Preliminary studies suggest that this can be done. Last year, for example, Nicholson and his colleagues showed that a fingerprint of the metabolites in urine could predict which rats would suffer liver damage from the drug paracetamol[3]. He says he has now shown the same in humans, and is preparing the study for publication. A team led by Douglas Kell at the University of Manchester, UK, has developed a computer model based on metabolite profiles in blood plasma that can identify pregnant women with the dangerous condition called pre-eclampsia[4].

Lab on a chip

But just as with genomics and proteomics, finding profiles that reliably predict the onset of disease will be a major undertaking, because it will typically require sampling regular profiles from many thousands of people and then following them for years to see which ones develop a particular condition. Researchers are hopeful that biobanks — large collections of people's biological samples and medical records — will in future supply this information, but such studies could take decades. They will also have to learn from those working on gene-expression or proteomic profiles, who have sometimes struggled to show that a test that works in one group also works in another, or that the changes they see are actually involved in a disease. "In my opinion we should know why this metabolite is going up or down," says William Bigbee, an expert in biomarkers and proteomics at the University of Pittsburgh Cancer Institute, Philadelphia.

In the long run, the best way to predict an individual's disease risk is likely to come from understanding the biology behind each disease — and that will come from a combination of genomics, proteomics and metabolomics. "I don't want to buy six machines," says Ben van Ommen of the Netherlands Organization for Applied Scientific Research in Zeist. "I want a lab on a chip that measures metabolites, proteins and gene expression." ■

Helen Pearson

1. Wishart, D. S. *et al. Nucleic Acids Res.* **35,** D521–D526 (2007).
2. Stella, C. *et al. J. Proteome Res.* **5,** 2780–2788 (2006).
3. Clayton, T. A. *et al. Nature* **440,** 1073–1077 (2005).
4. Kenny, L. C. *et al. Metabolomics* **1,** 227–234 (2005).

POLAR RESEARCH
Get International Polar Year started with science from the ends of the Earth.
www.nature.com/news/infocus/polarresearch.html

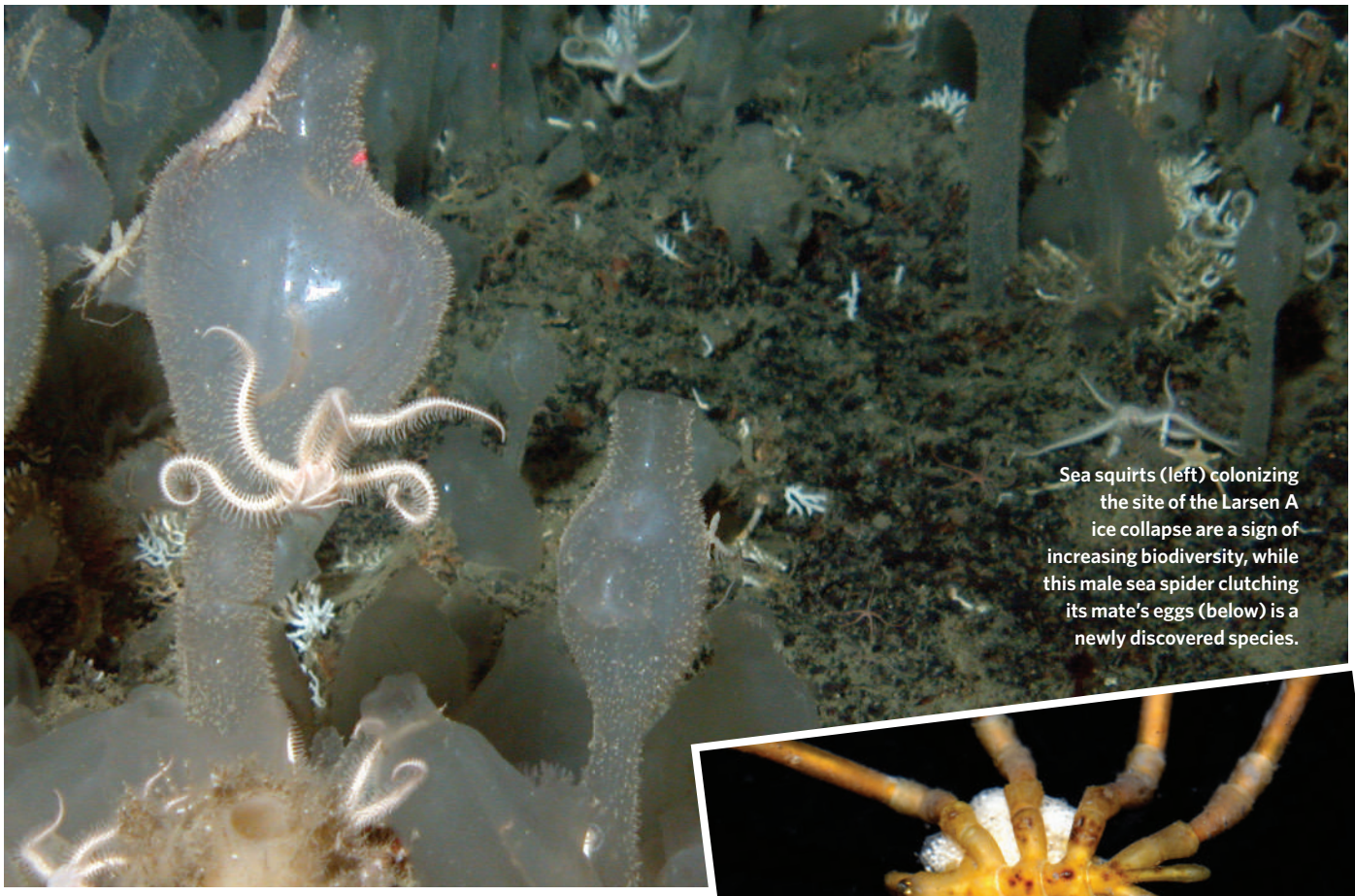

J. GUTT/ALFRED WEGENER INST.

Sea squirts (left) colonizing the site of the Larsen A ice collapse are a sign of increasing biodiversity, while this male sea spider clutching its mate's eggs (below) is a newly discovered species.

Letting the light in on Antarctic ecosystems

In just over a decade, two major ice shelves have collapsed on the eastern side of the Antarctic peninsula, uncovering a part of the sea floor that had not seen sunlight for several thousand years. A ten-week expedition that ended in late January has shed light on the biology of these waters, and has recovered samples of some 1,000 species from the region, several of which may be new to science.

"This is one of the first opportunities to see what will happen when climate change alters the conditions in the polar seas," says Jesse Ausubel, programme director at the Alfred P. Sloan Foundation in New York. The foundation is funding the Census of Antarctic Marine Life, an initiative for International Polar Year that has 13 voyages scheduled.

From the German research vessel *Polarstern*, around 50 marine biologists from 14 countries used various approaches, including a remotely operated vehicle equipped with a camera, to scour the depths and trawl for samples. They surveyed an area of seabed roughly the size of Jamaica beneath what used to be the Larsen A and B ice shelves, to a depth of 850 metres.

The biologists had two main aims: to discover what kinds of creatures live beneath ice shelves, and to track what happens to those communities once the ice disappears. Unexpected inhabitants of the relatively shallow waters were species more commonly found at greater depth.

"We found a species of sea urchin that has previously been found only at depths of 2,000 to 3,000 metres off Peru," says Gauthier Chappelle, the expedition's outreach officer and a biologist at the Brussels-based International Polar Foundation. Presumably, such species are better able to adapt to conditions where resources are scarce, as they would have been under the ice.

Another find was juvenile forms of glass sponges in the Larsen A region; the Larsen A ice shelf collapsed 12 years ago, whereas the Larsen B region opened up only 5 years ago. Glass sponges take hundreds of years to mature into adults, but are key members of Antarctic marine ecosystems, as they provide habitats for other species. "It seems like the system is shifting towards supporting the rich communities found in other parts of the Antarctic," says Julian Gutt, a marine ecologist at the Alfred Wegener Institute for Polar and Marine Research in Bremerhaven, Germany, and chief scientist on the *Polarstern* expedition.

It would probably take between 1,000 and 5,000 years for the region to mature into the kind of community typical of Antarctic coastal regions, says Gutt. And future climate change could result in soils from the coast degrading the crystal-clear waters and potentially blocking any further succession to a rich community of Antarctic filter-feeders. ■

Lucy Odling-Smee

Federal agency rescinds primate stem-cell patents

Three key stem-cell patents have been revoked by the US Patent and Trademark Office. Scientists have complained that the patents, held by the Wisconsin Alumni Research Foundation (WARF), are so broad that they impeded US research.

The patents were granted between 1998 and 2006, but last July several nonprofit groups requested that they be re-examined, arguing that the work described in the patents was not sufficiently novel to deserve protection. The patents claim to cover primate embryonic stem cells — including human embryonic stem cells — derived by any means. The patent office agreed, on reconsideration, that the work was not novel enough to deserve a patent.

WARF has two months to contest the decision, and could then initiate a lengthy appeals process.

Nobel laureate named as NASA chief scientist

NASA's science directorate has been boosted by the appointment of astronomer John Mather as the agency's chief scientist.

Formerly a somewhat isolated position, the chief scientist will now have his own staff and work closely with the new associate administrator for space science, planetary scientist Alan Stern. Mather shared the 2006 Nobel Prize in Physics for work to probe the cosmic microwave background, the relic radiation left over from the Big Bang.

But the news is mixed for the agency. Last week, some members of Congress moved towards ousting NASA's inspector-general, Robert Cobb. His position is meant to oversee the agency from an independent standpoint, but several Congressmen charge that Cobb was too close to a former agency chief to perform his duties properly.

An independent government committee last week passed a report to the House Committee on Science and Technology alleging that Cobb had misused his authority and created a hostile work environment. Several lawmakers have asked President George W. Bush to fire Cobb and may hold Congressional hearings on the matter. Cobb has not responded to the allegations.

Arctic sea-ice cover reaches near-record low

This year, the extent of winter sea ice in the Arctic came close to breaking the record for being the smallest ever.

On 4 April, scientists at the National Snow and Ice Data Center in Boulder, Colorado, announced that the maximum sea-ice cover last month was 14.7 million square kilometres. The record was set in March 2006, when the Arctic was covered by just 14.5 million square kilometres. This finding is consistent with the marked trend of sea-ice shrinkage and thinning that has been observed in recent decades.

NASA, meanwhile, reported last week that less ice may be persisting from year to year in the Arctic, so less is available to replenish the perennial pack ice each winter. A study by Ron Kwok, of the Jet Propulsion Laboratory in Pasadena, California, found that only 4% of the seasonal ice that formed in the winter of 2004–05 survived the summer melt and helped build up the perennial ice in the winter of 2005–06.

UK report calls for change to stem-cell rules

British politicians have criticized their government for proposing a ban on the creation of 'chimaeric' embryos, made from human DNA inserted into an animal egg.

The Select Committee on Science and Technology, which is drawn from all the major parties, released a report on 5 April calling for a 'permissive' set of rules to be put in place that would allow the Human Fertilisation and Embryology Authority more freedom to adjudicate on the scientific merit of new embryological procedures.

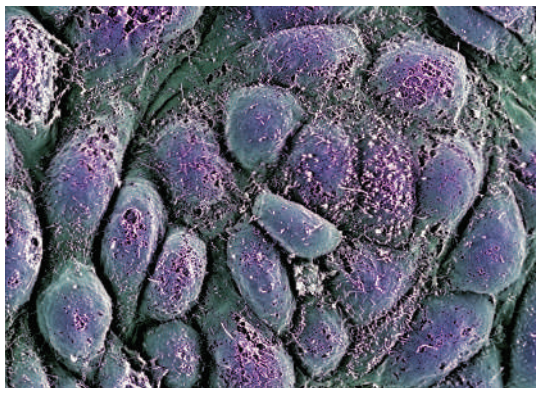

The creation of human stem-cell lines from 'chimaeric' embryos is controversial.

M. STOJKOVIC/SPL

The committee hopes the government will change the rules when it releases a draft bill next month. Only that would end the limbo for researchers at King's College London and the University of Newcastle, both of which have applied for licences to create chimaeric embryos to generate human stem-cell lines.

University decides not to investigate smoking study

Officials at the University of California have decided not to examine a controversial 2003 research article disputing the dangers of second-hand smoke.

In recent months, questions had been raised about whether the article, published in the *British Medical Journal*, involved scientific misconduct because it relied on purportedly faulty smoke-exposure data (see *Nature* 446, 242; 2007).

Epidemiologist James Enstrom of the University of California, Los Angeles, (UCLA) was the lead author of the article (J. E. Enstrom and G. C. Kabat *Br. Med. J.* 326, 1057; 2003), which reported that spouses of smokers were no more likely to develop lung cancer or heart disease than were spouses of non-smokers. Enstrom denied any impropriety.

Late last month, UCLA officials reviewed concerns raised by the American Cancer Society about Enstrom's article, and decided that the allegations were not worth a formal inquiry or investigation.

Correction

In our News story "Letting the light in on Antarctic ecosystems" (*Nature* **446,** 9; 2007), the credit for the photo of the sea spider was inadvertently omitted. The picture should have been credited to P. J. López, University of Seville/Climant-Ecoantha.

Pictures of clouds reveal a Venus in twirls

Images beamed back from Venus are revealing complex cloud features above the planet that seem to vary from equator to pole.

In this picture, clouds near the Alpha Regio area — close to the planet's equator — show turbulent eddies, possibly caused by local convection set up by daytime heating from the Sun's rays. At higher latitudes, venusian clouds spread out into streaky bands, powered by the winds that zip around the planet in just four days.

The latest images were generated by a spectrometer on board the European Space Agency's Venus Express spacecraft, which has been probing the planet since it arrived there a year ago.

ESA/VIRTIS/INAF-IASF/OBS. DE PARIS-LESIA

The lab that asked the wrong questions

PRINCETON

A medley of random-event machines, including a kaleidoscopic crystal ball on a pendulum, a pipe spurting water and a motorized box straddled by a toy frog, came to the end of their working lives yesterday at the Princeton Engineering Anomalies Research (PEAR) laboratory in New Jersey.

Only romantics — and some parapsychologists — are likely to lament the loss of this unique institution, which investigated whether people can alter the behaviour of machines using their thoughts. Many scientists think the lab's work was pointless at best. But the closure highlights a long-running question: how permissive should science be of research that doesn't fit a standard theoretical framework, if the methods used are scientific?

The PEAR lab was founded in 1979 by Robert Jahn, former dean of Princeton's school of engineering and applied sciences, and an expert on electric propulsion. Start-up funds came from aerospace pioneer James McDonnell, who believed that aircraft machinery was influenced by the mental states of pilots. The lab has relied on private funds ever since.

Over 28 years, PEAR researchers collected data from tens of millions of trials using random-event machines. When all the data are considered together, they show that human intention has a very slight effect, the researchers say. Whether the machine is a screen that flashes numbers or a fountain of water droplets, they say that, on average, people can shift 2–3 events out of 10,000 from chance expectations.

It was Jahn's decision to close the lab. He set out to prove the existence of the effect and, at 76, believes the work is done. But such tiny deviations from chance have not convinced mainstream scientists, and the lab's results have been studiously ignored by the wider community. Apart from a couple of early reviews (R. G. Jahn *Proc. IEEE* **70,** 136–170; 1982 and R. G. Jahn and B. J. Dunne *Found. Phys.* **16,** 721–772; 1986), Jahn's papers were rejected from mainstream journals. Jahn believes he was unfairly judged because of the questions he asked, not because of methodological flaws.

Even in other areas of parapsychology, opinion is divided on the lab's results. The difficulty is that it's virtually impossible to prove that such subtle effects aren't caused by some flaw in the methods or equipment. A recent meta-analysis (H. Bösch *et al. Psychol. Bull.* **132,** 497–523;

PEAR lab researchers feel that their parapsychology work was unfairly judged.

A. KANE PHOTOGRAPHERS, PEAR LAB.

Data sharing: the next generation

The Internet has already become a place for people to share knowledge, opinions, music and videos. Now, in a slightly geekier aspect of the same trend, social software is allowing people to share data too. More than 1 million data sets have been uploaded to the data-sharing site Swivel since its launch in December. And on 23 January, IBM labs launched Many Eyes, which allows users to visualize their data with tools previously available only to experts.

Once data are uploaded to these sites (which are still being tested), people can reanalyse the numbers, mix them with other data and visualize them in different ways. Swivel focuses on letting users combine data sets, with some basic ways to present the results such as scatter graphs and bar charts. Many Eyes allows users to generate more complicated graphs such as network diagrams, which depict nodes and connections within networks, and treemaps, which display data as groups of nested rectangles.

The idea is to make data analysis more democratic, as tools such as Google Earth have done for geographic visualization, says Fernanda Viégas of IBM's Visual Communication Lab in Cambridge, Massachusetts. "We want to provide the masses with access to visualization tools, especially interactive ones," she says. Governments, international agencies and research organizations generate huge silos of publicly available data on almost every aspect of society, but the public has never been able to explore, share and discuss these data sets easily, she points out.

Making such tools available will not only empower individuals, Viégas predicts, the collective intelligence and expertise of users will result in new insights. "Just three weeks in, people were using some of the most sophisticated visualization types," she says. Since Many Eyes launched, users have uploaded data and created graphics on everything from the stock price of Heineken against temperature, to collaborations of prostate cancer researchers, to co-occurrences of

2006) combined 380 studies on the phenomenon, often termed psychokinesis, including data from the PEAR lab. It concluded that although there is a statistically significant overall effect, it is not consistent and relatively few negative studies would cancel it out, so biased publication of positive results could be the cause.

Robert Park, a physicist at the University of Maryland, adds that if you run any test often enough, it's easy to get the "tiny statistical edges" the PEAR team seems to have picked up. If a coin is flipped enough times, for example, even a slight imperfection can produce more than 50% heads.

In the end, the decision whether to pursue a tiny apparent effect or put it down to statistical flaws is a subjective one. "It raises the issue of where you draw the line," says sceptic Chris French, an 'anomalistic psychologist' at Goldsmiths, University of London, who tries to explain what seem to be paranormal experiences in straightforward psychological terms. French thinks that even though the chances of a real effect being discovered are low, the implications of a positive result would be so interesting that work such as Jahn's is worth pursuing.

"Parapsychologists have a hard time trying to publish in mainstream journals."

Many scientists disagree. Besides being a waste of time, such work is unscientific, they argue, because no attempt is ever made to offer a physical explanation for the effect. Park says the PEAR lab "threatened the reputation" of both Princeton and the wider community. He sees the persistence of such labs as an unfortunate side effect of science's openness to new questions. "The surprising thing is that it doesn't happen more often," he says.

William Happer, a prominent physicist at Princeton, takes the middle ground. He believes the scientific community should be open to research that asks any question, however unlikely, but that if experiments don't produce conclusive results after a reasonable time, researchers should move on. "I don't know why this took up a whole lifetime," he says.

The status of paranormal research in the United States is now at an all-time low, after a relative surge of interest in the 1970s. Money continues to pour from philanthropic sources to private institutions, but any chance of credibility depends on ties with universities, and only a trickle of research now persists in university labs.

Elsewhere the field is livelier. Britain is a lead player, with privately funded labs at the universities of Edinburgh, Northampton and Liverpool Hope, among others. Parapsychologist Deborah Delanoy at the University of Northampton suspects that the field is stronger in Britain because researchers tend to work in conventional psychology departments, and also do studies in 'straight' psychology to boost their credibility and show that their methods are sound. "We're seen to be in the same business as other psychologists," she says.

But parapsychologists are still limited to publishing in a small number of niche journals. French thinks the field is treated unfairly. "I'm convinced that parapsychologists have a hard time trying to publish in mainstream journals," he says, adding that he even has difficulty publishing his 'straight' papers on why people believe in paranormal events: "Simply because the paper mentions the word telepathy or psychokinesis, it isn't sent out to referees. People think the whole thing is a waste of time." ■

Lucy Odling-Smee

names in the New Testament.

The new sites might also provide a model for better communication among scientists, says Brent Edwards, director of the Starkey Hearing Research Center in Berkeley, California, who blogs on innovation in science. He points out that journals could use the Internet to share information and move science forward much more effectively, rather than being facsimiles of their print cousins, with static graphs and figures.

"I'm often frustrated by my inability to analyse in a different way data that are printed in peer-reviewed publications, when I'm interested in looking at a relationship that the authors didn't think of," he says. If research organizations and journals linked the raw data behind papers to social software tools such as Swivel and Many Eyes, he argues, "it would have considerable value to the scientific community as a whole".

David Lipman, director of the US National Center for Biotechnology Information in Bethesda, Maryland agrees, adding that his centre might explore related possibilities. He finds it ironic that scientists have been slow to adopt social software, given how useful it could be for them. "Scientists are more interested in their careers and grants than using tools that promote better communication and data sharing," Lipman says.

He's optimistic that this attitude may change in the future, however, especially as a new generation — used to communicating through social sites such as MySpace — enters research. ■

Declan Butler

SCORECARD

A. PATERSON/ALAMY

▲ Australian lightbulbs
Australia, yet to sign the Kyoto Protocol, has boosted its green credentials by pledging to replace all conventional lightbulbs with energy-efficient ones.

▼ DVD games
A new game called *Body Mechanics* aims to teach kids about healthy lifestyles by battling the evil Col Esterol and his cronies — while sitting in front of the television.

N. EMM/ALAMY

ON THE RECORD

"Red hot ... Better performance. Better price."

The caption accompanying a picture of a scantily clad female model featured in an advert for optical company Edmund Optics. Offended scientists of both sexes have accused the firm of insulting the scientific community.

"I always knew that a geek would make a great husband."

Minneapolis resident Melinda Kimberly, who retrieved her stolen laptop because her husband was using it to run the alien-hunting SETI@home software. The program revealed the laptop's location when it checked in with SETI's server.

NUMBER CRUNCH

£18,000 (roughly US$35,000) was spent by the UK Ministry of Defence in 2002 to investigate the potential use of psychic powers to detect hidden objects.

12 self-proclaimed psychics declined to participate in the research, meaning the ministry had to rely on novice volunteers.

1 participant fell asleep during the study, which ultimately concluded that psychic techniques are of "little value".

Sources: news.com.au, Associated Press, CosmicVariance, BBC

SIDELINES

Scientists rethink approach to HIV gels

Scientists and activists struggling to combat the HIV epidemic were shattered by last month's failure of a candidate microbicide gel in large clinical trials. Microbicides aim to block HIV infection, but the candidate product — cellulose sulphate — seemed to increase women's susceptibility. In the wake of this setback, some are now warning that the field must change its approach.

Dozens of candidate microbicides are being tested in labs around the world. But advocates of change say the field must make hard choices about which of these should graduate to phase III clinical trials — extended trials to confirm that a product works — because these trials are expensive and time-consuming. Such choices have not previously been made: the gels tested so far were the first to be ready, not necessarily the most promising.

"How many more clinical trials are we going to be able to do with dramatic failures like this?" asks Ronald Veazey, chair of the division of comparative pathology at the Tulane National Primate Research Center in Covington, Louisiana.

The microbicides tested in phase III trials so far all belong to a 'first generation' of products that aim to make the vagina less hospitable to HIV, but don't target the virus directly. So far, none of these has worked. One, Savvy gel, failed, and two — cellulose sulphate and the spermicide nonoxynol-9 — led to higher HIV infection rates. Phase III trials of three other products are ongoing, a redundancy that is now unavoidable as the trials have already begun.

Meanwhile, most researchers see more promise in a batch of microbicides at an earlier stage of development. These products contain gel formulations of antiretroviral drugs that target HIV. But for these microbicides, too, there are many similar products in the pipeline.

For instance, different groups are testing at least four microbicide candidates belonging to a class of drug known as non-nucleoside reverse transcriptase inhibitors (NNRTIs). Two of these will probably be ready for phase III trials before 2009. The question now is whether all the products should automatically be pushed into such trials.

"Are we really going to proceed with two different NNRTIs, or should we be doing a study comparing them head-to-head, to help us determine which move forward?" says Salim Abdool Karim, director of an AIDS research centre at the University of KwaZulu-Natal in Durban, South Africa.

Right now, it is difficult to choose the best candidates without doing large human studies because different research groups use different preclinical testing methods, and there is no agreement on which of these tests best predict how a microbicide will act in patients.

R. JANTILAL/AFP/GETTY

The recent failure of clinical trials of a microbicidal gel has highlighted the need to make tough decisions.

The failure of cellulose sulphate may actually help solve this problem. CONRAD, the Virginia-based agency that organized trials of cellulose sulphate in five countries, is determined to find out why the compound was harmful. "We'll probably put together a blinded panel of compounds, including cellulose sulphate, and send it out to various individuals working on different models and see if they can come up with any clues," says Henry Gabelnick, CONRAD's executive director. Testing the same products across different models could help researchers compare different microbicides in future.

But that will leave a bigger obstacle: each research group is investing in its own product, so will be reluctant to step aside for others. The field may need a guiding hand from an impartial body, which doesn't exist at the moment.

It has been suggested that a working group on microbicides currently being set up by the US National Institutes of Health's Office of AIDS Research may serve this role. Its composition and role have not been clearly defined, but advocates suggest it could solicit advice from independent experts about which products should proceed to clinical trials.

Some, including Gabelnick, say it would be a mistake to jettison products just to avoid redundancy. "We don't know enough to say these are all the same," he argues.

But others, such as Polly Harrison, director of the Alliance for Microbicide Development based in Silver Spring, Maryland, say someone has to help the field reach a consensus. "Prioritization has to occur, and it has to go all the way along the pipeline," Harrison says. "We know we need this." ■

Erika Check

See Editorial, page 1.

Trio of studies makes headway in HIV battle

The search for new ways to curb HIV transmission received a badly needed boost last week.

On 22 February, researchers reported that drug treatment against the herpes simplex 2 virus cuts levels of HIV RNA in the blood and genitals of women infected with both viruses (N. Nagot *et al. N. Engl. J. Med.* **356,** 790–799; 2007). The researchers suggest that controlling herpes may thus also control the spread of HIV. Studies are under way to test the idea.

The following day, two large controlled trials on male circumcision in Uganda and Kenya were published (M. L. Newell & T. Bärnighausen *Lancet* **369,** 617–619; 2007). Both trials had been stopped early by their funder, the US National Institutes of Health, because the effects of the procedure were already clear. Together with a previous study in South Africa, the results show that circumcision can reduce a man's risk of HIV infection by 50–60%.

The task now is to roll out circumcision in countries that would most benefit, where HIV rates are high and the virus is spread mainly through heterosexual sex. A working group convened by the Joint United Nations Programme on AIDS and the World Health Organization will hold a consultation on 6 March to discuss how and where circumcision should be provided. **Erika Check**

California hands out grants for stem-cell research

The California Institute for Regenerative Medicine (CIRM) has approved its first research grants, awarding US$45 million in 72 grants to 20 research institutions in the state. The total is more than the National Institutes of Health is expected to spend on human embryonic stem-cell work this year.

The grants range from around $250,000 to $800,000 to support a range of projects, including efforts to study the flexibility of embryonic stem cells and how they can be used to treat disease. CIRM president Zach Hall says the grants are designed to attract new investigators: 30 went to scientists who have never worked with stem cells, and 27 have gone to researchers who have run their labs for six years or less.

The institute is embroiled in litigation over its right to exist. But stopgap funding from private investors and the state has permitted the first round of grants. The next round, for more established investigators, is expected to be awarded in March.

Virgin Galactic launches collaboration with NASA

Burt Rutan, who built the first private spaceship, has often criticized NASA for its bureaucracy and slowness. But now a successor to the craft that Rutan built could enter commercial service in 2009 — with a little help from NASA.

The private spaceflight company Virgin Galactic, which licensed technology developed for Rutan's SpaceShipOne, is talking to NASA about the possibility of collaborating on technology projects. Officials at NASA's Ames Research Center at Moffett Field, California, said on 21 February that they would talk to Virgin engineers about working together to develop spacesuits, heatshields for spaceships, hybrid rocket motors and hypersonic craft.

Britain cuts funding for research councils

It is only a small cut, but the fact it has happened at all is worrying UK science managers. After years of boosting research spending, the British government is to cut almost £100 million (US$196 million) from the science budget over the next two years.

The money will come from a pot used to smooth the transition from one financial year to the next and amounts to about 1.5% of the £6.6 billion allocated to science during that period. But some disciplines will still suffer: the Engineering and Physical Sciences Research Council says it will meet later this month to consider how to deal with the £29 million it will lose. The second worst-hit council is the Medical Research Council, which loses some £11 million.

"It is disturbing that the science budget is vulnerable in this way," says Martin Rees, president of the Royal Society in London. He called the decision, by the Department of Trade and Industry, "a worrying message about the priority accorded to science" in Britain.

New Horizons head named as NASA science boss

NASA will have a new lead space scientist on 2 April, when planetary scientist Alan Stern, of the Southwest Research Institute in Boulder, Colorado, takes over from Mary Cleave as the agency's associate administrator for space science.

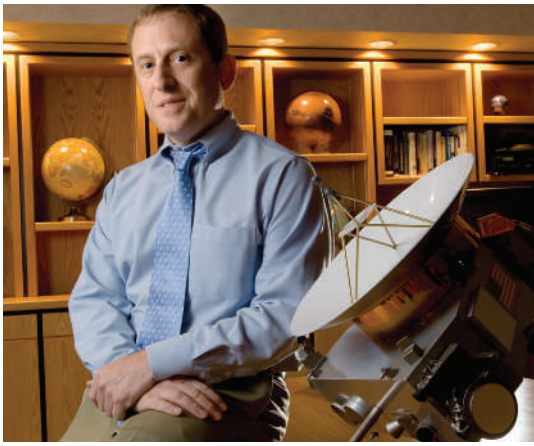

Change on the horizon: Alan Stern will become NASA's chief space scientist in April.

K. MOLONEY

Cleave, a former astronaut, had struggled to cope with increasing cuts to the agency's science budget. Many in the community now praise the appointment of Stern, who has a long history with NASA, including flying imaging instruments aboard the space shuttle (see *Nature* 436, 618–619; 2005).

Stern will also continue to serve as principal investigator for the New Horizons spacecraft, which was scheduled to fly past Jupiter on 28 February on its way to a 2015 flyby of Pluto. In a deal worked out by NASA chief Michael Griffin, Stern will not deal as associate administrator with any matters involving New Horizons.

South Africa doubles its science budget

South Africa's finance minister Trevor Manuel announced on 21 February that the nation has more than doubled its science budget. In the fiscal year 2007–08, the government will spend US$450 million on research, up from about $200 million last year. Next year, the budget is expected to increase by a further 16%, which should enable South Africa to meet the target set by the African Union of spending 1% of its gross domestic product on research and development.

The money for this year includes $14 million to allow institutions to share information over a cheap broadband network; $9 million for research chairs at universities; and $11 million for the Karoo Array Telescope, a prototype for the Square Kilometre Array (SKA) radio telescope. South Africa is competing against Australia to host the SKA, and an extra $64 million has been set aside between 2008 and 2010 should South Africa's bid be successful.

Blue Mars

Martian clouds appear an incandescent blue in this image taken by the European Space Agency's Rosetta spacecraft.

On 25 February, Rosetta came to within 250 kilometres of the martian surface on its way to Comet 67/P Churyumov-Gerasimenko, where it is expected to arrive in 2014.

On the way, though, it snapped a series of close-up shots of Mars. This false-colour image from the wide-angled camera in Rosetta's Optical, Spectroscopic, and Infrared Remote Imaging System (OSIRIS) is enhanced in the ultraviolet, bringing out details of the martian cloud systems.

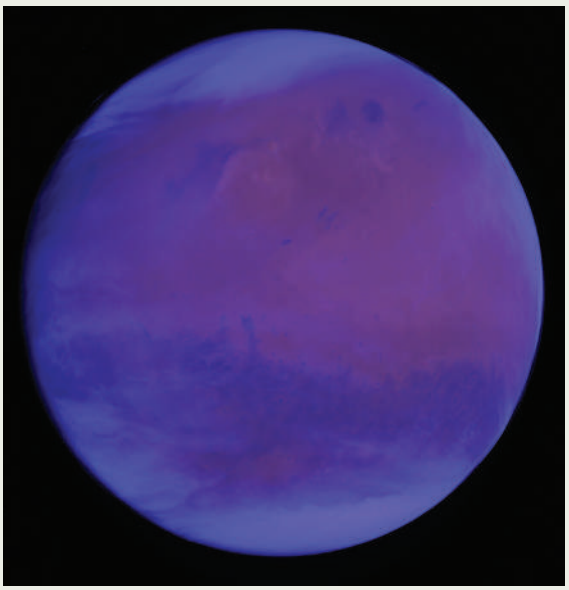

ESA

BUSINESS

A merger too far?

Bristol-Myers Squibb has been stoking its research productivity. **Meredith Wadman** investigates whether an acquisition would be the right prescription for the company.

Last month, the drug industry was abuzz with reports that Sanofi-Aventis was set to buy up Bristol-Myers Squibb. The move would make Paris-based Sanofi the world's second-largest drug maker, after Pfizer. And although talks between the two companies are said to have broken down, they could yet be revived once a key patent dispute involving both companies has been settled.

But some industry observers question the need for more aggregation. They argue that — short-term shareholder profits aside — Bristol-Myers Squibb could have plenty to gain from remaining independent. "Bristol-Myers Squibb is a turn-around story that has been neglected by many over an extended period of time," says Tim Anderson, an analyst with the Prudential Equity Group in Menlo Park, California.

A merger would streamline efforts to sell the blockbuster blood-thinner Plavix, which the companies now market jointly — but experts differ on whether that alone would justify such a move. "I don't know of many other reasons Bristol-Myers Squibb would want to merge," says Anderson, who last September recommended that investors stop selling shares and start buying them.

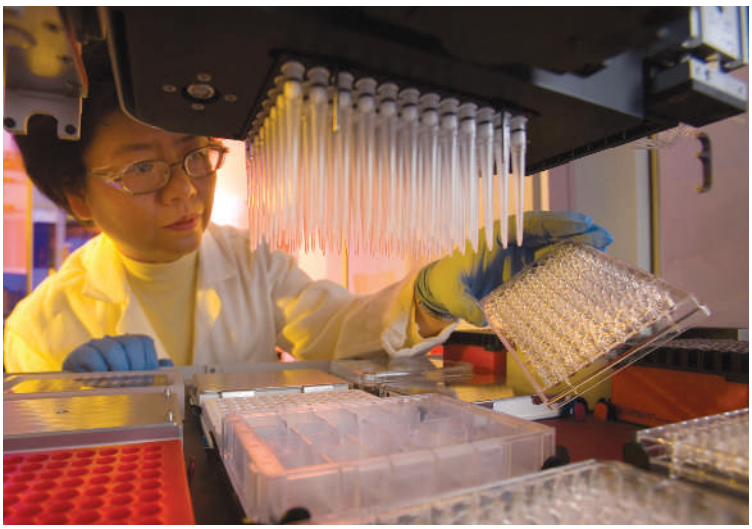

BRISTOL-MYERS SQUIBB

Drug development at Bristol-Myers Squibb's genomics lab in New Jersey — the firm's decision to focus research on speciality areas could help it to remain independent.

Niche market

In the process of weathering a series of scandals and blunders that culminated with the ousting of chief executive Peter Dolan last September, Bristol-Myers Squibb has done just what some say smart drug firms should be doing. The New York firm has established itself as a successful speciality-drug deliverer, in a business where most large firms are still chasing blockbusters for the general population.

"Bristol-Myers Squibb has done just what some say smart drug firms should be doing."

In 2003, Bristol-Myers Squibb launched a new research strategy. It slashed its number of therapeutic research areas to ten and "focused discovery and development efforts on patient populations with serious diseases that still had a high level of unmet need", says Brian Daniels, the company's vice-president of global clinical development. "That was a key to creating a successful research and development organization."

At its 17 research and development 'hubs' around the world, Bristol-Myers Squibb's 6,500 employees would focus not on discovering and developing the next Viagra or a slew of me-too cholesterol drugs, but on the pursuit of medicines for serious diseases that are not well served by existing remedies.

At the same time, Bristol-Myers Squibb boosted its efforts to discover biological drugs and narrowed its focus relentlessly to areas such as arthritis and cancer — in which specialists do the prescribing, and sales and marketing costs are thus lower. In the process, and by stark contrast with its bigger competitors, it virtually threw in the towel on chasing the drugs prescribed by generalist physicians to large populations. The new approach made a virtue of necessity — Bristol-Myers Squibb's pipeline of big primary-care drugs was all but dry — but it also yielded fruit and made the company's once-sluggish research operation look productive.

Since 2002, with an annual budget of about US$2.5 billion, Bristol-Myers Squibb has won approval for six novel drugs from the US Food and Drug Administration (FDA). Sanofi spent roughly twice as much in the same period — and had the same number of new drugs approved. And Pfizer, the leading research spender with a budget of around $7-billion, had just ten such drugs approved. What's more, Bristol-Myers Squibb's applications spent less time before US regulators than its competitors: the firm led the industry with a median review time of six months. This year, it expects to submit three new cancer drugs for FDA approval. And, unlike many of its peers, the firm is unlikely to have any major patents expire until 2011.

But all that seemed to count for little when merger talks, which have been widely reported but never officially confirmed, kicked off. Analysts were focused on the fact that the company has a number of key drugs that are due to come off patent in several years time, and that the Canadian generic drug maker Apotex has challenged the patent for the most successful product. Plavix, the world's second-best-selling drug, was invented by Sanofi but is marketed by Bristol-Myers Squibb in North America, bringing the company $3.2 billion in revenue, or roughly 17% of its sales, in 2005. Although a US court is expected to rule in favour of Bristol-Myers Squibb and Sanofi later this year, a loss would throw a major spanner in Bristol-Myers Squibb's works.

Daniels says that the focus on speciality drugs, together with the company's decision to pursue areas in which drugs are lacking, could provide its best insulation from a takeover. The strategy, he says, "gives us our best chance to remain independent".

Derek Lowe, a medicinal chemist whose blog 'In the Pipeline' has a devoted following in the industry, concurs. Focusing on speciality drugs, he says, "makes a lot of sense, because if you are going to compete in the primary-care market, you're going to be competing against some very big players". In speciality markets such as oncology, he points out, it is cheaper to play and therefore, perhaps, easier to win. ■

NATURE|Vol 446|1 March 2007

EXTREME LIGHT

Physicists are planning lasers powerful enough to rip apart the fabric of space and time. **Ed Gerstner** is impressed.

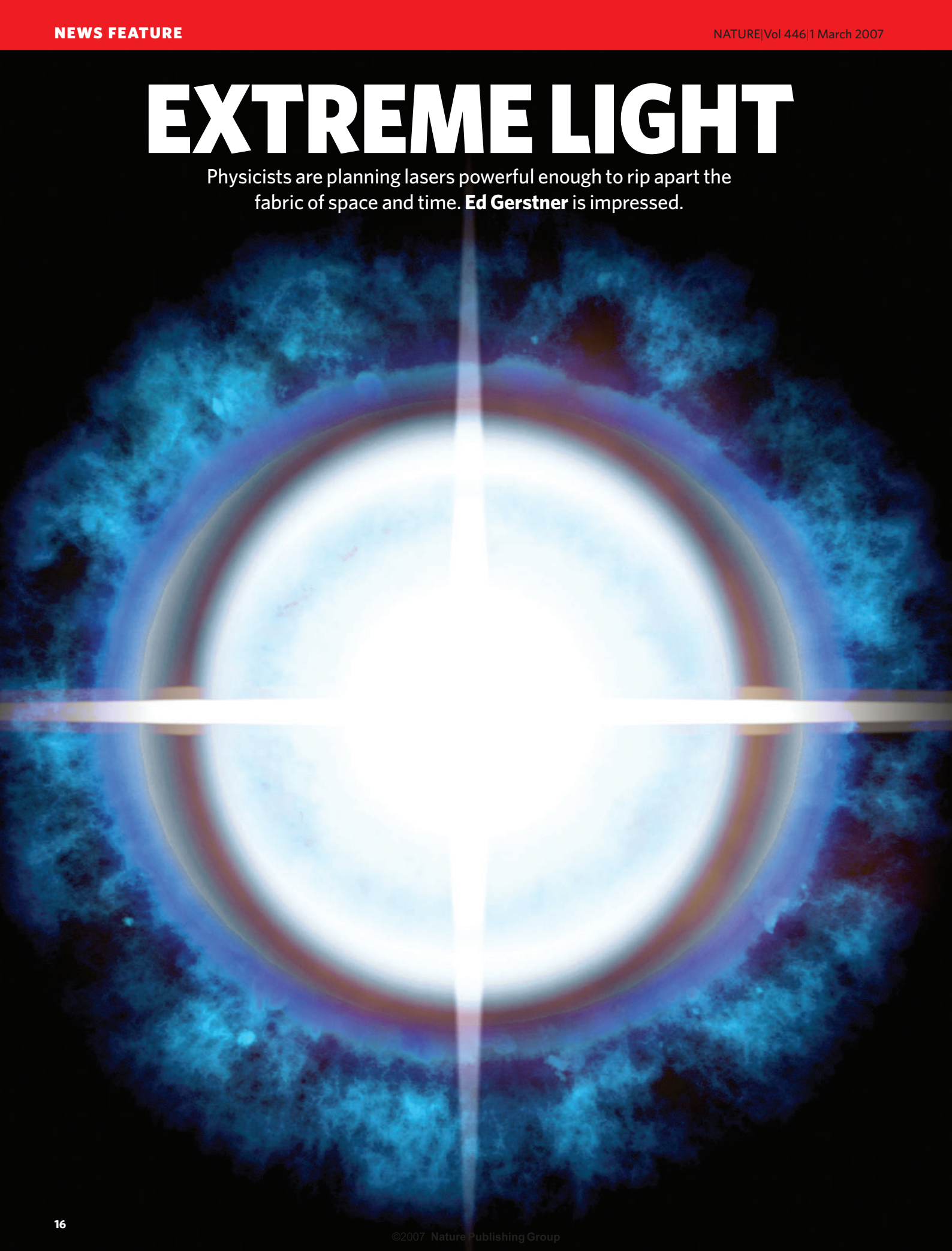

Almost 100 million times more powerful than its earliest ancestor, the Large Hadron Collider (LHC) is the latest triumph in a century of astounding physics. Officially inaugurated later this year, the €3.7-billion (US$4.9-billion) accelerator at CERN, Europe's particle-physics laboratory, will next year be fully up to speed in its search for exotic phenomena, such as the Higgs boson, that can only be discovered at the extreme energies it makes available. Yet even before it is turned on, the particle-physics community is already looking beyond it, with plans for an even more powerful machine, the International Linear Collider (ILC), which will cost some $6.7 billion.

At about the time that the LHC hopes to be homing in on the Higgs, construction of a much less feted multibillion-dollar physics research facility, the National Ignition Facility (NIF) at Lawrence Livermore National Laboratory in California, will be reaching completion. At a cost of about US$4 billion, NIF is an assembly of 192 lasers that, for a billionth of a second at a time, can pump out energy at more than 50 times the rate that it is generated in all of Earth's power stations put together. Its aim is to ignite a fusion reaction that turns a tiny pellet of hydrogen at the lasers' focus into helium.

Science at NIF will bring astrophysics into the laboratory by aping stars in microcosm, and it could conceivably provide the basis for future energy generation. But the main rationale for NIF, and the reason it has been able to command the budget that it has, is to help the United States assure the operability and safety of its nuclear arsenal. Similar motivations lie behind the French Laser MegaJoule (LMJ) facility, which is expected to achieve ignition a few years after NIF.

The lasers of the LMJ and NIF don't come close to an accelerator such as the LHC in terms of generating excitement among physicists. At least, not yet. But laser beams even more intense than NIF's — and far cheaper to generate — might in the next decades begin to take over from particle accelerators in exploring the outermost frontiers of the physical world. The world may never see conventional particle accelerators much more powerful than the LHC and ILC. But lasers a million times more intense than NIF are already to be found in the presentations of physicists looking for funding.

Let there be light

The guiding inspiration for extreme lasers lies in the way light interacts with the vacuum. Quantum field theory sees the vacuum as a strange sea of possibilities, where pairs of 'virtual' particles and antiparticles ceaselessly pop in and out of existence. When light is bright enough, the electromagnetic fields it is composed of begin to interact with that sea in unusual ways. The vacuum no longer behaves as a simple, predictable medium — it becomes something altogether more exotic, unpredictable and nonlinear.

Pump in enough energy, and the paired virtual particles become real, separated at birth by the extraordinarily strong fields involved. This energy level, currently thought to require fields of a little more than 8×10^{18} volts per metre, is known as the Schwinger limit, and it is the point at which the vacuum sea begins to boil.

"When I give talks to general audiences, that's the thing that they really seem to get drawn in by," says Tom Katsouleas, an extreme-laser enthusiast at the University of Southern California in Los Angeles. The problem is that the Schwinger limit is a long way away. For fields of 8×10^{18} V m^{-1} you need a laser with an intensity of more than 10^{30} W cm^{-2} — a thousand trillion times more intense than NIF. Given NIF's multibillion-dollar pricetag, that seems an overly ambitious target.

But a team led by Gérard Mourou, director of the Laboratory of Applied Optics near Paris, believes it can meet this target for a relatively moderate price. And the researchers predict all manner of wonders on the way to their eventual goal. Throughout their history, lasers have excited physicists by opening up new possibilities with light. In the 1960s, the fact that early lasers were powerful enough to change the refractive index of the medium through which they travelled opened up fresh vistas in 'nonlinear' optics. Today the frontier buzzword is 'relativistic optics' — systems in which the fields associated with the laser light can accelerate every electron in the medium the light is passing through close to the speed of light.

> **"I am always astonished at what experimentalists can actually do if they put their minds to it."**
> — William Unruh

Need for speed

Mourou's proposal — the Extreme Light Infrastructure (ELI) — would up the ante further, moving into 'ultrarelativistic systems' in which not only electrons but also the ions from which they have been stripped move close to the speed of light. Mourou notes that the nonlinear effects of lasers revealed in the 1960s far exceeded expectations. "Only the tip of the iceberg was predicted," he says. He is similarly optimistic about what the new energies available at the ELI could deliver.

On 15 February, the French government announced that it had bought into the vision enough to pay for a new laser beamline at the Laboratory of Applied Optics to show that the ELI could work. If it goes ahead, the full facility would provide unprecedented opportunities for scientists to pursue fundamental, curiosity-driven science, says Mourou. Perhaps more importantly, it would be relatively cheap, costing €138 million to build and €6 million per year to run — considerably less than the £380-million (US$746-million) Diamond synchrotron X-ray source recently opened in Britain, for example.

High-power lasers achieve their awesome intensities by squeezing moderate amounts of energy into very short-lived bursts, thus driving up the power — which is energy divided by time. So although the power of NIF's lasers sounds incredible, they actually use relatively small amounts of energy. A single pulse contains just 2,000 kilojoules — roughly half a kilowatt hour. It's just that all that energy is delivered in a few billionths of a second.

C. DARKIN

Power trip

The ELI takes the same principle further. By generating pulses a million times shorter than those of NIF — five femtoseconds — the ELI should fairly quickly be able to generate peak powers of more than a petawatt (10^{15} watts) from just a few joules of energy. This radically reduced need for energy makes things much easier than they are at NIF. By shortening the pulse lengths by a factor of a hundred more, down to tens of attoseconds (10^{-18} seconds), the ELI's proponents hope to reach peak intensities of more than 100 petawatts.

The ELI's extraordinarily short pulses will be made possible by a technique called chirped-pulse amplification (CPA), which Mourou developed at the University of Rochester, New York, in the mid-1980s. CPA works by decomposing the light in a laser pulse using a diffraction grating known as a stretcher, which acts like a prism. Having been stretched, the pulse's components, now spread out in space and time, are fed individually through an optical amplifier, before a similar grating designed for the opposite effect — a 'compressor' — reunites them into a pulse far shorter and more intense than the original.

These stretchers and compressors are currently used on almost all of the world's most powerful lasers except those, such as NIF and the LMJ, that need pulses that are relatively long (of the order of nanoseconds). Osaka University and the Central Laser Facility at Rutherford Appleton Laboratory in Didcot, UK, both have CPA lasers that can generate a petawatt, and the University of Rochester is also building one, as are other institutions. Mourou and others feel that the technique has, as yet, no obvious limitations; pulses can go on getting shorter and shorter.

In 2006, the ELI was one of 35 projects short-listed for consideration under the European Roadmap for Research Infrastructures, a programme that will provide money to help develop proposals for international projects. Also on the shortlist is another, costlier project that plans to use a CPA-enabled laser. A consortium led by the Central Laser Facility wants to build HiPER — the High Power Laser Energy Research facility — as a civilian equivalent to NIF and the LMJ, but pursuing a subtly different path to fusion. Whereas NIF

and the LMJ use megajoule beams to crush their targets into fusion, the €855-million HiPER would compress the target comparatively gently and then ignite it with a much shorter high-power pulse.

One advantage of this approach is that the laser could be fired far more frequently than NIF. With more pulses, and freed from the demands of weapons research, HiPER should offer physicists far greater scope for non-fusion research — NIF's non-fusion work is effectively limited to about one pulse a week. And the power would be greater. With further developments of CPA, Mike Dunne, director of the Central Laser Facility, predicts that amalgamating HiPER's beams could push the machine's limits beyond petawatts to exawatts (10^{18} watts). "If — and it's a big if — such beamlines could be coherently combined," Dunne says, "then we believe that a beam of up to 2 exawatts is feasible. Although horribly difficult in practice."

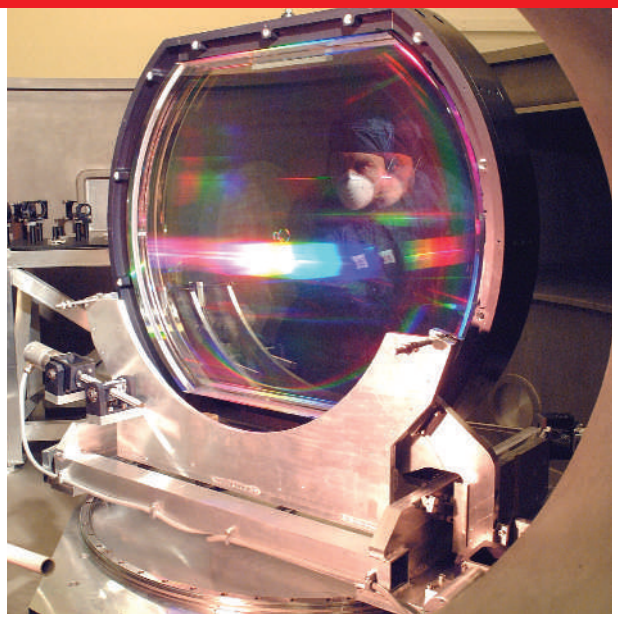

CCLRC RUTHERFORD APPLETON LAB.

A researcher examines one of the two diffraction gratings used by petawatt lasers to achieve their extreme power.

Curiouser and curiouser

In fundamental physics terms, energies at the exawatt level would offer some intriguing possibilities for producing strangeness from the vacuum, and so could allow physicists to study phenomena unreachable any other way, such as those found at the edges of black holes. In the 1970s, Stephen Hawking predicted that when a virtual particle–antiparticle pair is created just 'outside' a black hole, the warping of the local vacuum by the hole's gravity will be strong enough to tear the pair asunder, with one disappearing into the black hole and the other surviving as matter outside it.

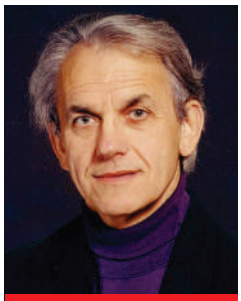

"We're going to change the index of refraction of the vacuum, and produce new particles."
— Gérard Mourou

The effect is analogous to the production of electron–positron pairs by electric fields at the Schwinger limit. "The vacuum really doesn't care if it's an electric field, a magnetic field, a gravitational field, or even if it's a weak nuclear field or a strong nuclear field," says Bob Bingham of the Rutherford Appleton Laboratory. "If you can pack enough energy in, you can excite particles out of the vacuum." The attraction of Hawking radiation is that its dependence on a gravitational field means that its subtleties will depend on interactions between quantum field theory and general relativity, the sort of thing that could throw light on quantum theories of gravity.

The laser-builders don't want to create black holes with which to look for Hawking radiation — but they don't have to. General relativity's equivalence principle means that to something experiencing one of them, a gravitational field and an acceleration are indistinguishable. So, as theorist William Unruh pointed out in the 1970s, when a particle is accelerated at a sufficient rate, it should see and be affected by Hawking-like radiation in its own frame of reference — if, that is, certain assumptions about the curvature and structure of space-time are correct.

The accelerations involved in Unruh radiation are far too extreme for a traditional particle accelerator, but perhaps not for lasers on the scale of the ELI. "Nothing generates fields even close to those produced by an ultra-high-intensity laser — except perhaps a black hole," says Bingham. "Some of the lasers at the Rutherford Appleton Laboratory will produce a field of about 3 trillion volts per centimetre. Nothing else comes close to that!"

Using their lasers to accelerate electrons fast enough to feel Unruh effects could be a tantalizing problem for the ELI, HiPER or other extreme lasers to tackle. "It seems to me to be a very hard experiment — creating such strong and short intense pulses," says Unruh, now at the University of British Columbia in Vancouver. "But I am always astonished at what experimentalists can actually do if they put their minds to it."

This is not the only way in which lasers could beat accelerators at their own game — or help them to greater heights. By definition, relativistic optics requires that electrons be accelerated close to the speed of light. Get them very close and researchers might be able to do particle physics beyond the reach of the LHC and ILC. One approach to this would build on the idea of a 'wakefield' accelerator, in which electrons hitch a ride on the wake left behind by an intense pulse of laser light blasting through a plasma.

"If you look at the progress that has gone on in laser wakefield accelerators," says Katsouleas, "and extrapolate that to the kinds of powers that people are talking about for the ELI, then it becomes possible to think about accelerating particles to [ILC energies] in just a short section of plasma." But even if the vast engineering challenges of such an accelerator could be met, it would hardly be a replacement for what the current and planned accelerators do, because the average power would be far lower: big accelerators store large amounts of energy in their beams.

"To get the luminosity one needs for doing high-energy physics," says Katsouleas, "and for events to be detectable on a reasonable timescale, the average power of the laser isn't sufficient. It's about three orders of magnitude away. But there are already many ways you could think about doing this."

Follow the light

Barry Barish, director of the global design effort for the ILC, is intrigued by the possibility of using lasers to accelerate particles, and agrees that it might be one of the future technologies that keeps the field going. "It's certainly a very promising avenue to pursue, because up front there doesn't seem to be any obvious limitation to it, and it could be that it will help in the long term," he says. But he doesn't see it as the only game in town, or as a sure thing. "It's just hard to know where the show-stoppers will be. But at the level where it won't require enormous resources, this is the sort of thing that needs to be pursued."

Mourou, on this as on much else, is bullish. "Probably within 20 years!" he says of laser-driven follow-ons to the ILC, before backpedalling, at least a little. "The time constant to design it and to build it is ten years. And you always build these things with the previous technology. So I have to be very careful when I say 20 years. But in 10 to 20 years we will have this technology, and then it would take another 10 years to build." Beyond that, he and his colleagues say, there are even more remarkable technologies: gamma–gamma colliders that can reach energies millions of times higher than today's accelerators; and 'relativistic mirrors' that can push light to the Schwinger limit and beyond.

"We're going to change the index of refraction of the vacuum," enthuses Mourou, evoking the ultimate fulfilment of the laser's original promise. "And we're going to produce new particles — the vacuum is the mother of all particles. And I'm sure we're going to discover more." ■

Ed Gerstner is a senior editor on *Nature Physics*.

The roots of accomplishment

From a New Jersey beauty parlour to cutting-edge genetics by way of her own alopecia, Angela Christiano's life has all been tied up with hair. **Helen Pearson** meets a woman whose head is full of the stuff that covers it.

C. E. MANLEY, CENTER FOR BIOMEDICAL COMMUNICATIONS

Ectodermal appendages: Angela Christiano leads a research life that is shaped by hair.

No one forgets their first encounter with Angela Christiano. For Jorge Frank, it was in an office at New York's Columbia University in 1995. "In walks this blizzard of a woman with the bright smile and the big hair and these long fingernails," recalls Frank, a molecular dermatologist at University Hospital Maastricht in the Netherlands. "I thought: 'This is a rock star not a scientist'."

Christiano certainly cuts an arresting figure. Deep-brown and bronze tresses erupt from her head in a gravity-defying explosion and surge over her shoulders. Her perfect make-up and carefully manicured nails complete an image that is the antithesis of a stereotypical scientist.

But for Christiano, hair is not just an adornment. It is a filament that binds together her appearance, her family, her personal life and her work. Descended from two generations of hairdressers, she came to appreciate hair's true importance when her own locks began to fall out in an episode of alopecia areata. Working at Columbia, she immediately shifted the focus of her research from skin disease to hunting down the genes that underlie human hair disorders, such as an atavistic condition in which people sprout thick hair all over their faces. Her scientific work may even end up with a cosmetic use, saving men and women with normal but nevertheless unwanted hair from shaving, waxing and depilation.

Grooming talent

Christiano grew up in New Jersey with an unusual appreciation for the importance of personal grooming. Hair and nails — "ectodermal appendages", as she now calls them — were her family's bread and butter. Her grandparents had set up a barber's shop after immigrating from Italy; her mother worked as a hairdresser and beautician. Christiano spent after-school hours sweeping up hair in her mother's shop. "I didn't realize it at the time," she says, "but I was becoming a keen observer."

Many of her schoolmates went on to become hairdressers and beauticians, and Christiano's family expected her to stay at home until she got married. But by that time, school had already kindled in her a love for genetics, and she was the first of her family to attend college and earn a PhD, at Rutgers University in New Jersey. She didn't abandon her roots though. Having watched so many hours of beautification, she found herself drawn to dermatology. "It is one of the only areas in medicine where visual things provide clues," she says. "Once I was exposed to a skin disease it was like instant love."

The subject is rarely the focus of such enthusiasm; indeed, dermatology is sometimes given short shrift in medicine. Very few dermatological conditions are life threatening, and a concern with unsightly skin or hair can be dismissed as vanity. As a result, those working in the field take great pains to spell out the difficulties faced by those with alopecia and other disorders. "Every day I have someone in my clinic crying and saying they want to commit suicide," says Abraham Zlotogorski, a specialist in hair disorders at Hadassah University Medical Center in Jerusalem, Israel, and a collaborator of Christiano's.

> **"Every day I have someone in my clinic saying they want to commit suicide."** — Abraham Zlotogorski

Christiano established herself in the science of skin during her postdoctoral position at Thomas Jefferson University in Philadelphia, Pennsylvania. While there, she studied the genes underlying epidermolysis bullosa — a condition in which the skin is incredibly fragile, blisters and falls off, and one of very few life-threatening skin diseases.

First signs

When she was 30, Christiano had just started a faculty position at Columbia, and felt under pressure to establish her own group in dermatology. Then one day, her hairdresser in New Jersey asked her whether she'd had a biopsy: "You have a little spot." The next day, a colleague who worked across the hall took a closer look and let out "the most blood-curdling scream I've ever heard", Christiano recalls. The spot was the size of an orange. In her new apartment, the blocked shower that she had attributed to bad Manhattan drains turned out to contain a clump of her hair.

Christiano was diagnosed with alopecia areata, a disease in which the immune system attacks hair follicles, causing hair to fall out in patches, or sometimes completely. Because the stem cells in the follicles escape the attack, the hair sometimes grows back, and the condition can come and go throughout life. Christiano had known that hair problems ran in her family: her mother and grandmother both developed female pattern baldness and wore wigs. Now she learned that a distant cousin had a more severe form of

alopecia areata and did not have any hair at all.

As soon as she was diagnosed, she decided to refocus her work on alopecia. Alopecia areata is known to involve several genes and is hard to trace through families. But Christiano found a Pakistani family in the scientific literature who had a simple, inherited form of alopecia called papular atrichia. The gene involved causes a specific phenotype in which babies lose their first hair from the front of the head to the back and then remain bald.

By looking for genetic landmarks inherited alongside the condition, Christiano's team narrowed its search for the responsible gene to a large region of chromosome 8. But the group was not able to narrow it down any further until Christiano attended a meeting of the Society for Investigative Dermatology and heard a talk about a mutant mouse called hairless that also loses its hair in a wave from head to tail. The human equivalent to the gene turned out to sit on that suspicious section of chromosome 8, and when she sequenced it in her Pakistani patients, they all had mutations that seem to prevent hair growth and destroy the hair follicle[1].

From mice to men

Since then, Christiano has tracked down genes in two other hair disorders in a similar way, using human families alongside mouse models. In one disorder, she showed that a type of cadherin, a protein that holds cells together in the hair follicle, is mutated in people whose hair breaks off near the head like razor stubble[2]. With time, the gene hunting has become easier, thanks to human sequence data and high-resolution genome maps. Last year, she and her colleagues took only six weeks to show that some families who had no nails on any of their fingers or toes had a mutation in a gene normally active in the embryo's developing nails[3].

Christiano is sensitive to the accusation that she is merely 'stamp collecting' — bagging genes for the sake of it — and tries to delve into what each gene does and how they drive skin and hair development. But she admits that the hunt has an addictive rush: "It's one of the most exciting things we do. When we have a new gene, it's like having a new baby." And it's not as if all gene hunting is now easy. One of Christiano's most intractable puzzles is in her "Mexican hair people", who have thick, 'terminal' hair all over their faces rather than the finer 'vellus' hair, which is normal. Christiano and her team have spent more than five years studying one of the only reported cases of a family with this disorder — called hypertrichosis[4]. But although they sequenced 82 genes in the relevant region of the X chromosome and every snippet of microRNA, they could not find a causative mutation. Some kind of genetic trickery could be afoot: perhaps a mutated RNA outside the protein-coding genes is failing to regulate a gene on another chromosome.

H. BAZZI

Mice provided some clues for tracking down genes involved in human hair disorders.

B. WALTON/EPA/CORBIS

MEDICAL-ON-LINE/ALAMY

Hypertrichosis (above) and alopecia areata both have genetic underpinnings.

To her obvious delight, last year Christiano made headway in the genetics of her own affliction. Various researchers have identified families in which several members have the disease, and Christiano and her collaborators have been able to pinpoint four locations in the genome that are strongly associated with the condition in these families[5]. If they find the actual genes, they might be able to unravel the immune system's antipathy to hair follicles, and even suggest ways that drugs could abate it.

Christiano had hoped that a company called Sirna Therapeutics, which is based in San Francisco, would find a use for her discoveries. Sirna had licensed some of the patents from her work and, before the company was acquired by Merck in late 2006, researchers with the company were trying to find a way to deliver inhibitory RNA to the skin to curb hair growth, with an eye to the cosmetic market. Despite her background and impeccable grooming, Christiano says that she is not interested in developing cosmetic applications from her work. She wants the company to find a way to deliver the inhibitory RNA to the skin so that she and other researchers can use it to hinder genes involved in conditions such as alopecia.

Her own case didn't need such interventions. Over two years she lost ten large patches of hair and became obsessed with her tresses, checking them constantly and carefully styling and dyeing them to hide the nude spots. But her hair came back, although with an odd, wiry texture. "Now every day I have hair, it's like an accomplishment."

The flamboyance of her accomplishment with her ectodermal appendages can lead to some teasing. When she goes to conferences that have hairdryer-free accommodation: "I have to bring my entire arsenal, and people make fun of my luggage." The teasing may, on occasion, give way to unfair criticism, says skin researcher Elaine Fuchs of Rockefeller University in New York: "Some scientists tend to judge people by their scientific pedigree and their appearance, and Christiano doesn't fit the mould."

"What I so admire about Christiano [is that] she proves these people wrong by her accomplishments." And Fuchs isn't talking about that hair. "I've learned that it's a phenotype really," Christiano says. "Everyone has a phenotype and this just happens to be mine." ■

Helen Pearson is a reporter for *Nature* in New York.

1. Ahmad, W. *et al. Science* **279,** 720–724 (1998).
2. Kljuic, A. *et al. Cell* **113,** 249–260 (2003).
3. Blaydon, D. C. *et al. Nature Genet.* **38,** 1245–1247 (2006).
4. Tadin-Strapps, M. *et al. Clin. Genet.* **63,** 418–422 (2003).
5. Martinez-Mir, A. *et al. Am. J. Hum. Genet.* **80,** 316–328 (2007).

NATURE|Vol 446|1 March 2007

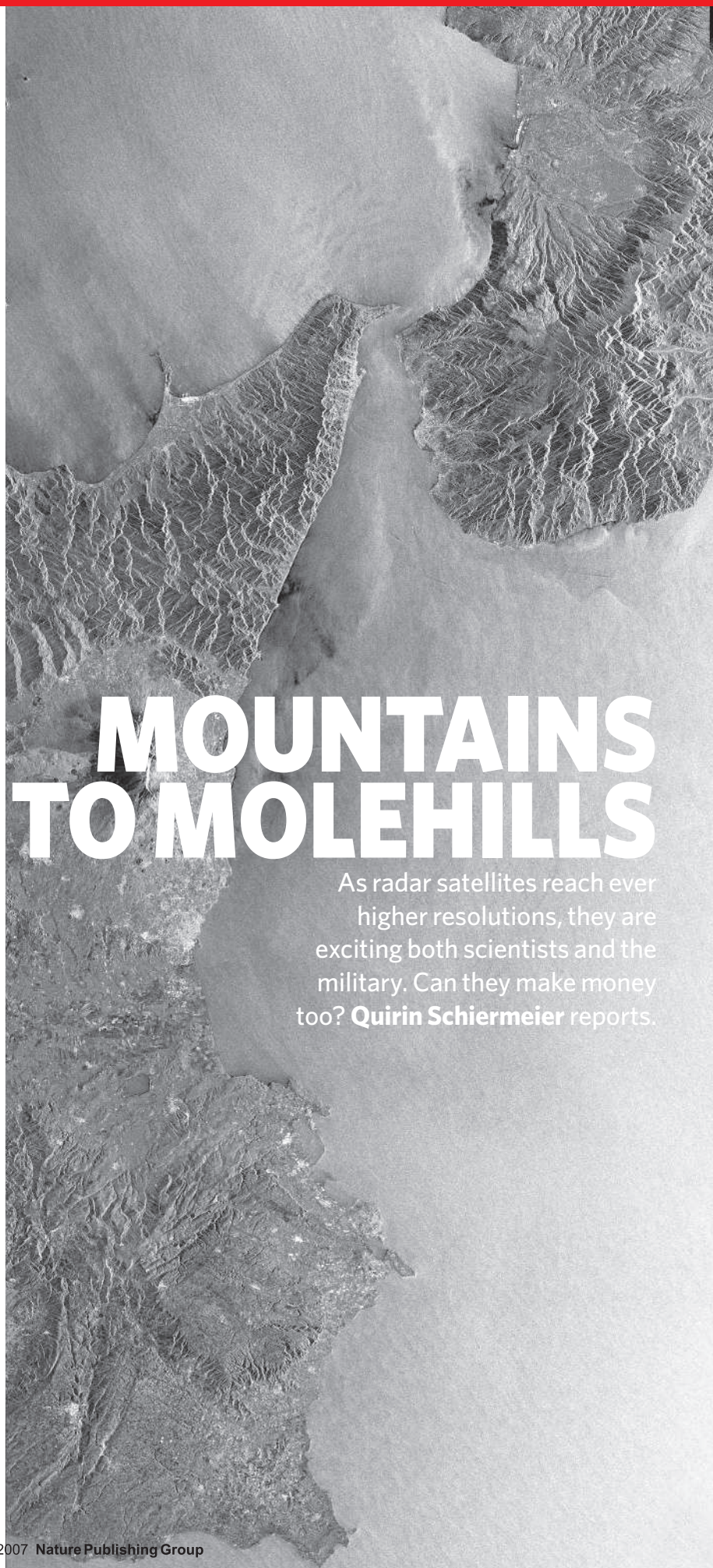

MOUNTAINS TO MOLEHILLS

As radar satellites reach ever higher resolutions, they are exciting both scientists and the military. Can they make money too? **Quirin Schiermeier** reports.

Rolf Werninghaus is getting used to tenterhooks. The TerraSAR-X mission that he and his team have been working on for the past five years was due to lift off on a Russian Dnepr-1 rocket launched from the Baikonur cosmodrome in Kazakhstan at the end of last year. Then it was meant to go in February. Now it's sometime in late March or early April.

When the converted nuclear missile finally does blast off, it will take with it more than just a satellite and the dreams of the team that built it. It will be carrying the prospects of a new industry. The €130-million (US$170-million) TerraSAR-X is a radar remote-sensing satellite conceived from the beginning as a public–private partnership between the German Aerospace Center (DLR) and EADS Astrium, a wholly owned subsidiary of EADS, the European Aeronautic Defence and Space Company. The amount of money it generates will determine, among other things, whether it gets a successor when its operational life ends five years down the line. But will the world want to buy what it is selling?

Radar satellites have advantages over optical systems in that they can see things in all weathers and all levels of light, which means that they can monitor sites reliably and regularly. TerraSAR-X can routinely take images of any given spot on Earth every four days or so — and it doesn't care whether clouds are present. "From tropical rainforests to arctic coastlines there are just so many regions where not enough optical data exist," says Susanne Lehner, head of radar oceanography at the DLR's remote-sensing technology institute in Wesseling, Germany. Lehner and her colleagues in Germany and the United States will use data from TerraSAR-X to study wave heights, wind stress and air–sea fluxes off the coast of Florida and in the Southern Ocean.

In focus

The instrument on the satellite that will let her take these measurements is a synthetic-aperture radar (SAR) that operates at a frequency of 9.65 gigahertz, which puts it in the X-band of the radio spectrum: hence, TerraSAR-X. SAR techniques use the distance that the radar moves between emitting a pulse and receiving back its echoes to add detail to the images produced. By adding together and analysing various echoes from the same spot as it passes over, the satellite mimics the performance of a much larger antenna.

The fine resolution and flexibility of the satellite's active antenna are its selling points. The antenna's 384 subarrays allow it to point its beam in different directions without having to tilt the satellite and to produce several types of image. In the 'spotlight' mode, TerraSAR-X can take images of an area measuring 5 kilometres by 10 kilometres with a resolution of down to one metre, making objects as small as cars easy to distinguish. This resolution is much higher than those of previous civilian radar satellites and of satellites operating in the visual range. It is at least ten times better than those of the Envisat satellites developed by the European Space Agency (ESA) or Canada's ten-year-old RADARSAT-1, which had commercial aspirations that were never really met, in part because it was optimized to observe sea ice. In the commercial world, this level of resolution is matched only by the optical images produced by the American Ikonos and QuickBird systems.

Missions equipped with SAR have been flying for almost 30 years, inspired by the success of the first such mission, NASA's short-lived 1978 Seasat, the data from which are still in use today. But only now is the technology considered by some mature enough to stand a chance of commercialization.

The hope at Infoterra — the EADS Astrium subsidiary in Friedrichshafen, Germany, that markets TerraSAR-X

ESA

products — is that as governments and others latch on to the new possibilities of radar, they will be increasingly willing to pay for them. Jörg Herrmann, Infoterra's managing director, says he thinks that the market for radar remote-sensing products will increase from some €10 million to €100 million in the next three years. He hopes that TerraSar-X will get between €20 million and €50 million of that action as it splits the market with radar data from Japan's advanced land-observing satellite (ALOS), which has a long-wavelength L-band system, and Canada's soon-to-be-launched RADARSAT-2, which will use the intermediate C-band. Optical-satellite imagery generated global revenues of more than US$500 million in 2006, according to Mark Brender, a vice-president at GeoEye, the Virginia-based company that operates the high-resolution Ikonos and Orbview satellites.

Private eye

Not everyone is so optimistic. "There is a lot of speculation going on as to what the commercial potential of radar sensing might be," says Urs Wegmüller, chief executive of Gamma Remote Sensing near Bern, Switzerland, which is developing data-processing software for radars. He cautions that radar products require a lot of work and are expensive, making them something of a luxury. "The civilian market is rather small, and we don't expect it will grow as fast as some believe," he says. "I doubt that a privately funded radar mission will be feasible in the near future." Both ESA and the United Kingdom have found insufficient interest from industry to develop a commercialized radar satellite.

Infoterra expects that its main customers for the radar data will be national governments — the Japanese have already signed a €10-million contract — and the European Union, with more than half of the expected revenue in the first few years expected to come from military users. Private companies will probably take longer to start buying, if they ever do. "Even with electro-optical satellite imagery, commercial markets have been slow to come on line," says Brender. "We expect that radar would also be slow to penetrate commercial markets. But sophisticated users, such as military and defence agencies, may be a ready-made market for radar products."

Indeed, interest from the military and intelligence sectors is strong enough that a second German X-band SAR system is being deployed: SAR-Lupe, built by a consortium led by OHB System of Bremen. The system has less sophisticated antennas than TerraSAR-X's but, because it will eventually consist of five identical satellites, it will be able to revisit any spot on Earth every ten hours or so. This development of radar-based intelligence by Germany is intended to complement France's optical capabilities, as seen in the commercial Spot satellites and, for those with the appropriate clearances, the military Helios system. The French–Italian CosmoSkymed spacecraft, which are to become operational in 2008, have been designed for use by the military and by civilians.

Although spooks and generals pay for their radar, scientists will get TerraSAR-X's data for free throughout the satellite's proposed lifespan. Quite what the scientists will do with them, though, remains to be seen. Previous radar remote sensing, which has provided spectacular interferometer images that show how the surface buckles and snaps before and during earthquakes, for instance, has used longer wavelength bands. "X-band radar, despite very high resolution, is not the most suitable wavelength for geoscience applications," says Wegmüller, who leads a project to monitor motion in mining regions to predict dangerous subsidence or collapses. "But with its different modes of operation, TerraSAR-X can respond very nicely to customer needs."

Particularly interesting is the information that TerraSAR-X can provide on the properties of features such as crops, ice crystals or ocean waves. Marine scientists interested in that last possibility have high hopes for TerraSAR-X , even though it was designed mainly for looking at land. Its experimental 'along-track interferometry' mode, in which the antenna is separated electrically into two halves to allow the detection of moving objects, could be used to detect sea ice, or to measure wave heights and currents in coastal areas.

DLR

Rolf Werninghaus and his team hope that the TerraSAR-X satellite will find its way to the commercial market.

Banding together

Data from different wavelengths could also be combined to provide a picture that no one instrument could match. "X-band radar is an ideal supplement to other wavelengths and to optical imagery," says Christiane Schmullius, a geographer at the Friedrich Schiller University in Jena, Germany. To assess the world's forest resources for a project funded by the United Nations Food and Agricultural Organization, she and her team plan to combine X-band data from TerraSAR-X, L-band data from Japan's ALOS mission and optical data from various other sources, including another new German satellite, RapidEye, being built by Surrey Satellite Technology in Britain.

So far, the DLR has accepted more than 200 scientific proposals for use of its data. Some of the projects, such as those for detecting subsidence around mines, or for measuring the swell and the wind around offshore wind farms, have commercial potential. More than a third of the approved projects include principal or co-principal investigators from industry.

And in 2009, the DLR and EADS Astrium plan to launch a nearly identical satellite — TanDEM-X — to fly in close formation with its older sibling. By combining their antennas electronically, the two will provide, among other things, a global 'digital elevation model' of unprecedented accuracy: a world map with a resolution of at least 10 metres, and elevations accurate to a metre. The pairing will also explore ways to get new types of information out of SAR data, such as an improved ability to measure the speed of traffic flows. Again, Infoterra will market the data.

As newcomers such as Argentina and South Korea join the club with their own satellites in the next few years, there's no doubt that high-resolution radar sensing is about to enjoy a boom. Whether it will be a profitable one — especially with so many players in the game — remains to be seen. "Perhaps we'll soon have a radar version of Google Earth," says Lehner. "I for one would certainly like to plaster my office walls with real-time radar films — if I could afford it." ■

Quirin Schiermeier is *Nature*'s Germany correspondent.

"X-band radar is an ideal supplement to other wavelengths and to optical imagery."
— Christiane Schmullius

For a full list of missions using SAR technology see http://tinyurl.com/37k64w

Potential downsides of perfect pain relief

SIR — J. J. Cox and colleagues present an exciting aspect of using drugs targeting SCN9A as analgesic agents, in their Article "An SCN9A channelopathy causes congenital inability to experience pain" (*Nature* **444,** 894–898; 2006). As clinicians, we need better tools to treat the high prevalence of non-malignant chronic pain syndromes such as back pain, arthritis, fibromyalgia, migraines and irritable bowel syndrome. These afflict a large number of people and severely reduce their quality of life, as well as creating a vast financial burden.

Several novel analgesics, targeting pain-specific molecular transduction pathways, are at various levels of clinical and preclinical development. The high drug specificity potentially allows profound pain relief without the dose-limiting toxicities seen with current drugs. But what if these medicines are even better than expected?

Pain is a protection mechanism, serving to prevent injury, deter repetitive harmful behaviour and allow healing. It is usually the first indication of disease or trauma that triggers the individual to seek treatment. Our current approaches to treating pain often provide effective relief, but it is 'incomplete', in that activity-related breakthrough pain continues — and this can be useful.

The problem will arise with long-term use of a potentially perfect analgesic drug to alleviate a specific symptom, such as chronic back pain. The medications that block the targeted pain generator could also prevent the warning pain caused by a new, more serious condition such as stroke, myocardial infarction or bowel obstruction. The results could be catastrophic: diagnosis may be delayed, leading to irreversible damage, long-term disability or worse.

Using a perfect analgesic to relieve pain from sports injuries such as sprain, repetitive injury or overuse may allow the athlete to ignore the bio-warning signs of pain, impair the healing process and risk more serious injury.

Should we be deterred from the search for superior pain medications? In patients with advanced life-threatening disease seeking palliation, the question is easily answered: no. But a young patient with disabling lower-back pain on chronic medication presents a different situation. Relieving the back pain may restore function, but could hinder the rapid diagnosis of life-threatening disease.

Our choice is whether to limit the use of these medications to a defined population, on the basis of risk assessment, or to embrace these innovations and attempt to adjust the practice of medicine fast enough to accommodate the potential consequences. In the latter case, clinicians would have to remove 'pain' from the list of symptoms currently used in diagnosis. For instance, myocardial infarction may present with more flu-like symptoms — sudden onset of nausea, weakness, diaphoresis and shortness of breath, instead of the classically described patient clutching his or her chest. Appendicitis and bowel perforation may present with painless nausea, vomiting and loss of appetite.

On the other hand, denying a known therapy to a patient with unrelenting pain is difficult to accept, when a novel analgesic could normalize function, improve quality of life, reduce the financial impact by replacing ineffective treatments and allow an earlier return to work.

The dilemma outlined here, although theoretical, should be considered before these therapies are approved. If these much-needed therapeutic advances are to be used in a truly effective fashion, anticipating and preventing any possible untoward events could facilitate their safe implementation. Data collected in clinical trials would be helpful in determining the importance of this response.

Andrew Mannes*, Michael Iadarola†
*Department of Anesthesia and Surgical Services, Warren Grant Magnuson Clinical Center, National Institutes of Health, 10 Center Drive, Bethesda, Maryland 20892, USA
†Neurobiology and Pain Therapeutics Section, National Institute of Dental and Craniofacial Research, 49 Convent Drive, MSC 4410, Bethesda, Maryland 20892, USA

Need to distinguish science (good or bad) from ethics

SIR — Although I share John Horgan's concern about the misrepresentation of science by the current US administration and others, expressed in his Book Review of Seth Shulman's *Undermining Science* ("Dark days at the White House" *Nature* **445,** 365–366; 2007), he and other commentators need to distinguish clearly between science and ethics in their arguments. It is bad science to claim that reducing environmental protection will not have adverse effects on rare species, for example, but the decision whether we should protect rare species or not is an ethical one.

With regard to research on embryonic stem cells, I know of no one who denies that there would be at least some scientific insights and medical benefit from such research. However, the real question with regard to stem-cell research is whether the potential medical benefit and scientific knowledge outweigh any harm done to the embryo. The answer depends strongly on the value assigned to the embryo, which is not a scientific question. Thus, instead of being an example of science versus anti-science, this is a case of competing ethical claims. Replacing an advocate of stem-cell research on the President's Council on Bioethics with someone morally opposed to it reflects support for an ethical position (although the fact that this particular example involved replacing a biologist with a political philosopher does also raise the possibility that science was getting less say).

By invoking science as supporting a particular position on ethical questions, which science cannot directly answer, critics are making an error of logic similar to the one made by the Bush administration itself.

David Campbell
Department of Biological Sciences, 425 Scientific Collections Building, University of Alabama, Box 870345, Tuscaloosa, Alabama 35487-0345, USA

Never mind the footprint, get the mass right

SIR — Your correspondent Geoffrey Hammond is being somewhat pedantic in calling for the 'carbon footprint' — amounts of carbon expressed in tonnes — to be called instead the 'carbon weight', because the essential property of a footprint is its area ("Time to give due weight to the 'carbon footprint' issue" *Nature* **445,** 256; 2007).

A true pedant would, however, have gone the full distance! If units of carbon are expressed in kilograms, tonnes and so on, the proper term is 'carbon mass'. Weight is the vertical force acting on a body as a result of gravity. The SI unit of weight is a newton, which has base dimensions of $kg\ m\ s^{-2}$. Balances measure weight, but are calibrated to give the answer in units of mass.

'Footprint' has become an accepted term throughout the ecological and environmental sciences, irrespective of dimensions and units, such as my domestic carbon footprint (tonnes) or my flux-tower carbon footprint (metre radius or hectares). 'Footprint' is evocative and has meaning, with relevant and appropriate units.

A far more serious issue is that journalists and commentators frequently confuse the mass of carbon and the mass of CO_2, sometimes within the same article. The mass of a mole of CO_2 is almost 4 times (44/12) larger than the mass of a mole of carbon. With errors of this size in articles and reports, it is not surprising that the public at large is confused by apparently conflicting reports on atmospheric CO_2 concentrations and terrestrial carbon budgets. Absolute clarity and consistency in definition is essential.

Paul Jarvis
Institute of Atmospheric and Environmental Science, School of Geosciences, University of Edinburgh, Edinburgh EH9 3JN, UK

Contributions to Correspondence may be submitted to corres@nature.com.

BOOKS & ARTS

Into the darkness

Cosmologists face some tough challenges as they explore the composition of the Universe.

Dark Cosmos: In Search of our Universe's Missing Mass and Energy
by Dan Hooper
Smithsonian Institution: 2006. 256 pp. $24.95

Volker Springel

Galaxies such as the Milky Way make up just a tiny fraction of the structure of the Universe.

M. J. DORF/CORBIS

Since the discoveries of Copernicus, astronomy has taught us that there is nothing special about the position of Earth in the Universe. The Sun lies in an unpretentious spiral arm of the Milky Way and is just an ordinary star among 100 billion others in our own Galaxy. Furthermore, the Milky Way itself is just one galaxy among billions of other similar stellar islands in the Universe around us. One cannot help but feel a sense of insignificance in the light of these myriad systems.

Some may find it comforting that the Milky Way is at least a beautiful spiral galaxy. However, any pride about this must surely be challenged by the revelations of modern cosmology. Over the past two decades it has become clear that all the rich cosmic structure we see in the form of luminous stellar systems accounts for only 0.5% of the cosmic energy density. Even including all the rest of the ordinary matter in the space between the stars — such as planets, moons, diffuse gas and interstellar dust — raises this fraction up to 5% at most. All the rest, a good 95%, is made up of two elusive components that astrophysicists call 'dark matter' and 'dark energy'. Galaxies mark only the peaks of the vast mountain ranges of cosmic structure present in the dark sector, and the ordinary baryonic matter is only a minor perturbation in the cosmic mix. In fact, even if we removed Earth, the Sun and every star in all the galaxies in our Universe, its evolution and fate would hardly be affected at all.

Although this could be viewed as yet another setback for human self-esteem, the discovery of dark matter and dark energy is undoubtedly one of science's most significant achievements. However, it is still rather incomplete, as we simply do not yet know the precise nature of dark matter and dark energy.

Particle physicist Dan Hooper addresses this fundamental puzzle in his book *Dark Cosmos*. He explains why astronomers believe that dark matter is made up of an as yet unidentified elementary particle, and tells how physicists around the world have embarked on a fascinating search for this mystery particle. He also discusses the disturbing discovery of a hidden dark-energy field, which counteracts gravity and is responsible for an accelerated expansion of the Universe.

Before Hooper delves into the evidence for these two dark components and their physical interpretation, he takes the reader through a brief yet amazingly clear introduction to quantum physics, general relativity and even string theory. This entertaining and enlightening journey through much of modern physics is a tour de force, enriched with historical accounts of some of the key developments. It paints a colourful picture of the way physicists work and explains their passion for finding a final 'theory of everything'.

In his introductory remarks, Hooper recounts how popular physics books had sparked his scientific interest as a college freshman. He still enjoys reading them today, no longer to learn something new about physics, but for the inspiration and sense of awe that a clear exposition of the essence of scientific discoveries can provide. This is also how I read Hooper's book. Although I am familiar with dark matter and dark energy from my own work, I found Hooper's account of recent discoveries in cosmology refreshing; it reminded me how exciting and amazing these findings really are. Niels Bohr once said that anyone who is not shocked by quantum mechanics has not understood it. The same could be said about the existence of dark matter and dark energy.

At the end of the book, Hooper makes an entertaining prediction, with an imaginary *Encyclopaedia Britannica* article written in the year 2100 reporting the history of cosmology in the twenty-first century. His article refers to the identification of the dark-matter particle in 2010, when a number of new elementary particles are discovered at the Large Hadron Collider at CERN, the European particle-physics laboratory near Geneva. This is followed by a direct detection of the particle in deep underground detectors some ten years later. The nature of dark energy proves more problematic, and is understood only after a unified theory of quantum gravity has finally been developed sometime in the 2070s.

Hooper also provides an alternative worst-case scenario for the future of cosmology in which little progress is made beyond what we know today. I agree with Hooper's more optimistic view; it is not only more attractive, but also more likely. If that's the case, the revolution in cosmology we have seen in recent decades is far from over. ■

Volker Springel is at the Max Planck Institute for Astrophysics, 85740 Garching, Germany.

The roots of complex problems

Fearless Symmetry: Exposing the Hidden Patterns of Numbers
by Avner Ash & Robert Gross
Princeton University Press: 2006. 302 pp.
$24.95, £15.95

Timothy Gowers

If you ask somebody who knows a little mathematics what is meant by the symbol i, they will probably tell you, correctly, that it stands for the square root of -1. But there is a subtlety to the question that is easy to overlook. Suppose that you pedantically point out that there are two square roots of -1. The response is likely to be that the other square root is $-i$. But now comes a much harder question: which square root is i and which one is $-i$?

The more one thinks about this question, the more one realizes that it does not have an answer. In fact, the question doesn't really make sense, and mathematicians even have a way of proving that it doesn't make sense. The rough idea of the proof is this. If z is any complex number, written in its usual form $a+ib$, where a and b are real numbers, then we define the complex conjugate of z to be $a-ib$, and denote this number by $\bar{z}$. It can then be proved that, for any two complex numbers z and w, $\overline{z+w}=\bar{z}+\bar{w}$ and $\overline{zw}=\bar{z}\,\bar{w}$. In mathematical terminology, the function that takes each complex number to its conjugate is an automorphism, because it 'preserves' the basic arithmetical operations.

Because of this automorphism, there is no true mathematical sentence about i that is not equally true when all occurrences of i (both implicit and explicit) are replaced by $-i$. This is the sense in which i and $-i$ are indistinguishable and is the reason that one cannot answer the question: "Which square root of -1 is i?" By contrast, it is possible to distinguish between 1 and -1, for example, as the square of 1 is itself, but the square of -1 is not itself.

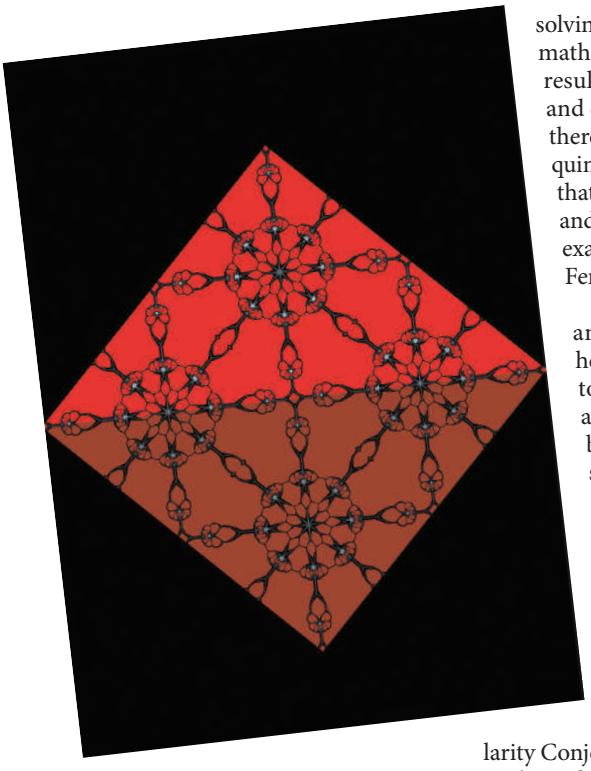

B. KALANTARI

Polynomiographs such as this one, *Acrobats*, are created using mathematical formulae.

Automorphisms such as this are the 'fearless symmetries' of the title of Avner Ash and Robert Gross's book. They can be thought of as symmetries because they are transformations of a mathematical object (which happens to be algebraic rather than geometrical) that leave its important properties unchanged. It turns out that understanding these symmetries in more complicated situations is the key to solving some of the deepest problems in mathematics. A notable example is the result, obtained by Niels Henrik Abel and extended by Évariste Galois, that there is no formula for solving general quintic equations, or at least no formula that involves just algebraic operations and taking roots. A much more recent example is Andrew Wiles' solution of Fermat's Last Theorem.

Fearless Symmetry started life as an expository paper intended to help mathematicians in other areas to understand Wiles' remarkable achievement. It then grew into a book, and to make it more accessible the authors added a lot of background material. The result is that to begin with there are plenty of gentle sentences such as: "We start our consideration of groups by thinking about a beautiful perfect sphere, one foot in radius, made of pure marble." By the end these are accompanied by sentences such as: "By the Modularity Conjecture, there is a cuspidal normalized newform f of level N and weight 2 such that for all primes w that are not factors of N, $aw(f)=aw(E)$, and hence these pairs of integers are congruent modulo p." In between, the level of sophistication rises steadily. A typical reader, therefore, will find that the book starts by covering familiar ground, then becomes interesting and informative, and finally becomes too difficult to understand. Where these transitions take place will vary from reader to reader: I learned a lot from about the middle third of the book and not much from the outer thirds. But that was enough to make it worth reading, and perhaps one day I will be ready to have another go at the later chapters.

One small disappointment was a section promisingly entitled: "Digression: What is so great about elliptic curves?" Anybody who has followed the story of the proof of Fermat's Last Theorem will have heard that elliptic curves are very important, but it is not at all obvious from the definition here why they should be. Eager for a better understanding, I turned to that section only to find that the answer is that elliptic curves are incredibly useful to number theorists. There are less question-begging answers later in the book, but by then the going is rather tough.

But that was just a digression. In general, the authors are to be admired for taking a very difficult topic and making it, if not fully accessible, then certainly more accessible than it was before. ■

Timothy Gowers is at the Centre for Mathematical Sciences, University of Cambridge, Wilberforce Road, Cambridge CB3 0WB, UK.

NEW IN PAPERBACK

The Evolution–Creation Struggle
by Michael Ruse (Harvard University Press, £10.95, €14.40, $16.95)
"In this book, Ruse aims not to attack but to understand. For that he wisely turns to history — specifically to the history of evolutionary theory." John Hedley Brooke, *Nature* **437,** 815–816 (2005).

The Revenge of Gaia
by James Lovelock (Penguin, £8.99)
"James Lovelock... offers his take on the future of energy. In brief, a vigorous turn towards nuclear power will be necessary to prevent the catastrophic climatic changes caused by an increase in atmospheric carbon dioxide." Tyler Volk, *Nature* **440,** 869–870 (2006).

Thinking With Animals: New Perspectives on Anthropomorphism
edited by Lorraine Daston & Gregg Mitman (Columbia University Press, $25, £16)
"An unusual book that will surely join the growing literature on consciousness, animal cognition and the continuity between human and animal minds." Juliette Clutton-Brock, *Nature* **434,** 958–959 (2005).

Terrors of the Table: The Curious History of Nutrition
by Walter Gratzer (Oxford University Press, £9.99, $16.95)
"[Gratzer's] purpose is 'to astonish, to instruct and, most especially, to entertain'. And what could possibly be more entertaining than the history of nutrition?" Marion Nestle, *Nature* **438,** 425–426 (2005).

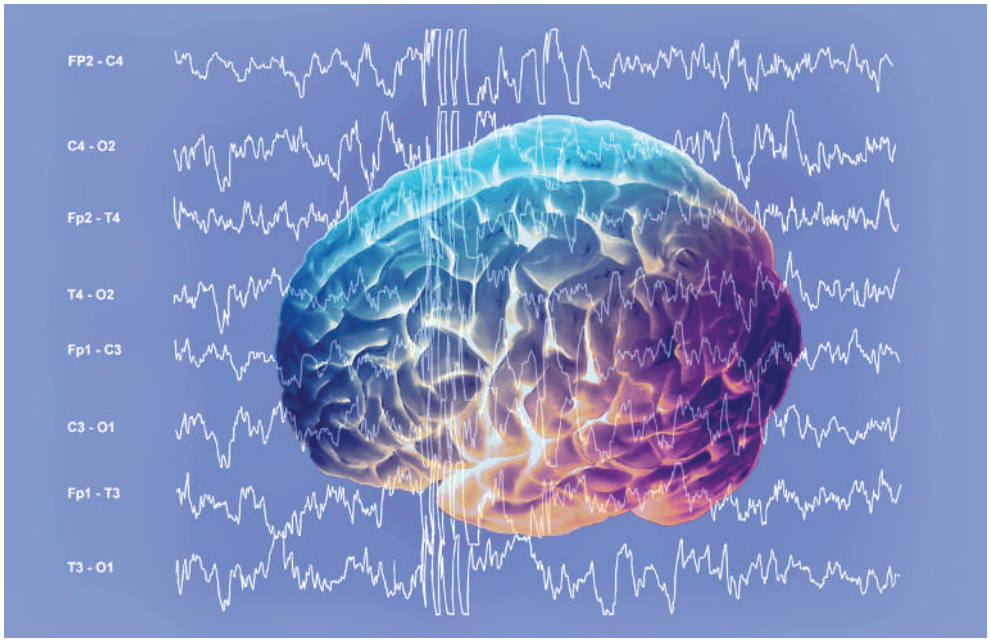

SOVEREIGN, ISM/SPL

Brain waves are chaotic during an epileptic attack, as this electroencephalogram shows.

Fascinating rhythm

Rhythms of the Brain
by György Buzsáki
Oxford University Press: 2006. 464 pp.
£42, $69.95

Mayank Mehta

The brain's primary task is probably to perceive environmental stimuli accurately and to generate appropriate responses quickly. Yet neurons not only respond to stimuli, but often do so in a rhythmic fashion. The strength of neural rhythms can predict a subject's performance on a task. Even when we sleep, neurons in most parts of the brain are active in a highly rhythmic fashion. By contrast, epileptic fits and Parkinson's disease are accompanied by an abnormal increase in certain brain rhythms.

What makes the brain rhythmic? What purpose do rhythms of the brain serve? These fascinating questions are being intensely investigated. In *Rhythms of the Brain*, György Buzsáki does a remarkable job of summarizing a vast body of literature on the topic.

This wonderful book seamlessly cycles between experimental results and theoretical concepts. It begins with an introduction to many topics related to brain rhythms, such as neuronal anatomy, physiology and the physics of self-organized systems. Here we learn about such things as scaling laws and complexity applied to simple neural circuits. Buzsáki describes a wide range of brain rhythms, ranging from very slow rhythms of the order of 1 cycle per second up to several hundred cycles per second. The frequency of rhythms changes as a function of development, ageing and disease. The frequency of oscillations often changes dramatically within a few seconds, as a function of the animal's behaviour. Subsequent chapters discuss various experimental methods used to measure neural activity, ranging from ion-channel measurements to multielectrode recordings and functional imaging, and their relative merits.

Buzsáki then moves on to describe possible functions of brain rhythms, such as resonance, synchronization of neural circuits, and improvement of signal-to-noise ratio by stochastic resonance. As with the rest of the book, these fascinating yet heavy topics are punctuated by entertaining stories, such as the origin of the word 'synchronicity', which refers to a key concept in systems neuroscience. According to Buzsáki, the physicist Wolfgang Pauli consulted the psychologist Carl Jung about the meaning of his dreams. After years of conversation, Pauli and Jung came up with the concept of synchronicity, which refers to the coincidence in time of multiple events that may not be causally unrelated.

The next few chapters summarize a vast amount of literature about the origin of neocortical oscillations and the joint effect of external stimuli and internally generated oscillations on perception. We learn that perception is largely governed by the brain's own internal, often involuntary, dynamics. Seemingly involuntary oscillations can dramatically enhance the perception of a stimulus. For example, neural activity is often modulated by a rhythm of 4–12 Hz, called the theta rhythm. The presence of theta oscillations can generate a fivefold increase in a rabbit's ability to respond to a stimulus. Further, neocortical activity is often modulated by a rhythm of 40–80 Hz, called the gamma rhythm. When there are strong gamma oscillations in certain parts of the neocortex, human subjects do better on learning and memory tasks.

The last few chapters are devoted to the functioning of a seahorse-shaped region called the hippocampus. This topic is the focus of Buzsáki's research, and he is one of the leading experts in this area. The hippocampus is essentially 'rhythm central', and hippocampal neurons probably show the widest range of oscillatory modulation. For example, these neurons mostly fire randomly when a rat sits around grooming itself. As soon as the rat starts to walk, the hippocampal neurons start to spike with a theta rhythm. The same theta rhythm appears when the rat is dreaming. When the rat stops walking and rests without dreaming, the theta rhythm is largely gone, and is replaced by occasional, short bursts of oscillations of about 200 cycles per second, called ripples. In addition to this range of rhythms, hippocampal neurons also fire selectively as a function of the rat's position in space. So, just by listening to the neural activity, one can gain information on where the rat is in space and whether it is resting or running. Hearing the rat hippocampus on a loudspeaker is an unforgettable experience. Buzsáki's book describes the amazing influence of oscillations on information encoding in the hippocampus and how this may be critical for learning facts and events. It ends with a discussion of some of the toughest problems in the field, such as what consciousness is, and how to irrefutably demonstrate the role of oscillations in brain function.

The book is clearly written and points the reader to the literature on a wide range of issues related to oscillations. Most chapters are accessible to a lay audience, and even practising neuroscientists would find much to learn here. The book is a 'must read' for anyone interested in understanding the functioning of large and complex brain circuits. ■

Mayank Mehta is in the Department of Neuroscience, Brown University, Providence, Rhode Island 02912, USA.
http://neurophysics.brown.edu

Protecting biostructure

Biodiversity researchers have focused on diversity at the cost of ignoring the networks of interactions between organisms that characterize ecosystems.

Kevin McCann

That biodiversity is in sharp decline is no longer in question, but scientists still heatedly debate the functional consequences of this loss. Attempts to tackle the problem have mainly involved trying to establish a direct link between species diversity and the sustainability of ecosystems. But in taking this approach, scientists have concentrated on diversity at the expense of ignoring the biological structure that maintains ecosystems. This is akin to the physiologist cataloguing animal parts and ignoring the anatomical structure that connects them. Clearly it is the underlying architecture, not just the parts by themselves, that maintains the bodily functions necessary for life. Analogously, the network of interactions between organisms, not diversity per se, breathes life into ecosystems. To understand the implications of biodiversity loss, it is crucial to monitor changes to the underlying 'biostructure'.

Perhaps the main reason why researchers have tended to focus on diversity is that it is easier to count species than to document their interactions. Empirically mapping biological networks such as food webs is no small chore. Like realist painters, some intrepid scientists have attempted to render the topology of these wildly complex webs by meticulously piecing together stomach-content analyses and many hours of field observations. But stomach contents are difficult to decipher, so it is often impossible to quantify energy fluxes that pulse through these networks.

Recently, ecologists have begun to use stable isotopes to trace the flow of energy through food webs. Because the concentration of the ^{15}N isotope tends to increase by a certain amount with each step of the food chain, patterns in ^{15}N fractionation provide a wonderfully simple measure of a species' position in the web. Similarly, signatures in ^{13}C can be used to determine a given predator's prey — although only prey organisms that have very different carbon sources can be differentiated (for example, C3 versus C4 plants).

A fuzzy but fluid empirical sketch of a food web emerges from stable-isotope analyses. Importantly, these 'sketches' can reveal changes in major network attributes across ecological gradients; for example, increased omnivory by fish as lake size decreases.

On the horizon, DNA-barcoding may soon provide a more highly resolved and precise understanding of both network topology and energy flux, by allowing ecologists to rigorously identify and quantify prey species taken from a predator's stomach. Here, bits of mitochondrial DNA are used to identify species, much like a barcode is used to identify the price of an item in a grocery store.

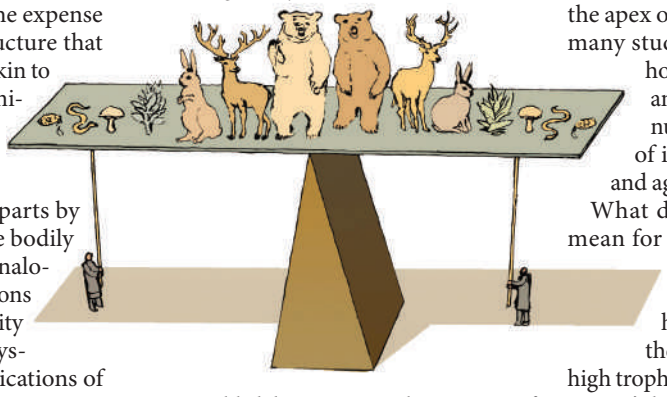

J. KAPUSTA/IMAGES.COM

To establish how structural properties of an ecological network change with human impact, an obvious starting point is to sketch ecological networks across a gradient of human-induced diversity. I know of only one study that has directly explored network patterns across such gradients, but the early results suggest that clear patterns may exist. By using stable isotopes to sketch food webs, our group has shown that human-induced diversity gradients consistently correlate with changes in the structure of tropical seagrass food webs.

Intact seagrass beds are wonderfully diverse and productive coastal ecosystems, but natural variation in human densities around different beds has repeatedly created gradients in species diversity. As human density increases, these ecosystems lose top predators, detritus, specialist consumers and edible seagrass. At high enough human densities the systems are reduced to a very homogenized habitat dominated by a single, relatively inedible seagrass and an explosion of sea urchins. The reason for this changing structure is not fully known but early findings suggest that generalist urchins consume increased algal production driven by an increased load of nutrients in the water. The human-induced nutrient subsidy, and the loss of top-level predators, promotes an elevated density of urchins that drives habitat homogenization.

Results from long-term ecological research are consistent with the seagrass story. Fisheries researchers, for example, have used historical catch records to argue that humans preferentially harvest large organisms in the higher levels of food webs. Similarly, terrestrial ecologists have found that habitat fragmentation and culling has led to the extirpation of many large mobile terrestrial organisms. Thus, indirect evidence is accumulating that humans are exerting a strong top-down force on the apex of food webs. At the same time, many studies indicate that humans are homogenizing the base of aquatic and terrestrial food webs, through nutrient run-off, the introduction of invasive species, urbanization and agriculture.

What does structural deterioration mean for ecosystem function and sustainability? Recent food-web theory predicts that the homogenization of habitats and the loss of mobile predators from high trophic levels is seriously threatening nature's balance. In the most simplified sense, this theory argues that the variation in species occupying lower levels in the food webs allows an ecosystem to elicit a range of responses to a variable world. The mobile larger organisms interact with this landscape of species variability in a way that prevents any single species from monopolizing space and energy. The large organisms, in other words, promote the balance and maintenance of a diverse and variable assemblage of organisms, which in turn buffers against an ever-changing world.

According to this theory, nature is a beautiful balance of bottom-up (driven by habitat heterogeneity) and top-down (driven by predators) forces. By homogenizing habitats and truncating higher-order predators, we may be inadvertently testing this theory — it remains to be seen whether the balance of critical ecosystem functions survives. ■

Kevin McCann is at the Department of Zoology, University of Guelph, Guelph, Ontario, N1G 2W1 Canada.

FURTHER READING
Ecological Effects of Biodiversity. http://en.wikipedia.org/wiki/Ecological_effects_of_biodiversity.
Food Webs. www.foodwebs.org
Barcode of Life Data Systems. www.barcodinglife.com
Tewfik, A., Rasmussen, J. B. & McCann, K. *Ecology* **86,** 2726–2736 (2005).

For other essays in this series, see http://nature.com/nature/focus/arts/connections/index.html

NEWS & VIEWS

PHYSICS

Gravity passes a little test

Clive Speake

Newton's gravity, that old classical warhorse, is well established on scales as large as the Solar System. The latest experimental confirmation of its validity is tiny in scale, but big in implications.

Isaac Newton's inverse-square law of gravity has given faultless service ever since that infamous encounter with an apple in the late seventeenth century. It might seem surprising, therefore, that physicists still feel compelled to verify it. But they do: writing in *Physical Review Letters*[1], Kapner *et al.* detail the latest high-precision test, showing that the gravitational forces between laboratory masses separated by as little as 55 μm — a scale at which there are good reasons to believe that the inverse-square law will break down — are consistent with Newton's law. But why should we prick up our ears at the news, "Gravity doesn't fail again"?

Of course, it could be argued that Newton's law is so fundamental that it should be subject to the most stringent tests on offer at any time. But the true significance of Kapner and colleagues' result lies in its implications for resolving the 'cosmological constant problem'. This problem, in turn, brings into sharp focus a conflict at the heart of efforts to develop a 'theory of everything', a theoretical framework that would treat gravitation and the other forces of nature on an equal footing. The incompatibility of gravitation with quantum mechanics is central to this conflict.

To illustrate where Kapner and colleagues' study fits in, let us work backwards from this impasse. One promising approach to breaking it is string theory, which endows fundamental matter and field particles with internal degrees of freedom that can be likened to the harmonics of a string. A well-known result of quantum mechanics is that a harmonic oscillator (or, to give another example, a mass on a spring) has a finite amount of energy even at a temperature of absolute zero, at which its thermal vibrations would have ceased entirely. This idea of a non-zero 'ground state' energy can also be applied to electromagnetic radiation contained in, say, a metal box. Here, each resonant mode (like the resonances of a drum head) carries the zero-point energy. The total energy density is the sum of the contributions from all the modes, and the magnitude of the sum is determined largely by the highest (or cut-off) frequency.

If this picture is applied to the vibrating quantum fields that suffuse the vacuum of the cosmos, a surprising result emerges. Simple thermodynamics shows that the vacuum must produce a negative pressure to balance out its non-zero, positive energy density. Furthermore, relativity theory suggests that negative pressure — the 'sucking' of the vacuum — creates a repulsive component to gravity. We therefore expect the zero-point energy of all the quantum fields at large in the Universe to act against the mutual attraction of ordinary matter. If this effect were big enough, it could create a Universe in which the recession speeds of distant galaxies would increase with time.

Albert Einstein, in a bid to recreate the static Universe that was *de rigueur* at the time, included, in an ad hoc way, such a repulsive term in his dynamical equations of general relativity, and referred to it as the cosmological constant. This term was thought to have been made redundant in the 1920s, when Edwin Hubble observed that the Universe was expanding and not static. But more recently, Einstein's constant was brought back into service — this time to account for observations that imply that the Universe's expansion is indeed accelerating[2].

It is too soon to say whether this acceleration is definitely caused by a vacuum energy — now dubbed 'dark energy' on account of its unresolved nature. But it is a strong possibility. If the measured geometry of space (which depends on its gravity) is to be reconciled with the total amount of visible matter in the Universe, unseen dark energy must account for about 70% of all the energy in the Universe[3].

This might seem astonishing in itself, but the biggest surprise comes when we ask what value, a priori, we would expect the vacuum-energy density to have. A naive, but not unreasonable, assumption would be that the cut-off frequency for summing up the relevant resonant modes of the vacuum would correspond to the reciprocal of the Planck time, the smallest timescale for which we have any physical insight. But in this case, the zero-point energy density would exceed that required by some 120 orders of magnitude. This enormous discrepancy is the nub of the cosmological-constant

E. LESSING/AKG-IMAGES

'Personification of man limited by reason.' The English poet, artist and mystic William Blake decried the "single vision" of scientific materialism, describing it as "Newton's sleep". In this 1795 painting by Blake, Newton, absorbed in geometrical calculations, has his back turned on the true fabric and colour of the Universe. Mirroring this depiction, Newton's avowedly classical gravity stands oddly detached from the other, quantum forces of modern physics — despite passing test after test[1].

problem. Even plausible extensions of the standard model of particle physics, such as postulating the existence of 'supersymmetrical' partners for each known particle, cannot narrow the gap to less than 60 orders.

There have been many attempts to fix this problem, and all have involved new physics of some sort. One possible mechanism[4] assumes that the particle proposed to mediate gravity, the graviton, is a 'fat' string. Such a particle would be blind to scales smaller than its own dimensions, and if this scale were smaller than the spatial scale corresponding to the cut-off frequency, the cosmological-constant problem would be solved. The spatial scale implied by the dark-energy density turns out to be about 90 μm. But if this is so, it must inevitably also reduce the newtonian gravitational attraction between masses in the laboratory on this scale.

Kapner and colleagues' detector for such aberrant gravity took the form of a disc about 1 mm thick suspended from a classical 'Cavendish' torsion balance, which exploits the low torsional stiffness of a fine suspension wire to measure small forces very sensitively. Two further discs acting as 'attractors'— the top one of a similar thickness to the detector disc, and the lower one much thicker — were rotated under the test mass at distances of as little as 55 μm. All three discs were drilled through with holes that can be thought of as 'negative' masses (Fig. 1).

In this set-up, the role of the lower attractor was to cancel the newtonian gravity acting between the upper attractor and the detector. If the graviton were indeed fat, the larger, more distant attractor would overcompensate for the enfeebled short-range gravity from the smaller, closer attractor. This would give a torque signal where essentially none would be expected if Newton's theory were correct. Given the size of the masses involved, Kapner *et al.* had to be certain of this cancellation to an accuracy of about 0.1%. Such experiments are arduous, as spurious forces resulting from residual ground vibration and thermal, magnetic, electrostatic and Casimir forces (these last due to the vacuum energy of electromagnetic fields) have to be eliminated to a fastidious level. The possible perturbing effects of all these forces increase as the separation between detector and attractor decreases. In the experiment, a metallic diaphragm stretched across the gap between the upper source and test discs was used to isolate the masses from non-gravitational couplings, and the whole apparatus was encased in a magnetically shielded, evacuated enclosure.

Kapner and colleagues' confirmation[1] of the inverse-square law at this tiny scale thus nullifies the fat-graviton hypothesis. It also provides strong constraints on other new physics that seeks to resolve the cosmological-constant problem. As such, it represents something of a milestone in tests of the law, and will certainly make the theorists take a long, hard look. Other groups should perhaps attempt to reproduce such an important result, as would be done for a non-null experiment such as the determination of Newton's gravitational constant itself.

There are many more predictions from string theory, from other theories of quantum gravity and from extensions of the standard model of particle physics that can be targeted by tests of Newton's familiar law at ever-smaller mass separations. String theory, for instance, suggests the possibility of extra spatial dimensions for the gravitational interaction. Tests for their existence will demand even greater sensitivity at ever-shorter separations than used in Kapner and colleagues' experiments. New techniques might well be required for researchers to take up the challenge. ■

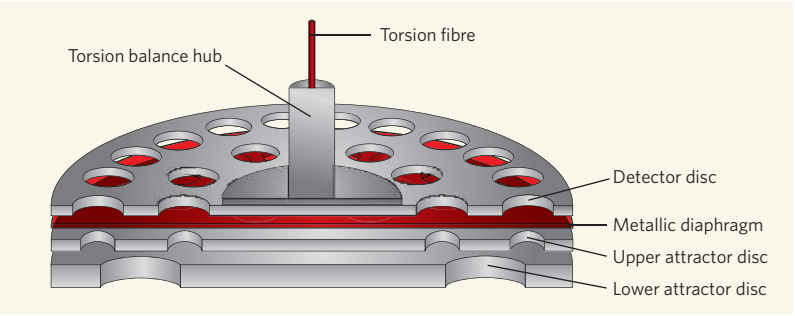

Figure 1 | Gravitational balance. In Kapner and colleagues' experimental set-up[1], the gravitational torque on a disc-shaped test mass suspended on a tungsten fibre is measured using a torsion balance whose hub contains detector mirrors and calibration masses. The torque is caused by tiny variations in gravity owing to the passage of holes drilled in two 'attractor' discs rotating beneath the test mass, which is also drilled through with holes. The distance between the upper of these two discs and the test mass was as little as 55 μm. At such short distances, deviations from Newton's gravity would have been made apparent by the overcompensation of the more massive lower rotating disc — but no such effect was observed. To ensure that spurious forces are kept to a minimum, a metallic diaphragm is placed between the detector and the upper attractor, and the whole apparatus is placed in a shielded, evacuated enclosure. (Figure not to scale.)

Clive Speake is at the School of Physics and Astronomy, University of Birmingham, Edgbaston, Birmingham B15 2TT, UK.
e-mail: c.c.speake@bham.ac.uk

1. Kapner, D. J. *et al. Phys. Rev. Lett.* **98,** 021101 (2007).
2. Reiss, A. G. *et al. Astron. J.* **116,** 1009–1038 (1998).
3. Bennett, C. L. *et al. Astrophys. J. Suppl. Ser.* **148,** 1 (2003).
4. Sundrum, R. *Phys. Rev. D* **69,** 044014 (2004).

PHYSIOLOGY

Legacy of leaky channels

Richard Horn

Mutations that affect the opening and closing of ion channels in cell membranes are associated with disease. Defects in other properties of these channels can also cause ion leakage, with equally devastating consequences.

Hundreds of millions of years ago, when the first cell emerged from the primordial ooze, it was enclosed by a membrane that was impermeable to many of the substances needed to sustain life. To overcome this obstacle, the cell had to invent transporters, exchangers, pumps and ion channels. An early trick developed by the first cells was to exploit the ion gradients created by protein pumps as batteries of potential energy. These gradients could be discharged to produce electrical signals in excitable cells, such as the neurons and muscle cells that subsequently evolved. The discharge happens when ion channels open their gates and allow ions to flow rapidly across the membrane down their concentration gradients.

For this process to work efficiently, the channel gates must be kept securely closed most of the time to prevent the transmembrane ion gradients from dissipating. Leakage of ions through these channels under a cell's resting condition, when the gates should be closed, can have unwelcome consequences, as Sokolov *et al.*[1] report on page 76 of this issue. The authors show that leakage of Na^+ ions is associated with an inherited dysfunction of the sodium channel (a channelopathy) in skeletal muscle cells. This underlies one form of a disorder known as hypokalaemic periodic paralysis, in which patients suffer from episodic attacks of muscle weakness or paralysis.

How could an inherited mutation make an ion channel leaky? The most obvious possibility is through a defect in the activation gate that, in voltage-gated ion channels of excitable cells, lies at the intracellular end of the pathway for ion flux. Normally, the activation gate of a sodium channel is closed at a cell's resting potential (around −90 millivolts in skeletal muscle cells). It opens fleetingly when input from a nerve impulse causes a muscle cell to become depolarized (the inside becomes more

positive than at rest). The sudden influx of Na^+ ions produces a regenerative spike, or action potential, after which the gate slams shut. A mutation might result in an activation gate that is open with a low, but finite, probability when it should be closed, or is unable to close tightly.

Remarkably, the Na^+ leak in the channelopathies studied by Sokolov *et al.*[1] has nothing to do with the central pathway normally associated with Na^+ flux. Rather, it concerns one of the four gating pores that surround the central pore domain. Like the central pathway, a gating pore is a thoroughfare for cation movement across the membrane. But in this case, instead of mobile ions in solution, the cation is a portion of the channel's S4 transmembrane segment, in which every third amino-acid residue is the cationic arginine, and which moves through this specialized pore (Fig. 1). On depolarization, the S4 segment with its positively charged side-chains moves outwards through the gating pore, a movement that is energetically coupled to the opening of the activation gate (Fig. 2a). When the membrane potential returns to its resting, hyperpolarized value (with the inside more negative), the S4 segment is drawn back inwards (Fig. 2b), causing the activation gate to close. Because this mobile protein entity is tethered at either end, the gating pore is never empty. Not surprisingly, then, gating pores are typically impermeable to the ions in the aqueous solutions that border the channel.

However, mutation of the two outermost S4 arginines to a neutral amino acid produces a cationic leak through the gating pore[2,3]. And in potassium channels, the mutation of arginine to a histidine results in a leakage pathway for protons[4]. This occurs only at hyperpolarized potentials, when the S4 segment is in its inwards, resting conformation (Fig. 2b). At these voltages, the outermost arginine side-chains usually lie in the narrowest region of the gating pore, where they can interact electrostatically with the anionic side-chains of other transmembrane segments, thereby preventing ions from moving through the gating pore. If one of these arginines is neutralized, however, it can no longer interfere with the movement of small monovalent cations through the pore. Until now, this gating-pore current has been merely a biophysical tool for studying the movement and environs of the S4 segment[5]. But Sokolov *et al.*[1] show that naturally occurring mutations of S4 arginines can also produce a leakage current through the gating pore, and that this functional defect is linked to episodic paralysis.

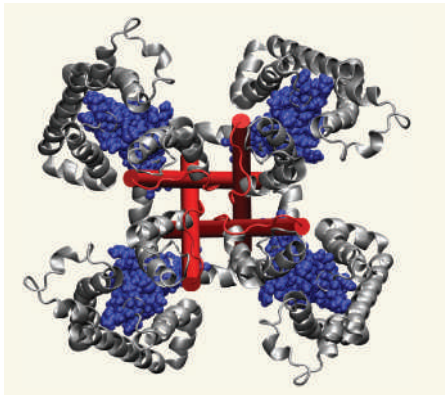

Figure 1 | Extracellular view of a voltage-gated membrane ion channel. A model of a potassium channel (Kv1.2), which is similar to the sodium channel studied by Sokolov *et al.*[1], is shown in a closed state at a hyperpolarized membrane potential. The pore domain is surrounded by four voltage-sensing domains. The central permeation pathway for ion flux (red) is lined by the selectivity filter and four helical S6 segments. The S4 segments are coloured blue and are shown as partially surrounded by other transmembrane segments. (Figure based on ref. 12.)

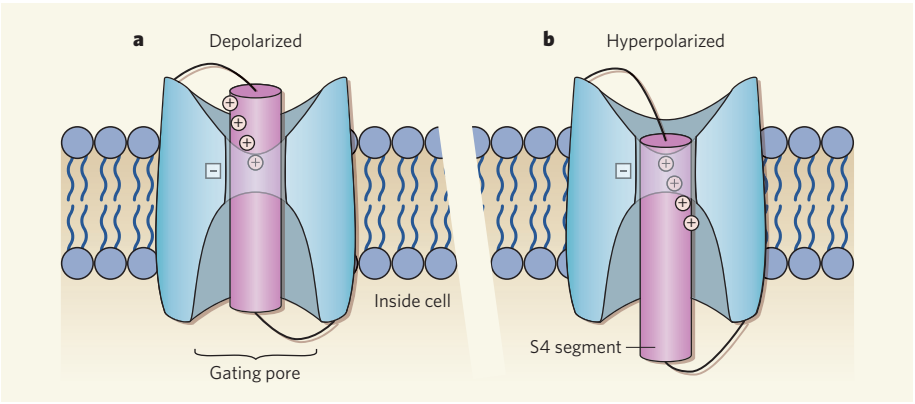

Figure 2 | Speculative model of the gating pore at two different membrane potentials. The S4 segment (pink), with its four outermost arginine residues (+), is shown within the confines of a gating pore. Water-filled vestibules surround much of this segment. **a**, When a cell is depolarized, the S4 segment moves outwards, opening the activation gate. **b**, The gate shuts when the cell returns to its resting, hyperpolarized state and the S4 segment moves back inwards. Normally, negatively charged residues (−) near the gating pore form electrostatic interactions with positively charged arginines in the S4 segment, preventing ion leakage. However, if one of these arginines is mutated to a neutral residue, current leakage occurs.

Two properties of this current indicate that it is not associated with a defective activation gate in the central pore. First, it is not selective for Na^+ ions, but instead allows the passage even of a monovalent cation as large as *N*-methyl-D-glucamine, to which the central pore is completely impermeable. More importantly, blocking the central pore with tetrodotoxin does not affect the gating-pore current.

Sokolov and colleagues found that the arginine mutations do not open gaping holes in the gating pore, however. When open, the permeability of the central pore is 800 times larger than that of an individual gating pore. Moreover, the gating pore of mutated sodium channels remains impermeable to small divalent cations, such as Ca^{2+} and Ba^{2+}.

These features are consistent with a water-inundated gating pore that, at hyperpolarized voltages, narrows to embrace the S4 segment snugly in the vicinity of its two outermost arginine residues (Fig. 2b). Sokolov and colleagues' conclusion that there is a short region of S4 in close contact with the pore is in agreement with several other observations. These include studies showing that S4 segments are largely accessible to hydrophilic reagents[6,7]; simulations showing that water-filled crevices invade the space around S4 segments[8]; and evidence that the electric field across the gating pore is highly focused at hyperpolarized potentials[9]. The fact that mutated pores show such a striking difference in permeability to large monovalent cations and small divalent cations indicates that the narrowest region of the pore in disease mutants is energetically unfavourable to the passage of a hydrated divalent cation.

Normally, skeletal muscle cells respond unwaveringly to every nerve impulse they receive by firing an action potential and contracting. In this type of periodic paralysis, however, the cells are sufficiently depolarized by the leak for the sodium channels to be inactivated, resulting in a breakdown of this normally reliable process and leading to the associated muscle weakness. But this is not the end of the story. For example, decreased plasma levels of K^+ ions exacerbate the muscle weakness seen in patients carrying these mutations[10], and the underlying mechanism for this remains a mystery. Furthermore, the mutations probably have other effects on the channels' gating properties that contribute to the observed weakness[10].

Nevertheless, Sokolov and colleagues' study[1] reveals a new way in which a naturally occurring ion-channel mutation can alter the excitability of muscle cells. Because of the prevalence of S4 mutations among the channelopathies[11], we can expect that a gating-pore leak will arise again as a malicious participant in such diseases. ■

Richard Horn is in the Department of Molecular Physiology and Biophysics, Institute of Hyperexcitability, Jefferson Medical College, 1020 Locust Street, Philadelphia 19107, USA.
e-mail: richard.horn@jefferson.edu

1. Sokolov, S., Scheuer, T. & Catterall, W. A. *Nature* **446,** 76–78 (2007).
2. Tombola, F., Pathak, M. M. & Isacoff, E. Y. *Neuron* **45,** 379–388 (2005).

50 YEARS AGO

In an article on "Nuclear Knowledge and Christian Responsibility" in the *London Quarterly* for January 1957, Prof. C. A. Coulson emphasizes that if the under-developed countries are also to enjoy the benefits of civilization, or indeed if our civilization is to continue, a fair and reasonable distribution of nuclear energy is an absolute necessity... he argues that it is a Christian responsibility to see that nuclear energy, like any other scientific discovery, is rightly used... Urging that we should be profoundly grateful for our nuclear knowledge, Prof. Coulson indicates some of the ways in which we should share and develop nuclear energy and its applications... We should also rejoice in new possibilities for curing disease and improving health in parts of the world where disease is rampant and health poor and should see that no one makes personal profit out of this situation to the detriment of the world-wide distribution of the new products.

From *Nature* 2 March 1957.

100 YEARS AGO

On Leprosy and Fish Eating. A Statement of Facts and Explanations. By Jonathan Hutchinson — The object of this work is stated in the preface to be "to carry conviction to the reader that the fundamental cause of the malady known as true leprosy is the eating of fish in a state of commencing decomposition."... Mr. Hutchinson would associate the former prevalence of leprosy in the British Isles and in Europe with the Roman Catholic ordinances prescribing fish-food on two out of every three weekdays... We think that Mr. Hutchinson goes much too far in thus ascribing *all* variations in the prevalence of leprosy as being correlated with those of a fish-diet; even in the fact that the disease is more prevalent among men than among women he sees support for his hypothesis, for he suggests that women are more fastidious feeders than men.

From *Nature* 28 February 1907.

50 & 100 YEARS AGO

3. Sokolov, S., Scheuer, T. & Catterall, W. A. *Neuron* **47,** 183–189 (2005).
4. Starace, D. M. & Bezanilla, F. *Nature* **427,** 548–553 (2004).
5. Tombola, F., Pathak, M. M., Gorostiza, P. & Isacoff, E. Y. *Nature* **445,** 546–549 (2007).
6. Larsson, H. P., Baker, O. S., Dhillon, D. S. & Isacoff, E. Y. *Neuron* **16,** 387–397 (1996).
7. Yang, N., George, A. L. Jr & Horn, R. *Neuron* **16,** 113–122 (1996).
8. Freites, J. A., Tobias, D. J. & White, S. H. *Biophys. J.* **91,** L90–L92 (2006).
9. Ahern, C. A. & Horn, R. *Neuron* **48,** 25–29 (2005).
10. Struyk, A. F., Scoggan, K. A., Bulman, D. E. & Cannon, S. C. *J. Neurosci.* **20,** 8610–8617 (2000).
11. Cannon, S. C. *Neuromusc. Disord.* **12,** 533–543 (2002).
12. Yarov-Yarovoy, V., Baker, D. & Catterall, W. A. *Proc. Natl Acad. Sci. USA* **103,** 7292–7297 (2006).

MICROSCOPY

Atomic fingerprinting

Alexander Shluger and Tom Trevethan

Atomic force microscopy is a well-established technique to image all kinds of surfaces at the atomic scale. But the force patterns that emerge can also pin down the chemical identity of individual atoms.

Picking lentils from ashes is one of the many challenging tasks delegated to fairy-tale characters. In a famous story, Cinderella completes this chore assisted by some helpful doves. Sugimoto *et al.*, in work that appears on page 64 of this issue[1], tackle a similar, but potentially more useful problem: how to identify a particular element on a surface that contains a mixture of elements using only a mechanical probe.

This is, in fact, one of the thorniest problems in surface science. Although the atomic force microscope (AFM) is starting to be used routinely to 'image' surfaces on the atomic scale, interpreting its images is still extremely difficult. The AFM was invented just over 20 years ago, and is now the most widely used scanning probe. Unlike the more mature scanning tunnelling microscope (STM), which can be used only for conducting surfaces, the AFM can image both insulating and conducting samples. But its evolution into a metrology tool capable of discriminating, or even determining, the chemical identities of individual atoms is a new development. It is akin to asking Cinderella to perform her sorting task blindfolded, relying only on the sensation in her fingers.

An AFM works by probing the force acting between its sharp tip and the atoms of the sample's surface. Over the past decade, there have been many spectacular achievements in the imaging and even manipulation of surface structures and individual atoms using an AFM in its dynamic or 'non-contact' mode[2–5]. In this mode, the AFM's tip is attached to the end of a flexible cantilever, which is oscillated at its resonant frequency and with constant amplitude in a direction perpendicular to the sample surface.

As the tip vibrates, it interacts with the sample's surface, causing the resonant frequency of its oscillations to change. These variations can be measured precisely as a function of tip position, and converted into a three-dimensional image of the surface that contains details at the atomic scale. But relating even simple image patterns to the position of surface atoms and their chemical identities is a tricky task. The imaging mechanism is complex, and, crucially, the exact composition of the tip's apex on the atomic scale — and so its contribution to the strength of the interaction — is impossible to establish with certainty[2,4].

So how does one sort the lentils from the ashes — or, less figuratively, tell apart atoms such as silicon (Si), tin (Sn) and lead (Pb) — using such a method? Sugimoto *et al.*[1] first looked at whether Sn and Pb atoms adsorbed on a silicon surface could be distinguished from each other by correlating topographic AFM images with the adsorbates' known concentrations. To create a transferable mechanistic 'sensation' of these atoms, they then measured with very high accuracy the dependence of the force on the distance between the AFM's tip and the individual atoms on the surface, in a similar way to previous studies[6,7].

After repeating their measurements many times, the authors realized that the forces measured above Si, Sn or Pb atoms vary from experiment to experiment. That is most probably because the shape and composition of the tip apex on the atomic scale differed between experiments. If the tip's structure were impossible to determine or control, and the experiments were to be deemed irreproducible, then the whole exercise would be ruined.

Trying to identify a characteristic that would allow force curves measured with different tip terminations to be compared, the authors noticed that the strongest interaction was always between the tip and Si atoms on the surface. So they divided the maximum attractive forces for Sn and Pb adsorbates by the maximum force measured with the surface Si atoms. In this way, they managed to obtain what seemed to be distinct, reproducible force 'fingerprints' for each different type of atom.

How can one be sure that the subtle differences between the force fingerprints are in fact due to the different chemical identities of the atoms? To understand and support their findings, the authors used atomistic modelling[1] to determine plausible atomic structures for the

tip, and used these structures to calculate the forces. This sort of realistic theoretical modelling of the interaction between the tip and the surface, and even of the entire experimental procedure, has become an integral and essential component of many AFM experiments[4,7]. The results of Sugimoto and colleagues' simulations matched well with those of their experiments. With increased confidence in their fingerprinting technique, the authors prepared an alloy of Si, Sn and Pb atoms on the silicon surface. By measuring the dependence of the force on the distance between the AFM's tip and individual surface atoms, and comparing it with the atomic fingerprints, they could label all atoms in the image with their chemical identity.

Sugimoto and colleagues' work marks an important step in establishing the AFM as a metrology tool on the atomic scale. It demonstrates that, as is possible with tunnelling current and scanning tunnelling microscopy[8], a statistical approach to measuring force can provide the local composition and structure of a semiconductor surface at the atomic level. Their findings will inspire similar studies of more complex, truly insulating surfaces, and stimulate further development of such extremely discriminatory chemical analyses. ■

Alexander Shluger and Tom Trevethan are in the London Centre for Nanotechnology and the Department of Physics and Astronomy, University College London, Gower Street, London WC1E 6BT, UK.
e-mail: a.shluger@ucl.ac.uk

1. Sugimoto, Y. *et al. Nature* **446,** 64–67 (2007).
2. Morita, S., Wiesendanger, R. & Meyer, E. (eds) *Non-Contact Atomic Force Microscopy* (Springer, New York, 2002).
3. Giessibl, F. J. *Rev. Mod. Phys.* **75,** 949–983 (2003).
4. Foster, A. S. & Hofer, W. *Scanning Probe Microscopes: Atomic Scale Engineering by Forces and Currents* (Springer, New York, 2006).
5. Sugimoto, Y. *et al. Nature Mater.* **4,** 156–159 (2005).
6. Lantz, M. A. *et al. Science* **291,** 2580–2583 (2001).
7. Hoffmann, R., Kantorovich, L. N., Baratoff, A., Hug, H. J. & Güntherodt, H.-J. *Phys. Rev. Lett.* **92,** 146103 (2004).
8. Schmid, M., Stadler, H. & Varga, P. *Phys. Rev. Lett.* **70,** 1441–1444 (1993).

VIROLOGY

Holed up in a natural crystal

Felix A. Rey

Insect viruses that cause polyhedrosis produce infectious microcrystals within a cell. These inclusions were used in a study that pushed the state of the crystallographic art to explain their exceptional stability.

Much of structural biology relies on obtaining highly ordered crystals of proteins and other macromolecules, and it often takes considerable time and effort to produce crystals of adequate quality. In some cases, however, proteins crystallize spontaneously *in vivo*. In such situations the crystals themselves have a biological role (usually storage), examples being insulin[1] and eosinophil major basic protein[2]. Also, the insect polyhedrosis viruses encode a protein called polyhedrin that forms polyhedric crystals, or polyhedra, within an infected cell[3]. The virus particles, or virions, are protected within these polyhedra and can remain infectious for years outside cells, even in harsh environmental conditions. The polyhedra break down and release the virus only when ingested into the very alkaline environment of the midgut of insect larvae (pH 10–11), resulting in infection of a new host.

Until now, the *in vivo* polyhedra were considered to be too small for single-crystal diffraction experiments. On page 97 of this issue, however, Coulibaly *et al.*[4] report the use of the latest X-ray diffraction techniques to determine the structure of the polyhedrin protein of silkworm cytoplasmic polyhedrosis virus (CPV) at 2 Å resolution from microcrystals grown *in vivo*. The crystals came from insect cells infected with either wild-type CPV or with a recombinant baculovirus expressing the CPV polyhedrin gene (Fig. 1a).

Several insect viruses have converged on the strategy of forming polyhedric inclusion bodies to protect themselves and remain infectious for long periods. As well as CPV, which is an RNA virus, baculoviruses such as the nuclear polyhedrosis virus (NPV), and the insect pox viruses (both from families of DNA viruses that are otherwise completely unrelated), use this strategy[3]. Described in technical terms, the CPV polyhedra are body-centred-cubic crystals of space group I23. Intriguingly, polyhedra from CPV and NPV, which show no homology detectable by amino-acid sequence similarity, have the same I23 symmetry and identical crystal unit-cell parameters[5,6], a coincidence that is hardly fortuitous. So, what's special about the three-dimensional lattice of polyhedra?

Electron micrographs of infectious CPV polyhedra clearly show the virions incorporated within the crystal; they appear as spherical disruptions in an otherwise regular lattice (Fig. 1b). The diameter of CPV particles is about 700 Å (ref. 7), about seven times greater than the unit-cell edge of polyhedra (103.8 Å per side). Each virion incorporated in the crystal thus takes up the space of about 150 unit cells. Several thousand infectious particles are incorporated in an average polyhedron with edges 2 micrometres long, occupying about 10–15% of the total volume of the crystal. Therefore, the polyhedrin packing contacts must be strong enough to make this sort of 'Gruyère' crystal very stable.

Remarkably, Coulibaly *et al.*[4] found no difference in the diffraction patterns of wild-type infectious polyhedra and those made by recombinant polyhedrin, which have a regular lattice with no virions incorporated. Polyhedrin thus seems to have special packing properties.

Crystals of insulin or eosinophil major basic protein form only within secretory vesicles and dissolve when exposed to the extracellular milieu. Large enough crystals of these two proteins for structural studies could thus be obtained after their isolation and recrystallization under biochemically controlled conditions. In contrast, polyhedrin crystals grow in the cytoplasm (or in the nucleus in the case of NPV) of the infected cell, within a highly heterogeneous

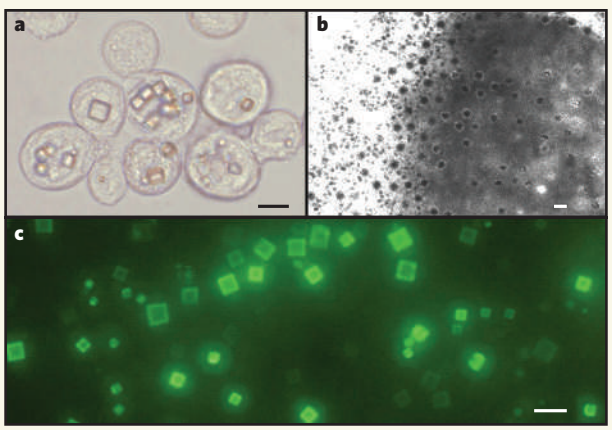

Figure 1 | Intracellular microcrystals. a, Insect cells of the Sf21 cell line infected with a recombinant baculovirus expressing the CPV polyhedrin gene. Cubic crystals are evident inside the cells. **b**, Transmission electron micrograph of a polyhedron recovered from a CPV-infected cell. The crystal (dark grey) has many CPV particles visible at the surface. Virions are included throughout the volume of the polyhedron, not just at the surface. **c**, Sf21 cells co-infected with two recombinant baculoviruses, one carrying the CPV polyhedrin gene and the other the gene encoding green fluorescent protein fused with the sequence for the amino-terminal segment of the CPV outer protein VP3. This latter observation points to potential applications in nanotechnology. Scale bars, 20 μm (**a**, **c**) and 0.1 μm (**b**). (Photos courtesy H. Mori, Protein Crystals Corp., Kyoto Inst. Technol., Japan.)

MATERIALS SCIENCE

Flaky research

Urban legend has it that American engineers spent more than a million dollars inventing an 'astronaut pen' that could work in space, while the Russians simply used a pencil. True or not, the tale shows that the best solutions can sometimes be found in mundane objects. And, indeed, that they can be found in pencils.

Pencils contain graphite, a form of carbon in which atoms are ordered in thin sheets stacked regularly on top of each other. The interaction between these sheets is small, so layers of graphite rub off easily, for example when a pencil draws a line on paper.

Not satisfied with such an obvious, practical use, physicists have long been fascinated by the electronic properties of a single sheet of graphite, called graphene. Graphene is unlike any other material because electrons within it can behave as massless particles, which means they can mimic relativistic physics. Exotic effects that normally require huge particle accelerators might therefore be observed in a simple device — if only it were possible to rub off one, and only one, sheet of graphene.

Despite concerted efforts, this proved problematic. In 2004, researchers at the University of Manchester, UK, finally isolated graphene when they peered through a conventional optical microscope at flakes of graphite that they had simply ripped off from a larger piece with sticky tape (K. S. Novoselov *et al. Science* **306,** 666–669; 2004). Graphene, being a layer just one atom thick, is transparent to light. But, as the picture here shows, there is just enough contrast from the thickness variation in a graphite shaving to locate the graphene layer under the microscope (here, the faint, semi-transparent region on the right, indicated by an arrow).

The image was obtained by Hubert Heersche and colleagues, who in this week's issue describe an experiment in which they attached a graphene sheet to two superconducting electrodes (H. B. Heersche *et al. Nature* **446,** 56–59; 2007). Previous experiments had thrown up the unexpected finding that graphene has a small electrical conductivity even in the absence of mobile charge carriers.

Heersche *et al.* add to the surprise by showing that the same holds true for a superconducting current. Moreover, it was not at all clear that a supercurrent could flow in graphene. As it turns out, not only does a conventional electron supercurrent flow, but so does one consisting of holes, which carry positive charge.

This experiment shows yet again that novel and surprising effects can be observed in simple materials — good news for those who don't have a million dollars to spend on discovering something new.

Liesbeth Venema

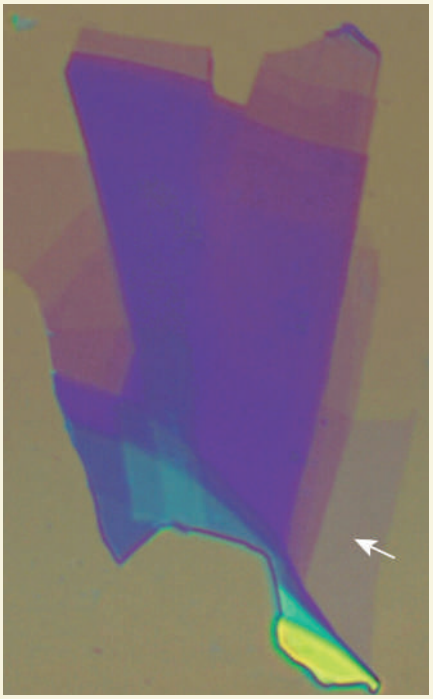

H. B. HEERSCHE *ET AL.*

mixture of proteins and other macromolecules. They do not readily dissolve to release soluble polyhedrin that could be recrystallized. Artificially exposing polyhedra to destabilizing conditions — such as very alkaline pH — leads to polyhedrin aggregation, and sometimes also to the breakdown of the protein[8].

The data needed to determine the structure therefore had to be obtained from microcrystals grown *in vivo*. Diffraction data were collected using a third-generation synchrotron — the Swiss Light Source — equipped with a micro-diffraction set-up[9]. This beamline, together with the ID13 beamline at the European Synchrotron Facility in Grenoble (which has the first dedicated single-crystal micro-diffraction facility to be installed at a synchrotron[10]), have had a major impact in structural biology by reducing the crystal size necessary for single-crystal diffraction experiments.

What does Coulibaly and colleagues' structure[4] tell us about the three-dimensional lattice of polyhedra? It shows that polyhedrin is a trimer, in the shape of a pyramid with a triangular base (Fig. 2). The vertices of the base are extended by amino-terminal, α-helical arms involved in creating a network of packing interactions among trimers in the crystal. The packing surfaces show striking complementarity, having a score for matching[11] higher than that of an antibody–antigen complex.

One remarkable feature is that the polyhedron solvent content is below 20% of the crystal volume, which is extremely low for a protein crystal: solvent content usually ranges between 40% and 70%, with rare cases reaching 27% or 85%[12]. This implies extremely close packing of the protein molecules, and the pyramidal shape of the polyhedrin trimer is clearly important in achieving such tight packing. For instance, the interstitial volume of the densest possible packing of rigid spheres is 26% of the crystal volume, and the solvent content in crystals of globular proteins rarely approaches this lower limit[12]. Also, in most protein crystals the solvent channels connect to the outside, allowing diffusion of small molecules within the crystals. By contrast, in the CPV polyhedra the solvent cavities are completely sealed off from the external environment.

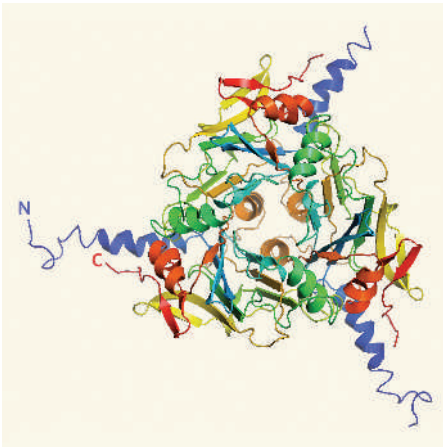

Figure 2 | Ribbon illustration of the polyhedrin trimer. Each subunit is rainbow-coloured from blue (amino terminus) to red (carboxy terminus). As Coulibaly *et al.*[4] show, the trimer has the shape of a pyramid (here viewed from the top) with a triangular base. An amino-terminal α-helical arm extends from each vertex of the base (one for each subunit of the trimer), and is involved in packing interactions in the crystal. (Data from ref. 4; illustration prepared with PyMOL software[15].)

If the packing between polyhedrin trimers is so tight, how do the virions get incorporated during crystal growth? This is not entirely clear, but we do know that they are included in polyhedra through the recognition of an 'inclusion signal' composed of a segment of the CPV outer virion protein VP3 (ref. 13). The interaction between polyhedrin and VP3 must be very strong so that crystal growth proceeds by surrounding the virion, instead of displacing it. The inclusion signal is contained within the amino-terminal 70 amino acids or so of CPV-VP3, and has biotechnological applications: fusion of this sequence to any protein leads to its incorporation into polyhedra[14], as illustrated in Figure 1c.

In principle, then, to take one example, it is possible to use these polyhedra to make ultra-stable protein chips, in which the protein of interest is protected from dehydration and other damage, as well as presented at the surface[14]. The next steps will be to carry out structure-based engineering of polyhedrin to derive mutants for various purposes, so that,

for instance, the crystals can be dissolved and reconstituted at less extreme pH values, with the aim of controlling the release of the incorporated protein. Thus, a further angle of interest to the remarkable polyhedrin structure is that it opens the door to exciting prospects in nanotechnology. ■

Felix A. Rey is in the Unité de Virologie Structurale (CNRS URA 3015), Département de Virologie, Institut Pasteur, 25 rue du Dr Roux, 75724 Paris Cedex 15, France.
e-mail: rey@pasteur.fr

1. Dodson, G. & Steiner, D. *Curr. Opin. Struct. Biol.* **8,** 189–194 (1998).
2. Giembycz, M. A. & Lindsay, M. A. *Pharmacol. Rev.* **51,** 213–340 (1999).
3. Rohrmann, G. F. *J. Gen. Virol.* **67,** 1499–1513 (1986).
4. Coulibaly, F. *et al. Nature* **446,** 97–101 (2007).
5. Fujiwara, T. *et al. Appl. Entomol. Zool.* **19,** 402–403 (1984).
6. Anduleit, K. *et al. Protein Sci.* **14,** 2741–2743 (2005).
7. Hill, C. L. *et al. Nature Struct. Biol.* **6,** 565–568 (1999).
8. Di, X., Sun, Y. K., McCrae, M. A. & Rossmann, M. G. *Virology* **180,** 153–158 (1991).
9. http://sls.web.psi.ch/view.php/beamlines/px/index.html
10. Riekel, C., Burghammer, M. & Schertler, G. *Curr. Opin. Struct. Biol.* **15,** 556–562 (2005).
11. Lawrence, M. C. & Colman, P. M. *J. Mol. Biol.* **234,** 946–950 (1993).
12. Kantardjieff, K. A. & Rupp, B. *Protein Sci.* **12,** 1865–1871 (2003).
13. Ikeda, K. *et al. J. Virol.* **75,** 988–995 (2001).
14. Ikeda, K. *et al. Proteomics* **6,** 54–66 (2006).
15. www.pymol.org

PHOTONICS

Light localized on the lattice

Z. Valy Vardeny and Mikhail Raikh

Photonic lattices are materials specially designed to cage light. By shaking the mesh of the cage, we can see how light, initially passing freely, finds its room for manoeuvre progressively restricted.

Unchecked, light's stamina as a messenger is unsurpassed. In outer space, with no scattering medium, it travels for billions of years and allows us to glimpse deep into the Universe's antiquity. In the past few decades, it has become apparent that light can also be confined within very small spaces. Out in the cosmos, this occurs in black holes, in which light is restricted to a sphere of just a few kilometres' radius by an immense gravitational field. Back on Earth, fibre optics exploits the fact that light can be confined in two dimensions by internal reflection, while propagating freely in the third. Constructs known as laser cavities are used to trap light through mirror reflections, allowing very high light intensities to build up. On page 52 of this issue, Schwartz *et al.*[1] provide the first observations of light being pinned down in a further type of confining space: the latticed cage of a specially manipulated material known as a photonic crystal.

In a perfect atomic crystal, visible light travels ballistically, only occasionally scattering off a lattice atom. As disorder increases — for example, through the introduction of a foreign atomic species — so does the frequency of scattering, and the light's passage through the crystal becomes diffusive. Ultimately, if the disorder is such that interference occurs between individual scattering events, then light can become spatially localized. Philip Anderson[2] first introduced this kind of localization in 1958, for electrons and their spins confined in a semiconductor.

Anderson went on to pioneer the field of light localization in the 1980s, at the same time as Sajeev John[3,4]. These two researchers' theoretical predictions were followed by the observation of a weak form of light localization using coherent backscattering[5,6]. A stronger form of light localization has been observed more recently in highly scattering, insulating (dielectric) media, in which the deviation from classical diffusion was measured by transmission spectroscopy[7,8].

The idea of a photonic crystal — a structure explicitly designed to trap light in the same way that electrons are trapped in a semiconductor — was advanced in 1987 (refs 9, 10). In photonic crystals, the refractive index varies in a periodic fashion, causing multiple light scattering and thus destructive interference. This effect prevents light from flowing in a range of frequencies known as the photonic bandgap. In this gap, the usual features of electromagnetism, as described by Maxwell's equations, can be partially or completely suspended. The resulting microscopic control of photons is even more remarkable than the control of electrons in microelectronic circuits based on semiconductor technology.

Schwartz *et al.*[1] prepared a photonic crystal with a hexagonal patterning of triangles in two dimensions (Fig. 1). The medium they used was a nonlinear dielectric, whose refractive index can be manipulated by high intensities of incident light. Using a technique known as optical induction, Schwartz and colleagues transformed the diffraction pattern of three laser 'pump beams' into a periodic refractive-index change in the medium. Much as in an optical fibre, this patterning means that light can be trapped in two dimensions, while being free to propagate ballistically in the third. Without the transverse trapping, the optical

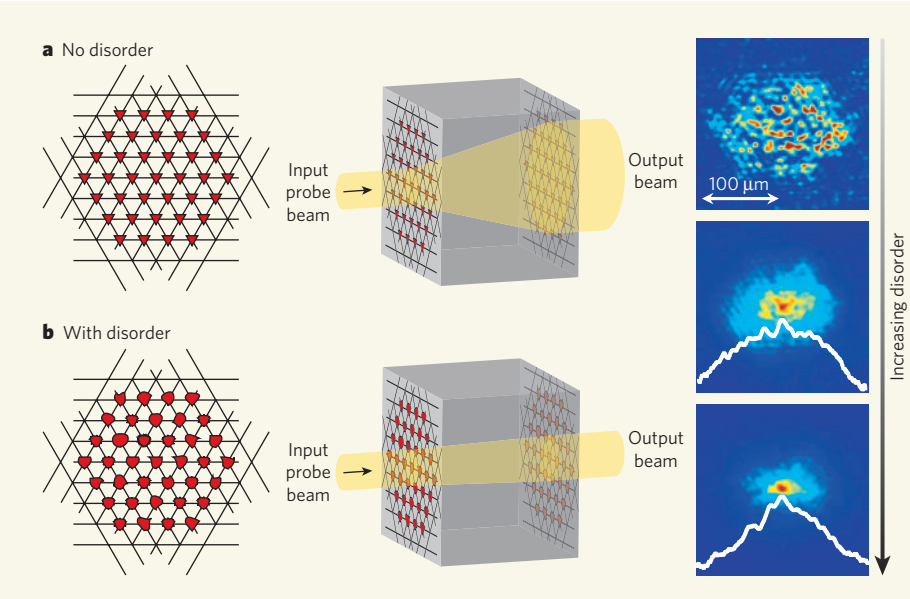

Figure 1 | Localizing disorder. Schwartz and colleagues[1] form their two-dimensional photonic lattice by imprinting the diffraction pattern of three laser beams intersecting at 60° onto the refractive index of a nonlinear optical dielectric. **a**, Without the addition of disorder, the areas of altered refractive index at the beam intersections are themselves regular triangles. In this 'ballistic' case, the width of a laser probe beam increases linearly as it propagates through the third dimension of the optical lattice, and the hexagonal patterning of the lattice is clearly visible in the pattern of the output beam. **b**, If disorder in the form of 'speckled' light is added to the diffraction pattern, the centres of altered refractive index are no longer triangular, but have arbitrary shapes. As more and more speckled light is added, the output pulse becomes gradually more localized in the plane transverse to the direction of propagation.

information would simply diffract, scatter and escape from the medium.

The authors introduced disorder into their transverse periodic structure by adding 'speckled' light. They created this by passing a laser beam through a diffuser whose pattern was linked to the interference pattern of the pump beams. The level of disorder in the lattice, from perfectly periodic to strongly disordered, was set by the intensity of the speckled beam. Once all this was set up, the authors launched a 'probe beam' into the disordered photonic crystal to monitor the image-intensity distribution at the lattice output.

When there was no transverse disorder, Schwartz *et al.* recorded[1] ballistic light transport through the lattice, in the form of a perfectly reproduced hexagonal intensity pattern (Fig. 1a). When transverse disorder was introduced, however, this patterning disappeared, to be gradually replaced by a single, ever-narrower exponential tail distribution at high disorders — a characteristic of Anderson-type localization (Fig. 1b). Extensive and elegant averaging over many different experiments unravelled the underlying evolution of the light transport processes, from diffusive transport among the lattice sites at moderate disorder through to localization at higher disorder.

So far, so expected. But certain aspects of Schwartz and colleagues' experiments make it worthy of special note. The first is that, whereas the original Anderson localization dealt with the evolution in time of a wave-packet[2], here that evolution takes place in space, as the light travels through the third 'free' dimension perpendicular to the disordered plane. The way in which light evolves in the free dimension under these circumstances has previously been shown to mimic the time evolution implied by the equation describing a light wave[11]. Second, this is the first observation of light localization in 'real time', rather than its deduction from optical transmission spectroscopy[7,8].

The third aspect of note is that there is the possibility, when working with the kind of nonlinear optical dielectric used by Schwartz *et al.*, of seeing interesting effects such as 'self-focusing'. In this effect, the diameter of an incident laser beam becomes thinner, because its more intense central part sharply increases the refractive index of the region of the medium it is passing through, thus turning the beam in on itself. By increasing the intensity of the probe beam, the authors could for the first time study the interplay of Anderson light localization and nonlinear effects. This interplay does not exist in electron transport, so it really is an exciting development. Specifically, it seems that in the presence of positive, or attractive, nonlinearity (such as that which causes self-focusing), localization is enhanced and occurs at lower disorder. That much is not unpredictable. In contrast, the influence of a negative, or repulsive, nonlinearity, also touched on by Schwartz and colleagues, is truly unpredictable. For this reason, their work[1] will no doubt spur on many further experimental and theoretical studies. ■

Z. Valy Vardeny and Mikhail Raikh are in the Department of Physics, University of Utah, Salt Lake City, Utah 84112, USA.
e-mails: val@physics.utah.edu; raikh@physics.utah.edu

1. Schwartz, T. *et al. Nature* **446,** 52–55 (2007).
2. Anderson, P. W. *Phys. Rev.* **109,** 1492–1505 (1958).
3. John, S. *Phys. Rev. Lett.* **53,** 2169–2172 (1984).
4. Anderson, P. W. *Phil. Mag. B* **52,** 505–509 (1985).
5. Van Albada, M. P. & Lagendijk, A. *Phys. Rev. Lett.* **55,** 2692–2695 (1985).
6. Wolf, P. W. & Maret, G. *Phys. Rev. Lett.* **55,** 2696–2699 (1985).
7. Wiersma, D. S. *et al. Nature* **390,** 671–673 (1997).
8. Chabanov, A. A. *et al. Nature* **404,** 850–853 (2000).
9. John, S. *Phys. Rev. Lett.* **58,** 2486–2489 (1987).
10. Yablonovitch, E. *Phys. Rev. Lett.* **58,** 2059–2062 (1987).
11. De Raedt, H. *et al. Phys. Rev. Lett.* **62,** 47–50 (1988).

CELL BIOLOGY

Aneuploidy and cancer

David Pellman

Aneuploidy is the condition in which a cell has extra or missing chromosomes, and is often associated with tumours. But whether it is a cause or a consequence of cancer remains a vexed question.

Aneuploid cancers are like Tolstoy's unhappy families: each aneuploid cancer has its own particular abnormal chromosome content, and thus its own abnormal characteristics. This variability has long frustrated biologists trying to establish whether aneuploidy is a cause or a consequence of malignant transformation. Two papers in *Cancer Cell*[1,2] advance the argument for 'cause', but with qualifications.

There are two ways in which cells can become aneuploid: they can develop alterations in the number of intact chromosomes, which is known as whole-chromosome aneuploidy and originates from errors in cell division (mitosis); and they can undergo rearrangements in chromosome structure — deletions, amplifications or translocations — that arise from breaks in DNA. Such rearrangement is a well-established cause of tumour development. By contrast, the contribution of whole-chromosome aneuploidy to cancer is the subject of controversy.

Weaver *et al.*[2] studied a line of genetically engineered mice that tend to gain or lose whole chromosomes with each cell division because of a defect in mitosis. These mice are heterozygous for the *Cenp-e* (centromere protein E) gene — that is, they have only one functional copy. This gene encodes a motor protein that is involved in aligning chromosomes normally on the mitotic spindle[3,4], and complete loss of the gene is lethal. Heterozygous cells, however, have only partly defective mitotic spindles and are viable, but develop whole-chromosome aneuploidy more frequently than normal cells (Fig. 1a). The CENP-E protein has roles not only in chromosome segregation, but also in modulating the spindle checkpoint[4], which is a signalling system that senses spindle defects and delays mitosis to prevent errors in chromosome segregation. Thus, loss of CENP-E is a double whammy: cells make more mistakes and fail to respond to them properly.

Mutations in spindle-checkpoint genes have been shown to promote aneuploidy and tumorigenesis[4,5]. But the signalling molecules investigated in these studies might have had functions other than modulating the checkpoint. This reservation also applies in part to work with *Cenp-e* (ref. 6), although loss of the protein should have a more restricted effect on mitosis because CENP-E has a direct role in chromosome segregation and is expressed only in dividing cells — specifically during mitosis.

Weaver *et al.*[2] found that mice with compromised CENP-E did indeed develop cancer, accompanied by an age-dependent increase in whole-chromosome aneuploidy. In contrast with control strains, at 19–21 months of age — old age for a mouse — 10% of the *Cenp-e*-heterozygous animals developed splenic lymphomas, and were three times more likely to develop benign lung tumours. These findings provide additional support for Theodor Boveri's much-discussed but still-unproved theory[7] that aneuploidy promotes tumorigenesis.

However, there are qualifiers. Weaver *et al.* also found that *Cenp-e* heterozygosity inhibited tumorigenesis in animals that lacked a tumour-suppressor gene known as *p19/ARF*. *In vitro* experiments further supported the conclusion that aneuploidy due to compromised CENP-E generally inhibits cell growth, but could also increase the frequency of rare transforming events.

At first glance, these observations seem complex, but the results in fact dovetail neatly with work on genetic instability and cells' ability to acquire new traits[8]. Chromosomal instability can increase the frequency both of growth-promoting mutations that could initiate cancer, and of deleterious mutations that could block cell growth or trigger cell death. The outcome depends on factors such as the population size of the cells at risk, the frequency of growth-promoting mutations relative to deleterious mutations, and the degree of dominance of these

mutations. A similar evolutionary balancing act is evident from work on telomere attrition[9] — the erosion of the ends of chromosomes.

Weaver and colleagues' experiments aptly illustrate the basic principles through which aneuploidy can affect tumorigenesis. But we are still left asking the question of how aneuploidy arises in human cancers. Sotillo *et al.*[1] extended previous work by their own group and collaborators[10] to suggest a general mechanism.

Hernando *et al.*[10] reported that the expression of the spindle-checkpoint protein Mad2 is inhibited by the retinoblastoma tumour-suppressor (Rb) pathway. During early G1 phase of the cell cycle, Rb inhibits members of the E2F family of gene-transcription factors. Then, before the ensuing S phase, Rb is itself inactivated, freeing the E2F proteins to activate their target genes. The authors showed[10] that Rb-pathway inhibition induces E2F-dependent transcription of Mad2, causing a partial blockade of mitosis and eventually resulting in tetraploid cells (with doubled chromosome content) and aneuploid cells (Fig. 1b). The Rb pathway is compromised in most human cancers, and the authors found that Mad2 was overexpressed in a variety of human cancers. This provided a satisfyingly simple link between malignant transformation and aneuploidy. But it remained unclear whether the resulting aneuploidy promoted tumour development, or whether it was just a passive consequence of Rb loss.

Sotillo *et al.*[1] answer this question by generating mice in which Mad2 is overexpressed. More than 50% of the mice developed a wide range of tumours, and, of these, those analysed had extensive chromosomal rearrangements. Unlike many signalling molecules that promote cancer, shutting off Mad2 after tumours had formed had no effect on tumour growth, supporting the view that Mad2 overexpression acts early to promote tumour formation, probably by triggering genetic instability. Although the main effect was enhanced tumorigenesis, tissue degeneration also occurred. Thus, as with *Cenp-e*-heterozygous mice, Mad2 overexpression can produce mutagenesis and cancer, or growth arrest and cell death.

What tips the balance causing Mad2 overexpression to favour tumorigenesis, whereas CENP-E loss pushes cells more towards cell death? It is tempting to pin the difference on how these genetic alterations produce aneuploidy. Mad2 overexpression blocks an essential step in cell division, the separation of sister chromatids, which — after a half-hearted attempt at mitosis — often results in the formation of tetraploid cells (Fig. 1b). Tetraploidy facilitates the development of cancer; and tetraploid-cell-derived tumours have both whole-chromosome aneuploidy and chromosomal rearrangements[11]. By contrast, heterozygous loss of *Cenp-e* results in the gain and loss of intact chromosomes, at least *in vitro*, without inducing failed cytokinesis (failed separation of the daughter cells) and tetraploidy[12]. The extra chromosomes in tetraploid cells may buffer the effects of deleterious mutations, allowing cells to survive until they acquire growth-promoting mutations. Tetraploidy might also increase the frequency of growth-promoting mutations if it acts in animal cells, as in yeast[13], to promote gross chromosomal rearrangements.

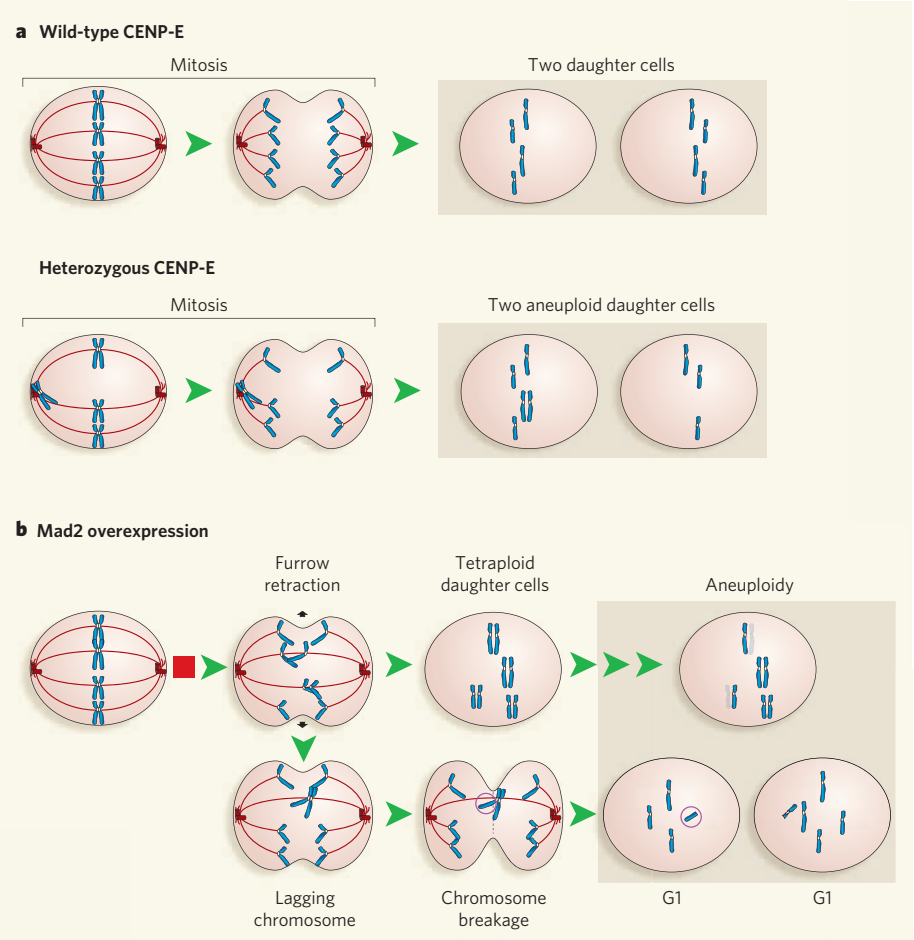

Figure 1 | Different routes to aneuploidy. a, In wild-type cells, each daughter cell inherits one copy of a chromosome after mitosis (top panel). However, in CENP-E-deficient cells, sister chromatids of some chromosomes do not separate, resulting in whole-chromosome aneuploidy (bottom panel). **b**, Overexpression of Mad2, which results in a delay in mitosis and entrapment of chromosomes in the cleavage furrow, can lead to aneuploidy in two ways. Furrow retraction can result in failure of cytokinesis and thus tetraploidy, with subsequent errors in the division of tetraploid cells causing aneuploidy (top panel). Alternatively, incomplete separation of chromosomes, with a lagging chromosome, might lead to chromosome breakage during cytokinesis (bottom panel); but how frequently this might occur, and the underlying mechanism, are not known.

Alternatively, Mad2 overexpression might lead more directly to DNA breaks. Partly separated chromatids generated by Mad2 overexpression may be trapped in the furrow between dividing cells, then broken during cytokinesis[1]. Finally, Mad2 overexpression could induce tumours by mechanisms unrelated to its role in the spindle checkpoint. Given the widespread overexpression of Mad2 in human cancers, this will clearly be the subject of future work.

Together, these studies help to move us beyond the question of whether aneuploidy causes cancer. They show that, like other types of genetic instability, cancer is a potential, but not obligatory, outcome of aneuploidy. The challenge for the future will be to define how different paths to aneuploidy, different cell types and different genetic contexts combine to determine whether aneuploidy leads to cell death or cancer. ■

David Pellman is at the Dana-Farber Cancer Institute, Children's Hospital, Harvard Medical School, Boston, Massachusetts 02115, USA.
e-mail: david_pellman@dfci.harvard.edu

1. Sotillo, R. *et al. Cancer Cell* **11,** 9–23 (2007).
2. Weaver, B. A., Silk, A. D., Montagna, C., Verdier-Pinard, P. & Cleveland, D. W. *Cancer Cell* **11,** 25–36 (2007).
3. Kapoor, T. M. *et al. Science* **311,** 388–391 (2006).
4. Kops, G. J., Weaver, B. A. & Cleveland, D. W. *Nature Rev. Cancer* **5,** 773–785 (2005).
5. Baker, D. J., Chen, J. & van Deursen, J. M. *Curr. Opin. Cell Biol.* **17,** 583–589 (2005).
6. Abrieu, A., Kahana, J. A., Wood, K. W. & Cleveland, D. W. *Cell* **102,** 817–826 (2000).
7. Boveri, T. *The Origin of Malignant Tumors* (Williams & Wilkins, Baltimore, 1914).
8. Rajagopalan, H., Nowak, M. A., Vogelstein, B. & Lengauer, C. *Nature Rev. Cancer* **3,** 695–701 (2003).
9. Maser, R. S. & DePinho, R. A. *Science* **297,** 565–569 (2002).
10. Hernando, E. *et al. Nature* **430,** 797–802 (2004).
11. Fujiwara, T. *et al. Nature* **437,** 1043–1047 (2005).
12. Weaver, B. A., Silk, A. D. & Cleveland, D. W. *Nature* **442,** E9–E10 (2006).
13. Storchova, Z. *et al. Nature* **443,** 541–547 (2006).

CLIMATE MODELLING

Uncertainty in climate-sensitivity estimates

Arising from: G. C. Hegerl, T. J. Crowley, W. T. Hyde & D. J. Frame *Nature* **440,** 1029–1032 (2006)

Based on reconstructions of past temperatures from proxy data, Hegerl *et al.*[1] estimate a confidence interval for climate sensitivity that suggests a substantially reduced probability of very high climate sensitivity compared with previous empirical estimates. Here I show that the inference procedure used by Hegerl *et al*. neglects uncertainties in temperature reconstructions and in the estimated climate sensitivity and can even be used to infer that the climate sensitivity is zero with vanishing uncertainty. Similar procedures based on temperature reconstructions from proxy data generally underestimate uncertainties in climate sensitivity.

Hegerl *et al.*[1] relate a given univariate time series, θ_i, composited from climate proxies, to a time series, T_i, of mean temperatures by using an errors-in-variables model

$$T_i - \langle T\rangle = \beta(\theta_i - \langle\theta\rangle + \eta_i) + \varepsilon_i \qquad (1)$$

with regression coefficient β and uncorrelated errors η_i and ε_i with zero mean and variances σ_η^2 and σ_ε^2. The subscript i indexes time, and $\langle\cdot\rangle$ denotes a temporal mean. Estimating the mean values $\langle T\rangle$ and $\langle\theta\rangle$ by sample means $\bar{T}$ and $\bar{\theta}$, Hegerl *et al.* obtain an estimate $\hat{\beta}$ of the regression coefficient β from a calibration period in which proxy data, θ_i, and instrumental temperature data, T_i, overlap. With model (1) and the estimated parameters, they infer expected values of past temperature anomalies ("reconstructed temperature anomalies") as $\hat{T}_i'(\hat{\beta}) = \hat{\beta}\,(\theta_i - \bar{\theta})$, given proxies θ_i in a reconstruction period. They then simulate temperature anomalies, $\hat{T}_i'$ (EBM), with an energy-balance model (EBM) for a range of forcing and model parameters including the climate sensitivity and determine the likelihoods of the temperature-anomaly time series $\hat{T}_i'(\hat{\beta})$ given EBM parameters from the sum of squares of the residuals $r_i(\hat{\beta}) = \hat{T}_i'(\mathrm{EBM}) - \hat{T}_i'(\hat{\beta})$. From these likelihoods, varying $\hat{\beta}$ within estimated confidence intervals, they obtain the marginal distribution of climate sensitivities that led to the conclusion of a reduced probability of high climate sensitivity.

Because this procedure treats reconstructed temperature anomalies, $\hat{T}_i'(\hat{\beta})$, as if they were known temperature anomalies, taking into account uncertainty only in $\hat{\beta}$, it neglects uncertainties in reconstructed temperature anomalies that contribute to uncertainties in the estimated climate sensitivity. The procedure does not take into account the uncertainties in reconstructed temperature anomalies $\hat{T}_i'(\hat{\beta})$ that arise because the mean values $\bar{T}$ and $\bar{\theta}$ are estimated rather than known and the uncertainties reflected in the error terms ε_i and η_i in model (1). (As a result, the estimated margins of error of reconstructed temperature anomalies vanish if the temperature anomalies vanish; see Table S1 of Hegerl *et al.*[1].)

What should enter the calculation of the likelihoods of the temperature-anomaly time series $\hat{T}_i'(\hat{\beta})$ is the estimated variance of the residuals $r_i(\hat{\beta})$, not just the sample variance proportional to their sum of squares, $\Sigma_i r_i^2$. In addition to the contribution taken into account by Hegerl *et al.*[1] — the contribution associated with the variance $\mathrm{var}(\hat{\beta})$ of the regression-coefficient estimate — a variance associated with the sample means and the variance $\beta^2\sigma_\eta^2 + \sigma_\varepsilon^2$ of the error terms, contribute to the residual variance. The error variance $\beta^2\sigma_\eta^2 + \sigma_\varepsilon^2$ would contribute to the residual variance even if the parameters β, $\langle\theta\rangle$ and $\langle T\rangle$ were known, which demonstrates that the unaccounted variance contribution is generally non-zero, irrespective of how parameters are estimated. Adding estimates of the unaccounted variances to the sample variance of the residuals does not affect the combination of EBM parameters that minimize the residual variance, but it does affect uncertainty estimates by increasing the minimum residual variance. It is inconsistent to estimate temperature variances as sample variances from the reconstructed anomalies $\hat{T}_i'(\hat{\beta})$ as if they were known anomalies while modelling temperatures according to model (1) (ref. 2). If an inference procedure for instrumental temperatures is used for reconstructed temperatures, the additional variance contributions must be taken into account to avoid underestimation of variances and uncertainties.

As an example of how the procedure used by Hegerl *et al.* leads to underestimation of uncertainties in climate sensitivity, consider a hypothetical proxy time series that is constant and equal to the sample mean $\theta_i = \bar{\theta}$ in the reconstruction period and is otherwise arbitrary. The reconstructed temperature anomalies, $\hat{T}_i'(\hat{\beta})$, are zero for any $\hat{\beta}$. It follows that the sample variance ($\propto \Sigma_i r_i^2$) of the residuals $r_i(\hat{\beta})$ between the reconstructed and simulated temperature anomalies is minimized and is equal to zero for zero climate sensitivity and any value of the forcing parameters (provided that the EBM simulation yields vanishing temperature anomalies for zero climate sensitivity, which can always be achieved with the normalizations of Hegerl *et al.*). For non-zero climate sensitivity, which leads to non-zero residuals, the procedure of Hegerl *et al.* gives a vanishing likelihood of the corresponding time series of reconstructed temperature anomalies, $\hat{T}_i'(\hat{\beta})$. The result for the reconstruction period would be an estimate of zero climate sensitivity with probability one — that is, without any uncertainty. If, additionally, instrumental temperature data in the calibration period are taken into account to estimate climate sensitivity, their relative influence can be made arbitrarily small by extending the hypothetical proxy time series into the distant past, leaving the result of zero climate sensitivity with vanishing uncertainty unchanged.

Even if the inferential errors are corrected, similar procedures based on temperature reconstructions from proxy data generally underestimate uncertainties in reconstructed temperatures and hence in climate sensitivity. Climate proxies are often selected on the basis of their correlations with instrumental temperature data, as in the reconstruction[3] underlying the analysis of Hegerl *et al.*[1]. Using such proxies in regression models to reconstruct past temperatures leads to selection bias[4], resulting in an overestimation of the correlation between proxies and temperatures and an underestimation of uncertainties. There are also structural uncertainties: in the structure of the regression model used to reconstruct temperatures (for example, error terms may be correlated if there are non-climatic, low-frequency variations of proxies) and in the structure of the EBM. Hegerl *et al.* acknowledge such structural uncertainties but do not scrutinize them quantitatively. The structural uncertainties may be large compared with the parametric uncertainties taken into account in the inference procedure[5].

For these reasons, uncertainties in temperature reconstructions and climate sensitivity are greater than those given by Hegerl *et al.*[1].

Tapio Schneider
California Institute of Technology, Pasadena, California 91125-2300, USA
e-mail: tapio@caltech.edu

1. Hegerl, G. C., Crowley, T. J., Hyde, W. T. & Frame, D. J. *Nature* **440,** 1029–1032 (2006).
2. Little, R. J. A. & Rubin, D. B. *Statistical Analysis with Missing Data* 2nd edn (Wiley, New York, 2002).
3. Hegerl, G. C. *et al. J. Climat.* (in the press).
4. Miller, A. J. *J. R. Statist. Soc. A* **147,** 389–425 (1984).
5. Draper, D. *J. R. Statist. Soc. B* **57,** 45–97 (1995).

Received 19 May 2006; accepted 13 December 2006.
Competing financial interests: declared none.
doi:10.1038/nature05707

CLIMATE MODELLING

Hegerl et al. *reply*

Replying to: T. Schneider *Nature* **446,** doi:10.1038/nature05707 (2007)

Despite Schneider's claim[1], the method we use to estimate equilibrium climate sensitivity from multiple proxy-based reconstructions of the temperature in the Northern Hemisphere[2] does account for uncertainty in reconstructions, including that associated with non-temperature and sampling error in the reconstruction. We arrive at a tighter constraint on climate sensitivity not by neglecting uncertainties, but by combining our wide-tailed proxy-based estimate with an independent estimate of climate sensitivity based on twentieth-century warming.

Schneider maintains that incomplete treatment of uncertainties in proxy reconstructions in our estimate yields an overly narrow estimate of equilibrium climate sensitivity[1]. This impression may have been caused by an inconsistency between the reconstruction erroneously attached to the Supplementary Information of ref. 2, which contained only uncertainty in the amplitude of the reconstruction, and its caption, which referred to both amplitude and sampling uncertainty (this error has now been corrected).

We account for uncertainty in temperature reconstructions as fully as possible. Our estimate of climate sensitivity is based on the sample variance of the residual T_i (using Schneider's terminology) between the proxy reconstruction and energy-balance model (EBM) simulations in response to external forcing. We estimate the probability that the difference between the minimum mean-squared residual and that the residual for any other parameter combination is due to noise by using the statistics $\Sigma_i r_i(\text{parameter})^2 - \Sigma_i r_{i,\min} / \bar{v}ar(r_{i,\min})$ (refs 2, 3).

The residual variance is a sum of the sampled variances of internal climate variability, of non-temperature and spatial sampling noise of the reconstruction η_i, and of model error, which varies with model parameters. Therefore η_i, as sampled in each reconstruction (over hundreds of years), is part of the total residual variance and is accounted for in our estimate. Reconstructions with larger η_i yield larger residual variances, resulting in wider probability density functions for climate sensitivity. Our overall estimate of climate sensitivity from the last millennium is based on several reconstructions, which should have largely independent realizations of η_i, thus reducing dependence of our estimate on a particular realization of η_i.

Furthermore, the hypothetical example given by Schneider[1] assumes a reconstruction that has zero variance over the reconstruction period, while varying randomly over the period of overlap with instrumental data. This example would yield numerical degeneracy in the statistic given here, whereas related examples with small preindustrial variance and poor correlations over the calibration period would yield very wide estimates of climate sensitivity owing to large uncertainty in β. Schneider's example violates the assumption that the relationship between proxy data and target of reconstruction can be estimated from the calibration period. It bears no resemblance to reconstructions used here, where the correspondence to (independently reconstructed) forcing is a strong indication that the reconstructions have skill over the pre-instrumental period[4].

We stress that our overall result of a tighter constraint on climate sensitivity does not arise from palaeoclimatic reconstructions alone, which yield a very wide-tailed probability density function (see Fig. 3a of ref. 2). The tighter constraint arises from combining that estimate with an independent estimate of climate sensitivity based on climate change in the late twentieth century. As our sensitivity probability density function also broadly agrees with other, at least partly independent, evidence that we have not used[5,6], we think that our estimate is conservative and valid, despite remaining uncertainties.

Gabriele C. Hegerl*, Thomas J. Crowley†, William T. Hyde† & David J. Frame‡

*Division of Earth and Ocean Sciences, Nicholas School of the Environment and Earth Sciences, Duke University, Durham, North Carolina 27708, USA

e-mail: hegerl@duke.edu

†Present address: Department of Physics, University of Toronto, Toronto M5S 1A7, Canada

‡Climate Dynamics Group, Department of Physics, University of Oxford, Oxford OX1 3PU, UK

1. Schneider, T. *Nature* **446,** doi: 10.1038/nature05707 (2007).
2. Hegerl, G. C., Crowley, T. J., Hyde, W. T. & Frame, D. J. *Nature* **440,** 1029–1032 (2006).
3. Forest, C. E., Stone, P. H., Sokolov, A. P., Allen, M. R. & Webster, M. D. *Science* **295,** 113–117 (2002).
4. Hegerl, G. C. *et al. J. Climat.* **20,** 650–666 (2007).
5. Annan, J. D. & Hargreaves, J. C. *Geophys. Res. Lett.* **33,** L06704 (2006).
6. Schneider von Deimling, T., Held, H., Ganopolski, A. & Rahmstorf, S. *Climat. Dynam.* **27,** 149–163 (2006).

doi:10.1038/nature05708

ARTICLES

CD38 is critical for social behaviour by regulating oxytocin secretion

Duo Jin[1,2]*, Hong-Xiang Liu[1,2]*, Hirokazu Hirai[1,5,6]*, Takashi Torashima[4,5], Taku Nagai[7], Olga Lopatina[1,2], Natalia A. Shnayder[1,2], Kiyofumi Yamada[1,7], Mami Noda[9], Toshihiro Seike[9], Kyota Fujita[9], Shin Takasawa[10], Shigeru Yokoyama[1,2], Keita Koizumi[1,2,5], Yoshitake Shiraishi[3], Shigenori Tanaka[3], Minako Hashii[2], Toru Yoshihara[1,5], Kazuhiro Higashida[2], Mohammad Saharul Islam[1,2], Nobuaki Yamada[1,5], Kenshi Hayashi[2,12], Naoya Noguchi[10], Ichiro Kato[14], Hiroshi Okamoto[11], Akihiro Matsushima[15], Alla Salmina[16], Toshio Munesue[13], Nobuaki Shimizu[8], Sumiko Mochida[17], Masahide Asano[1,5] & Haruhiro Higashida[1,2,4]

CD38, a transmembrane glycoprotein with ADP-ribosyl cyclase activity, catalyses the formation of Ca^{2+} signalling molecules, but its role in the neuroendocrine system is unknown. Here we show that adult CD38 knockout ($CD38^{-/-}$) female and male mice show marked defects in maternal nurturing and social behaviour, respectively, with higher locomotor activity. Consistently, the plasma level of oxytocin (OT), but not vasopressin, was strongly decreased in $CD38^{-/-}$ mice. Replacement of OT by subcutaneous injection or lentiviral-vector-mediated delivery of human CD38 in the hypothalamus rescued social memory and maternal care in $CD38^{-/-}$ mice. Depolarization-induced OT secretion and Ca^{2+} elevation in oxytocinergic neurohypophysial axon terminals were disrupted in $CD38^{-/-}$ mice; this was mimicked by CD38 metabolite antagonists in $CD38^{+/+}$ mice. These results reveal that CD38 has a key role in neuropeptide release, thereby critically regulating maternal and social behaviours, and may be an element in neurodevelopmental disorders.

CD38 has been identified as a transmembrane receptor that triggers proliferation and immune responses in lymphocytes and is used as a malignancy or differentiation marker in leukaemia or HIV infection[1–3]. CD38 is also present in many tissues other than haematopoietic cells, including the brain and pancreas[1,4,5]. It can catalyse the formation of cyclic ADP-ribose (cADPR) and nicotinic acid adenine dinucleotide phosphate (NAADP) by ADP-ribosyl cyclase from NAD^+ and NAD phosphate[1,4–8]. cADPR and NAADP mobilize Ca^{2+} from ryanodine-sensitive intracellular Ca^{2+} stores in the endoplasmic reticulum or other pools located in lysosomes or secretory granules, and thus act as second messengers[1,4–12]. Although the CD38-dependent cADPR or NAADP signalling pathway of Ca^{2+} regulation has been shown in cultured anterior pituitary tumour cells[13,14], information on posterior pituitary (neurohypophysial) hormone function has not yet been described.

Oxytocin (OT) and arginine vasopressin (AVP), which belongs to the same posterior pituitary hormone family, are secreted into the blood stream from axon terminals or into the brain from dendrites of hypothalamic neurons[15]. These peptides regulate the function of peripheral target organs, such as uterine contraction, lactation, penile erection, and urine concentration[15–17], but they also exert many behavioural effects via the amygdala and other brain regions[18–20]. In particular, OT seems to modulate a wide range of sexual and social behaviours from social recognition, pair bonding, mate guarding and parental care in rodents, to love, trust or fear in humans[18–25]. Pharmacological studies indicate that OT administration may facilitate social recognition in rats[26] and increase feelings of trust in healthy human males[23], or reduce repetitive behaviour in autistic and Asperger's disorders[27]. Mice that are mutant for the OT gene[28] and OT receptor gene[29] failed to develop social memory or maternal care. Thus, the OT signalling system is believed to be a neurobiological basis for attachment[19,22,30] and is thought to have some relationship to human diseases associated with abnormal social behaviour[31].

Depolarization–secretion coupling of OT release has been reported in both somato-dendritic and neurohypophysial terminals of hypothalamic neurons[15,32,33]. Although Ca^{2+} release from intracellular Ca^{2+} stores is involved in the stimulated OT release[33,34], Ca^{2+} signalling mechanisms underlying OT secretion are not fully understood. To assess this, we used mice with CD38 gene disruption ($CD38^{-/-}$)[11], and show that CD38-dependent cADPR- and NAADP-sensitive intracellular Ca^{2+} mobilization has a key role in OT release from soma and axon terminals of hypothalamic neurons, with profound consequential changes in social behaviours. Alteration of CD38 function and the resultant disturbance of OT secretion may explain some forms of impaired human behaviour in the spectrum of autism disorders.

Defects in maternal nurturing in $CD38^{-/-}$ mice

$CD38^{-/-}$ mice apparently grow normally and are viable and healthy[11] (Supplementary Fig. 1), but showed a significantly greater

[1]Kanazawa University 21st Century COE Program on Innovative Brain Science on Development, Learning and Memory, Kanazawa 920-8640, Japan. [2]Department of Biophysical Genetics, and [3]Department of Anatomy, and [4]Department of Cellular Neurophysiology, Kanazawa University Graduate School of Medicine, Kanazawa 920-8640, Japan. [5]Advanced Science Research Center, Kanazawa University, Kanazawa 920-8640, Japan. [6]SORST, Japan Science and Technology Agency (JST), Kanazawa 920-8640, Japan. [7]Laboratory of Neuropsychopharmacology, School of Natural Science and Technology, and [8]Institute of Nature and Environmental Technology, Kanazawa University, Kanazawa 920-1192, Japan. [9]Laboratory of Pathophysiology, Graduate School of Pharmaceutical Sciences, Kyushu University, Fukuoka 812-8582, Japan. [10]Department of Biochemistry, and [11]Department of Advanced Biological Sciences for Regeneration, Tohoku University Graduate School of Medicine, Sendai 980-8575, Japan. [12]Central Clinical Laboratory, and [13]Department of Psychiatry, Kanazawa University Hospital, Kanazawa 920-8641, Japan. [14]Department of Biochemistry, Toyama University School of Medicine, Toyama 930-0194, Japan. [15]Nanao National Hospital, Nanao 920-8531, Japan. [16]Department of Biochemistry and Medical Chemistry, Krasnoyarsk State Medical Academy, Krasnoyarsk 660022, Russia. [17]Department of Physiology, Tokyo Medical University, Tokyo 160-8402, Japan.
*These authors contributed equally to this work.

locomotor activity than their wild-type ($CD38^{+/+}$) littermates (Supplementary Fig. 2). The $CD38^{-/-}$ mice, however, showed no or few abnormalities in emotional behaviours such as anxiety and fear (Supplementary Fig. 3), except for a change in maternal behaviour when we monitored the responses of postpartum dams whose 6–14-day-old pups were returned to them after a 10 min separation (Fig. 1). A dam was put in a corner of a cage and her three pups were placed in different corners of the same cage. We then examined how the female retrieved them during 20 min (Fig. 1a). The wild-type dam approached the first pup after a very short latency, retrieved it to her corner and crouched over it; she subsequently collected all the pups with equally short latencies (Fig. 1b, c), and crouched over them for a long time to keep them warm and to nurse them (Fig. 1e, f). A CD38 mutant mother, however, approached the three pups infrequently and irregularly during supervision, though she could observe and sniff them (Fig. 1d). Thus, $CD38^{-/-}$ dams showed a longer latency to retrieve the pups with a significantly shorter duration of crouching (Fig. 1e, f). We also confirmed abnormal behaviour by mutant mothers with their newborn pups in their home cages (Supplementary Fig. 4). These results clearly show the mother's abnormal nurturing behaviour in $CD38^{-/-}$ postpartum mice. Eventually the mothers fed the pups sufficiently well for them to grow to the same weight as the control pups (Supplementary Fig. 1b), although the weaning rate was slightly lower in $CD38^{-/-}$ mice (83%) than that of control mice (96%).

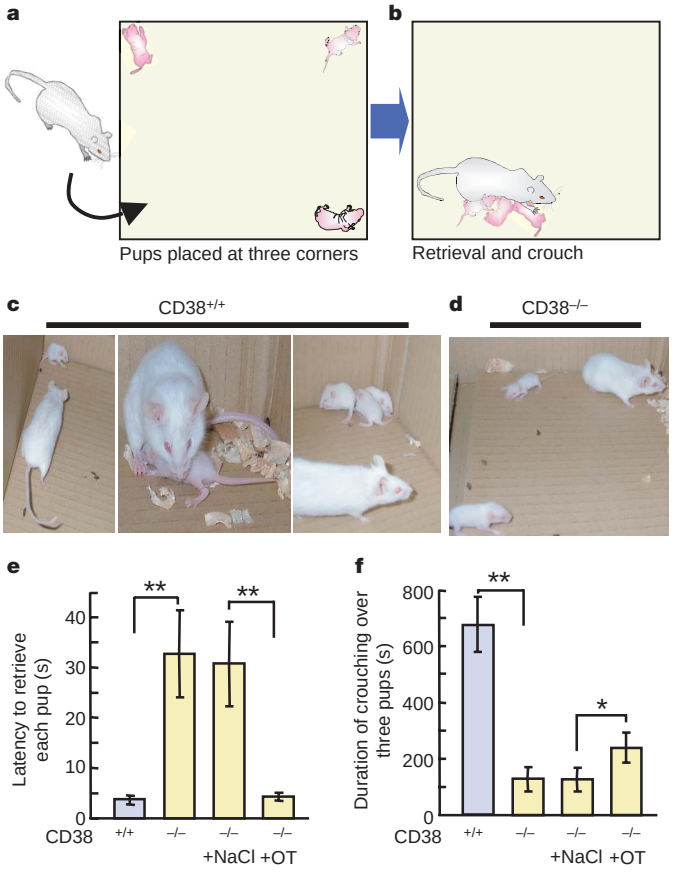

Figure 1 | Nurturing behaviour is impaired in $CD38^{-/-}$ mothers. **a**, **b**, Diagrams showing nurturing analysis of postpartum females. A mother was deprived of her pups from her first litter for 10 min and then re-challenged with three pups placed individually in the corners of her cage (**a**). The mother retrieves them into her nest and crouches over them to nurture (**b**). Typical behaviour of a $CD38^{+/+}$ mother shown approaching one pup immediately (**c**, left panel) and retrieving it to her corner and crouching over it (**c**, centre panel) or collecting all three pups in one corner within a short latency (**c**, right panel). **d**, A $CD38^{-/-}$ mother typically ignores the pup and does not retrieve immediately. **e**, Latency to retrieve each pup by maternal $CD38^{+/+}$ or $CD38^{-/-}$ mice, and by maternal $CD38^{-/-}$ mice treated with subcutaneous injection of 0.4 ml saline or 3 ng oxytocin (OT) per kg body weight. **f**, Time spent crouching over all three pups in the nest by the same set of mothers. $^{*}P < 0.05$; $^{**}P < 0.01$. $N = 6$ wild types and $N = 10$ mutants. Error bars, s.e.m.

Amnesia in social memory in $CD38^{-/-}$ mice

Impaired maternal nurturing was recently reported in OT-receptor-deficient mice[29]. The OT receptor and OT gene knockout male mice fail to develop social familiarity[28,29]. This depends predominantly on olfactory cues and can critically influence reproductive success[35]. It can be identified as a consistent decrease in olfactory investigation during repeated or prolonged encounters with a conspecific female[28], if tested as in Fig. 2a. $CD38^{+/+}$ mice showed a significant decline in the time spent investigating a female on subsequent presentations of the same female in trials 3 and 4, as compared with trial 1 (Fig. 2b). This decrease was not due to a general decline in olfactory investigation, because presentation of a novel female during trial 5 resulted in a similar amount of investigation as trial 1 with the original female. In contrast, $CD38^{-/-}$ males showed sustained high levels of investigation at each encounter with the same female and

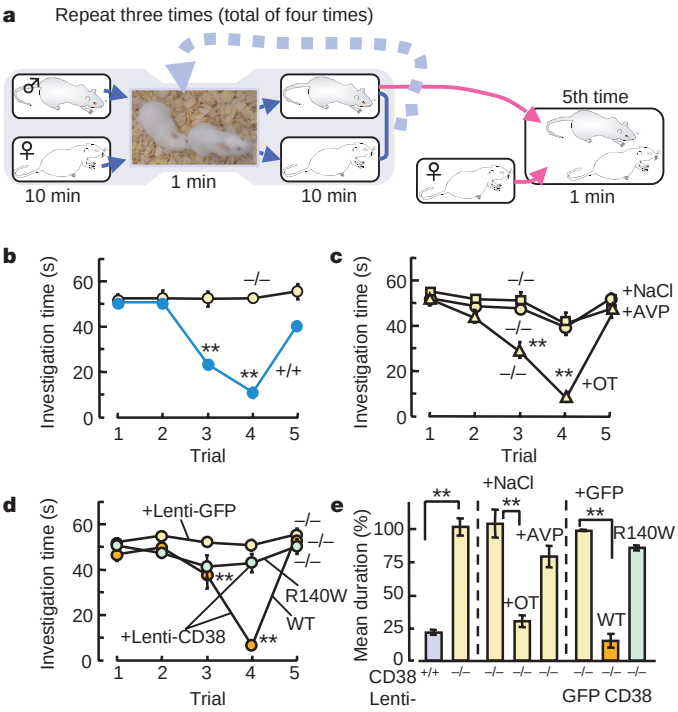

Figure 2 | Social recognition deficit in $CD38^{-/-}$ male mice. **a**, Olfactory investigation in $CD38^{-/-}$ mice used for social recognition test. Social memory by male mice was measured as a difference in anogenital investigation. Data depict mean ± s.e.m. for the amount of time allocated to investigating the same female during each of four successive 1-min trials. A fifth dis-habituation trial depicts the response of males to the presentation of a new female in a 1-min pairing 10 min after the fourth trial. **b**, Investigation time allocated to investigation of $CD38^{-/-}$ (yellow circle) and $CD38^{+/+}$ (blue circle) male mice. $^{**}P < 0.01$ for a significant decrease between each trial compared with the first trial. **c**, Olfactory investigation of $CD38^{-/-}$ males as in **b**. A single subcutaneous shot of 0.3 ml saline (NaCl, circles), OT (10 ng kg^{-1}; triangles) or vasopressin (AVP; 10 ng kg^{-1}; squares) to $CD38^{-/-}$ males was administered 10 min before the first pairing. $^{**}P < 0.01$ for a significant decrease between each trial compared with the first trial. **d**, The social recognition deficit and its rescue by lenti-GFP (yellow), lenti-R140W-CD38 (green) and lenti-CD38 (red) infection in male $CD38^{-/-}$ mice. **e**, Mean duration (per cent) of olfactory investigation of male mice in the fourth meeting relative to the first meeting with the same female in the tree different types of experiments from **b**–**d**. $^{**}P < 0.01$ compared with controls. $N = 6$–10 mice in each experiment. Error bars, s.e.m.

the same level of investigation when presented with a new female at trial 5 (Fig. 2b). CD38$^{-/-}$ mice did not have deficits in either olfactory guided foraging or habituation to a non-social olfactory stimulus as tested by the preference ratio of consumption of isovaleric acid solution in their drinking water (Supplementary Fig. 5). Furthermore, CD38 mutants trained in the passive avoidance test were able to learn the shock experience as well as wild-type animals (Supplementary Fig. 6), suggesting no global cognitive dysfunction. Therefore, it can be concluded that CD38$^{-/-}$ males with persistent interest during repeated presentations fail to develop their social memory, resembling a memory deficit found in OT gene or OT receptor knockout mice[28,29].

Plasma oxytocin and vasopressin levels

Next, we found significantly lower plasma concentrations of OT in CD38$^{-/-}$ than in wild-type CD38$^{+/+}$ mice (Fig. 3a). The OT level in cerebrospinal fluid (CSF) in CD38$^{-/-}$ mice was also lower than that in CD38$^{+/+}$ mice (Supplementary Fig. 7a). In contrast, OT concentrations in the hypothalamus and neurohypophysis in CD38$^{-/-}$ mice were increased to a much higher level than in controls (Fig. 3b). AVP showed little or no changes in plasma (Fig. 3a) or CSF (Supplementary Fig. 7b) concentrations, and no significant change in tissue concentrations in CD38$^{-/-}$ mice.

Electron microscopic analysis of the neurohypophysis also revealed a higher level of neurosecretory hormones in the tissue (Fig. 3c, d), which is OT as detected by immunostaining (Supplementary Fig. 8). Neurohypophysial axon swellings were filled with secretory dense core vesicles in both types of mice. In CD38$^{+/+}$ mice the endings at the neurovascular contact zone contained many microvesicles and vacuoles but were generally devoid of dense core vesicles (Fig. 3c). This is evidence of strong secretory activity[15]. In CD38$^{-/-}$ mice, dense core vesicles occupied both axon swellings and endings (Fig. 3d), indicating excess storage. Thus, our results suggest that both synthesis and vesicular packaging of these hormones seem to be unaffected in CD38$^{-/-}$ mice, but that OT secretion (but not AVP secretion) is selectively and severely impaired *in vivo*.

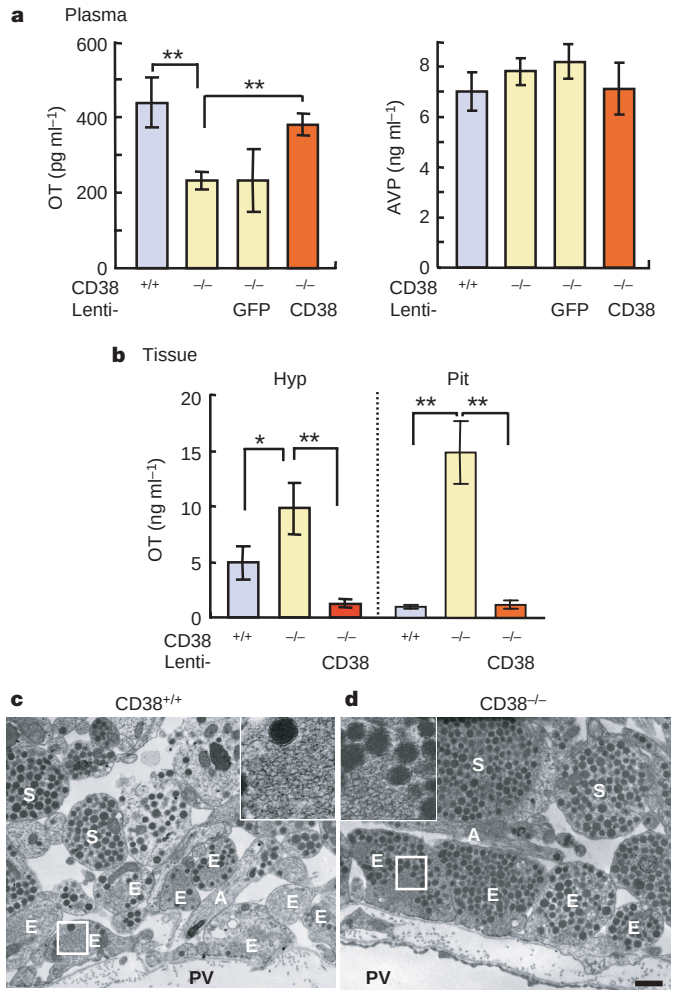

Figure 3 | Oxytocin and vasopressin concentrations. a, **b**, Levels of plasma OT or AVP (**a**) and tissue OT (**b**) concentrations in CD38$^{+/+}$ and CD38$^{-/-}$ mice, or CD38$^{-/-}$ mice injected with lenti-GFP or lenti-CD38. Hyp, hypothalamic cells. Pit, nerve endings in the posterior pituitary. $^{*,**}P < 0.05$ and 0.001, respectively. $N = 5$-8. **c**, **d**, Electron micrographs of the posterior pituitary gland in CD38$^{+/+}$ (**c**) and CD38$^{-/-}$ (**d**) mice. Axon (A) and axonal endings (E) near the perivascular space (PV) are empty (**c**) or full (**d**) of dense core vesicles. Bar indicates 500 nm (×8,000 magnification). Insets show typical nerve terminals with higher magnification images of the areas indicated by the squares in **c** and **d**. Axonal endings are identified from dense-core-vesicle-filled neurosecretory axonal swellings (Herring's body, S) with microvesicles. Error bars, s.e.m.

Rescue by injection of OT or CD38 re-expression

Because it has been reported that a single subcutaneous administration of OT affects memory storage within 10 min in rat[26], we used the same protocol after having confirmed that OT could transfer to the CSF after subcutaneous injection of OT in both wild-type and mutant male mice (Supplementary Fig. 7c and d). We found that acute subcutaneous OT injection substantially rescued the maternal nurturing behaviour of females (Fig. 1e, f) and the impaired social recognition in CD38$^{-/-}$ male mice (Fig. 2c), whereas AVP had no significant effect (Figs 2c). In addition, we observed that the social behaviour of CD38$^{-/-}$ males was rescued by acutely applying OT into the third ventricle (Supplementary Fig. 9).

A significant improvement achieved by OT with a single peripheral or central injection confirmed that a deficit in OT secretion is probably responsible for the social behaviour deficits in CD38$^{-/-}$ mice. To test this further, we examined the link between plasma and/or central OT decrease and loss of CD38 expression in hypothalamic neurons by selectively rescuing the human CD38 gene in the hypothamamic neuronal population. CD38$^{-/-}$ mice received infusion of lentiviral vectors carrying human CD38 (lenti-CD38) or green fluorescence protein (GFP) (lenti-GFP) genes in the third ventricle. Two weeks after the viral injection, mice receiving lenti-CD38 showed re-expression of human CD38 immunoreactivity within the hypothalamus and posterior pituitary, whereas mice receiving lenti-GFP did not (Supplementary Fig. 10). The low plasma and CSF concentrations of OT and high tissue concentrations of OT were reversed in lenti-CD38-injected CD38$^{-/-}$ mice, respectively, whereas no comparable change was observed in mice receiving lenti-GFP (Fig. 3a, b; Supplementary Fig. 7a). The plasma (Fig. 3a) and tissue (data not shown) AVP levels in lenti-CD38-injected CD38$^{-/-}$ mice were not significantly altered. Further, social memory in CD38$^{-/-}$ male mice receiving lenti-CD38, but not lenti-GFP, was rescued (Fig. 2d), with the comparable recovery rate in OT administration in CD38$^{-/-}$ mice or wild-type mice (Fig. 2e).

To further determine whether or not the enzymatic function of CD38 is important in rescuing the behaviour, we tested a mutant human CD38 (an amino acid substitution from Arg 140 (CGG) to Trp 140 (TGG)), R140W. This CD38 mutation has been found in human diabetes and contains roughly one-third of the control ADP-ribosyl cyclase activity[36]. The re-expression of the mutant CD38 in the hypothalamic region with lenti-R140W-CD38 did not significantly rescue the behavioural deficit in CD38$^{-/-}$ mice (Fig. 2d, e). The results indicate that enzyme activity is critically important for recovery of the amnesia phenotype and that the 'social brain system'[19,31] is not disrupted in CD38$^{-/-}$ mice.

CD38 expression and enzyme activity

Along with the loss of CD38 expression, brain tissue from CD38$^{-/-}$ mice shows a marked reduction of ADP-ribosyl cyclase activity as measured by both cADPR[11] and NAADP[37] generation. We reconfirmed

this phenotype by immunohistochemical analysis of hypothalamic periventricular regions and by other measurements (Supplementary Fig. 11). CD38 immunoreactivity in wild-type mice was present as punctate dots on or mostly outside oxytocinergic and/or AVP-ergic neurons, whereas staining in CD38$^{-/-}$ mice seemed to be at the background level (Supplementary Figs 11a and 12). Wild-type mice showed very high CD38 messenger RNA levels and ADP-ribosyl cyclase activity in the hypothalamic region but low levels in the posterior pituitary gland (Supplementary Figs 11b, c, and 13), whereas CD38$^{-/-}$ mice had much lower activity (Supplementary Fig. 11e). A correspondingly reduced content of cADPR was found in the hypothalamus and neurohypophysis of CD38$^{-/-}$ mice (Supplementary Fig. 11d). The reduced ADP-ribosyl cyclase activity in CD38$^{-/-}$ mice was partly restored following lentivector-mediated re-expression of human CD38 (Supplementary Fig. 11e).

OT secretion and Ca^{2+} transients *in vitro*

High-potassium-induced depolarization produced an extracellular Ca^{2+}-dependent increase in OT secretion from isolated hypothalamic neurons and axon terminals, and more so in CD38$^{+/+}$ mice than CD38$^{-/-}$ mice (Fig. 4a, b). In contrast, CD38$^{-/-}$ mice showed no deficit in AVP release from either brain region (Supplementary Fig. 14a). OT release from pituitary nerve endings was reduced by treatment with three antagonists to the level seen in CD38$^{-/-}$ mice. OT release was enhanced by extracellularly applied cADPR (100 μM) and inhibited by 8-bromo-cADPR (Fig. 4c) in the intact nerve endings of the wild-type mice. An identical increase was not observed in the CD38$^{-/-}$ mice, probably because of the lack of the transporter, CD38. However, when these CD38$^{-/-}$ nerve endings were permeabilized by digitonin, extracellular cADPR was now able to increase OT release. These results show that cADPR is essential for OT secretion, though the role of NAADP is relatively minor at best (Supplementary Fig. 14b). The results also indicate that the deficit in OT secretion and reduced plasma and CSF OT levels in CD38$^{-/-}$ mice might reasonably be attributed to the reduced ADP-ribosyl cyclase activity. However, this does not reflect a general defect in neurosecretion because AVP secretion was unaffected. As a further example, depolarization-induced secretion of dopamine in the striatum was unaffected in CD38$^{-/-}$ mice (Supplementary Fig. 15).

OT secretion in hypothalamic cells is triggered by increased intracellular calcium concentrations ($[Ca^{2+}]_i$) owing to the influx of extracellular Ca^{2+} through voltage-dependent Ca^{2+} channels associated with repetitive firing of action potentials[32,38]. Here, we investigated transient $[Ca^{2+}]_i$ increases in isolated nerve endings[34,39] with the Ca^{2+}-sensing dye, Oregon Green. Incubation with 50 mM KCl elevated $[Ca^{2+}]_i$ to 2.2-fold of the pre-stimulation level in CD38$^{+/+}$ but to 1.6-fold of that in CD38$^{-/-}$ mice (Fig. 4d). Interestingly, the $[Ca^{2+}]_i$ increase in CD38$^{+/+}$ mice was markedly inhibited in the presence of ryanodine, 8-bromo-cADPR or bafilomycin (Fig. 4e; Supplementary Fig. 14c). These results indicate that the mobilization of Ca^{2+} from intracellular stores in CD38$^{-/-}$ mice is inefficient and indicate that attenuation of the intracellular ryanodine-susceptible Ca^{2+} amplification in stimulation–secretion coupling for OT secretion may be the primary cause of behavioural abnormality.

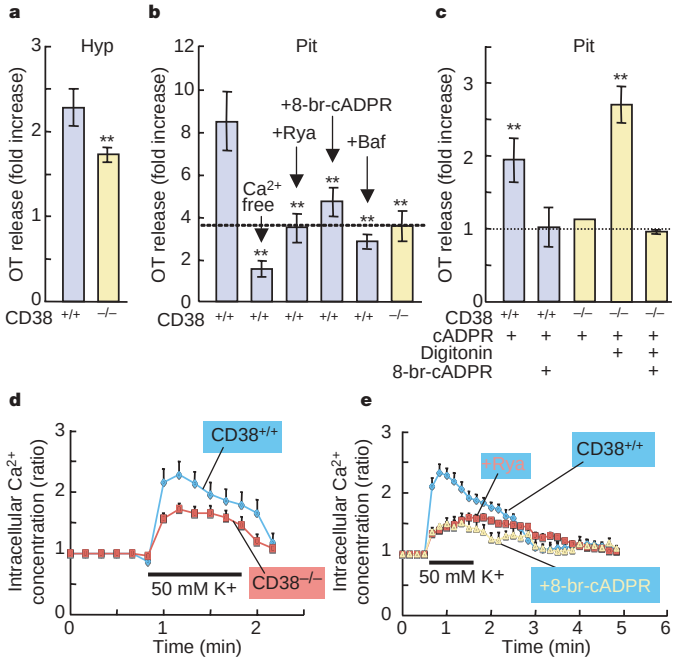

Figure 4 | Oxytocin secretion and calcium signalling. a, b, c, Enzyme-linked immunoassay of OT secreted from hypothalamic cells (Hyp; **a**) or nerve endings (Pit; **b**, **c**) in 35-mm culture dishes stimulated by 70 mM KCl for 2 min. The OT release was measured in the presence or absence of 200 μM ryanodine (Rya), 100 μM 8-bromo-cADPR (8-br-cADPR), or 2 μM bafilomycin (Baf) under conditions with or without extracellular 2.2 mM Ca^{2+}. Values represent the ratio of the concentrations in the perfusate after 70 mM KCl to that in control (5 mM KCl) solution. $N = 4$–12. $^{**}P < 0.01$, compared with control CD38$^{+/+}$. **c**, OT release for 5 min from nerve endings isolated from posterior pituitary of CD38$^{+/+}$ or CD38$^{-/-}$ mice and evoked by extracellularly applied 200 μM cADPR in the presence or absence of 100 μM 8-bromo-cADPR. In some experiments (**c**), nerve endings were treated with 1 μM digitonin to permeabilize the cell membranes for 5 min. Values represent the ratio of OT release during 5 min in the presence and absence of cADPR. $N = 4$–6. **d**, Time course of the increase in $[Ca^{2+}]_i$ stimulated with 50 mM KCl for the indicated period in oxytocinergic nerve endings isolated from the posterior pituitary of CD38$^{+/+}$ or CD38$^{-/-}$ mice. $N = 4$. **e**, Time course of the increase in $[Ca^{2+}]_i$ stimulated with 50 mM KCl for the indicated period in the presence or absence of 200 μM ryanodine or 100 μM 8-bromo-cADPR in oxytocinergic nerve endings isolated from CD38$^{+/+}$ mice. $N = 3$–4. See Supplementary Information for tissue preparation and details of each experiment. Error bars, s.e.m.

Discussion

In the present study we have demonstrated that the CD38 mutant mice showed normal exploratory and investigative behaviour towards pups and females, yet were less able to give normal nurturing or social recognition responses[19] to the cues received. The current paradigm of investigation time in wild-type mice used in our studies is normally maintained for an hour. It seems geared more towards the differentiation of conspecifics through short interactions or durations, and involves the ability to distinguish between two similar but different olfactory signatures[28], comparable with well-described long-term memories in pair-bonding in monogamous voles[22,30]. Thus, our results demonstrate a genetic requirement for CD38 in short-term social memory.

A significant observation of the present study is that AVP release is insensitive to the CD38 null mutation. It has been shown that OT and AVP neurons are relatively distinct from each other[40], although they are synthesized in the same supraoptic and paraventricular nuclei. But, only the secretion of OT seems to involve release of Ca^{2+} from ryanodine-sensitive stores. The simplest explanation for this is a difference in the targets for the enzymatic products of CD38, cADPR and NAADP[1,8–10]. Hence, even though CD38 is widely distributed throughout the hypothalamus and is not restricted to OT neurons (and so may exert a paracrine action through extracellular synthesis and cellular uptake of cADPR and NAADP[41]), this will only affect secretion of OT, not AVP. Thus, mice lacking the OT or AVP genes[18,22,28,30], OT- or AVP-receptor genes[29,42], and CD38 gene (this study) show similar and profound behavioural anomalies that collectively resemble those of human autism, a pervasive neuropsychiatric disorder with marked defects in social interaction. The dependence of OT levels on CD38 expression could potentially be of clinical significance because it has been reported that plasma OT levels are decreased in autistic children[43]. It would be interesting to test if disease-causing variants in the coding or non-coding sequence

of human CD38 can be detected in the spectrum of autistic patients, comparable to the CD38 mutations found in a subset of diabetes patients[36].

METHODS

See Supplementary Information for detailed methods.

Blood or tissues were sampled on the day of the experiment. Assays were performed according to the manufacturer's protocol (Assay Designs, Michigan). Vesicular Stomatitis Virus-G protein (VSV-G) pseudotyped lentiviral vectors[44] were designed to express human CD38 (ref. 6), R140W-CD38 (ref. 36) or GFP.

Received 18 October; accepted 11 December 2006.
Published online 7 February 2007.

1. Lee, H. C. Physiological functions of cyclic ADP-ribose and NAADP as calcium messengers. *Annu. Rev. Pharmacol. Toxicol.* **41,** 317–345 (2001).
2. Deaglio, S., Vaisitti, T., Aydin, S., Ferrero, E. & Malavasi, F. In-tandem insight from basic science combined with clinical research: CD38 as both marker and key component of the pathogenetic network underlying chronic lymphocytic leukemia. *Blood* **108,** 1135–1144 (2006).
3. Hunt, P. W. *et al.* The independent effect of drug resistance on T cell activation in HIV infection. *AIDS* **20,** 691–699 (2006).
4. Higashida, H. *et al.* Cyclic ADP-ribose as a second messenger revisited from a new aspect of signal transduction from receptors to ADP-ribosyl cyclase. *Pharmacol. Ther.* **90,** 283–296 (2001).
5. Okamoto, H. & Takasawa, S. Recent advances in the Okamoto model: the CD38-cyclic ADP-ribose signal system and the regenerating gene protein (Reg)-Reg receptor system in beta-cells. *Diabetes* **51,** S462–S473 (2002).
6. Takasawa, S. *et al.* Synthesis and hydrolysis of cyclic ADP-ribose by human leukocyte antigen CD38 and inhibition of the hydrolysis by ATP. *J. Biol. Chem.* **268,** 26052–26054 (1993).
7. Howard, M. *et al.* Formation and hydrolysis of cyclic ADP-ribose catalyzed by lymphocyte antigen CD38. *Science* **262,** 1056–1059 (1993).
8. Lee, H. C. Nicotinic acid adenine dinucleotide phosphate (NAADP)-mediated calcium signaling. *J. Biol. Chem.* **280,** 33693–33696 (2005).
9. Yamasaki, M. *et al.* Organelle selection determines agonist-specific Ca^{2+} signals in pancreatic acinar and beta cells. *J. Biol. Chem.* **279,** 7234–7240 (2004).
10. Gerasimenko, J. V., Sherwood, M., Tepikin, A. V., Petersen, O. H. & Gerasimenko, O. V. NAADP, cADPR and IP_3 all release Ca^{2+} from the endoplasmic reticulum and an acidic store in the secretory granule area. *J. Cell Sci.* **119,** 226–238 (2006).
11. Kato, I. *et al.* CD38 disruption impairs glucose-induced increases in cyclic ADP-ribose, $[Ca^{2+}]_i$, and insulin secretion. *J. Biol. Chem.* **274,** 1869–1872 (1999).
12. Johnson, J. D. & Misler, S. Nicotinic acid-adenine dinucleotide phosphate-sensitive calcium stores initiate insulin signaling in human beta cells. *Proc. Natl Acad. Sci. USA* **99,** 14566–14571 (2002).
13. Koshiyama, H., Lee, H. C. & Tashjian, A. H. Jr. Novel mechanism of intracellular calcium release in pituitary cells. *J. Biol. Chem.* **266,** 16985–16988 (1991).
14. Soares, S. M., Thompson, M. & Chini, E. N. Role of the second-messenger cyclic-adenosine 5′-diphosphate-ribose on adrenocorticotropin secretion from pituitary cells. *Endocrinology* **146,** 2186–2192 (2005).
15. Hatton, G. I. Emerging concepts of structure-function dynamics in adult brain: the hypothalamo-neurohypophysial system. *Prog. Neurobiol.* **34,** 437–504 (1990).
16. Russell, J. A., Leng, G. & Douglas, A. J. The magnocellular oxytocin system, the fount of maternity: adaptations in pregnancy. *Front. Neuroendocrinol.* **24,** 27–61 (2003).
17. Argiolas, A. & Melis, M. R. Central control of penile erection: role of the paraventricular nucleus of the hypothalamus. *Prog. Neurobiol.* **76,** 1–21 (2005).
18. Keverne, E. B. & Curley, J. P. Vasopressin, oxytocin and social behaviour. *Curr. Opin. Neurobiol.* **14,** 777–783 (2004).
19. Insel, T. R. & Fernald, R. D. How the brain processes social information: searching for the social brain. *Annu. Rev. Neurosci.* **27,** 697–722 (2004).
20. Bartels, A. & Zeki, S. The neural correlates of maternal and romantic love. *Neuroimage* **21,** 1155–1166 (2004).
21. LaBar, K. S. & Cabeza, R. Cognitive neuroscience of emotional memory. *Nature Rev. Neurosci.* **7,** 54–64 (2006).
22. Young, L. J. & Wang, Z. The neurobiology of pair bonding. *Nature Neurosci.* **7,** 1048–1054 (2004).
23. Kosfeld, M., Heinrichs, M., Zak, P. J., Fischbacher, U. & Fehr, E. Oxytocin increases trust in humans. *Nature* **435,** 673–676 (2005).
24. Fries, A. B., Ziegler, T. E., Kurian, J. R., Jacoris, S. & Pollak, S. D. Early experience in humans is associated with changes in neuropeptides critical for regulating social behavior. *Proc. Natl Acad. Sci. USA* **102,** 17237–17240 (2005).
25. Kirsch, P. *et al.* Oxytocin modulates neural circuitry for social cognition and fear in humans. *J. Neurosci.* **25,** 11489–11493 (2005).
26. Popik, P., Vetulani, J. & van Ree, J. M. Low doses of oxytocin facilitate social recognition in rats. *Psychopharmacol.* **106,** 71–74 (1992).
27. Hollander, E. *et al.* Oxytocin infusion reduces repetitive behaviors in adults with autistic and Asperger's disorders. *Neuropsychopharmacol.* **28,** 193–198 (2003).
28. Ferguson, J. N. *et al.* Social amnesia in mice lacking the oxytocin gene. *Nature Genet.* **25,** 284–288 (2000).
29. Takayanagi, Y. *et al.* Pervasive social deficits, but normal parturition, in oxytocin receptor-deficient mice. *Proc. Natl Acad. Sci. USA* **102,** 16096–16101 (2005).
30. Insel, T. R. & Young, L. J. The neurobiology of attachment. *Nature Rev. Neurosci.* **2,** 129–136 (2001).
31. Lim, M. M., Bielsky, I. F. & Young, L. J. Neuropeptides and the social brain: potential rodent models of autism. *Int. J. Dev. Neurosci.* **23,** 235–243 (2005).
32. Belin, V. & Moos, F. Paired recordings from supraoptic and paraventricular oxytocin cells in suckled rats: recruitment and synchronization. *J. Physiol. (Lond.)* **377,** 369–390 (1986).
33. Ludwig, M. & Leng, G. Dendritic peptide release and peptide-dependent behaviours. *Nature Rev. Neurosci.* **7,** 126–136 (2006).
34. De Crescenzo, V. *et al.* Ca^{2+} syntillas, miniature Ca^{2+} release events in terminals of hypothalamic neurons, are increased in frequency by depolarization in the absence of Ca^{2+} influx. *J. Neurosci.* **24,** 1226–1235 (2004).
35. Kendrick, K. M. *et al.* Neural control of maternal behaviour and olfactory recognition of offspring. *Brain Res. Bull.* **44,** 383–395 (1997).
36. Yagui, K. *et al.* A missense mutation in the CD38 gene, a novel factor for insulin secretion: association with Type II diabetes mellitus in Japanese subjects and evidence of abnormal function when expressed in vitro. *Diabetologia.* **41,** 1024–1028 (1998).
37. Chini, E. N., Chini, C. C., Kato, I., Takasawa, S. & Okamoto, H. CD38 is the major enzyme responsible for synthesis of nicotinic acid-adenine dinucleotide phosphate in mammalian tissues. *Biochem. J.* **362,** 125–130 (2002).
38. OuYang, W., Wang, G. & Hemmings H. C. Jr. Distinct rat neurohypophysial nerve terminal populations identified by size, electrophysiological properties and neuropeptide content. *Brain Res.* **1024,** 203–211 (2004).
39. Sasaki, N., Dayanithi, G. & Shibuya, I. Ca^{2+} clearance mechanisms in neurohypophysial terminals of the rat. *Cell Calcium* **37,** 45–56 (2005).
40. Yamashita, M., Glasgow, E., Zhang, B. J., Kusano, K. & Gainer, H. Identification of cell-specific messenger ribonucleic acids in oxytocinergic and vasopressinergic magnocellular neurons in rat supraoptic nucleus by single-cell differential hybridization. *Endocrinology* **143,** 4464–4476 (2002).
41. De Flora, A., Zocchi, E., Guida, L., Franco, L. & Bruzzone, S. Autocrine and paracrine calcium signaling by the CD38/NAD^+/cyclic ADP-ribose system. *Ann. NY Acad. Sci.* **1028,** 176–191 (2004).
42. Bielsky, I. F., Hu, S. B., Ren, X., Terwilliger, E. F. & Young, L. J. The V1a vasopressin receptor is necessary and sufficient for normal social recognition: a gene replacement study. *Neuron* **47,** 503–513 (2005).
43. Modahl, C. *et al.* Plasma oxytocin levels in autistic children. *Biol. Psychiatry* **15,** 270–277 (1998).
44. Torashima, T., Okoyama, S., Nishizaki, T. & Hirai, H. *In vivo* transduction of murine cerebellar Purkinje cells by HIV-derived lentiviral vectors. *Brain Res.* **1082,** 11–22 (2006).

Supplementary Information is linked to the online version of the paper at www.nature.com/nature.

Acknowledgements We acknowledge support from the COE programme of the Japanese Ministry of Education, Culture, Sports, Science and Technology. We thank D. A. Brown for discussion.

Author Contributions All authors contributed to this paper; in particular, K.Y., S.T., H.O. and A.S. contributed to experimental planning, and H. Higashida, H. Hirai and A.M. performed experimental work and project planning.

Author Information Reprints and permissions information is available at www.nature.com/reprints. The authors declare no competing financial interests. Correspondence and requests for materials should be addressed to H.H. (haruhiro@med.kanazawa-u.ac.jp).

ARTICLES

MAPK-mediated bimodal gene expression and adaptive gradient sensing in yeast

Saurabh Paliwal[1], Pablo A. Iglesias[1,2], Kyle Campbell[3], Zoe Hilioti[1], Alex Groisman[3] & Andre Levchenko[1]

The mating pathway in *Saccharomyces cerevisiae* has been the focus of considerable research effort, yet many quantitative aspects of its regulation still remain unknown. Using an integrated approach involving experiments in microfluidic chips and computational modelling, we studied gene expression and phenotypic changes associated with the mating response under well-defined pheromone gradients. Here we report a combination of switch-like and graded pathway responses leading to stochastic phenotype determination in a specific range of pheromone concentrations. Furthermore, we show that these responses are critically dependent on mitogen-activated protein kinase (MAPK)-mediated regulation of the activity of the pheromone-response-specific transcription factor, Ste12, as well as on the autoregulatory feedback of Ste12. In particular, both the switch-like characteristics and sensitivity of gene expression in shmooing cells to pheromone concentration were significantly diminished in cells lacking Kss1, one of the MAP kinases activated in the mating pathway. In addition, the dynamic range of gradient sensing of Kss1-deficient cells was reduced compared with wild type. We thus provide unsuspected functional significance for this kinase in regulation of the mating response.

The pheromone sensing MAPK pathway in the yeast *S. cerevisiae* affects the expression of an estimated 200 genes and directly participates in yeast chemotropism in pheromone gradients[1]. The pheromone response involves the formation of a diploid zygote from two haploid cells of opposite mating types through pheromone gradient sensing, directed localized cell growth (shmooing) and eventual cell fusion, and requires an integrated regulatory network. In spite of a long and productive research history, the control mechanisms involved in pheromone gradient sensing and chemotropism are still not completely understood. For example, it is not clear how the mean value and the gradient of the pheromone concentration are integrated by a chemotropic cell, whether the dose response in this pathway is graded, as suggested by a recent analysis[2], or switch-like, as observed in other MAPK cascades[3], and whether the response is affected by molecular-level noise. In addition, the respective roles of two MAP kinases activated by the pathway, Fus3 and Kss1, remain unclear.

Microfluidic chip-based experimental platform

To perform repeated high-throughput experiments on yeast pheromone response in precisely defined gradients, we developed a novel microfluidic device (Fig. 1a, b; Supplementary Fig. 1). Its functional area consists of an array of 5-μm-deep parallel rectangular test chambers of various lengths (short horizontal channels in Fig. 1a, b) and two 25-μm-deep mirror-symmetric flow-through channels adjacent to opposite edges of the test chambers (long vertical channels with kinks in Fig. 1a, b). Cells loaded into the test chambers are exposed to linear concentration profiles of pheromone (Supplementary Fig. 2). The pheromone gradient profiles are created by molecular diffusion between the left flow-through channel with a high concentration pheromone solution and the right flow-through channel with plain medium. In contrast to a previous microfluidic design for experiments on gradient response[4], cells in the test chambers are not exposed to any active flow, which is critical for experiments with non-adherent yeast cells. The pheromone gradient profiles in the test chambers remain stable over at least 20 h. A single microfluidic device contains multiple copies of test chambers of different lengths, allowing exposure of cells to a continuous range of pheromone concentrations presented in gradients of different steepness, as well as analysis of hundreds of cells per experiment. Therefore, long-term pheromone dose and gradient responses of individual cells can be analysed at high throughput. In addition, the cell phenotype and the expression level of specific fluorescently tagged genes can be monitored concurrently, an important capability unachievable with flow cytometry.

Phenotype co-existence versus bimodal gene expression

We used the device to study the phenotypic dose response of individual cells to pheromone concentration, c_{ph}, gradually varying from 0–80 nM. Although cell response was tracked continuously, the final analysis was performed six hours after pheromone exposure to reduce the effect of cell cycle stage variability at the beginning of the experiment. Specifically, cells past the G1-stage on pheromone exposure had sufficient time to complete their cell cycles and then attain their eventual phenotypic states. At six hours, cells adopted a variety of pheromone response phenotypes. At relatively high c_{ph}, cells formed multiple mating projections or exhibited prolonged chemotropism ('shmooing' or SHM phenotype), whereas at lower c_{ph} they underwent cell cycle arrest without formation of a shmoo (CCA phenotype). At yet lower c_{ph}, they showed no detectable response and continued dividing ('budding' or BUD phenotype)[5]. Additionally, some cells reverted from the SHM to the BUD phenotype ('reverted from shmooing' or RFS phenotype; see Supplementary Methods for cell phenotype determination). Surprisingly, distinct phenotypes often co-existed in cell subpopulations exposed to the same c_{ph} (Fig. 1e–g, i), indicating the existence of a range of c_{ph}, where the decision to acquire a specific phenotype might depend on stochastic features of the underlying biochemical reactions.

To gain insight into the phenotype co-existence, we generated cells expressing Fus3 and Fus1 proteins fused to yeast enhanced green

[1]Department of Biomedical Engineering and Whitaker Institute of Biomedical Engineering, and [2]Department of Electrical Engineering and Computer Engineering, The Johns Hopkins University, Baltimore, Maryland 21218, USA. [3]Department of Physics, University of California, San Diego, La Jolla, California 92093, USA.

fluorescent protein (EGFP), Fus3–EGFP and Fus1–EGFP, by genomic integration of *EGFP* at the respective native loci (referred to as wild-type strains henceforth, see Supplementary Methods). These two genes, known targets of the pheromone pathway[1,6], were selected as indicators of a more general gene expression response to pheromone. To exclude the effects of possible gradient variability between different chambers, we analysed Fus1–EGFP expression levels of cells in multicellular clusters (4–15 cells) with c_{ph} variation <5 nM across a cluster (Fig. 2a). (The same c_{ph} was assigned to all cells within one cluster for all further analysis.) At $c_{ph} = 20$–50 nM, cells within one cluster frequently exhibited different phenotypic responses uncorrelated with their positions in the cluster. In the same c_{ph} range, there was clear bimodality in the expression of Fus1–EGFP in individual cells (Fig. 2a; Supplementary Fig. 4). The fluorescence intensity of membrane-localized Fus1–EGFP measured with an epi-fluorescence microscope (as in Fig. 2a) correlated well with the total membrane-localized fluorescence estimated by confocal imaging (Supplementary Information and Supplementary Fig. 4). We subdivided cell clusters into groups of cells (4–11 cells per group) displaying one of the BUD/CCA/SHM/RFS phenotypes and explored the correlation between phenotype and gene expression. Strikingly, differences in Fus1–EGFP expression levels between BUD, CCA and RFS cells were insignificant, whereas the difference between SHM cells and cells of all other phenotypes was markedly significant (Fig. 2a). The dose response for Fus3–EGFP expression was qualitatively similar, but the bimodality was much less prominent (Supplementary Fig. 5).

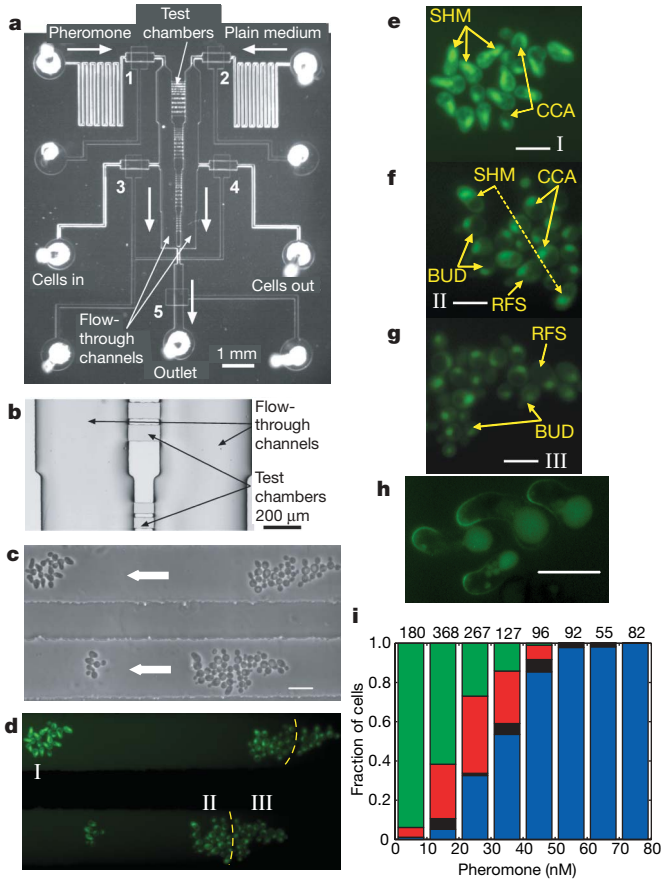

Figure 1 | Pheromone dose–response analysis using a microfluidic experimental setup. **a**, The microfluidic device consists of two layers of microchannels: a flow layer (labelled inlets) of flow-through channels and test chambers and a control layer, with 5 membrane valves[30] (numbered 1–5) actuated from 4 separate control inlets (not labelled). **b**, Magnified view of an area with two 25-μm-deep flow-through channels (wide vertical strips) and 5-μm-deep test chambers between them (see Supplementary Information for details). **c**, **d**, Phase contrast and fluorescence microscopy images of two adjacent chambers with Fus3–EGFP cells six hours after pheromone exposure. (c_{ph} in the field of view increases from right to left, from 10 to 50 nM). Yellow dashed lines indicate boundaries between cell clusters merged owing to cell division. Arrows in **c** denote the direction of increasing pheromone (see Supplementary Fig. 2 for gradient image). **e**–**g**, Close-up Fus3–EGFP fluorescence images of cell clusters I, II and III displaying mixtures of different phenotypes. **h**, Fus1–EGFP expressing cells displaying chemotropism in a similar chamber. Scale bars are 20 μm (**c**, **d**), 10 μm (**e**–**g**) and 5 μm (**h**). **i**, Fraction of different phenotypes of wild-type cells six hours after pheromone exposure. Phenotypes are colour coded as: BUD (green); CCA (red); RFS (black); and SHM (blue). Numbers on the top are the total numbers of cells in the bins.

Mathematical model for transcriptional regulation

The phenotype co-existence and bimodality in Fus1–EGFP and Fus3–EGFP expression indicated that the underlying gene regulation network might exhibit at least two distinct stable states (bistability). Many natural and engineered biochemical networks can exhibit bistability or multistability, usually as a consequence of one or more positive feedback interactions[7–14]. Deterministic bistable systems eventually converge to one of the two distinct steady states available under a given constant input, where the chosen steady state is determined by the system's history (hysteresis). Such systems produce histograms with unimodal distributions. In contrast, a combination of bistability with inherent stochastic noise might allow the system to switch between the two stable steady states, resulting in co-existence of two discrete response levels in cell populations exposed to the same level of stimulus, that is, response bimodality[3,15]. To investigate possible mechanisms of bistability in the pheromone pathway, we constructed a mathematical model incorporating the activity of the MAPKs Fus3 and Kss1, the pheromone-response specific transcription factor Ste12, and upregulation in expression of *FUS1, FUS3* and *STE12* by activated Ste12 (refs 1 and 6; Fig. 3a; Supplementary Figs 8–15). Unphosphorylated Kss1 exerts an inhibitory effect on the

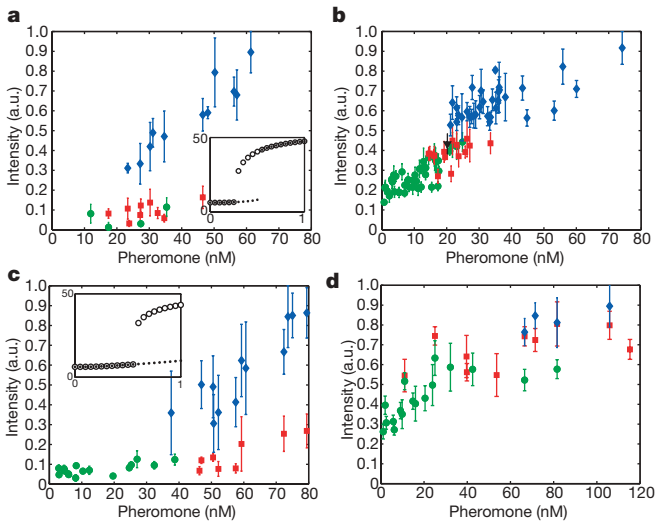

Figure 2 | Quantification of Fus1 protein and gene expression. **a**, Membrane-localized Fus1–EGFP in wild type (strain AL4). **b**, YFP driven by the *FUS1* promoter in wild type (strain SP42). **c**, Membrane-localized Fus1–EGFP in a $PSTE12_{3PREmut}$ strain (strain ZH579). **d**, YFP driven by the *FUS1* promoter in *fus3Δ* (strain SP44). The data (mean ± s.d.) from different cell groups ($n = 4$–11 cells, cell groups with $n < 4$ cells are neglected) are colour-coded as in Fig. 1i: BUD (green circles), CCA (red squares), RFS (black triangles) and SHM (blue diamonds). Fluorescence intensities are normalized so that the maximal (mean + s.d.) value in each experiment corresponds to unity. Insets in **a** and **c** are the corresponding predictions of the model (see also Supplementary Fig. 11). Expression levels of SHM and CCA cells in the region of co-existence are significantly different according to a two-sample *t*-test (assuming a two-tailed distribution and unequal variances): $P = 2.6 \times 10^{-4}$ for **a**; $P = 6.3 \times 10^{-6}$ for **b**; and $P = 1.1 \times 10^{-5}$ for **c**. a.u., arbitrary units.

pathway by binding to Ste12 and potentiating Dig1,2-mediated repression of Ste12 (ref. 16), whereas phosphorylated Fus3 and Kss1 can activate Ste12 thus enhancing the pathway activation[16–18]. Therefore, the model included activation of Ste12 by phosphorylated Fus3 and Kss1, and repression of Ste12 by unphosphorylated Kss1. The model generated *FUS1* and *FUS3* transcription dose–response curves with a combination of monostable and bistable regions (Figs 2a and 3b, insets; Supplementary Fig. 5d), thus reproducing the experimentally observed dose–response curves.

The bimodal expression of Fus1–EGFP and Fus3–EGFP (Fig. 2a; Supplementary Fig. 5a) suggested substantial stochastic variation in the concentrations of key pheromone pathway molecules across the cell population. Cell–cell differences in the signalling pathway components can be a significant source of variation in the pheromone response, especially at low pheromone concentrations[19]. Stochastic variability is also likely to diminish the effect of hysteresis in a bistable system[15]. Indeed, we did not observe any significant hysteretic effects in the response (Supplementary Figs 3 and 5b).

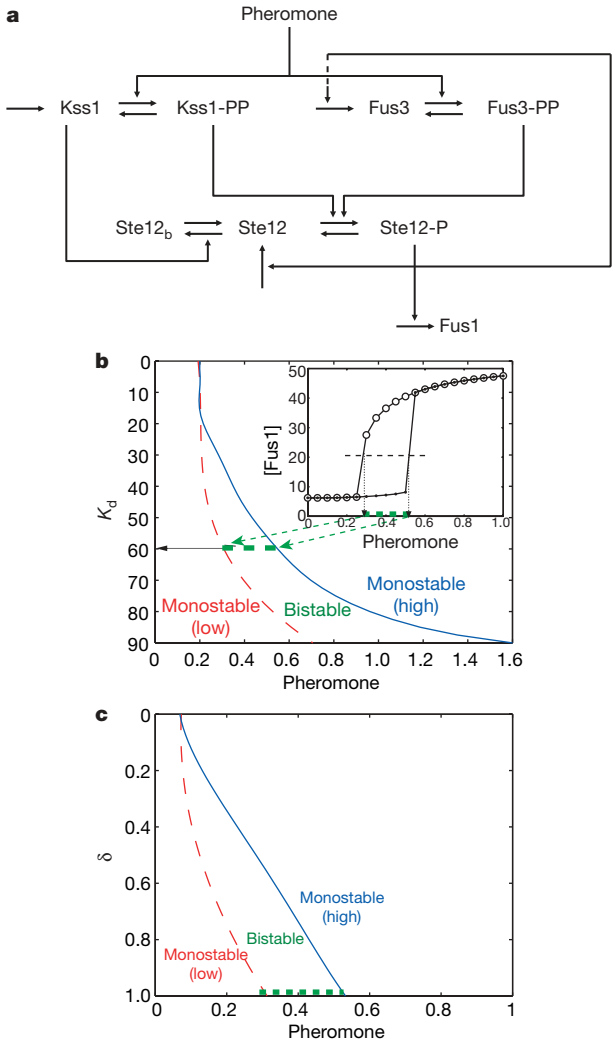

Figure 3 | Computational modelling of transcriptional regulation in the pheromone response. **a**, A simplified diagram of signalling and transcriptional regulation in the pheromone pathway. 'P' denotes phosphorylated forms of the species. $Ste12_b$ denotes the Kss1-bound repressed Ste12. **b**, Ste12 autoregulation is a critical determinant of bistability in the model. For each binding constant K_d of Ste12-P to the *STE12* promoter, the bistability region is confined between the red and blue curves. The inset shows the hysteretic dependence of [Fus1] (a.u.) on pheromone (a.u.) for nominal K_d. a.u., arbitrary units. Dashed green lines in the inset and **b** and **c** indicate the bistability ranges for nominal K_d. Filled and open circles in the inset correspond to low and high initial concentrations of the relevant species, respectively (Supplementary Table 1 and 2). **c**, Plot similar to **b** shows the region of bistability for various values of normalized Kss1 expression (δ). δ = 1 corresponds to the wild-type case and δ = 0 to the *kss1*Δ case (see Supplementary Information for a model description).

Transcriptional regulation: roles of MAPKs and Ste12

To verify that the bistability is regulated at the transcriptional level, as suggested by the model, we studied cells expressing yellow fluorescent protein (YFP) under the control of the *FUS1* promoter (also referred to as a wild-type strain, see Supplementary Methods). These cells gave a bimodal distribution of fluorescence intensity (Fig. 2b), which was qualitatively similar to but less pronounced than that of the Fus1–EGFP cells (see Supplementary Information for a discussion).

Analysis of the model further suggested that the nonlinear transcriptional autoregulation of Ste12 is essential for the bistable response. To investigate this, we mutated the three consensus pheromone response element (PRE) sequences in the promoter region upstream of *STE12* ($PSTE12_{3PREmut}$), leaving only non-consensus sites available for binding by activated Ste12 (Supplementary Information). We modelled this mutation by increasing K_d of Ste12 binding, which resulted in the bistability region moving to higher c_{ph} and becoming wider (Figs 2c, inset, and 3b; Supplementary Figs 11d and 12i). Both effects were observed experimentally, with the CCA phenotype in mutated cells found at much higher c_{ph} than in wild-type cells (Fig. 2c).

To investigate the respective roles of Fus3 and Kss1, we first analysed *fus3*Δ cells. Shmooing and polarized growth were severely hampered, occurring at much higher c_{ph} (Fig. 2d; Supplementary Figs 6 and 7), in agreement with previous studies that have highlighted the importance of Fus3 for the mating response[20–22]. Up to the highest c_{ph} tested ($c_{ph} > 100$ nM), these cells displayed a mixture of different phenotypes. We also observed hyperinvasive growth at low c_{ph}[18,23], and a moderate increase in the *FUS1*-promoter-driven transcription over the entire pheromone range. Results of the mathematical model agreed with the experiments regarding the important role of Fus3 in the pathway response (Supplementary Fig. 9).

To study the role of Kss1, we evaluated Fus1–EGFP expression (Fig. 4a) and *FUS1*-promoter-driven transcription (Fig. 4b) in *kss1*Δ cells as functions of c_{ph}. The model predicted substantial reduction of bistability in these cells, which was expected to lead to reduced bimodality in Fus1–EGFP expression. Additionally, knocking out *KSS1* was expected to reduce the c_{ph} at which *FUS1* expression starts to increase and saturate (Fig. 3c; Supplementary Figs 10 and 11a). In close agreement with the model, bimodality in gene expression in *kss1*Δ cells was drastically reduced, and the pheromone sensitivity saturated at substantially lower c_{ph}. Strikingly, in contrast to wild-type cells, the levels of gene expression in Kss1-deficient BUD and CCA cells were highly sensitive to variation in c_{ph}, whereas in SHM cells gene expression was essentially saturated (compare Fig. 2a, b with Fig. 4a, b). The increased activation of BUD cells is consistent with previously observed Fus1 upregulation without concomitant cell cycle arrest in *kss1*Δ cells[21].

We predicted that the graded increase of Fus1–EGFP expression in wild-type SHM cells was closely connected to pheromone-dependent phosphorylation of Kss1, leading to gradual reduction in Kss1-mediated repression of Ste12 (ref. 24). To test this hypothesis, we transformed Fus1–EGFP expressing *kss1*Δ cells either with the YCpU-*kss1*(AEF) or the YCpU-*kss1*(Y24F) plasmids[16,24,25]. $Kss1_{AEF}$ cannot be phosphorylated by the MAPKK Ste7, and hence lacks kinase activity. $Kss1_{Y24F}$ can be phosphorylated by Ste7 to the same level as wild-type, but its phosphorylated form lacks kinase activity. Unlike in *kss1*Δ cells, in both mutants, CCA cells showed only a modest increase in gene transcription, which was probably a consequence of repression of Ste12 by unphosphorylated $Kss1_{Y24F}$ and $Kss1_{AEF}$, which acted similarly to unphosphorylated Kss1 in wild-type cells. The bimodality and the growth of Fus1–EGFP expression with c_{ph} in $Kss1_{Y24F}$ SHM

cells were both similar to those in wild-type cells, indicating that the kinase activity of phosphorylated Kss1 is not essential for the observed behaviours (Fig. 4c). In contrast, the $Kss1_{AEF}$ mutant showed a stronger bimodality than wild type (Fig. 4d), and unlike wild-type SHM cells, $Kss1_{AEF}$ SHM cells showed no appreciable enhancement of Fus1–EGFP expression with increasing c_{ph}. This behaviour is predicted by the model: since Ste7 does not phosphorylate $Kss1_{AEF}$, the repression of Ste12 by $Kss1_{AEF}$ is not likely to be weakened with increasing c_{ph}. All major trends in Kss1 mutants were consistent with mathematical model predictions (Fig. 4 and Supplementary Fig. 11).

Gradient sensing of wild-type and *kss1*Δ cells

Our observations of wild-type SHM cells indicated that, as expected, the mating projections were predominantly oriented in the direction of increasing c_{ph}. Gradient sensing was strongest at lower c_{ph}, whereas, at higher c_{ph}, the orientation of projections became increasingly random. Interestingly, the c_{ph} range of gradient sensitivity seemed to coincide with the range of sensitivity of *FUS1* expression to variation of c_{ph}. Pheromone dependence of *FUS1* expression may be representative of a large subset of genes, some of which are likely to be essential for gradient sensing. Hence, we proposed that the c_{ph} sensitivity of gene expression reflects sensitivity of the signalling apparatus necessary for precise gradient sensing. Accordingly, the saturated *FUS1* expression in SHM *kss1*Δ cells might coincide with impaired gradient sensitivity. Therefore, we used the microfluidic device to further examine gradient sensing in wild-type and *kss1*Δ cells.

We found (Fig. 5a, d, e, h, i) that the directional bias in wild-type cells increased significantly with time, in general agreement with previous reports[26]. Moreover, the highest gradient sensitivity was consistently observed at high values of the gradient, $\gamma = \partial c_{ph}/\partial x$ and low c_{ph}. We quantified the precision of gradient sensing within a cluster of cells (4–11 SHM cells) by a parameter σ, the root mean square of the angles between the observed projections in the cluster and the direction of the gradient (precision decreases with increasing σ). σ values were binned into two equal intervals, 0–55° and 55–110°, covering the whole experimental range, and were plotted on the c_{ph}–γ plane, with bin-specific symbols (Fig. 5f). The results suggested a linear relationship between the γ and c_{ph} values for cell clusters having the same range of σ, that is $\gamma = \rho \cdot (c_{ph} - c_0) + \gamma_0$, where γ_0 and c_0 are constant and ρ is different for the two sets of cell clusters. We notice that $c_0 \approx 15$–20 nM, the value of c_{ph} where the two linear regression lines intersect, is also the lowest concentration at which SHM cells are observed. σ remained constant at constant fractional gradient, $\rho = (\gamma - \gamma_0)/(c_{ph} - c_0)$, and more precise gradient sensing (lower σ) corresponded to larger ρ (Fig. 5f). These findings suggest that yeast cells respond to the fractional rather than absolute gradient of pheromone, and that gradient sensing in yeast is optimized for exponential concentration profiles (see Supplementary Information). The sensitivity to the fractional gradient of a chemical cue is in surprising agreement with the results reported for gradient sensing by the amoeba *Dictyostelium discoideum* and grasshopper neurons[27,28].

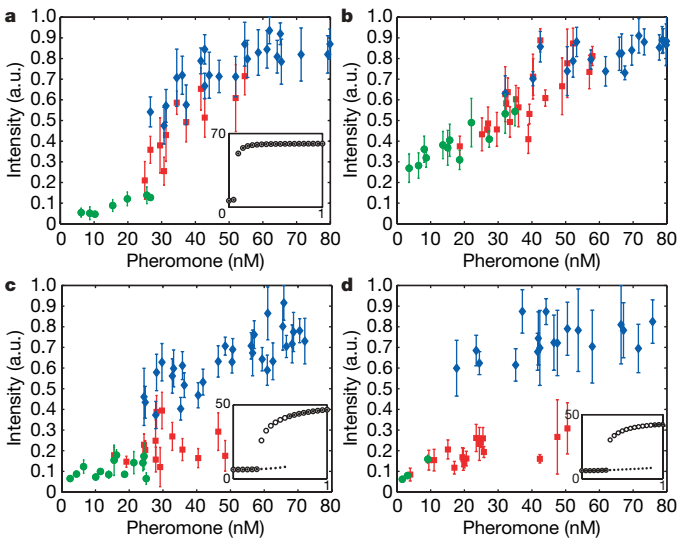

Figure 4 | Role of Kss1 in regulating the pheromone response. **a**, **b**, *kss1*Δ cells expressing Fus1–EGFP (ZH552) (**a**) and YFP driven by the *FUS1* promoter (SP43) (**b**) were exposed to the same conditions as in Fig. 2. Similar experiments were performed with a YCpU-*kss1*(Y24F) plasmid (**c**) and a YCpU-*kss1*(AEF) plasmid (**d**) introduced into the Fus1–EGFP *kss1*Δ strain used in **a**. Fluorescence intensities are normalized and plotted (mean ± s.d.) as in Fig. 2. a.u., arbitrary units. Insets (**a**, **c**, **d**) are the predictions of the mathematical model for the corresponding strains (see also Supplementary Fig. 11). *P*-values (calculated as in Fig. 2) were 1.0×10^{-8} for **c** and 3.2×10^{-11} for **d** indicating significant difference in expression levels of SHM and CCA cells. In contrast, this difference was relatively insignificant in **a** with a *P*-value of 0.017 and was insignificant in **b** with a *P*-value of 0.35.

Sensitivity of cells to fractional gradients further implies that gradient sensing can dramatically deteriorate at higher pheromone concentrations. We observed this deterioration in both wild-type and *kss1*Δ cells, but in *kss1*Δ cells it occurred at substantially lower c_{ph} than in wild type (Fig. 5g). Therefore, deficiency in Kss1 leads to a decrease in the range of c_{ph} in which gradient sensing is efficient, just as predicted above. Similarly, we observe that wild-type cells sense gradients substantially better than *kss1*Δ cells by comparing their values of σ for different ratios of γ to c_{ph} (Fig. 5i). Interestingly, wild-type cells performed only marginally better than *kss1*Δ cells in terms of the initial projection direction, but showed markedly better alignment along the gradient over time as compared to *kss1*Δ cells (Fig. 5h–i). It thus seems that the progressive improvement in gradient sensing in wild-type SHM cells is strongly correlated with the sensitivity of pheromone-induced gene expression to variation of c_{ph}. We also studied the gradient sensing of the strain containing the *STE12* promoter with three mutated consensus PRE sites (Supplementary Fig. 16), as well as the two Kss1 mutant strains, $Kss1_{Y24F}$ and $Kss1_{AEF}$ (Supplementary Fig. 17). In all cases, the existence of an extended dynamic range of gradient sensing was correlated with the c_{ph} sensitivity of the pheromone-induced gene expression in SHM cells.

Conclusions

This study yielded several important insights into the physiology of pheromone response in *S. cerevisiae*. The observed combination of switch-like and graded dose responses, combined with stochastic variability across a cell population, can provide significant benefits for mating yeast populations. First, bimodality in gene expression allows a cell population to diversify its transcriptional response at relatively low pheromone concentrations, reducing the cost of possible inappropriate engagement in expensive pheromone-dependent gene amplification. Thus, when exposed to weak pheromone signals, some cells continue to suppress the pheromone response, whereas others display amplified gene expression correlated with the formation of mating projections. These shmooing cells, capable of sensing fractional pheromone gradients, benefit from the particularly high gradient-sensitivity that we observe at low c_{ph} (higher fractional gradient). Second, continued sensitivity of gene expression in shmooing cells to increasing c_{ph} seems to extend the c_{ph} range in which cells can sense gradients. Thus, as cells approach the mating partner, they can adjust to increasing pheromone concentrations with only partial compromise of gradient sensing. Strikingly, many features of the wild-type pheromone response, including bimodality in gene expression and high dynamic range of gradient sensing, are critically dependent on the presence of Kss1. In particular, the switch-like increase of gene expression in shmooing cells is a result of the combined effect of Ste12 repression by unphosphorylated Kss1 and of Ste12 autoregulation. The graded increase of gene expression with increasing c_{ph} depends on pheromone-regulated phosphorylation of

Kss1, which results in graded reduction in Kss1-mediated repression of Ste12, and possibly, on the ability of phosphorylated MAPKs to activate the pathway. A reduction in the graded increase of gene expression in *kss1*Δ cells correlates with lower precision and reduced dynamic range of gradient sensing. Our results suggest that the role of Kss1 is not redundant with that of Fus3, and provide functional significance for the strong negative regulation exerted by inactive Kss1 on Ste12, the transcriptional factor essential for the pheromone response.

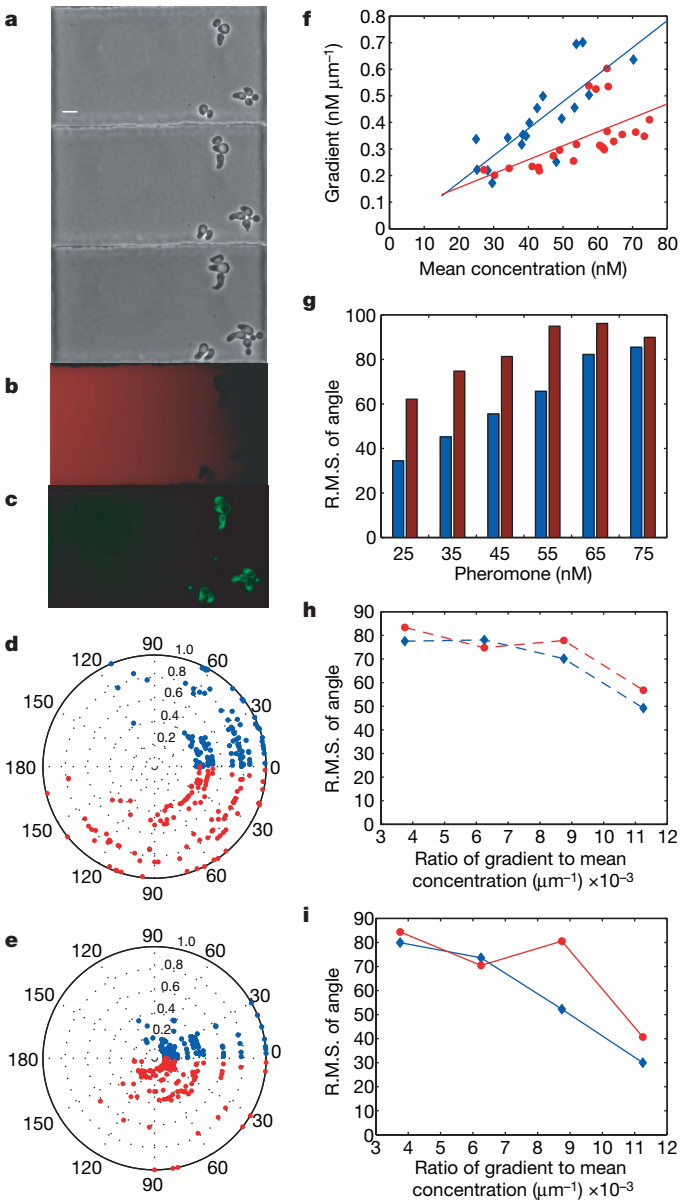

Figure 5 | Quantification of pheromone gradient sensing. a, Chemotropism at 4, 5 and 7 hours (top to bottom) following exposure to a pheromone gradient (scale bar, 10 μm). **b**, **c**, c_{ph} profile (visualized with Alexa Fluor 555 dye) and Fus3–EGFP, respectively, at 5 hours. **d**, **e**, Polar plots representing the dependence of the absolute value of the angle between individual cell projections and the gradient, on c_{ph} (radial dimension in **d**) and γ (radial dimension in **e**), normalized to the maximal values of c_{ph} and γ, respectively. Data are shown for the same cells at 4 hours (red) and 20 h (blue) post-stimulation. **f**, Cell clusters with $\sigma = 0–55^{\circ}$ and $\sigma = 55–110^{\circ}$ are plotted in the c_{ph}–γ plane in blue and red, respectively (σ is the root mean square, R.M.S., of the angle between the projection and the gradient direction); $n = 4–11$ SHM cells per cluster. Straight lines are the corresponding linear regression lines $R^2 = 0.64$ (blue) and $R^2 = 0.38$ (red). **g–i**, σ displayed by groups of SHM cells in wild-type (blue) and *kss1*Δ (red) backgrounds at $t = 4$ hours in **h** and $t = 9$ hours in **g** and **i**, as a function of the c_{ph} (**g**) and γ / c_{ph} (**h–i**). Each bar (or point) represents at least 5 clusters of SHM cells. Bars in (**g**) correspond to 10 nM widths in c_{ph}. Points in **h**, **i** represent bin widths of 0.0025 μm^{-1} in γ / c_{ph}.

METHODS

Yeast and nucleic acid manipulations were performed as previously described[29]. Details on strain construction are present in the Supplementary Information. Fabrication and operation of the microfluidic device is described in detail in Supplementary Information. Evaluation of the pheromone concentrations and gradients, and of the levels of fluorescent reporter expression was performed using custom-written Matlab programs (See Supplementary Information for details). Mathematical model simulations were run in Matlab.

Received 20 June; accepted 21 December 2006.
Published online 18 February 2007.

1. Roberts, C. J. *et al.* Signaling and circuitry of multiple MAPK pathways revealed by a matrix of global gene expression profiles. *Science* **287,** 873–880 (2000).
2. Poritz, M. A., Malmstrom, S., Kim, M. K., Rossmeissl, P. J. & Kamb, A. Graded mode of transcriptional induction in yeast pheromone signalling revealed by single-cell analysis. *Yeast* **18,** 1331–1338 (2001).
3. Ferrell, J. E. Jr & Machleder, E. M. The biochemical basis of an all-or-none cell fate switch in *Xenopus* oocytes. *Science* **280,** 895–898 (1998).
4. Jeon, N. L. *et al.* Neutrophil chemotaxis in linear and complex gradients of interleukin-8 formed in a microfabricated device. *Nature Biotechnol.* **20,** 826–830 (2002).
5. Moore, S. A. Comparison of dose–response curves for alpha factor-induced cell division arrest, agglutination, and projection formation of yeast cells. Implication for the mechanism of alpha factor action. *J. Biol. Chem.* **258,** 13849–13856 (1983).
6. Lee, T. I. *et al.* Transcriptional regulatory networks in *Saccharomyces cerevisiae*. *Science* **298,** 799–804 (2002).
7. Angeli, D., Ferrell, J. E. Jr & Sontag, E. D. Detection of multistability, bifurcations, and hysteresis in a large class of biological positive-feedback systems. *Proc. Natl Acad. Sci. USA* **101,** 1822–1827 (2004).
8. Becskei, A., Seraphin, B. & Serrano, L. Positive feedback in eukaryotic gene networks: cell differentiation by graded to binary response conversion. *EMBO J.* **20,** 2528–2535 (2001).
9. Biggar, S. R. & Crabtree, G. R. Cell signaling can direct either binary or graded transcriptional responses. *EMBO J.* **20,** 3167–3176 (2001).
10. Ferrell, J. E. Jr. Self-perpetuating states in signal transduction: positive feedback, double-negative feedback and bistability. *Curr. Opin. Cell Biol.* **14,** 140–148 (2002).
11. Gardner, T. S., Cantor, C. R. & Collins, J. J. Construction of a genetic toggle switch in *Escherichia coli*. *Nature* **403,** 339–342 (2000).
12. Ninfa, A. J. & Mayo, A. E. Hysteresis vs. graded responses: the connections make all the difference. *Sci. STKE* **232,** pe20 (2004).
13. Pomerening, J. R., Sontag, E. D. & Ferrell, J. E. Jr. Building a cell cycle oscillator: hysteresis and bistability in the activation of Cdc2. *Nature Cell Biol.* **5,** 346–351 (2003).
14. Sha, W. *et al.* From the cover: hysteresis drives cell-cycle transitions in *Xenopus laevis* egg extracts. *Proc. Natl Acad. Sci. USA* **100,** 975–980 (2003).
15. Ozbudak, E. M., Thattai, M., Lim, H. N., Shraiman, B. I. & Van Oudenaarden, A. Multistability in the lactose utilization network of *Escherichia coli*. *Nature* **427,** 737–740 (2004).
16. Bardwell, L., Cook, J. G., Zhu-Shimoni, J. X., Voora, D. & Thorner, J. Differential regulation of transcription: repression by unactivated mitogen-activated protein kinase Kss1 requires the Dig1 and Dig2 proteins. *Proc. Natl Acad. Sci. USA* **95,** 15400–15405 (1998).
17. Cook, J. G., Bardwell, L. & Thorner, J. Inhibitory and activating functions for MAPK Kss1 in the *S. cerevisiae* filamentous-growth signalling pathway. *Nature* **390,** 85–88 (1997).
18. Madhani, H. D., Styles, C. A. & Fink, G. R. MAP kinases with distinct inhibitory functions impart signaling specificity during yeast differentiation. *Cell* **91,** 673–684 (1997).
19. Colman-Lerner, A. *et al.* Regulated cell-to-cell variation in a cell-fate decision system. *Nature* **437,** 699–706 (2005); erratum *Nature* **439,** 502 (2006).
20. Elion, E. A., Satterberg, B. & Kranz, J. E. FUS3 phosphorylates multiple components of the mating signal transduction cascade: evidence for STE12 and FAR1. *Mol. Biol. Cell* **4,** 495–510 (1993).
21. Farley, F. W., Satterberg, B., Goldsmith, E. J. & Elion, E. A. Relative dependence of different outputs of the *Saccharomyces cerevisiae* pheromone response pathway on the MAP kinase Fus3p. *Genetics* **151,** 1425–1444 (1999).
22. Matheos, D., Metodiev, M., Muller, E., Stone, D. & Rose, M. D. Pheromone-induced polarization is dependent on the Fus3p MAPK acting through the formin Bni1p. *J. Cell Biol.* **165,** 99–109 (2004).
23. Roberts, R. L. & Fink, G. R. Elements of a single MAP kinase cascade in *Saccharomyces cerevisiae* mediate two developmental programs in the same cell type: mating and invasive growth. *Genes Dev.* **8,** 2974–2985 (1994).

24. Bardwell, L. *et al.* Repression of yeast Ste12 transcription factor by direct binding of unphosphorylated Kss1 MAPK and its regulation by the Ste7 MEK. *Genes Dev.* **12,** 2887–2898 (1998).
25. Ma, D., Cook, J. G. & Thorner, J. Phosphorylation and localization of Kss1, a MAP kinase of the *Saccharomyces cerevisiae* pheromone response pathway. *Mol. Biol. Cell* **6,** 889–909 (1995).
26. Segall, J. E. Polarization of yeast cells in spatial gradients of alpha mating factor. *Proc. Natl Acad. Sci. USA* **90,** 8332–8336 (1993).
27. Janetopoulos, C., Ma, L., Devreotes, P. N. & Iglesias, P. A. Chemoattractant-induced phosphatidylinositol 3,4,5-trisphosphate accumulation is spatially amplified and adapts, independent of the actin cytoskeleton. *Proc. Natl Acad. Sci. USA* **101,** 8951–8956 (2004).
28. Isbister, C. M., Mackenzie, P. J., To, K. C. W. & O'Connor, T. P. Gradient steepness influences the pathfinding decisions of neuronal growth cones *in vivo*. *J. Neurosci.* **23,** 193–202 (2003).
29. Guthrie, C. & Fink, G. R. (eds) *Methods in Enzymology. Guide to Yeast Genetics and Molecular Biology* (Academic, San Diego, 1991).
30. Unger, M. A., Chou, H. P., Thorsen, T., Scherer, A. & Quake, S. R. Monolithic microfabricated valves and pumps by multilayer soft lithography. *Science* **288,** 113–116 (2000).

Supplementary Information is linked to the online version of the paper at www.nature.com/nature.

Acknowledgements The authors would like to thank M. Piel from A. Murray's laboratory (Harvard) for the initial suggestion of the possible importance of Kss1 in controlling bimodality of pheromone response. They also want to thank P. Sternberg, J. Bruck, M. Peter, A. Colman-Lerner, J. Boeke, L. Bardwell and S. Quake for intellectual and material support of the study. This work was supported by NIH and NSF grants.

Author Contributions S.P., A.G. and A.L. conceived the framework of and wrote the paper, and A.L. oversaw the complete project. A.G., K.C., S.P. and A.L. conceptualized the microfluidic device design and the experimental setup, and K.C. and A.G. fabricated the devices. S.P., P.A.I. and A.L. were involved in the mathematical model setup. Z.H., S.P. and A.L. designed the yeast strains used in the study. S.P. performed the experiments, analysis of results and mathematical model simulations.

Author Information Reprints and permissions information is available at www.nature.com/reprints. The authors declare no competing financial interests. Correspondence and requests for materials should be addressed to A.L. (alev@jhu.edu) and A.G. (agroisman@ucsd.edu).

LETTERS

Transport and Anderson localization in disordered two-dimensional photonic lattices

Tal Schwartz[1], Guy Bartal[1], Shmuel Fishman[1] & Mordechai Segev[1]

One of the most interesting phenomena in solid-state physics is Anderson localization, which predicts that an electron may become immobile when placed in a disordered lattice[1]. The origin of localization is interference between multiple scatterings of the electron by random defects in the potential, altering the eigenmodes from being extended (Bloch waves) to exponentially localized[2]. As a result, the material is transformed from a conductor to an insulator. Anderson's work dates back to 1958, yet strong localization has never been observed in atomic crystals, because localization occurs only if the potential (the periodic lattice and the fluctuations superimposed on it) is time-independent. However, in atomic crystals important deviations from the Anderson model always occur, because of thermally excited phonons and electron–electron interactions. Realizing that Anderson localization is a wave phenomenon relying on interference, these concepts were extended to optics[3,4]. Indeed, both weak[5–7,31] and strong[8–11] localization effects were experimentally demonstrated, traditionally by studying the transmission properties of randomly distributed optical scatterers (typically suspensions or powders of dielectric materials). However, in these studies the potential was fully random, rather than being 'frozen' fluctuations on a periodic potential, as the Anderson model assumes. Here we report the experimental observation of Anderson localization in a perturbed periodic potential: the transverse localization of light caused by random fluctuations on a two-dimensional photonic lattice. We demonstrate how ballistic transport becomes diffusive in the presence of disorder, and that crossover to Anderson localization occurs at a higher level of disorder. Finally, we study how nonlinearities affect Anderson localization. As Anderson localization is a universal phenomenon, the ideas presented here could also be implemented in other systems (for example, matter waves), thereby making it feasible to explore experimentally long-sought fundamental concepts, and bringing up a variety of intriguing questions related to the interplay between disorder and nonlinearity.

During the past few decades, localization of light has drawn considerable attention, beginning with the suggestion that the concept of Anderson localization may be applied to electromagnetic waves[3,4]. These propositions were followed by the prediction[5] and observation[6,7,31] of coherent backscattering (weak localization). More recently, strong localization of light was observed in highly scattering dielectric media[8–11] (typically suspensions or powders of dielectric materials). These experiments demonstrated deviations from classical diffusion, signifying localization of light due to disorder. The past decade has also witnessed progress in random lasing[12], which is based on light localization in random gain media. In all of these studies, the underlying potential was fully random (no lattice), rather than 'frozen' (quenched) random fluctuations on a periodic potential, as Anderson's original model implied (see discussion in Supplementary Information).

Typical experiments studying localization of light examined transmission properties of disordered media. However, a different approach to localization of light was suggested in 1989 (ref. 13), referred to as 'transverse localization'. That concept proposed an optical system that is uniform in one ('longitudinal') direction but contains disorder in the two directions transverse to it. Such a system is described (in the paraxial limit) by a Schrödinger-like equation:

$$i\frac{\partial A}{\partial z}+\frac{1}{2k}\left(\frac{\partial^2 A}{\partial x^2}+\frac{\partial^2 A}{\partial y^2}\right)+\frac{k}{n_0}\Delta n(x,y)A=0 \qquad (1)$$

where $A(\mathbf{r})$ is the slowly-varying envelope of the time-harmonic optical field $E(\mathbf{r},t)=\mathrm{Re}[A(\mathbf{r})e^{i(kz-\omega t)}]$ of frequency ω and wavenumber $k=\omega n_0/c$, with c the vacuum light speed, n_0 and $\Delta n(x,y)$ being the average refractive index and the random fluctuations upon it, respectively. Equation (1) has no time dependence: the evolution of the light is only in space, where the propagation coordinate z replaces time in the Schrödinger equation of quantum mechanics. The localization occurs in the x–y (transverse) plane, as the diffraction-broadening of the beam is arrested by disorder[13]. Hence, the relevant wavenumber is not $k=\omega n_0/c$ but rather the transverse wavenumber, $k_\perp$, which is inversely proportional to the width of the beam, and can be much smaller (10–100 times). In our two-dimensional system, the localization length is given by[2] $\xi=l^*\exp(\pi k_\perp l^*/2)$ with $k_\perp \ll k$, where the mean free path l^* is related to the refractive-index fluctuations. We therefore recognize that even with l^* much larger than the optical wavelength $\lambda=2\pi/kn_0$, transverse localization may occur on reasonably short (experimentally accessible) propagation distances, and the fluctuations in the refractive index can be as small as 10^{-4}. Additionally, in analogy to the requirement of a time-independent potential in the corresponding quantum problem, the most stringent requirement for transverse localization is that the 'potential' $\Delta n(x,y)$ must not vary throughout propagation, otherwise Anderson localization would not occur. Thus far, there have been two pioneering attempts to observe transverse localization in arrays of optical waveguides[14,15]. However, neither has demonstrated Anderson localization, because the experiments lacked the necessary statistical aspect, and control over the disorder. Here, we demonstrate Anderson localization of light in a perturbed periodic potential: transverse localization caused by random fluctuations on a photonic lattice.

Our system (illustrated in Fig. 1a) is a two-dimensional photonic lattice with random fluctuations, represented by equation (1). The index change $\Delta n(x,y)$ contains a periodic term and fluctuations (of the same average period) superimposed on it, such that both the periodic potential and the fluctuations are z-independent. The lattice depth and the relative disorder strength are controlled independently. To make the disordered lattice, we use the optical induction technique[16], now commonly used for studying nonlinear phenomena in photonic lattices[17–23]. This technique transforms an optical

[1]Physics Department, Technion—Israel Institute of Technology, Haifa 32000, Israel.

interference pattern into a refractive-index change in a dielectric material (see Supplementary Information). Disorder is introduced by adding a speckled beam—created by passing a laser beam through a diffuser—to the interference pattern of the plane waves inducing the lattice. The disorder level is set by controlling the intensity of the speckled beam, and ranges continuously from a perfectly periodic lattice (without the speckled beam) to a strongly disordered lattice. We quantify the disorder strength by the ratio between the power of the speckled beam inducing the disorder, and the total power of the lattice-forming beams. As explained in Supplementary Information, we make the fluctuations in the lattice z-independent (propagation-invariant) by creating 'non-diffracting speckles' (a random superposition of diffraction-free Bessel beams).

After forming the disordered lattice, we launch a probe beam into it, and image the intensity distribution at the lattice output onto a CCD camera. Two representative output intensity patterns are displayed in Fig. 1. When the lattice is perfectly periodic (Fig. 1b), the probe beam undergoes 'ballistic transport', manifested by the symmetric hexagonal intensity pattern[24]. In the presence of 15% disorder (Fig. 1c), light tunnels randomly among lattice sites, producing a random intensity distribution at the lattice output after a distance L, $I(x,y,L)$. As we are dealing with a statistical problem in a finite system, it is most important to measure ensemble averages over many realizations of disorder—that is, to repeat the experiment many ($\sim$100) times under the same conditions (strength and statistics of disorder), each time with a different realization of the disorder. To do this, we vary the diffuser position, generating a new speckle pattern, which induces a new disordered lattice, with the same statistical properties as before (see Supplementary Information). The probe beam is launched into the new lattice (at the same location), and its output intensity is recorded. We test the propagation of the probe beam for 12 levels of disorder, and the statistical data for each disorder level is taken over 100 individual experiments.

Figure 2 presents the results of these statistical measurements. For each realization of disorder, the confinement of the beam at the output plane is quantified by the inverse participation ratio $P \equiv \left[\int I(x,y,L)^2 \mathrm{d}x\mathrm{d}y\right] \Big/ \left[\int I(x,y,L)\mathrm{d}x\mathrm{d}y\right]^2$, which has units of inverse area, and an average effective width $\omega_{\mathrm{eff}} = \langle P \rangle^{-1/2}$, where $\langle \cdots \rangle$ stands for averaging over multiple realizations of disorder (of the same level). Figure 2a shows the average (over 100 realizations) effective width at the lattice output as a function of disorder level, revealing that the effective width of the output probe beam decreases monotonically as the level of disorder is increased. That is, transport in the lattice is reduced by the presence of random fluctuations, even though these fluctuations are very weak ($|\Delta n|/n_0 < 2 \times 10^{-4}$). Figure 2b shows the corresponding average value of the inverse participation ratio, $\langle P \rangle$, as a function of the disorder level, along with its statistical standard deviation (marked by error bars). Figure 2b reveals that, when Anderson localization occurs, the relative fluctuations of the inverse participation ratio, $\Delta P/\langle P \rangle$, are very large—of the order of unity. This result agrees with the prediction[25,26] that the relative fluctuations in P are inversely proportional to the dimensionless diffusion coefficient ('conductance'). In our experiments, this coefficient is close to unity, so these large fluctuations are expected.

According to the scaling theory of localization, in two-dimensional systems Anderson localization always occurs, for any amount of disorder[25] (unlike three-dimensional systems, where localization occurs above some critical level of disorder). However, the localization length is exponentially large, posing a great challenge for the observation of two-dimensional localization. In the transverse localization scheme[13], a narrow beam propagating through the medium first undergoes diffusive broadening, until its width becomes comparable to the localization length. Then, localization takes place, and the beam stays localized, acquiring exponentially decaying 'tails'. As the disorder level is increased, the initial distance of diffusive propagation decreases, and the beam evolves faster into the localized

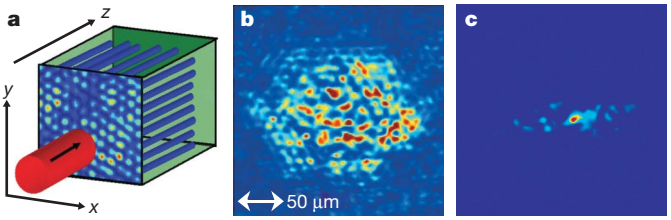

Figure 1 | Transverse localization scheme. a, A probe beam entering a disordered lattice, which is periodic in the two transverse dimensions (x and y) but invariant in the propagation direction (z). In the experiment described here, we use a triangular (hexagonal) photonic lattice with a periodicity of 11.2 μm and a refractive-index contrast of $\sim 5.3 \times 10^{-4}$. The lattice is induced optically, by transforming the interference pattern among three plane waves into a local change in the refractive index, inside a photorefractive SBN:60 ($Sr_{0.6}Ba_{0.4}Nb_2O_6$) crystal. The input probe beam is of 514 nm wavelength and 10.5 μm full-width at half-maximum (FWHM), and it is always launched at the same location, while the disorder is varied in each realization of the multiple experiments. **b**, Experimentally observed diffraction pattern after $L = 10$ mm propagation in the fully periodic hexagonal lattice. **c**, Typical experimentally observed intensity distribution after $L = 10$ mm propagation in one particular realization of the 15% disorder in the lattice.

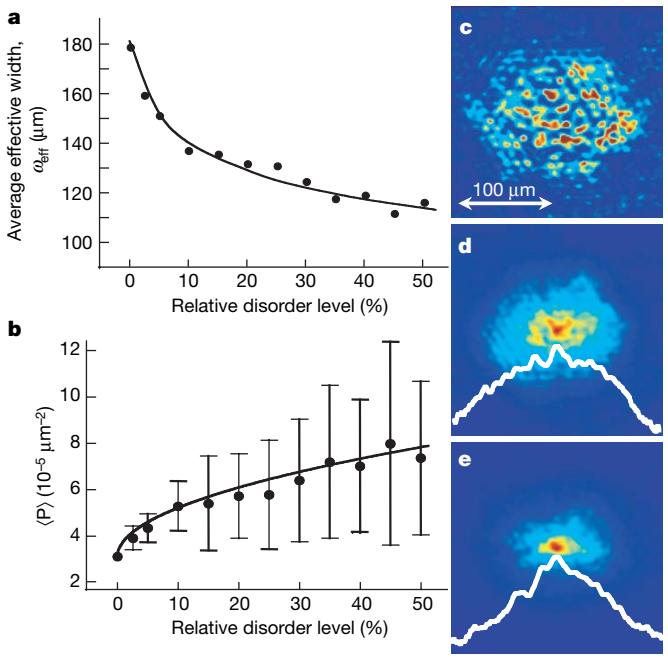

Figure 2 | Experimental results for propagation in disordered lattices. **a**, Ensemble-averaged effective width measured experimentally at the lattice output, as a function of disorder level. The ensemble average is taken over 100 realizations of disorder. **b**, Average inverse participation ratio as function of disorder level. The ensemble average is taken over 100 realizations of disorder. The error bars are the statistical standard deviations of P. **c**–**e**, Experimentally measured intensity distributions at the lattice output, without disorder (**c**) and with 15% (**d**) and 45% (**e**) disorder. **d** and **e** are averaged over 100 realization of disorder. The white curves show the logarithm of the averaged intensity profile, taken along the horizontal line passing through the beam's peak. In **d**, fitting the curve to a gaussian profile of the form $I \propto \exp(-2r^2/\sigma^2)$ yields the value $\sigma = 92$ μm. In **e**, the fitted curve corresponds to an intensity profile of the form $I \propto \exp(-2|r|/\xi)$, where $|r|$ is the distance from the centre of the beam, and $\xi = 64$ μm is the localization length as determined by the exponential fit. In terms of FWHM, the width of the fitted profile of **e** is 44 μm, compared to 108 μm FWHM for the gaussian fit in the diffusive case of **d**, and it is also three times narrower than the diffraction pattern observed in the absence of disorder: 120 μm (**c**). The transition from the gaussian curve of **d** to the exponentially decaying curve of **e** displays the crossover from diffusive transport (**d**) to Anderson localization (**e**).

state. Consequently, when examining the beam after a given propagation distance, the output beam should display a crossover, from diffusive transport to localization, as the disorder level is increased (to be distinguished from the localization transition, occurring in three-dimensional systems).

In order to reveal the transport properties of the disordered lattice, we average over the intensity distributions acquired at the lattice output, and examine the ensemble-average profile. Figure 2 shows $\langle I(x,y,L)\rangle$ in the absence of disorder (Fig. 2c), with moderate disorder (15%, Fig. 2d) and with strong disorder (45%, Fig. 2e). Figure 2 reveals that the (ensemble-averaged) beam intensity structure narrows as the disorder level is increased. Examining the logarithm of the intensity cross-section in Fig. 2d, taken through the peak of the ensemble-averaged intensity, reveals a gaussian shape (the parabolic curve of the logarithm, white curve in Fig. 2d), indicating diffusive broadening. This means that, for the particular level of disorder in Fig. 2d, the localization length is rather large, hence the localization effect is not observed yet. However, when the disorder is stronger (Fig. 2e), the best fit of the logarithm of the ensemble-averaged intensity profile is a linear curve, implying a structure decaying exponentially from its centre. That is, the ensemble-average intensity profile displayed in Fig. 2e exhibits Anderson localization. The transition from Fig. 2d to Fig. 2e manifests the crossover from diffusive transport to localization as the disorder level is increased.

In order to corroborate our experimental results, we simulate the propagation of the probe beam under typical experimental parameters, repeating the process with 100 different random realizations of the disorder, at each disorder level. Figure 3a shows the averaged effective width as a function of propagation distance (on a double-logarithmic scale), where each curve represents a different level of disorder, and the dashed lines designate a power-law ($\omega_{\mathrm{eff}} \propto z^{\nu}$) relation, with $\nu = 1$ and $\nu = 1/2$. For a perfectly periodic lattice, the curve approaches a constant slope with $\nu = 1$, meaning that the beam broadens linearly as it propagates in the lattice, signifying ballistic transport. When weak disorder (2.5%) is introduced, the behaviour is completely different: the curve approaches $\nu = 1/2$, indicating that the (mean) transport is now diffusive (over the range of the simulated propagation). With stronger disorder the beam first expands diffusively, but after a short propagation distance the exponent ν decreases to a value in the range $0 < \nu < 1/2$ (depending on the disorder strength), and the broadening of the beam becomes slower. At disorder levels higher than 20%, ν approaches zero, and the only change in the beam width is due to statistical fluctuations. At this stage the light is localized, and the further broadening of the beam is arrested by the disorder. This is again confirmed by calculating the logarithm of the intensity profile. As in the experimental results, in the localization regime (30% disorder, Fig. 3c), the average intensity pattern decays exponentially from the centre. In contrast to that, in the diffusive regime (2.5% disorder, Fig. 3b), the average beam has a gaussian-like profile. Following our experimental findings, corroborated by our numerical simulations, we conclude that we have indeed observed Anderson localization in disordered photonic lattices.

Finally, we study how nonlinearities affect Anderson localization. In solid-state physics, the interaction between electrons is usually considered to be an obstacle for observing Anderson localization. However, the interplay between disorder and nonlinearity may yield interesting new physical phenomena. This fundamental subject has been the subject of ongoing theoretical research[27–29], yet thus far it is not fully understood, and experimental studies are scarce[14,30]. Our system offers a convenient platform for such experiments, as nonlinearity can be added in a controlled fashion.

Figure 4a, b presents numerical results for a probe beam propagating in the disordered lattice, with focusing and defocusing Kerr-type nonlinearity. The system is described by:

$$i\frac{\partial A}{\partial z} + \frac{1}{2k}\left(\frac{\partial^2 A}{\partial x^2} + \frac{\partial^2 A}{\partial y^2}\right) + \frac{k}{n_0}\Delta n(x,y) + \sigma\frac{k}{n_0}n_2|A|^2 A = 0 \quad (2)$$

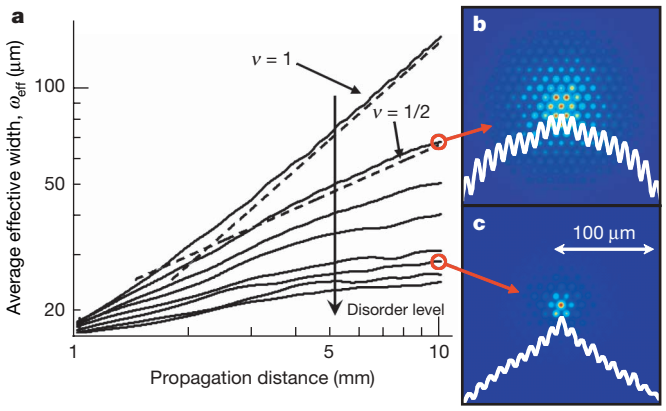

Figure 3 | Results of numerical simulations of linear propagation in disordered lattices. **a**, Averaged effective width, ω_{eff}, versus propagation distance, in a log–log plot, for different levels of disorder (0–50%). The dashed lines correspond to ballistic ($\omega_{\mathrm{eff}} \propto z$) and diffusive ($\omega_{\mathrm{eff}} \propto z^{1/2}$) transport. **b**, **c**, Averaged intensity distributions at the lattice output (after propagation of $L = 10$ mm), showing diffusive transport with a gaussian intensity profile with 2.5% disorder (**b**) and localization with an exponential decay of intensity at 30% disorder (**c**). The white curve shows the logarithm of the intensity profile, taken along the horizontal line passing through the beam's peak. The mean free path and the localization length evaluated from these simulations are approximately $l^* \approx 5$ μm and $\xi \approx 29$ μm, respectively (see calculation details in Supplementary Information).

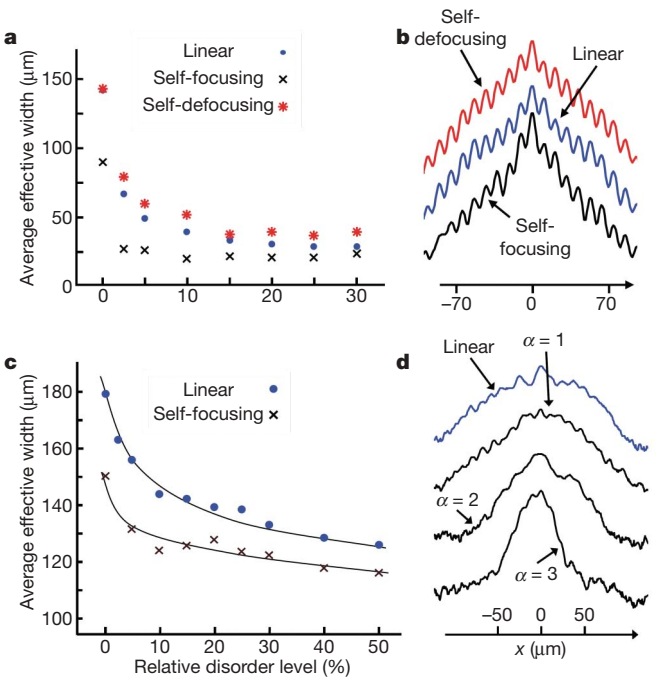

Figure 4 | Numerical (top row) and experimental (bottom row) results, showing the effects of nonlinearity on Anderson localization. **a**, Calculated effective width at the lattice output versus disorder level for linear and nonlinear propagation. **b**, Calculated intensity profiles (on a logarithmic scale) at the lattice output after linear and nonlinear propagation with 15% disorder. **c**, Experimentally measured effective width at the lattice output versus disorder level for linear propagation (upper blue curve) and under self-focusing conditions (lower black curve), for $L = 10$ mm of propagation (the lines are guides to the eye). **d**, Experimental results for the ensemble-average intensity profile (on a logarithmic scale) with 15% disorder, and increasing strengths of a focusing-type nonlinearity ($\alpha = 1$, 2 and 3, black curves), compared to linear propagation (blue curve). The ensemble average is taken over 100 different realizations of the disordered lattice, and all data are taken after $L = 10$ mm of propagation. The self-focusing nonlinearity enhances localization: the localization length decreases as the nonlinearity increases.

where n_2 scales the strength of the nonlinearity, $\sigma = 1$ ($\sigma = -1$) standing for self-focusing (self-defocusing). In Fig. 4a, the maximal nonlinear contribution $n_2|A|^2$ is 15% of the lattice depth. Figure 4a shows the output averaged effective width, for different values of disorder. In the absence of disorder, the self-focusing strength is insufficient to form a lattice soliton[17,18], yet it does reduce the diffraction broadening. The general trend of all three generic cases (linear, self-focusing and defocusing) is similar: disorder suppresses transport. In the presence of self-focusing, the initial (at low disorder levels) reduction in the width of the average output beam is much steeper than in the linear case. At high disorder levels, where localization takes place, the difference between linear and nonlinear propagation is reduced, and the behaviour is dominated primarily by disorder. In contrast, the effect of defocusing is minor at all disorder levels: the width of the average output beam is slightly increased due to self-defocusing (which acts to spread the beam faster than its linear diffraction). After a short propagation distance, in which the beam has broadened and its intensity has diminished, the remaining propagation is essentially as if the medium were linear. A more interesting behaviour is revealed in Fig. 4b, showing the logarithm of the intensity profile of the output beam, under the combined action of 15% disorder and self-focusing (lower graph), self-defocusing (top) and linear propagation (middle). For this disorder level, the localization regime, during linear propagation, is not yet reached, as the average beam profile is non-exponential. Again, the defocusing effect is minor: the average intensity profile is only slightly broader. However, under self-focusing, the beam becomes localized with exponentially decaying tails (bottom curve in Fig. 4b). This clearly indicates that self-focusing enhances localization. That is, in the presence of an 'attractive nonlinearity', localization is observed at lower levels of disorder, for a given (finite) propagation distance. We therefore study the combined effects of disorder and nonlinearity experimentally, for the particular case studied numerically in Fig. 4a.

The results are shown in Fig. 4c, where we compare the averaged effective width as a function of disorder level, for the linear case (upper curve, circles), and under self-focusing nonlinearity (lower curve, crosses), where the nonlinearity strength is set by making the probe intensity equal to the interference maxima of the lattice-writing beams (for a perfect lattice). These experiments show that self-focusing enhances localization effects. Figure 4d emphasizes this observation: shown are the ensemble-averaged intensity profiles (logarithmic scale) for a lattice with 15% disorder at various strengths of nonlinearity. We denote by α the ratio between the peak intensity of the probe beam and the maximum intensity of the lattice-forming beams, and perform statistical measurements for $\alpha = 1$, 2 and 3 (black curves in Fig. 4d). Comparing the logarithm of the averaged intensity profile to that of linear propagation (blue curve in Fig. 4d), we observe the effect predicted by the simulation: for $\alpha = 1$, self-focusing enhances localization, altering the intensity profile from diffusive-like to exponentially decaying. As the nonlinearity is made stronger, the intensity profile narrows down further ($\alpha = 2$), until, at $\alpha = 3$, the output beam profile resembles the input profile, suggesting the formation of a soliton. This kind of 'average soliton', forming in the highly nonlinear disordered lattice, is in fact an ensemble-average over many realizations of disorder, which survives the lattice imperfections. Such an 'average soliton' has not, to our knowledge, been observed before.

Our methods for real-time induction of photonic lattices with controlled disorder embedded in them, which have facilitated the observation of Anderson localization and the effects of nonlinearity on localization, offer an elegant means for its statistical exploration. We anticipate that the methods presented here will become a standard tool in future experimental research on transverse localization. They should also prove useful in future work on the influence of nonlinearity on localization, where a variety of intriguing questions arise. For example, can solitons form in the presence of random fluctuations in a nonlinear periodic structure? Can modulation instability and spontaneous pattern formation occur in perturbed nonlinear lattices? These and related questions are now accessible experimentally in our system.

Received 6 November 2006; accepted 25 January 2007.

1. Anderson, P. W. Absence of diffusion in certain random lattices. *Phys. Rev.* **109,** 1492–1505 (1958).
2. Lee, P. A. & Ramakrishnan, T. V. Disordered electronic systems. *Rev. Mod. Phys.* **57,** 287–337 (1985).
3. John, S. Electromagnetic absorption in a disordered medium near a photon mobility edge. *Phys. Rev. Lett.* **53,** 2169–2172 (1984).
4. Anderson, P. W. The question of classical localization: a theory of white paint? *Phil. Mag. B* **52,** 505–509 (1985).
5. Akkermans, E. & Maynard, R. Weak localization of waves. *J. Phys. Lett.* **46,** 1045–1053 (1985).
6. Van Albada, M. P. & Lagendijk, A. Observation of weak localization of light in a random medium. *Phys. Rev. Lett.* **55,** 2692–2695 (1985).
7. Wolf, P. E. & Maret, G. Weak localization and coherent backscattering of photons in disordered media. *Phys. Rev. Lett.* **55,** 2696–2699 (1985).
8. Wiersma, D. S., Bartolini, P., Lagendijk, A. & Righini, R. Localization of light in a disordered medium. *Nature* **390,** 671–673 (1997).
9. Berry, M. V. & Klein, S. Transparent mirrors: rays, waves and localization. *Eur. J. Phys.* **18,** 222–228 (1997).
10. Chabanov, A. A., Stoytchev, M. & Genack, A. Z. Statistical signatures of photon localization. *Nature* **404,** 850–853 (2000).
11. Störzer, M., Gross, P., Aegerter, C. M. & Maret, G. Observation of the critical regime near Anderson localization of light. *Phys. Rev. Lett.* **96,** 063904 (2006).
12. Cao, H. *et al.* Random laser action in semiconductor powder. *Phys. Rev. Lett.* **82,** 2278–2281 (1999).
13. De Raedt, H., Lagendijk, A. & de Vries, P. Transverse localization of light. *Phys. Rev. Lett.* **62,** 47–50 (1989).
14. Pertsch, T. *et al.* Nonlinearity and disorder in fiber arrays. *Phys. Rev. Lett.* **93,** 053901 (2004).
15. Eisenberg, H. *Nonlinear Effects in Waveguide Arrays*. PhD thesis (supervisor Y. Silberberg) Weizmann Institute of Science (2002).
16. Efremidis, N. K., Sears, S., Christodoulides, D. N., Fleischer, J. W. & Segev, M. Discrete solitons in photorefractive optically induced photonic lattices. *Phys. Rev. E* **66,** 046602 (2002).
17. Fleischer, J. W., Carmon, T., Segev, M., Efremidis, N. K. & Christodoulides, D. N. Observation of discrete solitons in optically induced real time waveguide arrays. *Phys. Rev. Lett.* **90,** 023902 (2003).
18. Fleischer, J. W., Segev, M., Efremidis, N. K. & Christodoulides, D. N. Observation of two-dimensional discrete solitons in optically induced nonlinear photonic lattices. *Nature* **422,** 147–150 (2003).
19. Neshev, D. N. *et al.* Observation of discrete vortex solitons in optically induced photonic lattices. *Phys. Rev. Lett.* **92,** 123903 (2004).
20. Fleischer, J. W. *et al.* Observation of vortex-ring "discrete" solitons in 2D photonic lattices. *Phys. Rev. Lett.* **92,** 123904 (2004).
21. Cohen, O. *et al.* Observation of random-phase lattice solitons. *Nature* **433,** 500–503 (2005).
22. Trompeter, H. *et al.* Bloch oscillations and Zener tunneling in two-dimensional photonic lattices. *Phys. Rev. Lett.* **96,** 053903 (2006).
23. Freedman, B. *et al.* Wave and defect dynamics in nonlinear photonic quasicrystals. *Nature* **440,** 1166–1169 (2006).
24. Bartal, G. *et al.* Brillouin zone spectroscopy of nonlinear photonic lattices. *Phys. Rev. Lett.* **94,** 163902 (2005).
25. Abrahams, E., Anderson, P. W., Licciardello, D. C. & Ramakrishnan, T. V. Scaling theory of localization: Absence of quantum diffusion in two dimensions. *Phys. Rev. Lett.* **42,** 673–676 (1979).
26. Mirlin, A. D. Statistics of energy levels and eigenfunctions in disordered systems. Phys. Rep. **326,** 259–382 (2000).
27. Devillard, P. & Souillard, B. Polynomially decaying transmission for the nonlinear Schrödinger equation in a random medium. *J. Stat. Phys.* **43,** 423–439 (1986).
28. Doucot, B. & Rammal, R. Invariant-imbedding approach to localization. II. Nonlinear random media. *J. Phys.* **48,** 527–546 (1987).
29. Li, Q., Soukoulis, C. M., Pnevmatikos, St & Economou, E. N. Scattering properties of solitons in nonlinear disordered chains. *Phys. Rev. B* **38,** 11888–11891 (1988).
30. McKenna, M. J., Stanley, R. L. & Maynard, J. D. Effects of nonlinearity on Anderson localization. *Phys. Rev. Lett.* **69,** 1807–1810 (1992).
31. Etemad, S., Thompson, R. & Andrejco, M. J. Weak localization of photons: universal fluctuations and ensemble averaging. *Phys. Rev. Lett.* **57,** 575–578 (1986).

Supplementary Information is linked to the online version of the paper at www.nature.com/nature.

Acknowledgements We are indebted to our colleagues B. Shapiro and E. Akkermans for discussions on Anderson localization. This research was supported by the Israeli Science Foundation, by the German-Israeli DIP Project, and by the Russell Berrie Nanotechnology Institute at the Technion, Israel.

Author Information Reprints and permissions information is available at www.nature.com/reprints. The authors declare no competing financial interests. Correspondence and requests for materials should be addressed to M.S. (msegev@tx.technion.ac.il).

Vol 446|1 March 2007|doi:10.1038/nature05555

LETTERS

Bipolar supercurrent in graphene

Hubert B. Heersche[1]*, Pablo Jarillo-Herrero[1]*, Jeroen B. Oostinga[1], Lieven M. K. Vandersypen[1] & Alberto F. Morpurgo[1]

Graphene—a recently discovered form of graphite only one atomic layer thick[1]—constitutes a new model system in condensed matter physics, because it is the first material in which charge carriers behave as massless chiral relativistic particles. The anomalous quantization of the Hall conductance[2,3], which is now understood theoretically[4,5], is one of the experimental signatures of the peculiar transport properties of relativistic electrons in graphene. Other unusual phenomena, like the finite conductivity of order $4e^2/h$ (where e is the electron charge and h is Planck's constant) at the charge neutrality (or Dirac) point[2], have come as a surprise and remain to be explained[5–13]. Here we experimentally study the Josephson effect[14] in mesoscopic junctions consisting of a graphene layer contacted by two closely spaced superconducting electrodes[15]. The charge density in the graphene layer can be controlled by means of a gate electrode. We observe a supercurrent that, depending on the gate voltage, is carried by either electrons in the conduction band or by holes in the valence band. More importantly, we find that not only the normal state conductance of graphene is finite, but also a finite supercurrent can flow at zero charge density. Our observations shed light on the special role of time reversal symmetry in graphene, and demonstrate phase coherent electronic transport at the Dirac point.

Owing to the Josephson effect[14,16], a supercurrent can flow through a normal conductor placed between two closely spaced superconducting electrodes. For this to happen, transport in the normal conductor must be phase coherent and time reversal symmetry (TRS) must be present. In graphene, the Josephson effect can be investigated in the 'relativistic' regime[15], where the supercurrent is carried by Dirac electrons. However, it is not clear a priori that graphene can support supercurrents, because other quantum interference phenomena that require both phase coherence and TRS were found to be absent or strongly suppressed in previous experiments[17]. Below we show experimentally that the Josephson effect in graphene is a robust phenomenon, and argue that its robustness is intimately linked to graphene's unique electronic structure.

Single- and few-layer graphene Josephson junctions are fabricated on oxidized Si substrates by mechanical exfoliation of bulk graphite[1], followed by optical microscope inspection to locate the thinnest graphitic flakes, and electron beam lithography to define electrical contacts. Figure 1a shows an atomic force microscope image of a typical device. We use as superconducting contacts a Ti/Al bilayer (10/70 nm). Titanium ensures good electrical contact to graphene, and Al establishes a sufficiently high critical temperature to enable the observation of supercurrents in a dilution refrigeration set-up[18]. Before discussing their superconducting properties, we first characterize the devices with the superconducting electrodes in the normal state. Figure 1c shows the two-terminal resistance, R, versus gate voltage, V_G, for one of our samples. The strong V_G-dependence of R provides a first indication that the device consists of at most a few layers of graphene[1], since, owing to screening, V_G affects the carrier density only in the bottom one or two layers. For single layers, the position of the resistance maximum corresponds to the gate voltage at which the Fermi energy is located at the Dirac point, V_D, and we typically find that $|V_D| < 20$ V. We unambiguously determine the single layer character of a device by quantum Hall effect (QHE) measurements. Because the superconducting proximity effect requires two closely spaced electrodes, we can only perform magnetoconductance measurements in a two terminal configuration. In general, the conductance, G, measured in this way is a mixture of longitudinal and Hall signals, but at high fields $G \approx |G_{Hall}|$ (this approximation is exact at the Hall plateaus[19]). Indeed, the measurement of G versus V_G at $B = 10$ T shows clearly identifiable Hall plateaus at half-integer multiples of $4e^2/h$ (Fig. 1d), characteristic of the QHE in single layer graphene[2,3]. This demonstrates that, even in

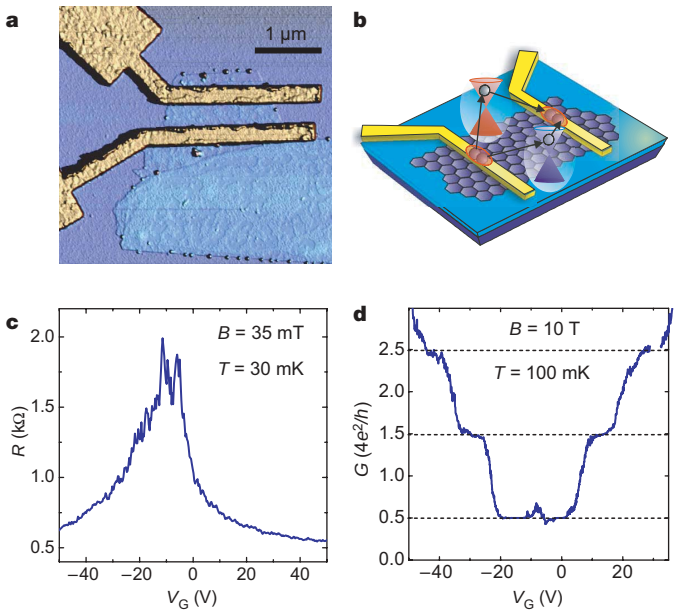

Figure 1 | Sample characterization. a, Atomic force microscope image of a single layer graphene device between two superconducting electrodes. We have fabricated devices with electrode separations in the range 100–500 nm. **b**, Schematic representation of graphene between superconducting electrodes. The two electrons in a Cooper pair entering graphene go into different K-valleys, represented by the red and blue cones (see text). **c**, Two-terminal resistance versus gate voltage, V_G, at $T = 30$ mK and a small magnetic field, $B = 35$ mT, to drive the electrodes into the normal state. The aperiodic conductance fluctuations are due to random quantum interference of electron waves (see also Fig. 4). **d**, Two terminal conductance, G, versus V_G at high magnetic field, $B = 10$ T, and $T = 100$ mK, showing a series of steps at half-integer values of $4e^2/h$, characteristic of the anomalous QHE in single layer graphene.

[1]Kavli Institute of Nanoscience, Delft University of Technology, PO Box 5046, 2600 GA, Delft, The Netherlands.
*These authors contributed equally to this work.

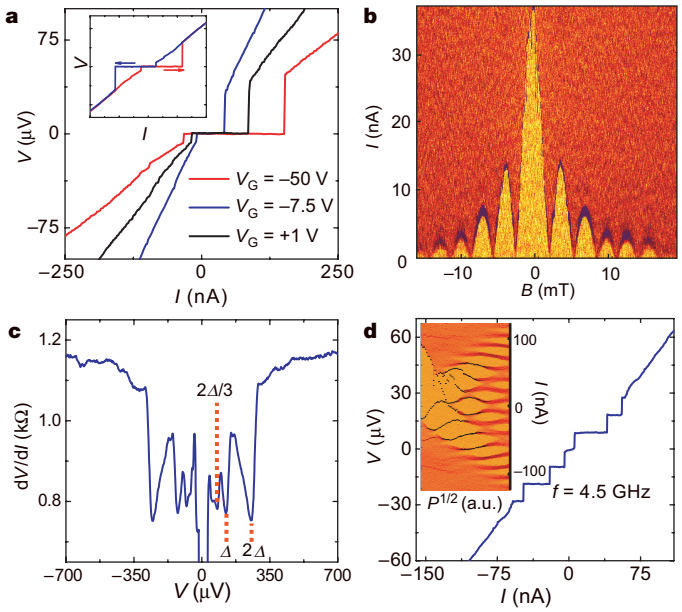

Figure 2 | Josephson effect in graphene. **a**, Voltage, V, versus current bias, I, characteristics at various V_G, showing a modulation of the critical current. Inset, current bias sweeps from negative to positive (red) and vice versa (blue), showing that the asymmetry in the main panel is due to hysteretic behaviour (the retrapping current is smaller than the switching current, as is typical for an underdamped junction). **b**, Colour-scale representation of $dV/dI(I,B)$ at $T = 30$ mK (yellow-orange is zero, that is, the supercurrent region, and red corresponds to finite dV/dI). The critical current exhibits a series of oscillations described by a Fraunhofer-like pattern. **c**, Differential resistance, dV/dI, versus V, showing multiple Andreev reflection dips below the superconducting energy gap. The dips in dV/dI occur at values of $V = 2\Delta/en$, where n is an integer number. **d**, a.c. Josephson effect. The Shapiro steps in the I–V characteristics appear when the sample is irradiated with microwaves. In the example, we applied 4.5 GHz microwaves, resulting in 9.3 μV voltage steps. Inset, colour-scale plot showing the characteristic microwave amplitude ($P^{1/2}$; a.u., arbitrary units) dependence of the a.c. Josephson effect (orange and red correspond respectively to zero and finite dV/dI).

mesoscopic samples, the QHE can be used to identify single layer devices.

Cooling down the devices below the critical temperature of the electrodes ($T_c \approx 1.3$ K) leads to proximity-induced superconductivity in the graphene layer. A direct proof of induced superconductivity is the observation of a Josephson supercurrent[20]. Figure 2a shows the current–voltage (I–V) characteristics of a single layer device. The current flows without resistance (no voltage drop at finite current) below the critical current, I_c (what we actually measure is the switching current; the intrinsic I_c may be higher[20,21]). In our devices, I_c ranged from ~10 nA to more than 800 nA (at high V_G). Remarkably, we have measured proximity-induced supercurrents in all the devices that we tested (17 flakes in total, with several devices on some flakes), including four flakes that were unambiguously identified as single layer graphene via QHE (the rest being probably two to four layers thick). This clear observation demonstrates the robustness of the Josephson effect in graphene junctions. (The data shown are representative of the general behaviour observed; the measurements shown in Figs 1, 2a, c, d and 3 have been taken on the same device, whereas those in Figs 2b and 4 correspond to a different single layer device, shown in Fig. 1a.)

To investigate further the superconducting properties of our devices, we measured the dependence of I_c on magnetic field (Fig. 2b). The critical current exhibits an oscillatory Fraunhofer-like pattern, with at least six visible side lobes, which is indicative of a uniform supercurrent density distribution[22]. The periodicity of the oscillations is in the ideal case expected to be equal to a flux quantum Φ_o divided by the junction area. The area that corresponds to the 2.5 ± 0.5 mT period is $0.8 \pm 0.2\ \mu m^2$, which is in good agreement with the measured device area ($0.7 \pm 0.2\ \mu m^2$) determined from the atomic force microscope image. Applying a radio-frequency field to the sample results in the observation of quantized voltage steps, known as Shapiro steps, in the I–V characteristics[20]. The voltage steps, of amplitude $\hbar\omega/2e$ (ω is the microwave frequency), are a manifestation of the a.c. Josephson effect, and are evident in Fig. 2d. The induced superconductivity manifests itself also at finite bias in the form of subgap structure in the differential resistance due to multiple Andreev reflections[23], as shown in Fig. 2c. This subgap structure consists of a series of minima at source–drain voltages $V = 2\Delta/en$ ($n = 1,2\ldots$), which enables us to determine the superconducting gap, Δ. We find $\Delta = 125$ μeV, as expected for our Ti/Al bilayers[18]. For $V > 2\Delta/e$, the differential resistance returns to the

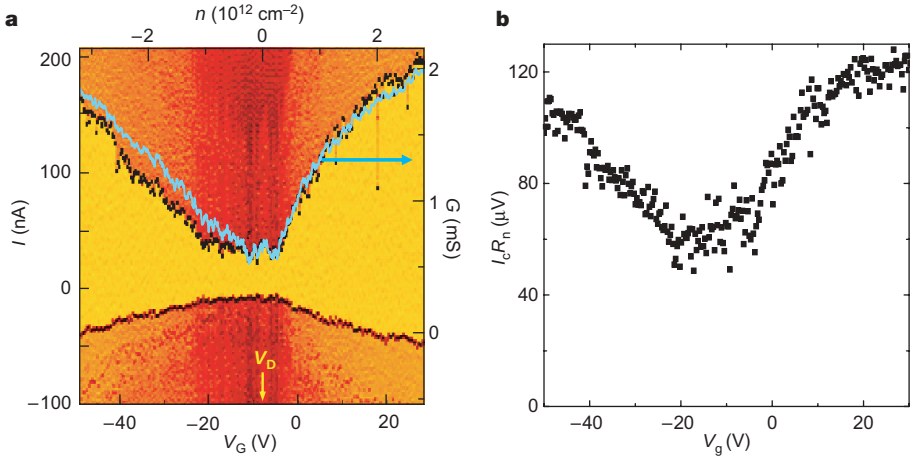

Figure 3 | Bipolar supercurrent transistor behaviour and finite supercurrent at the Dirac point. **a**, Colour-scale plot of $dV/dI(V_G,I)$. Yellow means zero, that is, the supercurrent region, and finite dV/dI increases via orange to dark red. The current is swept from negative to positive values, and is asymmetric owing to the hysteresis associated with an underdamped junction (see also Fig. 2a inset). The top axis shows the electron density, n, as obtained from geometrical considerations[1]. For large negative (positive) V_G the supercurrent is carried by hole (electron) Cooper pairs. The supercurrent at the Dirac point (V_D) is finite. Note that the critical current is not symmetric with respect to V_D. The origin of this asymmetry is not known, but a similar asymmetry is seen in the normal state conductance (blue curve). **b**, Product of the critical current times the normal state resistance versus V_G. The normal state resistance is measured at zero source–drain bias, at $T = 30$ mK and with a small magnetic field to drive the electrodes into the normal state. The I_cR_n product exhibits a dip around the Dirac point (see main text).

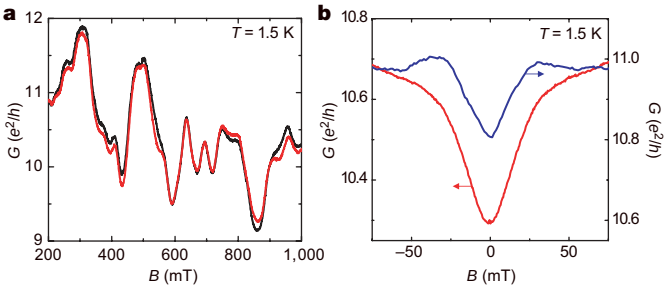

Figure 4 | Magnetoconductance measurements. **a**, Conductance versus magnetic field at $T \approx 1.5$ K for a single layer device at $V_G = V_D$. The red and black traces are two subsequent measurements, showing reproducible conductance fluctuations, whose root mean square amplitude is e^2/h. **b**, Low field magnetoconductance measured at $T \approx 1.5$ K (electrodes in the normal state) for two different single layer devices (the red trace corresponds to the device measured in **a**), showing that the amplitude of the weak localization effect is sample dependent and suppressed as compared to the expected value, $\sim e^2/h$. Each curve results from an ensemble average of 66 individual magnetoresistance measurements taken at different gate voltages near the Dirac point.

normal state value. From the suppression of the differential resistance observed while changing the bias from above to below the gap, we can estimate that the average transparency of the superconductor–graphene interface is ~0.7–0.8.

Having established the existence of the Josephson effect in graphene, we analyse the gate voltage dependence of the critical current. Figure 2a shows several I–V traces taken at different V_G, where it can already be seen that varying the gate voltage has a strong effect on the maximum supercurrent flowing through the device. This behaviour can be more readily seen in Fig. 3a, where the differential resistance is plotted as a function of current bias and gate voltage. By changing V_G we can continuously shift the Fermi energy from the valence band ($V_G < V_D$) to the conduction band ($V_G > V_D$): irrespective of the sign of V_G, we find a finite supercurrent. This demonstrates that the devices operate as bipolar supercurrent transistors: the supercurrent is carried by hole Cooper pairs when the Fermi level is in the valence band and by electron Cooper pairs when it is in the conduction band. Note that in going from valence to conduction band, we sweep the position of the Fermi level through the Dirac point. Strikingly, even then the supercurrent remains finite, despite the fact that for perfect graphene theory predicts[24] a vanishing density of states at $V_G = V_D$. This behaviour has been observed in all samples, and demonstrates that electronic transport in graphene is phase coherent irrespective of the gate voltage, including when the Fermi level is located at the Dirac point.

In conventional Josephson junctions, the critical current correlates with the normal state conductance, G_n (ref. 25). In graphene this correlation can be observed directly, as shown in Fig. 3a, because both I_c and G_n depend on V_G. To analyse this correlation, we plot the product of the measured critical current and the normal state resistance ($R_n = 1/G_n$), or I_cR_n product (see Fig. 3b). We find that at high gate voltage $I_cR_n \approx \Delta/e$, and that I_cR_n is suppressed by a factor of 2–3 around the Dirac point. The observed I_cR_n product is thus close to the theoretical value of $\sim 2.5\Delta/e$ for a model system of graphene in the ballistic regime[15]. The remaining discrepancy may be accounted for by the difference between the measured critical current (or switching current) and the intrinsic critical current[20,21]. This difference is in general hard to quantify and depends on the electromagnetic environment of the sample, but it is expected to be more pronounced when I_c itself is smaller (that is, at low V_G), and could thus well explain the observed V_G dependence of I_cR_n.

An interesting aspect of supercurrent in graphene is the special role of time reversal symmetry in the Josephson effect compared to that in phase coherent transport in the normal state. At low energy, the band structure of graphene consists of two identical, independent valleys centred on the so-called K_1 and K_2 points[24], which transform into each other under time reversal. As Cooper pairs are made out of time reversed electron states, the two electrons in Cooper pairs that are injected from the superconducting electrodes into graphene go to opposite K-points[15] (see Fig. 1b). In this way, the presence of a superconducting electrode provides an intrinsic mechanism that couples phase coherently electronic states belonging to opposite valleys. The dynamics of electrons is then described by the full (two-valley) hamiltonian of graphene that is time reversal symmetric.

The situation is very different for normal-state transport where the dynamics of the electrons is determined by a 'one-valley' hamiltonian. This has important consequences not only for the QHE[4,5], but also for quantum interference. When the two valleys are fully decoupled, interference originating from coherent propagation of electrons along time reversed trajectories cannot occur, as these trajectories involve quantum states from opposite K-points. As a consequence, quantum corrections to the conductivity, like weak localization, would be absent (note that for the single-valley hamiltonian there exists an effective TRS in the long wavelength limit, but in real samples this symmetry is easily broken[26–28]; see Supplementary Information). The contribution of time-reversed trajectories to quantum interference can be restored only up to the extent that there exists a coupling mechanism between the two valleys, such as short-range scattering at impurities or at the graphene edges[26–28]. This makes the occurrence of weak localization dependent on extrinsic defects, which explains why both in our own samples (see Fig. 4b) and other recent measurements[17,29] weak localization is found to exhibit a surprising sample dependent behaviour and is often suppressed (while, at the same time, we observe a supercurrent in all samples investigated). This interpretation, which illustrates the unique electronic properties of graphene, is consistent with the observation of aperiodic conductance fluctuations[30] of amplitude e^2/h (see Fig. 4a), whose occurrence requires phase coherence but not time reversal symmetry.

Received 5 September; accepted 28 December 2006.

1. Novoselov, K. S. *et al.* Electric field effect in atomically thin carbon films. *Science* **306**, 666–669 (2004).
2. Novoselov, K. S. *et al.* Two-dimensional gas of massless Dirac fermions in graphene. *Nature* **438**, 197–200 (2005).
3. Zhang, Y. B., Tan, Y. W., Stormer, H. L. & Kim, P. Experimental observation of the quantum Hall effect and Berry's phase in graphene. *Nature* **438**, 201–204 (2005).
4. Gusynin, V. P. & Sharapov, S. G. Unconventional integer quantum Hall effect in graphene. *Phys. Rev. Lett.* **95**, 146801 (2005).
5. Peres, N. M. R., Guinea, F. & Castro Neto, A. H. Electronic properties of disordered two-dimensional carbon. *Phys. Rev. B* **73**, 125411 (2006).
6. Fradkin, E. Critical-behavior of disordered degenerate semiconductors. II. Spectrum and transport properties in mean-field theory. *Phys. Rev. B* **33**, 3263–3268 (1986).
7. Ludwig, A. W. W., Fisher, M. P. A., Shankar, R. & Grinstein, G. Integer quantum Hall transition — an alternative approach and exact results. *Phys. Rev. B* **50**, 7526–7552 (1994).
8. Nersesyan, A. A., Tsvelik, A. M. & Wenger, F. Disorder effects in 2-dimensional d-wave superconductors. *Phys. Rev. Lett.* **72**, 2628–2631 (1994).
9. Altland, A., Simons, B. D. & Zirnbauer, M. R. Theories of low-energy quasi-particle states in disordered d-wave superconductors. *Phys. Rep.* **359**, 283–354 (2002).
10. Katsnelson, M. I. Zitterbewegung, chirality, and minimal conductivity in graphene. *Eur. Phys. J. B* **51**, 157–160 (2006).
11. Nomura, K. & MacDonald, A. H. Quantum transport of massless Dirac fermions in graphene. Preprint available at ⟨http://xxx.lanl.gov/abs/cond-mat/0606589⟩ (2006).
12. Aleiner, I. L. & Efetov, K. B. Effect of disorder on transport in graphene. *Phys. Rev. Lett.* **97**, 236801 (2006).
13. Altland, A. Low energy theory of disordered graphene. *Phys. Rev. Lett.* **97**, 236802 (2006).
14. Josephson, B. D. Possible new effects in superconductive tunnelling. *Phys. Lett.* **1**, 251–253 (1962).
15. Titov, M. & Beenakker, C. W. J. The Josephson effect in ballistic graphene. *Phys. Rev. B* **74**, 041401(R) (2006).
16. Degennes, P. G. Boundary effects in superconductors. *Rev. Mod. Phys.* **36**, 225–237 (1964).
17. Morozov, S. V. *et al.* Strong suppression of weak localization in graphene. *Phys. Rev. Lett.* **97**, 016801 (2006).

18. Jarillo-Herrero, P., van Dam, J. A. & Kouwenhoven, L. P. Quantum supercurrent transistors in carbon nanotubes. *Nature* **439,** 953–956 (2006).
19. Datta, S. *Electronic Transport in Mesoscopic Systems* (Cambridge Univ. Press, Cambridge, UK, 1995).
20. Tinkham, M. *Introduction to Superconductivity* (McGraw-Hill, Singapore, 1996).
21. Joyez, P., Lafarge, P., Filipe, A., Esteve, D. & Devoret, M. H. Observation of parity-induced suppression of Josephson tunneling in the superconducting single-electron transistor. *Phys. Rev. Lett.* **72,** 2458–2461 (1994).
22. Barone, A. & Paterno, G. *Physics and Applications of the Josephson Effect* (Wiley & Sons, New York, 1982).
23. Octavio, M., Tinkham, M., Blonder, G. E. & Klapwijk, T. M. Subharmonic energy-gap structure in superconducting constrictions. *Phys. Rev. B* **27,** 6739–6746 (1983).
24. Dresselhaus, M. S., Dresselhaus, G. & Eklund, P. C. *Science of Fullerenes and Carbon Nanotubes* (Academic, San Diego, 1996).
25. Likharev, K. K. Superconducting weak links. *Rev. Mod. Phys.* **51,** 101–159 (1979).
26. Morpurgo, A. F. & Guinea, F. Intervalley scattering, long-range disorder, and effective time reversal symmetry breaking in graphene. *Phys. Rev. Lett.* **97,** 196804 (2006).
27. Suzuura, H. & Ando, T. Crossover from symplectic to orthogonal class in a two-dimensional honeycomb lattice. *Phys. Rev. Lett.* **89,** 266603 (2002).
28. McCann, E. *et al.* Weak localisation magnetoresistance and valley symmetry in graphene. *Phys. Rev. Lett.* **97,** 146805 (2006).
29. Berger, C. *et al.* Electronic confinement and coherence in patterned epitaxial graphene. *Science* **312,** 1191–1196 (2006).
30. Lee, P. A. & Stone, A. D. Universal conductance fluctuations in metals. *Phys. Rev. Lett.* **55,** 1622–1625 (1985).

Supplementary Information is linked to the online version of the paper at www.nature.com/nature.

Acknowledgements We thank A. Geim, D. Jiang and K. Novoselov for help with device fabrication; L. Kouwenhoven for the use of experimental equipment, support and discussions; and C. Beenakker, J. van Dam, D. Esteve, T. Klapwijk, Y. Nazarov, G. Steele, B. Trauzettel, C. Urbina and B. van Wees for discussions.

Author Information Reprints and permissions information is available at www.nature.com/reprints. The authors declare no competing financial interests. Correspondence and requests for materials should be addressed to H.B.H. (h.b.heersche@tudelft.nl) or P.J.-H. (P.D.Jarillo-Herrero@tudelft.nl).

LETTERS

The structure of suspended graphene sheets

Jannik C. Meyer[1], A. K. Geim[2], M. I. Katsnelson[3], K. S. Novoselov[2], T. J. Booth[2] & S. Roth[1]

The recent discovery of graphene has sparked much interest, thus far focused on the peculiar electronic structure of this material, in which charge carriers mimic massless relativistic particles[1–3]. However, the physical structure of graphene—a single layer of carbon atoms densely packed in a honeycomb crystal lattice—is also puzzling. On the one hand, graphene appears to be a strictly two-dimensional material, exhibiting such a high crystal quality that electrons can travel submicrometre distances without scattering. On the other hand, perfect two-dimensional crystals cannot exist in the free state, according to both theory and experiment[4–9]. This incompatibility can be avoided by arguing that all the graphene structures studied so far were an integral part of larger three-dimensional structures, either supported by a bulk substrate or embedded in a three-dimensional matrix[1–3,9–12]. Here we report on individual graphene sheets freely suspended on a microfabricated scaffold in vacuum or air. These membranes are only one atom thick, yet they still display long-range crystalline order. However, our studies by transmission electron microscopy also reveal that these suspended graphene sheets are not perfectly flat: they exhibit intrinsic microscopic roughening such that the surface normal varies by several degrees and out-of-plane deformations reach 1 nm. The atomically thin single-crystal membranes offer ample scope for fundamental research and new technologies, whereas the observed corrugations in the third dimension may provide subtle reasons for the stability of two-dimensional crystals[13–15].

Whether a strictly two-dimensional (2D) crystal can exist was first raised theoretically more than 70 years ago by Peierls[4,5] and Landau[6,7]. They showed that, in the standard harmonic approximation[16], thermal fluctuations should destroy long-range order, resulting in melting of a 2D lattice at any finite temperature. Furthermore, Mermin and Wagner proved that a magnetic long-range order could not exist in one and two dimensions[17] and later extended the proof to crystalline order in 2D[8]. Importantly, numerous experiments on thin films have been in accord with the theory, showing that below a certain thickness, typically of dozens of atomic layers, the films become thermodynamically unstable (segregate into islands or decompose) unless they constitute an inherent part of a three-dimensional (3D) system (such as being grown on top of a bulk crystal with a matching lattice)[18–20]. However, although the theory does not allow perfect crystals in 2D space, it does not forbid nearly perfect 2D crystals in 3D space. Indeed, a detailed analysis of the 2D crystal problem beyond the harmonic approximation has led to the conclusion[13–15] that the interaction between bending and stretching long-wavelength phonons could in principle stabilize atomically thin membranes through their deformation in the third dimension[15]. Indeed, the experiments described here show that freely suspended graphene crystals can exist without a substrate, and exhibit random elastic deformations involving all three dimensions.

The preparation of graphene membranes used in this study is described in the text of the Supplementary Information and in Supplementary Fig. 1. Briefly, we used the established procedures[9] of micromechanical cleavage and identification of graphene, followed by electron-beam lithography and a number of etching steps, to obtain graphene crystallites attached to a micrometre-sized metallic scaffold. Figure 1 shows the bright-field transmission electron microscopy (TEM) image of one of our samples. The central parts of the prepared membranes normally appear on TEM images as homogeneous and featureless regions, whereas the membranes' edges tend to scroll (Fig. 1). Also, we often observed folded regions in which a graphene sheet became partly detached from the scaffold during microfabrication (right side of Fig. 1). Such folds provide a clear TEM signature for the number of graphene layers. A folded graphene sheet is locally parallel to the electron beam and, for monolayer graphene, a fold exhibits only one dark line (Fig. 2a), similar to TEM images from one-half of a single-walled carbon nanotube. For comparison, Fig. 2b shows a folded edge of bilayer graphene, which exhibits two dark lines, as in the case of double-walled nanotubes. One has to be careful, however, because scrolls and multiple folds can give rise to any number of dark lines even for monolayer graphene, as indeed observed experimentally.

In addition, we could directly distinguish between monolayer graphene and thicker samples by analysing nanobeam electron diffraction patterns from their flat areas as a function of incidence angle. This procedure effectively allowed us to probe the whole 3D reciprocal space. Figure 2 shows examples of diffraction patterns at three tilt angles for the graphene membrane of Fig. 1. As expected, there are

Figure 1 | Suspended graphene membrane. Bright-field TEM image of a suspended graphene membrane. Its central part (homogeneous and featureless region indicated by arrows) is monolayer graphene. Electron diffraction images from different areas of the flake show that it is a single crystal without domains. We note scrolled top and bottom edges and a strongly folded region on the right. Scale bar, 500 nm.

[1]Max Planck Institute for Solid State Research, Heisenbergstrasse 1, 70569 Stuttgart, Germany. [2]Manchester Centre for Mesoscience and Nanotechnology, University of Manchester, Oxford Road, Manchester M13 9PL, UK. [3]Institute for Molecules and Materials, Radboud University of Nijmegen, Toernooiveld 1, 6525 ED Nijmegen, The Netherlands.

two dominant reflections corresponding to periodicities of 2.13 and 1.23 Å, and weak higher-order peaks. The key for the identification of monolayer graphene is that its reciprocal space (Fig. 3) has only the zero-order Laue zone and, therefore, no dimming of the diffraction peaks should occur at any angle, in contrast to the behaviour of crystal lattices extended in the third dimension. This is exactly the behaviour we observed experimentally. Figure 2f plots the total intensity for diffraction peaks (0–110) and (1–210) as a function of tilt angle for monolayer graphene. One can see that changes in the total intensity are relatively small and, importantly, there are no minima, in agreement with our numerical simulations (see Fig. 2 legend). For comparison, Fig. 2g shows the corresponding behaviour for bilayer graphene, where the total intensities vary so strongly that the same peaks become completely suppressed at some angles and the underlying sixfold symmetry remains undisturbed only for normal incidence. The diffraction analysis also shows that our bilayer membranes retained the Bernal (AB) stacking of bulk graphite, in contrast to the AAA... stacking reported in "carbon nanofilms"[21]. Independently of stacking order, the weak monotonic variation of diffraction intensities with tilt angle is a signature specific to monolayer graphene and can be used for its unambiguous identification in TEM.

Notwithstanding the overall agreement, there is one feature in the observed diffraction patterns that strongly disagrees with our numerical simulations and, more generally, with the standard diffraction behaviour in 3D crystals[22,23]. We can clearly see that the diffraction peaks in Fig. 2 become broader with increasing tilt angle and this

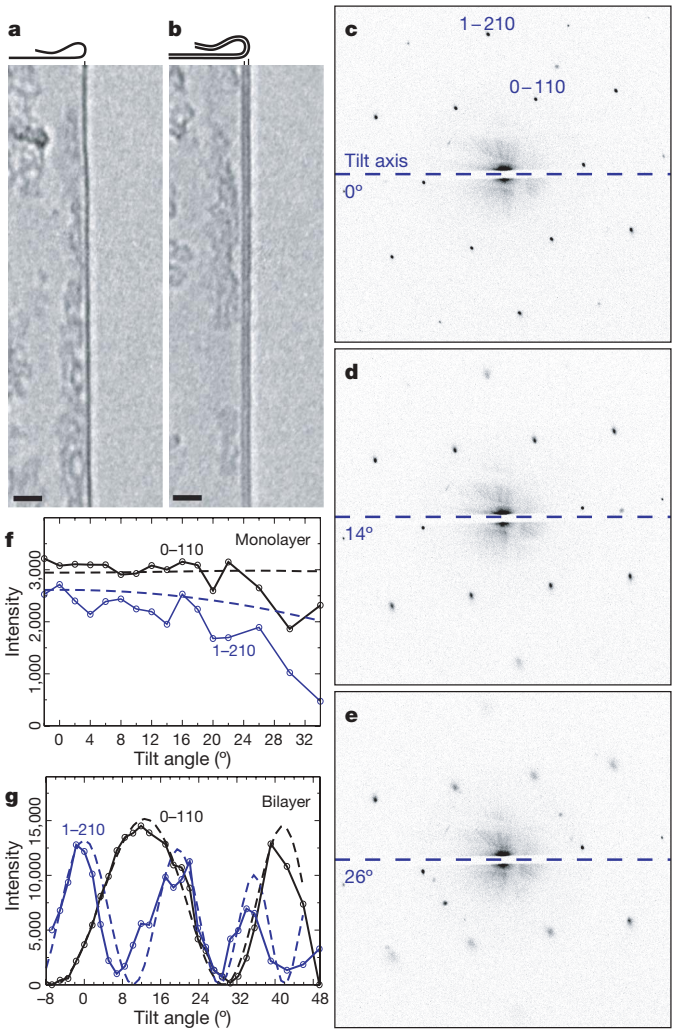

Figure 2 | Transmission electron microscopy of graphene. **a**, **b**, TEM images of folded edges for monolayer and bilayer graphene, respectively, using a Philips CM200 TEM. Scale bars, 2 nm. **c–e**, Electron diffraction patterns from a graphene monolayer under incidence angles of 0°, 14° and 26°, respectively. The tilt axis is horizontal. Here we used a Zeiss 912 TEM operated at 60 kV in the Köhler condition with the smallest (5 μm) condenser aperture. This allowed us to obtain a small, almost parallel beam with an illumination angle of 0.16 mrad and an illumination area of only 250 nm in diameter. The diffraction patterns were recorded on a charge-coupled device (CCD) for further quantitative analysis. The peaks become broader with increasing tilt, and this effect is strongest for peaks further away from the tilt axis. To label equivalent Bragg reflections, we use the Miller–Bravais indices (*hkil*) for graphite so that the innermost hexagon and the next one correspond to indices (0–110) (2.13 Å spacing) and (1–210) (1.23 Å spacing), respectively. **f**, Total intensity as a function of tilt angle for the peaks marked in **c**. To find the intensity values, each of the above Bragg reflections was fitted by a gaussian distribution for every angle, which yielded the peaks' intensities, positions, heights and widths. The dashed lines are numerical simulations, in which we used a Fourier transform of the projected atomic potentials[22,23,24] and the atomic form factors reported in ref. 29. **g**, The same analysis and simulations for a bilayer graphene membrane.

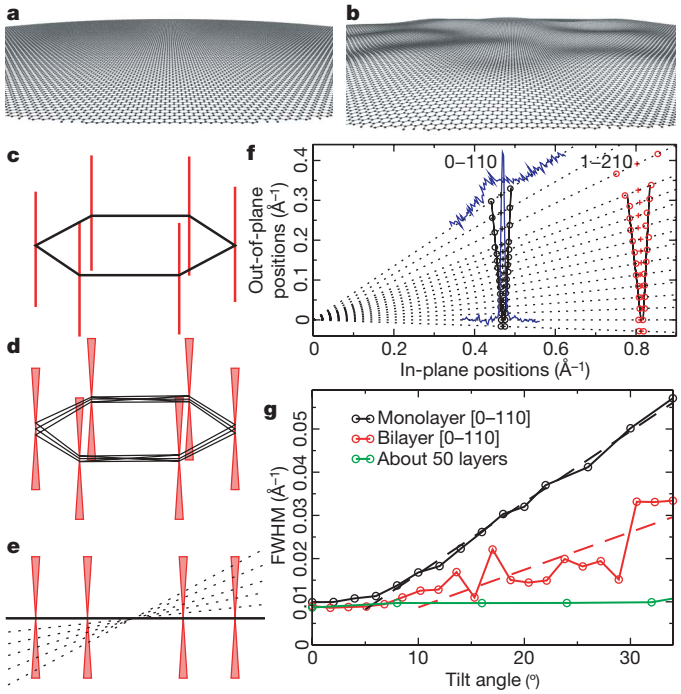

Figure 3 | Microscopically corrugated graphene. **a**, Flat graphene crystal in real space (perspective view). **b**, The same for corrugated graphene. The roughness shown imitates quantitatively the roughness found experimentally. **c**, The reciprocal space for a flat sheet is a set of rods (red) directed perpendicular to the reciprocal lattice of graphene (black hexagon). **d**, **e**, For the corrugated sheet, a superposition of the diffracting beams from microscopic flat areas effectively turns the rods into cone-shaped volumes so that diffraction spots become blurred at large angles (indicated by the dotted lines in **e**) and the effect is more pronounced further away from the tilt axis (compare with Fig. 2). Diffraction patterns obtained at different tilt angles allow us to measure graphene roughness. **f**, Evolution of diffraction peaks with tilt angle in monolayer graphene. The experimental data are presented in such a way that they closely resemble the schematic view in **e**. For each tilt angle, the black dotted line represents a cross-section for diffraction peaks (0–110) and (1–210). The peak centres and full widths at half maxima (FWHM) in reciprocal space are marked by crosses and open circles, respectively. In two cases (0° and 34°), the recorded intensities are shown in full by blue curves. All the intensity curves could be well fitted by the gaussian shape. The solid black lines show that the width of the diffraction spots reproduces the conical broadening suggested by our model (**d** and **e**). **g**, FWHM for the (0–110) diffraction peak in monolayer and bilayer membranes and thin graphite (as a reference), as a function of tilt angle. The dashed lines are the linear fits yielding the average roughness. The flat region between 0° to 5°, and also for the reference sample, is due to the intrinsic peak width for the microscope at our settings.

blurring is much stronger for those peaks that are further away from the tilt axis. This broadening is a distinctive feature of monolayer graphene. It becomes notably weaker in bilayer samples and completely disappears for multilayer graphene. From a theory point of view, the broadening is completely unexpected. To emphasize this, we note that, for example, thermal vibrations can only reduce the intensity of diffraction peaks (Debye–Waller factor) but do not lead to their broadening[22,24].

Figure 3 explains how the observed broadening explicitly reveals that graphene sheets are not flat within the submicrometre area of the electron beam. The full 3D Fourier transform of a flat graphene crystal (Fig. 3a) consists of a set of rods perpendicular to the plane of the reciprocal hexagonal lattice (Fig. 3c). Each diffraction pattern is then a two-dimensional slice (given by a section of the Ewald sphere) through this 3D space. In particular, this picture suggests that the intensity of diffraction peaks should vary without any singularities (monotonically) with changing tilt angle and the hexagonal symmetry is preserved for any tilt, as already discussed above. The increasing broadening of diffraction peaks without changes in their total intensity implies that the rods wander around their average direction (see Fig. 3d). This corresponds to a slightly uneven sheet (Fig. 3b) so that the diffraction pattern effectively comes from an ensemble of small flat 2D crystallites with different orientations with respect to the average plane. Figure 3e illustrates that such roughness results in sharp diffraction peaks for normal incidence, but that the peaks rapidly become wider with increasing tilt angle. This model also shows that their total intensity should be practically independent of the membrane's roughness and can be described by the angle dependence for a flat sheet; this is consistent with our simulations in Fig. 2f.

For quantitative analysis, Fig. 3f and g shows the detailed evolution of the broadening of the diffraction peaks with changing incidence angle. One can see that the peak widths increase linearly with tilt and also proportionally to the peaks' position in reciprocal space, in quantitative agreement with our simulations for corrugated graphene. The width of the cones or the linear slopes in Fig. 3f and g provide a direct measure of the membrane's roughness. For different monolayer membranes, we found cone angles between 8° and 11°, that is, the surface normal deviated from its mean direction on average by ±5°. For bilayer membranes, this value was found to be about 2° (Fig. 3g). We note that the diffraction peaks broaden isotropically (see Fig. 2c–e). This means that the surface normal in real space wanders in all directions, and the observed waviness is omni-directional. Otherwise, if a graphene membrane were curved only in one direction, diffraction peaks would spread into a line indicating the direction of curling. An absolutely incompressible sheet can only be curved in one direction, not two, and the isotropic waviness unambiguously implies local deformations of graphene. The curvature of 5° yields a local strain of up to 1%, which is large but sustainable without plastic deformation and generation of defects[25–27].

To estimate the spatial extent L of the corrugations we found, let us start with two observations. First, L cannot be drastically (more than a few times) smaller than the coherence length of the diffracted electrons. Otherwise, the above model of incoherent superpositions from locally flat pieces would be replaced by a coherent superposition where we would expect sharp peaks and also much stronger deviations between the experimental and calculated intensities in Fig. 2f. The coherence length is estimated to be about 10 nm, so the corrugations must have a mesoscopic (several nanometres) rather than atomic scale. Second, the smooth gaussian shape of the diffraction peaks requires a large number N of different orientations within the submicrometre illuminated area, which provides us with the upper limit for L. A minimalist assumption of $N = 100$ necessitates $L \leq 25$ nm. These qualitative considerations are in agreement with our simulated diffraction patterns for corrugated graphene sheets (see text on numerical simulations in the Supplementary Information and Supplementary Figs 2–5). From the known curvature and size L of the corrugations, we estimate their height to be about 1 nm.

The above order-of-magnitude estimates are also strongly supported by atomic-resolution TEM imaging of our membranes. Unfortunately, for monolayer graphene, such smooth waviness could not be visualized because diffraction intensities vary little with tilt angle, as discussed earlier (Fig. 2f), and no additional contrast due to corrugations could be expected or, in fact, observed. On the other hand, the visibility of the hexagonal lattice for two and more layers strongly depends on their tilt angle (Fig. 2g) and, accordingly, surface undulations of few-layer graphene can be expected to result in areas of different brightness. Such areas are clearly seen in Fig. 4 and have a characteristic size of a few nanometres, which is somewhat smaller than the above estimate for L in monolayer graphene where the ripples could also be larger laterally. Importantly, atomic-resolution images show that the corrugations are static, because otherwise, changes during the exposure would lead to blurring and disappearance of the additional contrast.

Perfect 2D atomic crystals cannot exist, unless they are of a limited size or contain many crystal defects[7,8]. The observed microscopic corrugations of 2D graphene in the third dimension provide another, unexpected way to reconcile the high quality of graphene with its thermodynamic stability. The fact that the microscopic roughness is reproducible for different positions on membranes and for different samples, becomes notably smaller for bilayer graphene and disappears for thicker membranes proves that the corrugations are intrinsic to graphene membranes. Theoretical investigations of 2D membranes have predicted their thermodynamic stability through static microscopic crumpling involving either bending or buckling[13–15]. The buckling mechanism requires the generation of a high density of dislocations[15] that are neither observed in our atomic-resolution images nor expected in the case of relatively small (micrometre-sized) membranes with strong interatomic bonds. However, the bending scenario assumes no defects and only requires out-of-plane deformations involving a significant elastic strain. The latter is in qualitative agreement with our observations, but further experimental and theoretical studies are needed to clarify the detailed mechanism of the corrugations in graphene.

Free-hanging graphene is the thinnest conceivable object and thus offers many exciting directions for future research. The observed

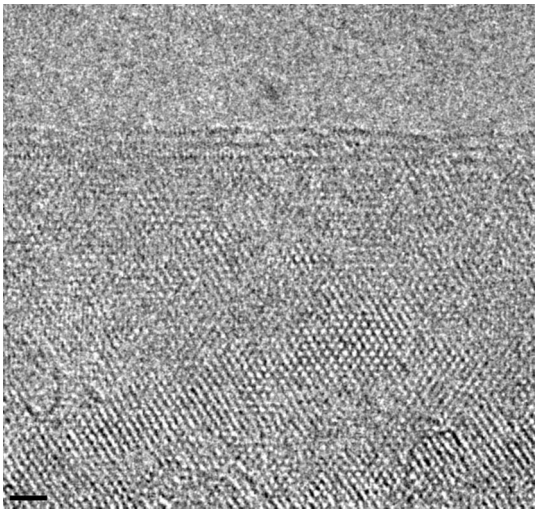

Figure 4 | Atomic resolution imaging of graphene membranes. TEM image of a few-layer graphene membrane near its edge, where the number of dark lines indicates the thickness of two to four layers. Because for few-layer graphene the electron contrast depends strongly on incidence angle, relatively small (a few degrees) variations in the surface normal become visible. The atomic-resolution imaging was achieved by using FEI Titan at an acceleration voltage of 300 kV. Scale bar, 1 nm.

microscopic roughening seems to be essential for the structural stability of 2D membranes; their mechanical, electronic, optical and other properties may be equally extraordinary. We also note that the presence of these elastic corrugations is consistent with high mobility of charge carriers in graphene[1–3] and may explain some of its unusual transport characteristics, such as the suppression of weak localization[28]. 2D crystal membranes also promise such tantalizing applications as almost-transparent substrates for high-resolution electron microscopy or sieving of atoms and small molecules through the atomic-size benzene rings. Such 2D membranes can be considered for any other technology in which ultrathin, transparent and robust substrates offer an advantage (for example, nanomechanical devices).

Received 11 September; accepted 21 December 2006.

1. Novoselov, K. S. *et al.* Electric field effect in atomically thin carbon films. *Science* **306,** 666–669 (2004).
2. Novoselov, K. S. *et al.* Two-dimensional gas of massless Dirac fermions in graphene. *Nature* **438,** 197–200 (2005).
3. Zhang, Y., Tan, J. W., Stormer, H. L. & Kim, P. Experimental observation of the quantum Hall effect and Berry's phase in graphene. *Nature* **438,** 201–204 (2005).
4. Peierls, R. E. Bemerkungen über Umwandlungstemperaturen. *Helv. Phys. Acta* **7,** 81–83 (1934).
5. Peierls, R. E. Quelques proprietes typiques des corpses solides. *Ann. Inst. Henri Poincare* **5,** 177–222 (1935).
6. Landau, L. D. Zur Theorie der Phasenumwandlungen II. *Phys. Z. Sowjetunion* **11,** 26–35 (1937).
7. Landau, L. D. & Lifshitz, E. M. *Statistical Physics* Part I, Sections 137 and 138 (Pergamon, Oxford, 1980).
8. Mermin, N. D. Crystalline order in two dimensions. *Phys. Rev.* **176,** 250–254 (1968).
9. Novoselov, K. S. *et al.* Two-dimensional atomic crystals. *Proc. Natl Acad. Sci. USA* **102,** 10451–10453 (2005).
10. Berger, C. *et al.* Electronic confinement and coherence in patterned epitaxial graphene. *Science* **312,** 1191–1196 (2006).
11. Ohta, T., Bostwick, A., Seyller, T., Horn, K. & Rotenberg, E. Controlling the electronic structure of bilayer graphene. *Science* **313,** 951–954 (2006).
12. Stankovich, S. *et al.* Graphene-based composite materials. *Nature* **442,** 282–286 (2006).
13. Nelson, D. R. & Peliti, L. Fluctuations in membranes with crystalline and hexatic order. *J. Phys.* **48,** 1085–1092 (1987).
14. Radzihovsky, L. & Le Doussal, P. Self-consistent theory of polymerized membranes. *Phys. Rev. Lett.* **69,** 1209–1212 (1992).
15. Nelson, D. R., Piran, T. & Weinberg, S. *Statistical Mechanics of Membranes and Surfaces* (World Scientific, Singapore, 2004).
16. Born, M. & Huang, K. *Dynamical Theory of Crystal Lattices* (Clarendon, Oxford, 1954).
17. Mermin, N. D. & Wagner, H. Absence of ferromagnetism or antiferromagnetism in one- or two-dimensional isotropic Heisenberg models. *Phys. Rev. Lett.* **17,** 1133–1136 (1966).
18. Venables, J. A., Spiller, G. D. T. & Hanbucken, M. Nucleation and growth of thin-films. *Rep. Prog. Phys.* **47,** 399–459 (1984).
19. Zinkeallmang, M., Feldman, L. C. & Grabow, M. H. Clustering on surfaces. *Surf. Sci. Rep.* **16,** 377–463 (1992).
20. Evans, J. W., Thiel, P. A. & Bartelt, M. C. Morphological evolution during epitaxial thin film growth: Formation of 2D islands and 3D mounds. *Surf. Sci. Rep.* **61,** 1–128 (2006).
21. Horiuchi, S. *et al.* Carbon nanofilm with a new structure and property. *Jpn. J. Appl. Phys.* **42,** L1073–L1076 (2003).
22. Buseck, P. R., Cowley, J. M. & Eyring, L. *High-Resolution Transmission Electron Microscopy* (Oxford Univ. Press, Oxford, 1988).
23. Spence, J. C. H. *High-Resolution Electron Microscopy* (Oxford Univ. Press, Oxford, 2003).
24. Peng, L. M. Electron atomic scattering factors and scattering potentials of crystals. *Micron* **30,** 625–648 (1999).
25. Yu, M. F., Files, B. S., Arepalli, S. & Ruoff, R. S. Tensile loading of ropes of single wall carbon nanotubes and their mechanical properties. *Phys. Rev. Lett.* **84,** 5552–5555 (2000).
26. Zhao, Q., Nardelli, M. B. & Bernholc, J. Ultimate strength of carbon nanotubes: a theoretical study. *Phys. Rev. B* **65,** 144105 (2002).
27. Huang, J. Y. *et al.* Superplastic carbon nanotubes. *Nature* **439,** 281 (2006).
28. Morozov, S. V. *et al.* Strong suppression of weak localization in graphene. *Phys. Rev. Lett.* **97,** 016801 (2006).
29. Doyle, P. A. & Turner, P. S. Relativistic Hartree-Fock x-ray and electron scattering factors. *Acta Crystallogr. A* **24,** 390–397 (1968).

Supplementary Information is linked to the online version of the paper at www.nature.com/nature.

Acknowledgements We thank B. Freitag and D. Beamer of FEI for providing access to their in-house TEM Titan. This work was supported by the EU project CANAPE, the EPSRC (UK) and the Royal Society. M.I.K. acknowledges financial support from FOM (Netherlands).

Author Information Reprints and permissions information is available at www.nature.com/reprints. The authors declare no competing financial interests. Correspondence and requests for materials should be addressed to J.C.M. (email@jannikmeyer.de) and A.K.G. (geim@man.ac.uk).

LETTERS

Chemical identification of individual surface atoms by atomic force microscopy

Yoshiaki Sugimoto[1], Pablo Pou[2], Masayuki Abe[1,3], Pavel Jelinek[4], Rubén Pérez[2], Seizo Morita[1] & Óscar Custance[1]

Scanning probe microscopy is a versatile and powerful method that uses sharp tips to image, measure and manipulate matter at surfaces with atomic resolution[1,2]. At cryogenic temperatures, scanning probe microscopy can even provide electron tunnelling spectra that serve as fingerprints of the vibrational properties of adsorbed molecules[3–5] and of the electronic properties of magnetic impurity atoms[6,7], thereby allowing chemical identification. But in many instances, and particularly for insulating systems, determining the exact chemical composition of surfaces or nanostructures remains a considerable challenge. In principle, dynamic force microscopy should make it possible to overcome this problem: it can image insulator, semiconductor and metal surfaces with true atomic resolution[8–10], by detecting and precisely measuring[11–13] the short-range forces that arise with the onset of chemical bonding between the tip and surface atoms[14,15] and that depend sensitively on the chemical identity of the atoms involved. Here we report precise measurements of such short-range chemical forces, and show that their dependence on the force microscope tip used can be overcome through a normalization procedure. This allows us to use the chemical force measurements as the basis for atomic recognition, even at room temperature. We illustrate the performance of this approach by imaging the surface of a particularly challenging alloy system and successfully identifying the three constituent atomic species silicon, tin and lead, even though these exhibit very similar chemical properties and identical surface position preferences that render any discrimination attempt based on topographic measurements impossible.

The chemical identification of single atoms and molecules at surfaces has been pursued since the invention of both the scanning tunnelling microscope and the atomic force microscope (AFM). Particularly promising in this quest is dynamic force microscopy, which achieves true atomic imaging resolution[8–10] by detecting the short-range forces associated with the onset of the chemical bond between the outermost atom of the tip apex and the surface atoms being imaged[14,15] (see Fig. 1 for schematic illustration of the method and imaging examples). Moreover, dynamic force spectroscopy[11–13] makes it possible to quantify these forces.

Figure 2a shows five sets of dynamic force spectra measured on a single atomic layer of Sn grown on a Si(111) substrate. Each set of force curves was obtained over an Sn atom and an Si atom having the same local surface configuration as the corresponding atoms highlighted in the topographic image shown in Fig. 1d, always using identical acquisition and analysis protocols (see Methods). However, the sets were collected over multiple measurement sessions, using tips that had different apex terminations. These tip apexes presumably differ in both structure and composition (Sn or Si), as sometimes slight tip–surface contacts were intentionally produced before the acquisition of each set of force curves. The sets seem to share only one feature: curves measured over the Si atoms are characterized by a stronger attractive interaction force. Given the high degree of stability, lateral positioning accuracy, and reproducibility provided by our acquisition protocol[12,16], we attribute the variability seen in the data in Fig. 2a to a strong tip dependence of both the registered

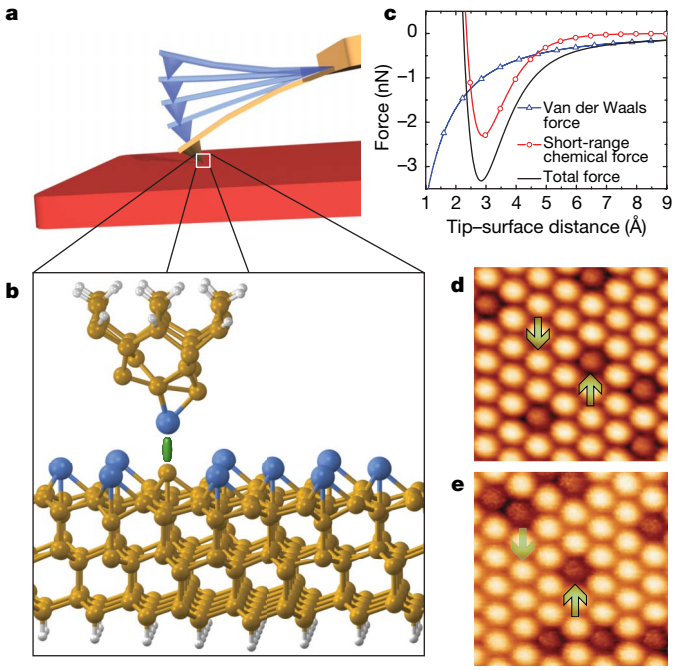

Figure 1 | Dynamic force microscopy with atomic resolution. Schematic illustration of AFM operation in dynamic mode (**a**), and of the onset of the chemical bonding between the outermost tip atom and a surface atom (highlighted by the green stick) that gives rise to the atomic contrast[14,15] (**b**). However, the tip experiences not only the short-range force associated with this chemical interaction, but also long-range force contributions that arise from van der Waals and electrostatic interactions between tip and surface (though the effect of the latter is usually minimized through appropriate choice of the experimental set-up). **c**, Curves obtained with analytical expressions for the van der Waals force, the short-range chemical interaction force, and the total force to illustrate their dependence on the absolute tip–surface distance. **d**–**e**, Dynamic force microscopy topographic images of a single-atomic layer of Sn (**d**) and Pb (**e**) grown, respectively, over a Si(111) substrate. At these surfaces, a small concentration of substitutional Si defects, characterized by a diminished topographic contrast[20], is usually found. The green arrows indicate atomic positions where force spectroscopic measurements were performed (see Fig. 2). Image dimensions are (4.3×4.3) nm^2; for the acquisition parameters see the Supplementary Information.

[1]Graduate School of Engineering, Osaka University, 2-1 Yamada-Oka, 565-0871 Suita, Osaka, Japan. [2]Departamento de Física Teórica de la Materia Condensada, Universidad Autónoma de Madrid, 28049 Madrid, Spain. [3]PRESTO, Japan Science and Technology Agency, Saitama 332-0012, Japan. [4]Institute of Physics, Academy of Sciences of the Czech Republic, Cukrovarnická 10, 1862 53, Prague, Czech Republic.

maximum attractive force value and the distance dependence of the attractive and repulsive regions of the curves.

A meaningful comparison of measured short-range forces requires some data processing to reduce the variability caused by the use of tips with different terminations. We have found that the relative interaction ratio, that is, the ratio of the maximum attractive short-range forces of the two curves within a set of measurements over Si and Sn (acquired using a tip that had the same apex termination), remains nearly constant. This is illustrated in Fig. 2b, where each curve within a given measurement set has been normalized to the absolute value of the maximum attractive short-range force of the Si curve of that set ($|F_{Si(set)}|$). The normalization reveals an average value for the relative interaction ratio of 0.77 ± 0.02. This approach has also been validated for elements such as Pb or In in similar surfaces (see Fig. 1e, Fig. 2c, d and Supplementary Information). Using the same acquisition and analysis protocols as applied when studying the mixed Sn/Si surface layer, several sets of short-range force curves were obtained over structurally equivalent atoms (for the Pb/Si layer, these are highlighted by arrows in Fig. 1e). The data revealed an average relative interaction ratio of 0.59 ± 0.03 for Pb and Si in the Pb-terminated surface (Fig. 2c, d), and an average relative interaction ratio for In and Si of 0.72 ± 0.04 in the In-terminated one.

To corroborate the experimental observations, we conducted large-scale first-principles calculations (see Methods) using atomically extended nanometre-scale asperities[17] as tip-apex models. In these calculations, homogeneous tip apexes that have different structures for probing the Sn and Si atoms of a model of the mixed Sn/Si surface layer (shown in Fig. 1b) produce different short-range force curves (Fig. 2e). If the tip apexes have the same termination structure but a different element at the outermost position, we obtain weaker short-range forces for Sn-terminated tips than for Si-terminated tips (Fig. 2e). In all these cases, as in the experiments, the tip–surface interaction is stronger over Si surface atoms than over Sn atoms (Fig. 2e). But independently of tip-apex structure and the chemical termination of the tips, the relative interaction ratios of the maximum attractive forces calculated over the Sn and Si atoms for a given tip are all similar, with an average value of 0.71 ± 0.07 (Fig. 2f) that is close to the experimental ratio.

To gain some insight into the behaviour of the short-range forces, we have developed a simple analytical model that assumes that tip and sample deform elastically in response to the short-range chemical interaction between the tip apex and the closest surface atoms (P.P., Y.S., P.J., M.A., S.M., O.C. and R.P., manuscript in preparation). The model indicates that although the shape of the force-versus-distance curves depends on the elastic response of the system, the value of the maximum attractive short-range force is determined only by the short-range chemical interaction (data not shown). The minimum short-range force value registered for a given surface atom (corresponding to maximum attractive force) is thus expected to depend significantly on the chemical composition and structure of the tip apex (an effect seen in the data in Fig. 2e), and will also depend on the relative orientation of the tip with respect to the surface[18,19]. These three factors explain the strong tip dependence found in the experiments (see Fig. 2a and c). However, when the relative interaction ratio of the maximum attractive short-range forces for two atomic species probed with the same tip is considered, the common features associated with the structural characteristics of the tip-apex cancel out, and the intrinsic strength of the chemical bonding interaction between the outermost tip atom and the closest surface atom is revealed (Fig. 2b, d and f). This explanation can be rationalized for semiconductor surfaces using accepted combination rules for covalent chemical interactions; it can, in fact, be generalized to multi-element systems by considering that when individually probing the atoms of such systems with a given tip apex, interactions between pairs of atomic species are obtained. This ensures that the relative strengths of the minimum short-range forces are almost independent from the tip-apex structure or chemical termination (see Supplementary Information for further details).

By determining the ratio of the maximum attractive short-range forces as outlined above, it is possible to identify individual atoms in

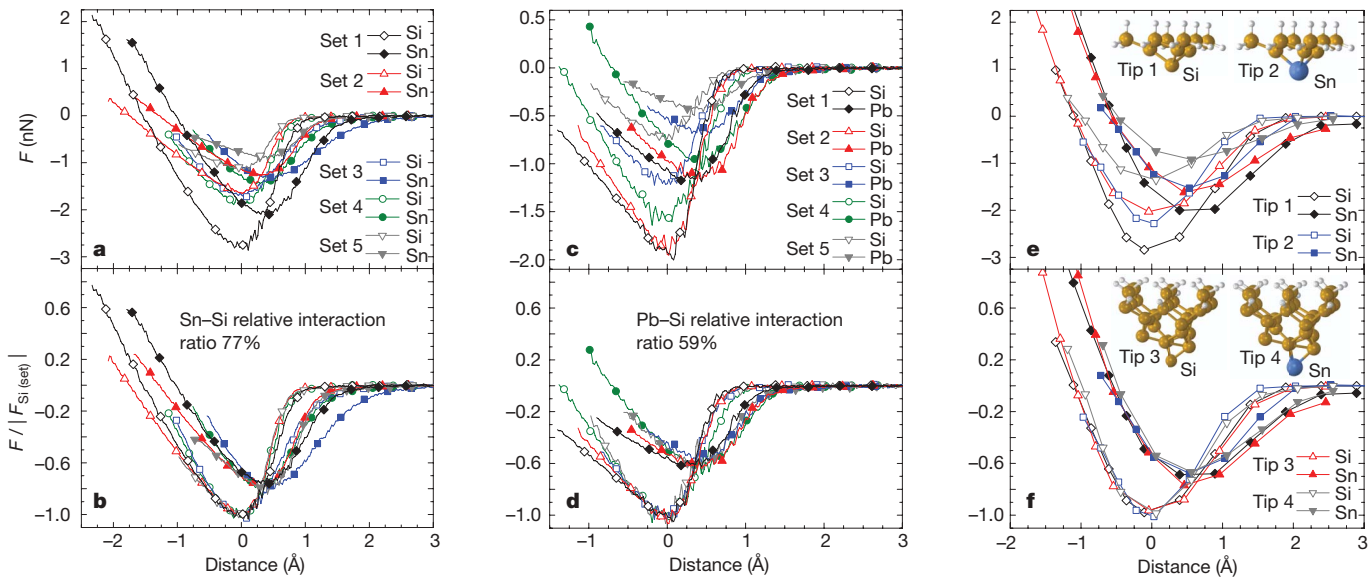

Figure 2 | Probing short-range chemical interaction forces. **a**, Sets of short-range force curves obtained over structurally equivalent Sn and Si atoms. All curves are obtained using identical acquisition and analysis protocols, but the tips differ from set to set. **b**, The same force curves as in **a**, but the curves in each set are now normalized to the absolute value of the minimum short-range force of the Si curve ($|F_{Si(set)}|$). **c**, **d**, Sets of short-range force curves for Pb and Si, obtained in the same way as for Sn and Si, before (**c**) and after (**d**) normalization. The average relative interaction ratios calibrated against Si, or the maximum attractive short-range forces for Sn and Pb relative to those of Si (77% and 59%, respectively), provide an intrinsic signature for the chemical identification of individual atoms. Each experimental force characteristic shown here was obtained from the measurement of a hundred spectroscopic curves (see Methods for details). The acquisition parameters are available in the Supplementary Information. **e**, **f**, Chemical force curves calculated for different tip-apex models (see insets for structural and chemical characteristics) over the Sn and Si atoms of the $(\sqrt{3} \times \sqrt{3})$ R30° surface model shown in Fig. 1b. The curves are shown before (**e**) and after (**f**) normalization. In both the experimental and the calculated short-range force curves, the distance axes denote the tip–sample relative displacement (see Methods for details).

multi-element systems. This capability of the AFM is demonstrated in Fig. 3, where we have unambiguously discriminated between the three species—topographically not clearly distinguishable—of a surface alloy comprised of Si, Sn, and Pb atoms mixed in equal proportions

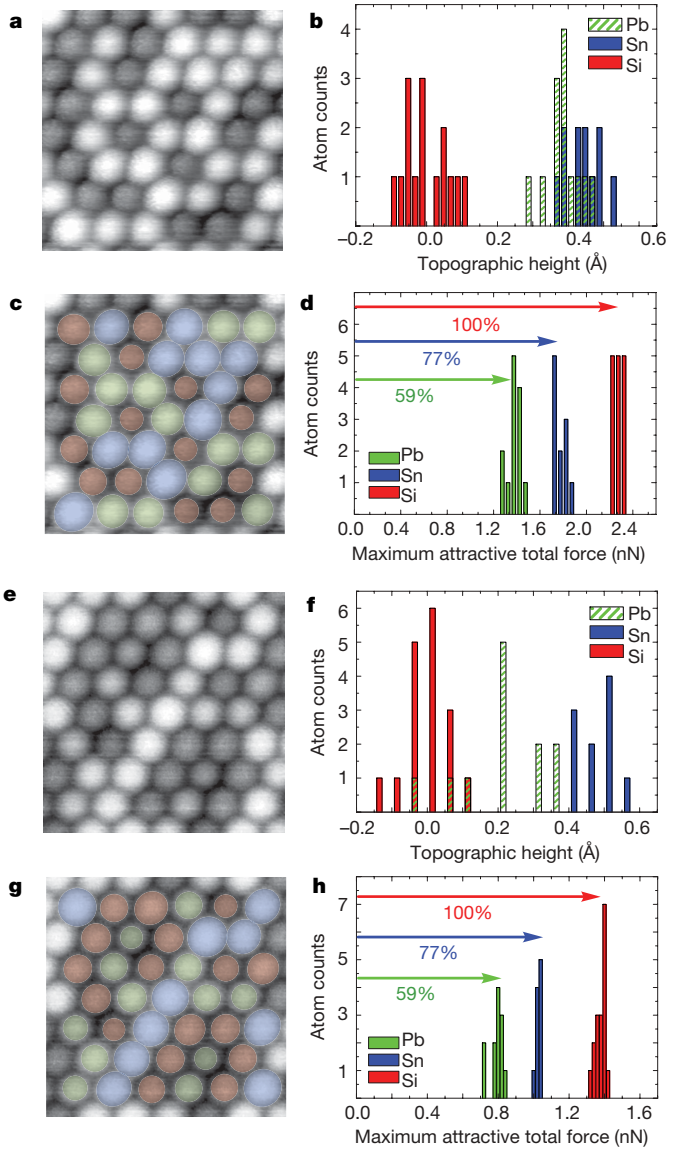

Figure 3 | Single-atom chemical identification. **a**, Topographic image of a surface alloy composed by Si, Sn and Pb atoms blended in equal proportions on a Si(111) substrate. **b**, Height distribution of the atoms in **a**, showing that Pb and Sn atoms with few nearest-neighbouring Si atoms appear indistinguishable in topography. **c**, Local chemical composition of the image in **a**. Blue, green, and red atoms correspond to Sn, Pb and Si, respectively. **d**, Distribution of maximum attractive total forces measured over the atoms in **a**. By using the relative interaction ratio determined for Sn/Si and Pb/Si (Fig. 2b and d), each of the three groups of forces can be attributed to interactions measured over Sn, Pb and Si atoms. **e**, Topographic image similar to that in **a**, but showing a region where some Pb atoms are almost completely surrounded by Si atoms. These Pb atoms (identified in **g** by a darker shade of green) are indistinguishable from the surrounding Si atoms, as illustrated by the topographic height distribution histogram (**f**). The local chemical composition, shown in **g**, can still be unambiguously assigned by measuring the total force values over each surface atom and using the relative interaction ratios for Sn/Si and Pb/Si to attribute the three groups of maximum attractive forces to interactions measured over Sn, Pb and Si atoms (**h**). The colour code for labelling the Pb, Sn and Si atoms in **g** is the same as in **c**. Image dimensions are (4. 3 × 4.3) nm^2. The images were acquired close to the onset of the short-range interaction[20]; for the acquisition parameters see the Supplementary Information.

(Fig. 3a and e). In this instance, we systematically recorded the total tip–surface interaction force over each atom seen in the images in Fig. 3a and e, respectively. The measured maximum attractive total forces were found to fall into three distinct groups (see histograms in Fig. 3d and h, respectively). When taking into account the relative interaction ratio for Sn and Si and for Pb and Si determined in our earlier experiments (Fig. 2b and d), these groups can be assigned to forces obtained over Sn, Pb and Si atoms (Fig. 3d and h) and hence the chemical identity of each surface atom can be determined (Fig. 3c and g). The significant discrepancy between the total force values in Fig. 3d and h—obtained in two separate measurement sessions using different tips—confirms that although tip characteristics strongly influence measured forces, they do not affect the ability to chemically identify surface atoms. These results also corroborate the robustness of the procedure, as the identification in Fig. 3 has been accomplished by using the maximum attractive total forces instead of the short-range forces. This more straightforward identification process, which avoids the non-trivial and time-consuming separation of the short- and long-range contributions to the total force[20], can be extended to other systems if the total force is not dominated by long-range interactions and there are no pronounced in-plane local spatial variations of the long-range forces. In the experiments shown in Fig. 3, for instance, the long-range contribution at the minimum positions was only 10% to 18% of the total interaction force (see the Supplementary Information).

We note that it would have been impossible to reveal the local atomic composition of these surface alloy regions using topographic information. For example, in areas with locally homogeneous distributions of Si atoms (Fig. 3a), Pb and Sn appear indistinguishable in topography; this is clearly illustrated by the atomic height distribution histogram (Fig. 3b). But in regions where Si atoms cluster together (Fig. 3e), any Pb atoms that are surrounded almost completely by Si atoms (differentiated from other Pb atoms in Fig. 3g by a darker shade of green) are indistinguishable from the Si atoms; again, this effect is clearly illustrated by the histogram shown in Fig. 3f. These topographic variations with the number of nearest-neighbouring Si atoms[20,21] have been attributed to a subtle coupling between charge transfer and atomic relaxations[22]. For closer tip–surface distances, relative variations in the atomic contrast—which would further hinder a topographic discrimination attempt—are expected owing to differences in the strength of the interaction forces over the atoms and tip-induced atomic relaxations[20]. Attempts to scan at tip–surface distances close to the maximum attractive forces—where the interaction between the outermost tip atom and a surface atom dominates the signal, and hence unambiguous chemical information of the atomic surface species can be obtained—result in most of the cases in unstable imaging, or even in modifications of the tip apex or surface due to strong tip–surface lateral forces.

The present approach to characterizing the local composition of a multi-element system at the atomic level, which is based on the detection of the short-range chemical forces between the outermost atom of an AFM tip and individual surface atoms, should be widely applicable. It does require prior calibration of the relative interaction ratio of the maximum attractive short-range forces between pairs of atomic species on a well-defined system; but once obtained, the ratios (which are practically independent of tip apex characteristics) can serve as fingerprints for chemical recognition in subsequent measurements. We believe that the chemical identification capabilities demonstrated here hold substantial promise for affecting research areas such as catalysis, materials science or semiconductor technology, in which important functional properties are controlled by the chemical nature and short-range ordering of individual atoms, defects, adsorbates or dopants.

METHODS

Dynamic force microscopy and spectroscopy measurements. We used a home-built ultrahigh vacuum dynamic AFM powered by a commercial scanning probe controller (Dulcinea, Nanotec Electrónica, Madrid, Spain) and operated at room

temperature under the frequency modulation detection method[23]. The cantilever was instantaneously excited to its first mechanical resonant frequency keeping the oscillation amplitude constant. The main observable was the shift of the first mechanical resonant frequency (Δf) from the free-oscillation value upon the forces acting on the tip at the cantilever free end[24]. Force spectroscopy was performed recording the Δf signal as a function of the tip–sample relative vertical displacement (Z). The determination of the corresponding cantilever stiffness and oscillation amplitude values is described elsewhere[12]. The absence of any tip or surface modification during the spectroscopic acquisition was carefully and properly checked[12]. During imaging, and for each spectroscopic measurement, the long-range electrostatic interaction was minimized by compensating the tip–surface contact potential difference. For the calibration of the relative interaction ratio in Fig. 2, we first performed the identification of Sn, Pb, and Si in the corresponding bi-atomic overlayers (Fig. 1d, e) by changing the relative concentration of the two elements[20].

In Fig. 2, a single spectroscopic measurement comprised the successive acquisition of a hundred equivalent $\Delta f(Z)$ curves over the topmost part of the surface atom with a lateral precision better than ± 0.1 Å, provided by our atom-tracking implementation[12,16]. In each case, these $\Delta f(Z)$ curves were averaged in a single $\Delta f(Z)$ characteristic from which we obtained the total interaction force using the inversion procedure proposed by Sader and Jarvis[25]. For each set of curves, the compensation of the topographic effects on Z associated with the spectroscopic acquisition[20] was then undertaken; this sets the separation distance between the two force minima and provides a common origin with respect to the surface plane[20]. The short-range chemical forces were obtained afterwards by the subtraction of an appropriate fit[11,12] over the long-range interaction region to the total force, where this long-range region is defined from the free oscillation to the Z position at which both curves start splitting owing to the onset of the short-range interaction. For clarity in the representation, the origin of the Z axis for each set was shifted to the position for the Si minimum (keeping the original separation between the minima constant), so that all the sets share the same distance origin when compared. In the case of the experiments shown in Fig. 3, only ten $\Delta f(Z)$ curves were measured over each atom. The surface alloy was prepared by the deposition of approximately one-sixth of a monolayer of Pb—one monolayer corresponds to the surface atomic density of a (111) plane of a Si crystal—and one-ninth of a monolayer of Sn over the Si(111)-(7×7) surface, followed by sample annealing at 700 K.

First-principles calculations. Calculations are based in density functional theory implemented with a local orbital basis using the FIREBALL code[26], which offers a very favourable accuracy-to-efficiency balance. The details of the minimal basis we used are described elsewhere[20]. To model the surface we considered a (6×6) periodic slab that includes six Si layers with H saturating the dangling bonds at the deeper layer (Fig. 1b). Only the Γ point was included in the sampling of the Brillouin zone. The tip–surface interaction energy was determined in a stepwise, quasistatic manner by approaching the tip parallel to the surface. At each step, the atoms in the slab and the tip model were allowed to relax to their ground-state configuration with convergence criteria for the total energy and forces of 10^{-6} eV and 0.05 eV Å^{-1}. Only the H-saturated atoms at the topmost part of the tip models (Fig. 2e and f) and the Si and H layers at the bottom of the slab were fixed during the relaxation process. The short-range forces were calculated as a numerical derivative of the total energy.

Received 12 August; accepted 4 December 2006.

1. Eigler, D. M. & Schweizer, E. K. Positioning single atoms with a scanning tunnelling microscope. *Nature* **344,** 524–526 (1990).
2. Sugimoto, Y. *et al.* Atom inlays performed at room temperature using atomic force microscopy. *Nature Mater.* **4,** 156–159 (2005).
3. Stipe, B. C., Rezaei, M. A. & Ho, W. Single-molecule vibrational spectroscopy and microscopy. *Science* **280,** 1732–1735 (1998).
4. Heinrich, A. J., Lutz, C. P., Gupta, J. A. & Eigler, D. M. Molecule cascades. *Science* **298,** 1381–1387 (2002).
5. Pascual, J. I., Lorente, N., Song, Z., Conrad, H. & Rust, H.-P. Selectivity in vibrationally mediated single-molecule chemistry. *Nature* **423,** 525–528 (2003).
6. Madhavan, V., Chen, W., Jamneala, T., Crommie, M. F. & Wingreen, N. S. Tunneling into a single magnetic atom: spectroscopic evidence of the Kondo resonance. *Science* **280,** 567–569 (1998).
7. Li, J., Schneider, W.-D., Berndt, R. & Delley, B. Kondo scattering observed at a single magnetic impurity. *Phys. Rev. Lett.* **80,** 2893–2896 (1998).
8. Morita, S., Wiesendanger, R. & Meyer, E. *Noncontact Atomic Force Microscopy*. *NanoScience and Technology* (Springer, Berlin, 2002).
9. García, R. & Pérez, R. Dynamic atomic force microscopy methods. *Surf. Sci. Rep.* **47,** 197–301 (2002).
10. Giessibl, F. J. Advances in atomic force microscopy. *Rev. Mod. Phys.* **75,** 949–983 (2003).
11. Lantz, M. A. *et al.* Quantitative measurement of short-range chemical bonding forces. *Science* **291,** 2580–2583 (2001).
12. Abe, M., Sugimoto, Y., Custance, O. & Morita, S. Room-temperature reproducible spatial force spectroscopy using atom-tracking technique. *Appl. Phys. Lett.* **87,** 173503 (2005).
13. Hoffmann, R., Kantorovich, L. N., Baratoff, A., Hug, H. J. & Güntherodt, H.-J. Sublattice identification in scanning force microscopy on alkali halide surfaces. *Phys. Rev. Lett.* **92,** 146103 (2004).
14. Pérez, R., Payne, M., Štich, I. & Terakura, K. Role of covalent tip-surface interactions in noncontact atomic force microscopy. *Phys. Rev. Lett.* **78,** 678–681 (1997).
15. Livshits, A. I., Shluger, A. L., Rohl, A. L. & Foster, A. S. Model of noncontact scanning force microscopy on ionic surfaces. *Phys. Rev. B* **59,** 2436–2448 (1999).
16. Abe, M., Sugimoto, Y., Custance, O. & Morita, S. Atom tracking for reproducible force spectroscopy at room temperature with non-contact atomic force microscopy. *Nanotechnology* **16,** 3029–3034 (2005).
17. Oyabu, N. *et al.* Single atomic contact adhesion and dissipation in dynamic force microscopy. *Phys. Rev. Lett.* **96,** 106101 (2006).
18. Ke, S. H., Uda, T., Pérez, R., Štich, I. & Terakura, K. First-principles investigation of tip-surface interaction on a GaAs(110) surface: implications for atomic force and scanning tunneling microscopies. *Phys. Rev. B* **60,** 11631–11638 (1999).
19. Hembacher, S., Giessibl, F. J. & Mannhart, J. Force microscopy with light-atom probes. *Science* **305,** 380–383 (2004).
20. Sugimoto, Y. *et al.* Real topography, atomic relaxations, and short-range chemical interactions in atomic force microscopy: The case of the α-Sn/Si(111)-$(\sqrt{3} \times \sqrt{3})$R30° surface. *Phys. Rev. B* **73,** 205329 (2006).
21. Sugimoto, Y. *et al.* Non-contact atomic force microscopy study of the Sn/Si(111) mosaic phase. *Appl. Surf. Sci.* **241,** 23–27 (2005).
22. Charrier, A. *et al.* Contrasted electronic properties of Sn-adatom-based $(\sqrt{3} \times \sqrt{3})$R30° reconstructions on Si(111). *Phys. Rev. B* **64,** 115407 (2001).
23. Albrecht, T. R., Grütter, P., Horne, D. & Rugar, D. Frequency modulation detection using high-Q cantilevers for enhanced force microscope sensitivity. *J. Appl. Phys.* **69,** 668–673 (1991).
24. Giessibl, F. J. Forces and frequency shifts in atomic resolution dynamic-force microscopy. *Phys. Rev. B* **56,** 16010–16015 (1997).
25. Sader, J. E. & Jarvis, S. P. Accurate formulas for interaction force and energy in frequency modulation force spectroscopy. *Appl. Phys. Lett.* **84,** 1801–1803 (2004).
26. Jelinek, P., Wang, H., Lewis, J. P., Sankey, O. F. & Ortega, J. Multicenter approach to the exchange-correlation interactions in ab initio tight-binding methods. *Phys. Rev. B* **71,** 235101 (2005).

Supplementary Information is linked to the online version of the paper at www.nature.com/nature.

Acknowledgements We thank F. J. Giessibl and M. Reichling for their comments on the manuscript, and T. Namikawa and K. Mizuta for technical assistance. This work was supported by the Handai FRC, the JST, the 21st Century COE programme, and the MEXT of Japan. The work of P.P. and R.P. is supported by the MCyT, the Juan de la Cierva Programme, the CCC-UAM (Spain), and the FORCETOOL project (EU). The work of P.J. is supported by the MSMT and GAAV.

Author Information Reprints and permissions information is available at www.nature.com/reprints. The authors declare no competing financial interests. Correspondence and requests for materials should be addressed to O.C. (oscar@afm.eei.eng.osaka-u.ac.jp).

LETTERS

Implications for plastic flow in the deep mantle from modelling dislocations in $MgSiO_3$ minerals

Philippe Carrez[1]*, Denise Ferré[1]* & Patrick Cordier[1]*

The dynamics of the Earth's interior is largely controlled by mantle convection, which transports radiogenic and primordial heat towards the surface. Slow stirring of the deep mantle is achieved in the solid state through high-temperature creep of rocks, which are dominated by the mineral $MgSiO_3$ perovskite. Transformation of $MgSiO_3$ to a 'post-perovskite' phase[1–3] may explain the peculiarities of the lowermost mantle, such as the observed seismic anisotropy[4], but the mechanical properties of these mineralogical phases are largely unknown[5–7]. Plastic flow of solids involves the motion of a large number of crystal defects, named dislocations[8]. A quantitative description of flow in the Earth's mantle requires information about dislocations in high-pressure minerals and their behaviour under stress. This property is currently out of reach of direct atomistic simulations using either empirical interatomic potentials or *ab initio* calculations. Here we report an alternative to direct atomistic simulations based on the framework of the Peierls–Nabarro model[9,10]. Dislocation core models are proposed for $MgSiO_3$ perovskite (at 100 GPa) and post-perovskite (at 120 GPa). We show that in perovskite, plastic deformation is strongly influenced by the orthorhombic distortions of the unit cell. In silicate post-perovskite, large dislocations are relaxed through core dissociation, with implications for the mechanical properties and seismic anisotropy of the lowermost mantle.

Silicate minerals are often characterized by a significant intrinsic resistance to plastic shear, called lattice friction. The dislocation dynamics in such cases depends strongly on the mobility of dislocations, and this mobility is governed by the dislocation core structure at the atomic scale[11]. Following earlier developments for olivine[12,13] and ringwoodite[14], we propose a new approach to the modelling of dislocation cores of minerals under high pressure. We couple atomistic simulation results (from the density functional theory, DFT) for generalized stacking faults to a continuum-based description of the dislocation core within the framework of the Peierls–Nabarro (PN) model. Dislocation cores have been described recently in complex materials[15–18]. However, these models rely on empirical interatomic potentials to describe atomic interactions (at least in the core region). The application of these models to minerals of the deep Earth is difficult, as reliable interatomic potentials are not available under a wide range of high-pressure conditions. *Ab initio* methods based on the DFT provide reliable and efficient methods to solve Schrödinger's equation for a solid, also at high pressure. Currently, standard techniques using DFT are limited to hundreds of atoms. This is not sufficient to model dislocation cores in complex minerals. Therefore, in our approach, tractable DFT calculations of generalized stacking faults are used as an input for the PN model.

Peierls, motivated by Orowan, proposed[9] an elegant model to account for the atomic-level nonlinear forces in the dislocation core within an essentially continuum framework[9]. This model was further developed by Nabarro[10]. It is now referred to as the Peierls–Nabarro (PN) model, and has been widely applied to simple structured materials[19–21] and recently to minerals[14]. Peierls divided the dislocation-containing crystal into three regions (Fig. 1): regions a and b where linear elasticity applies, and the interplanar region across the slip plane where atomic displacements are large and deviate from linear elasticity and where we use DFT calculations.

The balance within the A and B layers (see Fig. 1) of elastic and non-elastic forces leads to the PN equation:

$$\frac{K}{2\pi}\int_{-\infty}^{+\infty}\frac{1}{x-x'}\left[\frac{\mathrm{d}S(x')}{\mathrm{d}x'}\right]\mathrm{d}x' = \frac{K}{2\pi}\int_{-\infty}^{+\infty}\frac{\rho(x')}{x-x'}\mathrm{d}x' = F(S(x)) \quad (1)$$

where K is the energy coefficient (a function of the dislocation character, and calculated using anisotropic elasticity), $S(x)$ represents the disregistry across the glide plane, $\rho(x)$ is the planar continuous distribution of infinitesimal dislocations in the glide plane, x is the distance from the dislocation line along the glide direction, and x' is the location of every infinitesimal dislocation. An analytical solution of the PN equation can be found by introducing a sinusoidal restoring force (in the right-hand side of the equation). This leads to the standard expression of the Peierls stress found in most textbooks. However, most real cases deviate significantly from this ideal harmonic situation and therefore, this model is of little practical use.

The PN approach was rejuvenated when Vitek[22] showed that the restoring force F introduced in the PN model is simply the gradient of the so-called generalized stacking fault energy, γ:

$$\mathbf{F}(S) = -\nabla\gamma(S) \quad (2)$$

Here, the generalized stacking fault energy is calculated using DFT by imposing a shear displacement between two rigid blocks of a perfect crystal[12,13]. DFT calculations were performed using the

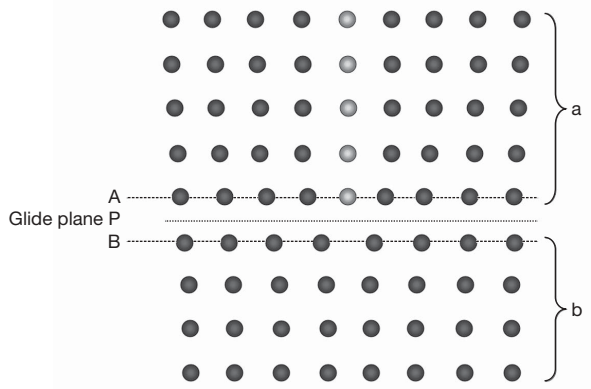

Figure 1 | Diagram of an edge dislocation in a simple square lattice. Adapted from ref. 9. The grey spheres highlight the extra half-plane; see text for details.

[1]Laboratoire de Structure et Propriétés de l'Etat Solide, UMR 8008 CNRS/Université de Lille 1, 59655 Villeneuve d'Ascq Cedex, France.
*These authors contributed equally to this work.

VASP code[23] based on the generalized gradient approximation[24] and the all-electron projector augmented-wave method[25,26]. The first achievement of the PN model is to provide an analytical function describing the dislocation profile, $\rho(x)$; a recent application of this technique to Mg_2SiO_4 ringwoodite is given in ref. 14. More importantly, it also provides insights about the critical stress required to move a dislocation in the lattice: the so-called Peierls stress. For that purpose, one must calculate the derivative of the misfit potential, calculated at the actual positions of the atomic planes[14]. We present here the application of this technique to the structure of dislocation cores in $MgSiO_3$ perovskite (Pv) and post-perovskite (pPv). We also demonstrate that the solution of the PN model can be used to build an atomic-scale model of a dislocation core. (Technical details concerning the *ab initio* calculations, the application of the PN model and how the solution of the PN equation $\rho(x)$ is used to derive the dislocation core models are given in Supplementary Methods.)

We first describe the implications of the $MgSiO_3$ pPv crystal structure for the plastic properties. The shorter vector of the unit cell is [100] ($a = 2.456$ Å, to be compared to $b = 8.042$ Å and $c = 6.093$ Å; ref. 3). It corresponds to the Burgers vector of the less energetic dislocations. A diagram of the core of a [100] edge dislocation gliding on (010) is presented Fig. 2a. The core is relatively wide (the half-width of the $\rho(x)$ dislocation distribution $\zeta = 1.88$ Å) compared to the lattice periodicity (2.456 Å). The Peierls stress of this edge dislocation is only 4 GPa and it is able to glide very easily. On the other hand, the Peierls stress of the related screw dislocation is 87 GPa. Therefore the screw dislocations will control plastic deformation on this slip system. Glide along [001] in the same plane corresponds to a significantly longer translation vector and is expected to be more difficult. However, Fig. 2b shows that this difficulty is overcome by the dissociation of the [001] dislocation into two collinear partial dislocations ($\zeta = 1.86$ Å for the partial dislocation) separated by a stacking fault ribbon 16.15 Å wide. This dissociation has profound implications for the mobilities, as the Peierls stresses are respectively 18 and 12 GPa for the screw and edge dislocations. Surprisingly, we find that [001](010) is intrinsically the easiest slip system in $MgSiO_3$ pPv. Let us examine the case of the largest Burgers vector: [010]. We find that this dislocation can be stabilized thanks to significant core relaxations. Figure 3 shows that in (100), this dislocation dissociates into three partial dislocations separated by a 13.4-Å-wide faulted ribbon. Here again, the implications for the mechanical properties are significant, as the Peierls stresses are 95 and 57 GPa for the screw and edge dislocations, respectively. These values are comparable to those encountered with [100] slip.

In the bulk of the lower mantle, $MgSiO_3$ exhibits a structure derived from the perfect perovskite structure by orthorhombic distortions. We present here (Fig. 4) the structure of a [010] dislocation gliding in a (001) plane. The core is relatively wide, but owing to the distortions, it does not lead to a well-defined dissociation. The Peierls stresses are 20 GPa and 30 GPa for the edge and screw dislocations, respectively. The Peierls stresses of [100](001) dislocations (a pseudo-equivalent slip system differing only by the distortions in the orthorhombic unit cell) are 48 and 76 GPa for the edge and screw

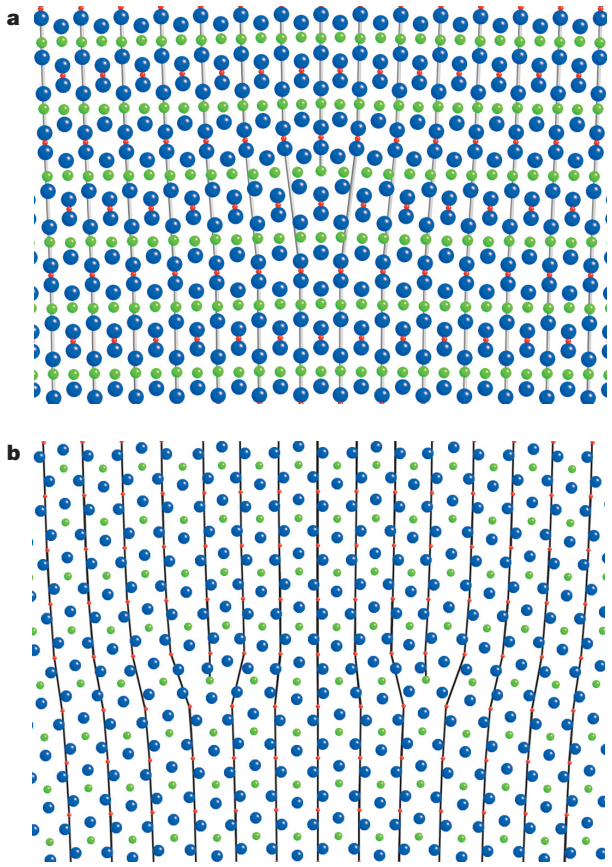

Figure 2 | PN models of dislocation cores in $MgSiO_3$ pPv at 120 GPa. **a**, A [100] edge dislocation gliding in the (010) plane (horizontal) viewed along [001]. The atomic positions are derived from the $S(x)$ profile calculated from the PN model, to which the elastic displacement field is added. Oxygen atoms are represented by blue spheres, silicon atoms are red and magnesium atoms are green. Some atomic planes are highlighted to help viewing the extra half-plane of the dislocation. **b**, A [001] edge dislocation gliding in the (010) plane (horizontal) viewed along [100]. Some atomic planes are highlighted. The two partial dislocations are seen to enclose a stacking fault.

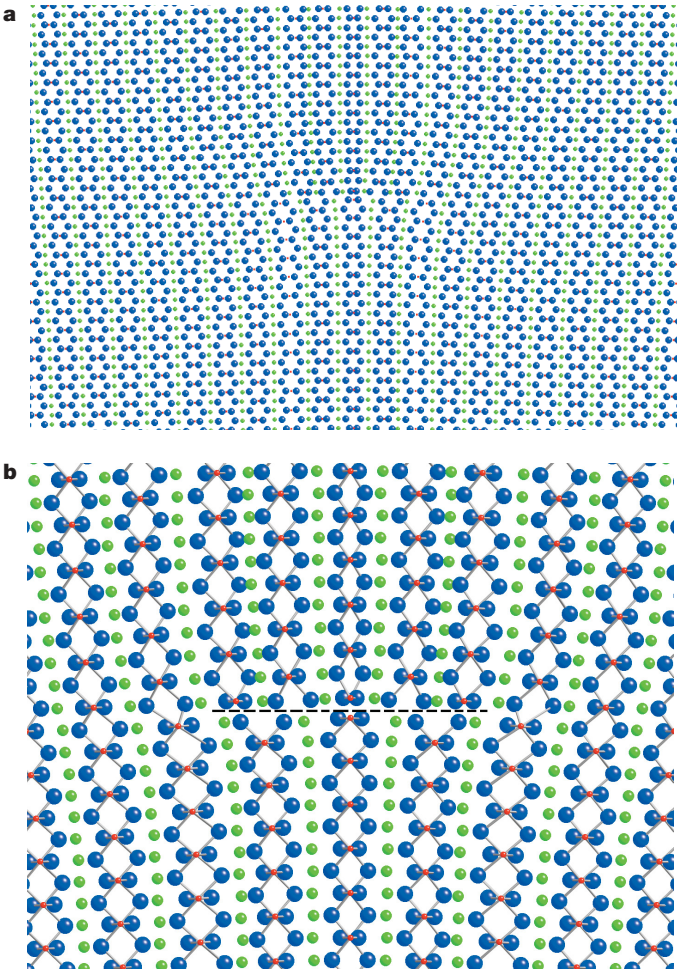

Figure 3 | An [010] edge dislocation in $MgSiO_3$ pPv at 120 GPa. **a**, PN model of the core of an [010] edge dislocation gliding in the (100) plane (horizontal) viewed along [001]. **b**, Enlargement of the core region showing spreading resulting from the formation of three overlapping partials. The stacking fault is underlined by the dashed line.

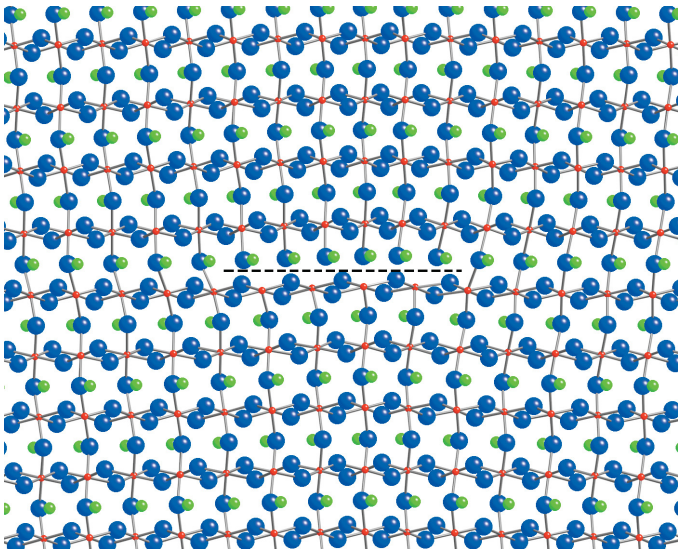

Figure 4 | $MgSiO_3$ pV at 100 GPa. PN model of the core of an [010] edge dislocation gliding in the (001) plane (horizontal) viewed along [100]. The stacking fault is underlined by the dashed line.

dislocations, respectively. This difference illustrates the contribution of small changes in the fine core structure (here the orthorhombic distortions) to the mechanical properties.

Our calculations yield the first (to our knowledge) models of dislocation cores in complex crystal structures under extreme pressure conditions. In $MgSiO_3$ Pv, we show that orthorhombic distortions affect the core and dislocation mobilities. This calls for a reinterpretation of existing data on $MgSiO_3$ Pv, often described within the framework of a pseudo-cubic symmetry. Beyond mineral physics, dislocations in perovskite-structured materials play a key role in industrial nanoelectronics and are at the focus of many studies[27]. Our work provides a theoretical counterpart to transmission electron microscopy determinations of dislocation cores in complex materials[28–30].

Dislocation core spreading has implications for the mechanical properties, as illustrated by the calculations of Peierls stresses. Examples presented for $MgSiO_3$ pPv show that counterintuitive results (such as [001](010) being the easiest slip system) can be the consequence of the fine structure of the dislocation core. Determining the easy slip systems in $MgSiO_3$ pPv is a major issue in understanding the seismic anisotropy in the lowermost mantle (the D″ layer). Several studies are now being conducted on the lattice preferred orientation (LPO) that develops in pPv phases. First-principles calculations suggest that LPO dominated by the {110} planes can result from shear transformation of the perovskite phase[6]. Experiments on the $MgGeO_3$ pPv analogue are compatible with this mechanism[7]. On the other hand, experiments on $CaIrO_3$ pPv lead to strong LPO, with (010) perpendicular to the compression axis[31]. Both signatures have been reported in Mn_2O_3 pPv, suggesting that LPO in pPv phases can be affected by phase transition and heating as well as differential stress[32]. Our study goes beyond educated guesses, and suggests that (010) is the easiest slip plane at low temperature in $MgSiO_3$ pPv. Moreover, we show that slip along [001] provides a major contribution to plastic deformation along this plane (this information is not contained in LPO obtained in compression, which provides no information about the slip direction). Our study suggests that shear transformation and dislocation activity involve different slip planes ({110} or (010)), which could lead to distinctly different LPO. Therefore, polarization anisotropy should be an indicator of the relative importance of phase transformation and plastic flow in the lowermost mantle.

Received 7 June 2006; accepted 8 January 2007.

1. Murakami, M., Hirose, K., Kawamura, K., Sata, N. & Ohishi, Y. Post-perovskite phase transition in $MgSiO_3$. *Science* **304,** 834–836 (2004).
2. Oganov, A. R. & Ono, S. Theoretical and experimental evidence for a post-perovskite phase of $MgSiO_3$ in Earth's D″ layer. *Nature* **430,** 445–448 (2004).
3. Itaka, T., Hirose, K., Kawamura, K. & Murakami, M. The elasticity of the $MgSiO_3$ post-perovskite phase in the Earth's lowermost mantle. *Nature* **430,** 442–445 (2004).
4. Wookey, J., Stackhouse, S., Kendall, J. M., Brodholt, J. & Price, G. D. Efficacy of the post-perovskite phase as an explanation for lowermost-mantle seismic properties. *Nature* **438,** 1004–1007 (2005).
5. Cordier, P., Ungár, T., Zsoldos, L. & Tichy, G. Dislocation creep in $MgSiO_3$ perovskite at conditions of the Earth's uppermost lower mantle. *Nature* **428,** 837–840 (2004).
6. Oganov, A. R., Martonák, R., Laio, A., Raiteri, P. & Parrinello, M. Anisotropy of Earth's D″ layer and stacking faults in the $MgSiO_3$ post-perovskite phase. *Nature* **438,** 1142–1144 (2005).
7. Merkel, S. *et al.* Plastic deformation of $MgGeO_3$ post-perovskite at lower mantle pressures. *Science* **311,** 644–646 (2006).
8. Hirth, J. P. & Lothe, J. *Theory of Dislocations* (Wiley & Sons, New York, 1982).
9. Peierls, R. E. On the size of a dislocation. *Proc. Phys. Soc. Lond.* **52,** 34–37 (1940).
10. Nabarro, F. R. N. Dislocations in a simple cubic lattice. *Proc. Phys. Soc. Lond.* **59,** 256–272 (1947).
11. Cai, W., Bulatov, V. V., Chang, J., Li, J. & Yip, S. in *Dislocations in Solids* (eds Nabarro, F. N. R. & Hirth, J. P.) 1–80 (Elsevier, Amsterdam, 2004).
12. Durinck, J., Legris, A. & Cordier, P. Influence of crystal chemistry on ideal plastic shear anisotropy in forsterite: first principle calculations. *Am. Mineral.* **90,** 1072–1077 (2005).
13. Durinck, J., Legris, A. & Cordier, P. Pressure sensitivity of forsterite slip systems: first-principle calculations of generalised stacking faults. *Phys. Chem. Miner.* **32,** 646–654 (2005).
14. Carrez, P., Cordier, P., Mainprice, D. & Tommasi, A. Slip systems and plastic shear anisotropy in Mg_2SiO_4 ringwoodite: insights from numerical modelling. *Eur. J. Mineral.* **18,** 149–160 (2006).
15. Walker, A. M., Slater, B., Gale, J. D. & Wright, K. Predicting the structure of screw dislocations in nanoporous materials. *Nature Mater.* **3,** 715–720 (2004).
16. Walker, A. M., Gale, J. D., Slater, B. & Wright, K. Atomic scale modelling of the cores of dislocations in complex materials part 2: applications. *Phys. Chem. Chem. Phys.* **7,** 3235–3242 (2005).
17. Cawkwell, M. J., Nguyen-Manh, D., Woodward, C., Pettifor, D. G. & Vitek, V. Origin of brittle cleavage in iridium. *Science* **309,** 1059–1062 (2005).
18. Cordier, P., Barbe, F., Durinck, J., Tommasi, A. & Walker, A. M. in *Mineral Behaviour at Extreme Conditions* (ed. Miletich, R.) 389–415 (Eötvös Univ. Press, Budapest, 2005).
19. Joos, B., Ren, Q. & Duesbery, M. S. Peierls-Nabarro model of dislocations in silicon with generalized stacking-fault restoring forces. *Phys. Rev. B* **50,** 5890–5898 (1994).
20. Lu, G., Kioussis, N., Bulatov, V. V. & Kaxiras, E. Generalized-stacking-fault energy surface and dislocation properties of aluminum. *Phys. Rev. B* **62,** 3099–3108 (2000).
21. Miranda, C. R. & Scandolo, S. Computational materials science meets geophysics: dislocations and slip planes of MgO. *Comput. Phys. Commun.* **169,** 24–27 (2005).
22. Vítek, V. Intrinsic stacking faults in body-centered cubic crystals. *Phil. Mag.* **18,** 773–786 (1968).
23. Kresse, G. & Furthmüller, J. Efficient iterative schemes for ab initio total-energy calculations using a plane-wave basis set. *Phys. Rev. B* **54,** 11169–11186 (1996).
24. Perdew, J. P., Burke, K. & Ernzerhof, M. Generalized gradient approximation made simple. *Phys. Rev. Lett.* **77,** 3865–3868 (1996).
25. Blöchl, P. E. Projector augmented-wave method. *Phys. Rev. B* **50,** 17953–17979 (1994).
26. Kresse, G. & Joubert, D. From ultrasoft pseudopotentials to the projector augmented-wave method. *Phys. Rev. B* **59,** 1758–1775 (1999).
27. Setter, N. & Waser, R. Electroceramic materials. *Acta Mater.* **48,** 151–178 (2000).
28. Hÿtch, M., Putaux, J. L. & Pénisson, J. M. Measurement of the displacement field of dislocations to 0.03 Å by electron microscopy. *Nature* **423,** 270–273 (2003).
29. Chisholm, M. F., Kumar, S. & Hazzledine, P. Dislocations in complex materials. *Science* **307,** 701–703 (2005).
30. Jia, C. L., Thust, A. & Urban, K. Atomic-scale analysis of the oxygen configuration at a $SrTiO_3$ dislocation core. *Phys. Rev. Lett.* **95,** 225506 (2005).
31. Niwa, K. *et al.* Lattice preferred orientation in $CaIrO_3$ perovskite and post-perovskite formed by the plastic deformation under pressure. *Geophys. Res. Lett.* (submitted).
32. Santillan, J., Shim, S.-H., Shen, G. & Prakapenka, V. B. High-pressure phase transition in Mn_2O_3: application for the crystal structure and preferred orientation of the $CaIrO_3$ type. *Geophys. Res. Lett.* **33,** L15307, doi:10.1029/2006GL026423 (2006).

Supplementary Information is linked to the online version of the paper at www.nature.com/nature.

Acknowledgements This work was supported by CNRS-INSU under the DyETI programme. Computational resources were provided by IDRIS and CRI-USTL supported by the Fonds Européens de Développement Régional and the Région Nord-Pas de Calais. D. Rodney is thanked for discussions.

Author Information Reprints and permissions information is available at www.nature.com/reprints. The authors declare no competing financial interests. Correspondence and requests for materials should be addressed to P.C. (Patrick.Cordier@univ-lille1.fr).

LETTERS

A topographic map of recruitment in spinal cord

David L. McLean[1], Jingyi Fan[2], Shin-ichi Higashijima[3], Melina E. Hale[2] & Joseph R. Fetcho[1]

Animals move over a range of speeds by using rhythmic networks of neurons located in the spinal cord[1–6]. Here we use electrophysiology and *in vivo* imaging in larval zebrafish (*Danio rerio*) to reveal a systematic relationship between the location of a spinal neuron and the minimal swimming frequency at which the neuron is active. Ventral motor neurons and excitatory interneurons are rhythmically active at the lowest swimming frequencies, with increasingly more dorsal excitatory neurons engaged as swimming frequency rises. Inhibitory interneurons follow the opposite pattern. These inverted patterns of recruitment are independent of cell soma size among interneurons, but may be partly explained by concomitant dorso-ventral gradients in input resistance. Laser ablations of ventral, but not dorsal, excitatory interneurons perturb slow movements, supporting a behavioural role for the topography. Our results reveal an unexpected pattern of organization within zebrafish spinal cord that underlies the production of movements of varying speeds.

Like all vertebrates, larval zebrafish move over a range of speeds. They can swim slowly using caudal tail bends of 20–40 Hz and swim faster using larger body bends of 80–100 Hz that propagate from the head to the tail[7–9]. We set out to understand how the spinal cord was organized to produce movements over such a broad range of swimming frequencies.

The zebrafish motor column contains large, early born, dorsally located primary motor neurons, which innervate fast muscle fibres and are known to be involved in faster movements[10], and a larger number of usually smaller and more ventral secondary motor neurons[11,12]. We recorded the activity of single motor neurons during swimming (Fig. 1a–c), while monitoring the fictive motor pattern from peripheral motor nerves. Initial observations indicated that more dorsal primary and secondary motor neurons did not fire at slow swimming speeds, as illustrated in Fig. 1d–f. This prompted us to look more closely for a relationship between neuronal location and activation frequency. A plot of the position of a motor neuron along the dorso-ventral axis of the spinal cord against an average of the three lowest swimming frequencies at which it was active revealed a linear relationship (Fig. 1g–i). Ventral motor neurons were active at low frequencies of swimming, and the minimal frequency of activation rose for motor neurons located at increasingly more dorsal positions ($R = 0.78$, $P < 0.0001$, $n = 40$). This relationship was evident even within the population of secondary motor neurons (Fig. 1h; $R = 0.79$, $P < 0.0001$, $n = 30$).

To rule out possible artefacts of patch recording, we used *in vivo* calcium imaging to visualize simultaneously the activity of groups of motor neurons distributed along the dorso-ventral axis during fictive swimming (Fig. 1j). As in the electrophysiological data, ventral neurons were recruited during episodes with lower peak frequencies, with more dorsal cells engaged as the peak frequency in an episode increased (Fig. 1k, l; $R = 0.80$, $P < 0.0001$, $n = 52$).

We next examined whether the same functional topography extended to premotor excitatory spinal neurons, including circumferential descending (CiD) interneurons with ipsilateral axons and multipolar commissural descending (MCoD) interneurons with contralateral axons[13,14] (Fig. 2a–f). In both classes, a neuron's position was related to the minimal frequency at which it was recruited. MCoDs, which are active at the lowest frequencies of swimming[15] and inhibited at higher frequencies[16], occupy a ventral location in the spinal cord. CiD interneurons, active over a wide range of higher swimming speeds than MCoD interneurons, are more dorsal in the spinal cord, with the most ventral CiD interneurons active at lower frequencies than the most dorsal ones. Like motor neurons, there was a significant relationship between position and recruitment frequency within the CiD population in the electrophysiological data (Fig. 2g; $R = 0.56$, $P < 0.05$, $n = 16$). This relationship was not significant in the calcium imaging data (see Supplementary Table 1) in which the definition of the exact recruitment frequency is more difficult. However, when the electrophysiological or calcium imaging data for these two interneuronal classes (which together span the range of frequencies of swimming) were superimposed upon those for motor neurons, as in Fig. 2g, h, we found that they overlapped. The relationship between position and activation frequency is therefore similar for all of these rhythmically active excitatory cell types.

We then asked whether rhythmically active inhibitory interneurons, which are mostly located dorsal to the motor neurons and excitatory interneurons, follow the same pattern of recruitment. We recorded from two classes of inhibitory cells: circumferential ascending (CiA) interneurons and commissural bifurcating longitudinal (CoBL) interneurons, which have ipsilateral and contralateral axons respectively. To target these neurons, we used an engrailed-1 green fluorescent protein construct (*En-1:GFP*), which labels CiA interneurons[17], and also generated a stable line of transgenic zebrafish in which GFP is expressed under control of the promoter for the *glycine transporter-2* gene. While the location of inhibitory interneurons was also systematically related to their order of activation, the relationship was in the opposite direction of that for excitatory interneurons and motor neurons (Fig. 3a–d). More-dorsal inhibitory interneurons were active during slower swimming frequencies, with more-ventral interneurons activated as the speed of swimming increased ($R = -0.61$, $P < 0.001$, $n = 30$).

The maps of recruitment frequency onto dorso-ventral location might be a consequence of gradients in cell size, with larger cells located more dorsally among excitatory neurons and more ventrally among inhibitory ones. We evaluated this by plotting the cross-sectional area of the somata of excitatory and inhibitory neurons against their location. As shown in Fig. 3e, the more-dorsal motor neurons, which are more difficult to recruit, tended to be larger than ventral ones ($R = 0.70$, $P < 0.0001$, $n = 40$), in accordance with the size principle[18]. In contrast, there was no significant relationship between the soma size of excitatory interneurons and their dorso-ventral location (Fig. 3f). Ventral MCoD interneurons recruited at low frequencies were spread over the same range of sizes as the more

[1]Department of Neurobiology and Behavior, Cornell University, Ithaca, New York 14853, USA. [2]Department of Organismal Biology and Anatomy, University of Chicago, Chicago, Illinois 60637, USA. [3]National Institutes of Natural Sciences, Okazaki Institute for Integrative Bioscience and National Institute for Physiological Sciences, Myodaiji Okazaki, Aichi 444-8787, Japan.

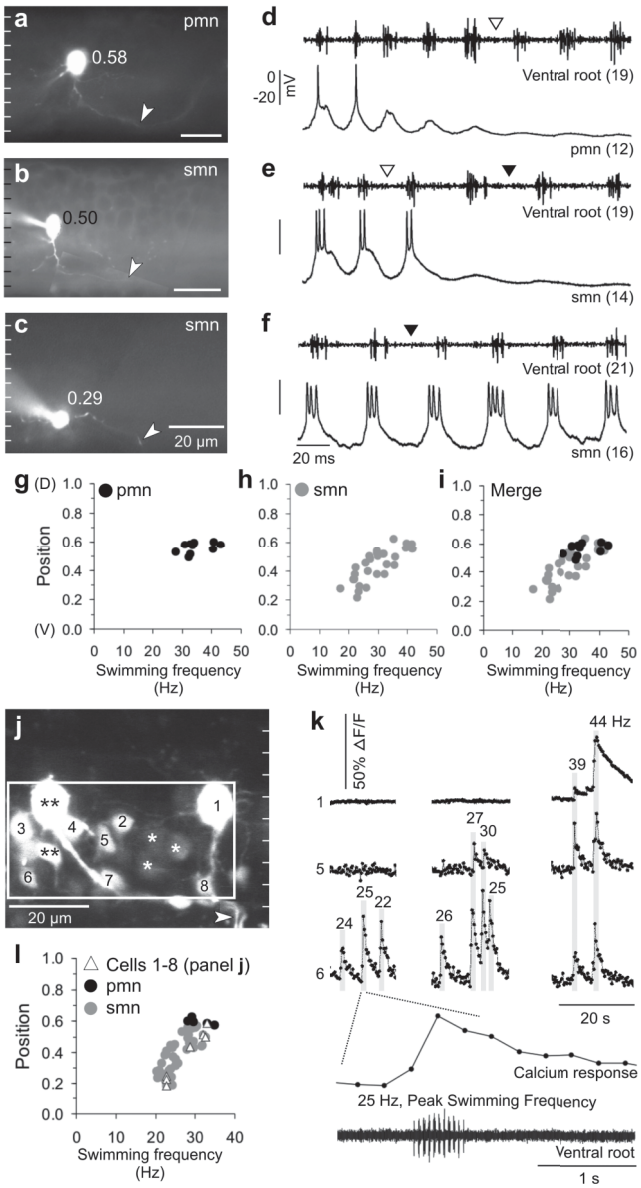

Figure 1 | Activation of motor neurons depends on their position in spinal cord. **a**–**c**, Fluorescent images of motor neurons whose respective activity is illustrated in **d**–**f**. Hash marks to the left indicate basis for numerical position measurements (labelled next to the somata). A white arrowhead indicates the axon. pmn, primary motor neuron; smn, secondary motor neuron. **d**–**f**, Activity patterns of the neurons illustrated in **a**–**c** along with ventral root recordings. Muscle segment locations are given in parentheses. Triangles mark comparable swimming frequencies (white, **d** and **e**; black, **e** and **f**). **g**–**i**, Plots of position versus minimum swimming frequency for ten primary motor neurons (black circles) and 30 secondary motor neurons (grey circles). Locations are normalized with respect to the dorsal (D; one) and ventral (V; zero) edges of spinal cord in all figures. **j**, Confocal image of eight motor neurons in one larva. A white arrowhead shows where the axons exit via the ventral root. A white box demarcates the imaging window. We could not detect fluorescence (F) changes in neurons that were either oversaturated (**) or too dimly labelled (*). **k**, Calcium responses ($\Delta F/F$) of three motor neurons numbered in **j**. The fastest swimming frequency (numbers given in Hz) within the episodes in which motor neurons showed a calcium response is indicated above the shaded grey bars. An expanded trace (bottom) illustrates a calcium response and the corresponding ventral root activity from which the peak frequency (here, 25 Hz) was derived. **l**, Plot of an average of the three lowest peak frequencies from the slowest swimming episodes in which a neuron responded with a 9% or greater increase in fluorescence intensity. The plot was compiled from 46 secondary motor neurons and six primary motor neurons from six larvae.

dorsally located CiD interneurons active at higher frequencies. Similarly, there was no significant relationship between soma size and position of inhibitory interneurons (Fig. 3g,h).

In contrast to soma size, the input resistance of the neurons declined from ventral to dorsal spinal cord for motor neurons (Fig. 3i; $R = -0.81$, $P < 0.0001$, $n = 40$) and for pooled excitatory interneuron classes (Fig. 3j; $R = -0.72$, $P < 0.0001$, $n = 38$), and did the opposite for pooled inhibitory interneurons (Fig. 3k, l; $R = 0.71$, $P < 0.0001$, $n = 32$). Neurons with higher input resistance will tend to depolarize more for a given excitatory synaptic input than those with lower resistance. These gradients might therefore contribute to a greater excitability of the most ventral excitatory neurons and the most dorsal inhibitory ones, consistent with their opposite recruitment patterns (Fig. 3m).

The correlations we observed and the direct connections of MCoD interneurons and CiD interneurons to motor neurons[16,19,20] strongly suggest that ventral excitatory cells play a part in driving motor output in slow movements, whereas dorsal ones drive fast movements. We predicted that removing ventral MCoD interneurons would impair slow movements, while removing dorsal CiD interneuron cells would not. This was tested by laser ablating bilateral groups of MCoD interneurons (Fig. 4a, b) or CiD interneurons in rostral spinal cord. The slowest swimming movements always involve alternating pectoral fin movements coordinated with slow axial bending movements[21]. During faster swimming, the fins are held against the body. Alternating fin movements without slow axial movements are

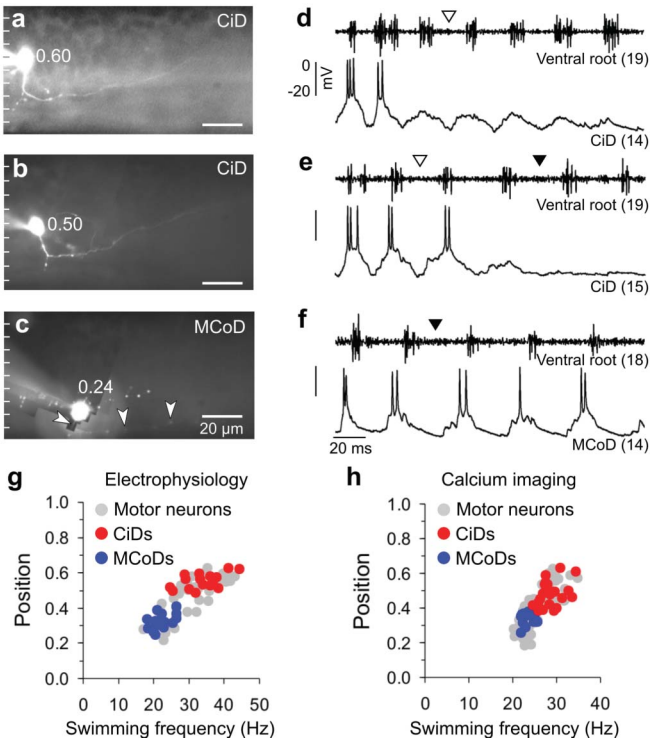

Figure 2 | Activity patterns of excitatory spinal interneurons are also correlated with position. **a**–**c**, Fluorescent images of CiD and MCoD interneurons, the activity of which is illustrated in **d**–**f**. Arrowheads mark the point at which the MCoD axon crosses the spinal cord and descends. The morphology of these interneurons is more evident in the Supplementary movies. **d**–**f**, Activity patterns of the neurons illustrated in **a**–**c**, with ventral root recordings. Triangles mark comparable swimming frequencies (white, **d** and **e**; black, **e** and **f**). **g**, Plot of position versus minimum swimming frequency of 40 motor neurons (grey circles), 16 CiD interneurons (red circles) and 14 MCoD interneurons (blue circles) recorded using patch electrophysiology from 70 larvae. **h**, Plot of position versus minimum swimming frequency of 52 motor neurons (grey circles), 22 CiD interneurons (red circles) and 14 MCoD interneurons (blue circles) recorded using calcium imaging from 14 larvae.

extremely rare in our experimental conditions (1 of 182 trials in 28 larvae). We therefore used the occurrence of alternating fin movements as an indication that the larva was attempting to engage in slow swimming movements.

Before the ablation of MCoD interneurons, only one out of 65 trials (1.5%) in six larvae showed alternating fin movements without axial movements (Fig. 4c). After MCoD ablations, however, 19 of 72 (26%) trials had fin movements occurring without accompanying axial movements (videos in Supplementary Information). In five out of the six larvae, the change was significant ($P < 0.05$). These ablations did not affect the ability of the larvae to produce fast swimming. In three larvae, a slightly greater number of dorsal CiD interneurons was ablated bilaterally. Prior to ablations, 34 out of 34 trials showed the typical pairing of fin movements and axial bending. All 32 trials after CiD interneuron ablations also showed paired fin and axial movements, with no evidence of isolated fin movements (Fig. 4d). These observations are consistent with a role for MCoD interneurons, but not CiD interneurons, in providing the excitatory drive necessary to produce the slowest swimming movements. Complementary experiments examining faster movements have revealed that the ablation of CiD interneurons, but not MCoD interneurons, leads to deficits in the kinematics of high-speed movements[22]. Together, these data argue that the topography we observe has behavioural consequences.

Although there has been much progress in identifying the regions and circuits responsible for rhythmic motor behaviours in vertebrate spinal cord[1–6], for many years it was unclear how these neurons and their functional identities emerged during development. Then developmental studies revealed a dorso-ventral transcriptional code that directs the differentiation of morphologically and functionally distinct cell types from different regions of spinal cord[23]. This transcriptional code does not, by itself, explain the pattern we observed, because the relationship we found is present both within classes derived from a single transcriptional domain (CiD interneurons from the V2 domain)[19] and across classes arising from different domains (CiD interneurons and motor neurons from the V2 and MN domains respectively)[17,19]. There may, however, still be direct links to development because the motor neurons and excitatory interneurons that develop earliest are located most dorsally in spinal cord[11,19]. The recruitment order for excitatory cells thus maps onto the time of neuronal differentiation, with younger ventral neurons active at low frequencies and older, dorsal ones at higher frequencies. We do not yet know whether an opposite age-related pattern exists among inhibitory neurons. Importantly, the gradients of recruitment and input resistance we found might also be associated with gradients of channel expression; these could be specified during development by molecular gradients, which are known to establish the dorso-ventral patterning of the transcription factor code[24].

Our findings reveal an unexpected pattern of organization in which the frequency of swimming at which a neuron is recruited varies in a continuous way with its position in the spinal cord. This topographic map of function underlies the ability of zebrafish to produce movements over a range of speeds. We do not yet know whether features of this pattern might be evident in the more complex spinal cords of reptiles, birds and mammals—creatures in which

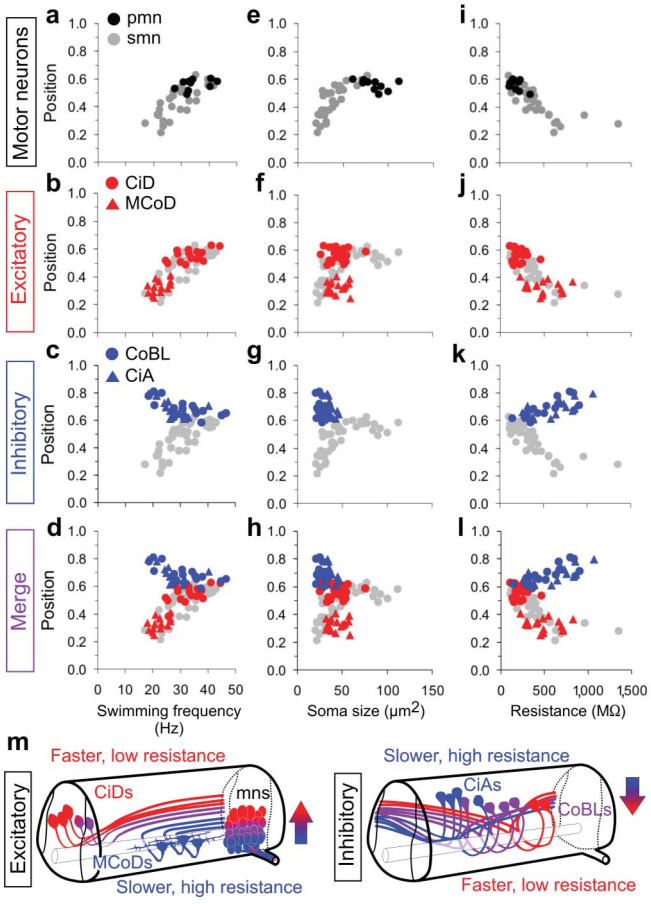

Figure 3 | Reverse gradients of recruitment for excitatory and inhibitory interneurons. a–d, Plots of position versus minimum swimming frequency for ten primary motor neurons (black circles), 30 secondary motor neurons (grey circles), 16 CiD interneurons (red circles), 14 MCoD interneurons (red triangles), 17 CoBL interneurons (blue circles) and 13 CiA interneurons (blue triangles) from 100 larvae. **e–h**, Plots of position versus maximum cross-sectional area of the somata for ten primary motor neurons, 30 secondary motor neurons, 21 CiD interneurons, 17 MCoD interneurons, 18 CoBL interneurons and 14 CiA interneurons from 110 larvae. **i–l**, Plots of position versus input resistance measurements for ten primary motor neurons, 30 secondary motor neurons, 21 CiD interneurons, 17 MCoD interneurons, 18 CoBL interneurons and 14 CiA interneurons from 110 larvae. All motor neurons are shown in light grey in **b–d**, **f–h**, **j–l** to provide a frame of reference. **m**, Summary diagram of recruitment pattern. Dorsal is up, rostral is to the left.

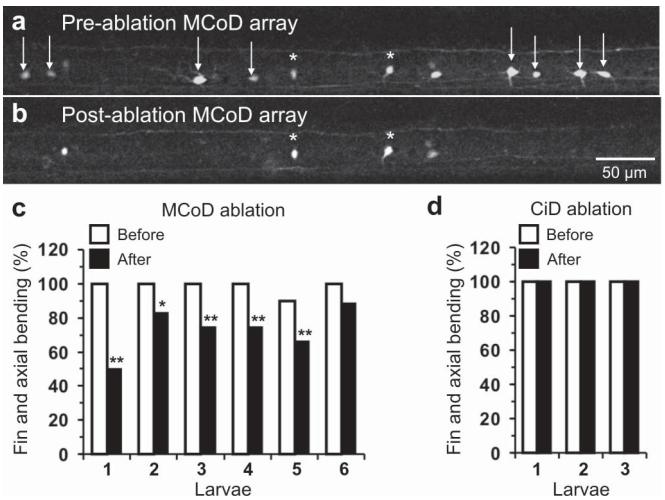

Figure 4 | Ablation of ventral excitatory interneurons perturbs slow swimming movements, while ablation of dorsal ones does not. a, Low-magnification confocal image of an array of back-filled interneurons. Arrows mark MCoD interneurons ablated in **b**, while asterisks mark examples of a different cell type not removed in **b**. **b**, The same region of cord illustrated in **a** after targeted laser ablation. **c**, A bar chart illustrating the percentage of trials in which axial movements occurred together with fin movements before and after MCoD interneuron ablations. **d**, A bar chart as in **c** before and after CiD interneuron ablations. The number of cells ablated on left and right sides in each case are as follows. For MCoD interneurons: larva 1, left/right = 9/6; larva 2, 7/7; larva 3, 10/5; larva 4, 6/6; larva 5, 8/6; larva 6, 7/7. For CiD interneurons: larva 1, left/right = 10/9; larva 2, 9/10; larva 3, 10/8. Significant changes are marked by asterisks: *$P < 0.05$, ** $P < 0.0001$.

motor neurons are clustered into discrete motor pools in a topographic arrangement that differs from those innervating axial muscles in fishes[25–27]. However, the conserved mechanisms of early spinal cord development among animals as divergent as fish, frogs, chicks and mice[17,19,23,28,29] suggest that a similar functional organization in other vertebrates might be most evident early in their development.

METHODS

Full details of methods are presented in the Supplementary Information. All procedures conform to the National Institutes of Health guidelines regarding animal experimentation and were approved by Cornell University's and the University of Chicago's Institutional Animal Care and Use committees.

Electrophysiology. Patch-clamp and ventral root recordings were performed as described previously[17,30]. Neurons were targeted between the 9th and 21st muscle segments. Motor neurons were targeted blindly. MCoD interneurons were targeted on the basis of their lateral location in the neuropil. CiD interneurons were targeted either blindly or by backfilling the previous day with fluorescein or calcium green dextran-conjugated dyes injected into the caudal spinal cord. CoBL interneurons were targeted either blindly or by using a stable transgenic line expressing green fluorescent protein driven by a *glycine transporter-2* promoter. CiA interneurons were targeted either blindly or by stochastic labelling using a bacterial artificial chromosome (BAC) in which GFP expression was driven by an *En-1* promoter[17]. After recordings, transmitted and fluorescent light images through the spinal cord were captured to confirm the morphology and location of the neurons.

Generation of the *glycine transporter-2* transgenic line. A BAC DNA construct in which GFP was placed under the control of the *glycine transporter-2 cis*-regulatory elements was made as previously described[17] and was used to generate stable transgenic lines. We obtained two lines, and electrophysiology was performed using compound homozygotes of the two.

***In vivo* calcium imaging.** Motor neurons and CiD and MCoD interneurons between the 9th and 21st segments were retrogradely filled three to four days post-fertilization with calcium green dextran by pressure injection into muscle or caudal spinal cord[15]. After 24 hours, larvae were anaesthetized, immobilized in α-bungarotoxin and pinned to a thin layer of Sylgard in a glass-bottomed Petri dish containing saline solution. The caudal tail skin was removed to provide access to the ventral roots. The preparation was imaged using an inverted Zeiss LSM confocal microscope set at low laser intensity, maximum pinhole diameter and high photomultiplier gain to avoid photodamage. Ventral root activity was recorded and time-locked to image collection. After recordings, higher-quality images of neurons were obtained to confirm their morphology and location in spinal cord.

Laser ablations and behaviour. MCoD or CiD interneurons in four-day-old larvae were backfilled with fluorescein dextran injected into spinal cord and screened with a dissecting microscope to identify larvae with an array of labelled interneurons. After backfilling, pre-ablation swimming bouts were recorded at 1,000 Hz with a high-speed camera. Neurons were then ablated bilaterally, one neuron at a time, by targeting the nucleus with a pulsed nitrogen laser. The behaviour of the larvae was assessed again by filming after ablations.

Data analysis. Neuron location was determined by averaging three measurements from the bottom of spinal cord to the middle of the cell body using either Image J or Zeiss software. This value was then normalized to an average of three measurements of the total dorso-ventral extent of spinal cord. Recruitment using patch physiology was assessed by averaging the three slowest instantaneous swimming frequencies from three to five swimming episodes. Instantaneous frequency was measured as the reciprocal of the interval between the first spikes in successive bursts of activity in motor neurons or interneurons. Spikes were simpler to threshold using our automated data analysis program and matched the frequency of the bursts recorded from ventral roots.

For calcium imaging, the temporal resolution of the imaging prohibited a similar approach. The slow calcium responses allowed us only to determine whether a neuron responded during a swimming episode, not exactly when it responded. We adopted a conservative approach to determining a neuron's minimal frequency of recruitment by using ventral root recordings to determine the fastest cycle within a swimming episode from the three to five slowest episodes during which a cell responded. We then plotted the mean of the three lowest of these against the position of the neuron. Location measurements were always performed first, so they would not be unduly influenced by frequency measurements, which were less subjective. To further rule out any observer bias, positions and frequencies were measured independently by two individuals, the one who collected the data and another who analysed blind a coded data set. Both observers arrived at the same conclusions.

Resistance measurements were calculated from an average of five hyperpolarizing square current pulses between 20–50 pA, in a linear current–voltage range for the neurons tested. Soma cross-sectional area was determined by averaging three measurements from DIC images. Electrophysiological analysis was performed using DataView (software by W. Heitler, University of St Andrews; http://www.st-andrews.ac.uk/~wjh/dataview/). Statistical significance was set at $P < 0.05$ and analysis was performed using Microsoft Excel and Statview 4.5. Changes in the frequency of the occurrence of axial and fin movements after ablations was assessed by a binomial analysis with a $P < 0.05$, as described in Supplementary Methods.

Received 16 November 2006; accepted 10 January 2007.

1. Grillner, S. The motor infrastructure: from ion channels to neuronal networks. *Nature Rev. Neurosci.* **4,** 573–586 (2003).
2. Jankowska, E. Spinal interneuronal systems: identification, multifunctional character and reconfigurations in mammals. *J. Physiol. (Lond.)* **533,** 31–40 (2001).
3. Kiehn, O. & Butt, S. J. Physiological, anatomical and genetic identification of CPG neurons in the developing mammalian spinal cord. *Prog. Neurobiol.* **70,** 347–361 (2003).
4. Roberts, A. How does a nervous system produce behaviour? A case study in neurobiology. *Sci. Prog.* **74,** 31–51 (1990).
5. Stein, P. S., McCullough, M. L. & Currie, S. N. Spinal motor patterns in the turtle. *Ann. NY Acad. Sci.* **860,** 142–154 (1998).
6. Combes, D., Merrywest, S. D., Simmers, J. & Sillar, K. T. Developmental segregation of spinal networks driving axial- and hindlimb-based locomotion in metamorphosing *Xenopus laevis*. *J. Physiol. (Lond.)* **559,** 17–24 (2004).
7. Fuiman, L. A. & Webb, P. W. Ontogeny of routine swimming activity and performance in *Zebra danios* (Teleostei, Cyprinidae). *Anim. Behav.* **36,** 250–261 (1988).
8. Budick, S. A. & O'Malley, D. M. Locomotor repertoire of the larval zebrafish: swimming, turning and prey capture. *J. Exp. Biol.* **203,** 2565–2579 (2000).
9. Muller, U. K. & van Leeuwen, J. L. Swimming of larval zebrafish: ontogeny of body waves and implications for locomotory development. *J. Exp. Biol.* **207,** 853–868 (2004).
10. Liu, D. W. & Westerfield, M. Function of identified motoneurones and co-ordination of primary and secondary motor systems during zebra fish swimming. *J. Physiol. (Lond.)* **403,** 73–89 (1988).
11. Myers, P. Z. Spinal motoneurons of the larval zebrafish. *J. Comp. Neurol.* **236,** 555–561 (1985).
12. Westerfield, M., McMurray, J. V. & Eisen, J. S. Identified motoneurons and their innervation of axial muscles in the zebrafish. *J. Neurosci.* **6,** 2267–2277 (1986).
13. Hale, M. E., Ritter, D. A. & Fetcho, J. R. A confocal study of spinal interneurons in living larval zebrafish. *J. Comp. Neurol.* **437,** 1–16 (2001).
14. Higashijima, S., Schaefer, M. & Fetcho, J. R. Neurotransmitter properties of spinal interneurons in embryonic and larval zebrafish. *J. Comp. Neurol.* **480,** 19–37 (2004).
15. Ritter, D. A., Bhatt, D. H. & Fetcho, J. R. *In vivo* imaging of zebrafish reveals differences in the spinal networks for escape and swimming movements. *J. Neurosci.* **21,** 8956–8965 (2001).
16. Masino, M. A., McLean, D. L. & Fetcho, J. R. Identification of an intersegmental interneuron that may drive slow swimming movements in larval zebrafish. *Soc. Neurosci. Abstr. Viewer/Itinerary Planner* Program 751.16, (Society for Neuroscience, Washington DC, 2005); ⟨http://sfn.scholarone.com/itin2005/⟩.
17. Higashijima, S., Masino, M. A., Mandel, G. & Fetcho, J. R. Engrailed-1 expression marks a primitive class of inhibitory spinal interneuron. *J. Neurosci.* **24,** 5827–5839 (2004).
18. Henneman, E., Somjen, G. & Carpenter, D. O. Functional significance of cell size in spinal motoneurons. *J. Neurophysiol.* **28,** 560–580 (1965).
19. Kimura, Y., Okamura, Y. & Higashijima, S. alx, a zebrafish homolog of Chx10, marks ipsilateral descending excitatory interneurons that participate in the regulation of spinal locomotor circuits. *J. Neurosci.* **26,** 5684–5697 (2006).
20. Bhatt, D. H., McLean, D. L., Hale, M. E. & Fetcho, J. R. Grading movement strength by changes in firing intensity versus recruitment of spinal interneurons. *Neuron* **53,** 91–102 (2007).
21. Thorsen, D. H., Cassidy, J. J. & Hale, M. E. Swimming of larval zebrafish: fin-axis coordination and implications for function and neural control. *J. Exp. Biol.* **207,** 4175–4183 (2004).
22. Fan, J. & Hale, M. E. Excitatory descending spinal interneurons influence the degree of axial bending during startles of larval zebrafish. *Soc. Neurosci. Abstr. Viewer/Itinerary Planner* Program 751.14, (Society for Neuroscience, Washington DC, 2005); ⟨http://sfn.scholarone.com/itin2005/⟩.
23. Briscoe, J., Pierani, A., Jessell, T. M. & Ericson, J. A homeodomain protein code specifies progenitor cell identity and neuronal fate in the ventral neural tube. *Cell* **101,** 435–445 (2000).
24. Briscoe, J. *et al.* Homeobox gene *Nkx2.2* and specification of neuronal identity by graded Sonic hedgehog signalling. *Nature* **398,** 622–627 (1999).
25. Fetcho, J. R. A review of the organization and evolution of motoneurons innervating the axial musculature of vertebrates. *Brain Res. Rev.* **434,** 243–280 (1987).

26. Landmesser, L. The distribution of motoneurones supplying chick hind limb muscles. *J. Physiol. (Lond.)* **284,** 371–389 (1978).
27. McHanwell, S. & Biscoe, T. J. The localization of motoneurons supplying the hindlimb muscles of the mouse. *Phil. Trans. R. Soc. Lond. B* **293,** 477–508 (1981).
28. Gosgnach, S. *et al.* V1 spinal neurons regulate the speed of vertebrate locomotor outputs. *Nature* **440,** 215–219 (2006).
29. Li, W. C., Higashijima, S., Parry, D. M., Roberts, A. & Soffe, S. R. Primitive roles for inhibitory interneurons in developing frog spinal cord. *J. Neurosci.* **24,** 5840–5848 (2004).
30. Drapeau, P., Ali, D. W., Buss, R. R. & Saint-Amant, L. *In vivo* recording from identifiable neurons of the locomotor network in the developing zebrafish. *J. Neurosci. Methods* **88,** 1–13 (1999).

Supplementary Information is linked to the online version of the paper at www.nature.com/nature.

Acknowledgements We are grateful to A. Hon and S. Kishore for performing *En-1:GFP* DNA injections and L. Heller for care and maintenance of the fish. We also thank A. Bass, D. Bhatt, P. Brehm, R. Harris-Warrick, A. Kinkhabwala, S. Kishore, M. Koyama, J. Liao and J. Olthoff for comments on the manuscript. This work was supported by grants from the National Institutes of Health and from the Ministry of Education, Science, Technology, Sports and Culture of Japan.

Author Information Reprints and permissions information is available at www.nature.com/reprints. The authors declare no competing financial interests. Correspondence and requests for materials should be addressed to J.R.F. (jrf49@cornell.edu).

LETTERS

Gating pore current in an inherited ion channelopathy

Stanislav Sokolov[1], Todd Scheuer[1] & William A. Catterall[1]

Ion channelopathies are inherited diseases in which alterations in control of ion conductance through the central pore of ion channels impair cell function, leading to periodic paralysis, cardiac arrhythmia, renal failure, epilepsy, migraine and ataxia[1]. Here we show that, in contrast with this well-established paradigm, three mutations in gating-charge-carrying arginine residues in an S4 segment that cause hypokalaemic periodic paralysis[2] induce a hyperpolarization-activated cationic leak through the voltage sensor of the skeletal muscle $Na_V1.4$ channel. This 'gating pore current' is active at the resting membrane potential and closed by depolarizations that activate the voltage sensor. It has similar permeability to Na^+, K^+ and Cs^+, but the organic monovalent cations tetraethylammonium and *N*-methyl-D-glucamine are much less permeant. The inorganic divalent cations Ba^{2+}, Ca^{2+} and Zn^{2+} are not detectably permeant and block the gating pore at millimolar concentrations. Our results reveal gating pore current in naturally occurring disease mutations of an ion channel and show a clear correlation between mutations that cause gating pore current and hypokalaemic periodic paralysis. This gain-of-function gating pore current would contribute in an important way to the dominantly inherited membrane depolarization, action potential failure, flaccid paralysis and cytopathology that are characteristic of hypokalaemic periodic paralysis. A survey of other ion channelopathies reveals numerous examples of mutations that would be expected to cause gating pore current, raising the possibility of a broader impact of gating pore current in ion channelopathies.

Skeletal muscle Na^+ channels generate action potentials in response to nerve stimulation and thereby initiate muscle contraction. They are complexes of pore-forming α and auxiliary β_1 subunits[3–6]. The periodic paralyses are dominantly inherited syndromes that cause episodic failure of skeletal muscle contraction[2]. Hyperkalaemic periodic paralysis and paramyotonia congenita are caused by mutations in the α subunit of skeletal muscle $Na_V1.4$ channels that are widely spread throughout the protein and usually cause a gain of function by impairing fast and/or slow inactivation[7]. Increased Na^+ channel activity leads to depolarization, hyperexcitability, and either repetitive firing or depolarization block. In contrast, hypokalaemic periodic paralysis (HypoPP) is caused by mutations in both the α subunit of the skeletal muscle $Na_V1.4$ channel and the homologous α_1 subunit of the skeletal muscle $Ca_V1.1$ channel, which initiates excitation–contraction coupling[7]. The mutations in both of these large channel proteins target only the outermost two gating-charge-carrying arginine residues in their S4 voltage sensors in domains II and/or IV. The convergence of these mutations on the outermost two gating charges of voltage sensors in two different proteins strongly implicates altered voltage sensor function in this disease. Studies of these mutant Na^+ channels expressed in heterologous cells revealed enhanced fast and/or slow inactivation as the primary common effect[8–11], but it is uncertain how this inhibitory effect causes the dominant inheritance of this disease or its apparent requirement for mutation of gating charges. We therefore explored the hypothesis that unrecognized gain-of-function changes that are unique to the voltage sensor might be caused by these mutations and might contribute to their dominant inheritance.

The voltage sensors of ion channels transduce changes in membrane potential into a conformational change that opens the pore. Gating charges in their S4 transmembrane segments move across the membrane under the influence of the electric field[12,13]. In one mechanistic model, the S4 segments are thought to move outwards through the voltage sensor module by means of a specialized gating pore formed by the segments S1 to S3 (refs 6, 13–18), as presented in detail in a recent high-resolution structural model of the gating process[19]. Consistent with this mechanism is our observation that mutations of the arginine gating charges to smaller, uncharged residues generates gating pore currents resulting from movement of protons and cations through the modified gating pore[20–22]. Mutations of outer gating charges cause gating pore current in the resting state[21,22], whereas mutations of more inward gating charges cause gating pore current in the activated state[22]. Because gating pore current is unique to voltage sensors and is a gain-of-function effect, we tested the HypoPP mutant $Na_V1.4$/R666G for gating pore current.

Wild-type $Na_v1.4$ and R666G channels were transiently expressed in *Xenopus* oocytes together with the Na^+ channel β_1 subunit, and their electrophysiological properties were examined with the cut-open oocyte voltage-clamp technique[23] (Fig. 1). Na^+ currents recorded during depolarizing voltage-clamp steps were generally similar in kinetics and voltage dependence for the wild-type and R666G channels

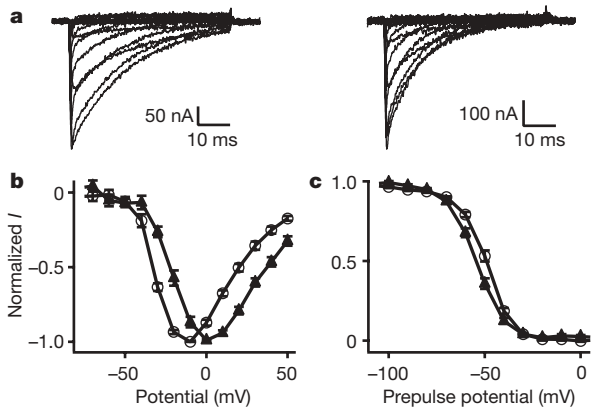

Figure 1 | Central pore Na^+ currents for wild-type $Na_v1.4$ and HypoPP mutant R666G channels. a, Representative Na^+ currents through the central pore of wild type $Na_v1.4$ (left) and R666G (right) channels. **b**, Current–voltage relationships. Mean normalized peak Na^+ current is plotted against test potential for $Na_v1.4$ channels (circles) and R666G (triangles). Voltages for half-maximal activation (V_a) were calculated from conductance-voltage relationships (Supplementary Methods): wild-type $Na_v1.4$, $V_a = -28 \pm 1$ mV, $n = 6$; R666G, $V_a = -15 \pm 3$ mV, $n = 8$. **c**, Voltage dependence of inactivation. The graph shows mean normalized peak Na^+ current during test pulses after 100-ms prepulses to the indicated membrane potentials. Half-inactivation values (V_h) were: wild-type $Na_v1.4$ (circles), $V_h = -49 \pm 1$ mV, $n = 6$; R666G (triangles), $V_h = -55 \pm 1$ mV, $n = 8$ ($P < 0.05$). Error bars denote s.e.m.

[1]Department of Pharmacology, University of Washington, Seattle, Washington 98195-7280, USA.

(Fig. 1a). However, as reported previously[11], there was a trend towards faster inactivation for R666G (Fig. 1a), current–voltage relationships revealed a positive shift in the voltage dependence of activation (Fig. 1b), and the voltage dependence of fast inactivation was shifted to more negative membrane potentials by 6 mV (Fig. 1c).

To detect gating pore currents, we blocked the central pore with 1 μM tetrodotoxin (TTX) and measured leak currents with the normal leak-subtraction protocol turned off. Ionic currents in response to 500-ms voltage steps from a holding potential of −100 mV to test potentials from −140 mV to +50 mV were substantially larger for R666G than for the wild-type channel (Fig. 2a, b). For the wild type, these leak currents were linear (Fig. 2c). In contrast, for R666G a nonlinear component of leak current was observed in the range −50 mV to −140 mV (Fig. 2d). Plotting the mean nonlinear component of ionic current for R666G and the wild type against voltage reveals a highly significant nonlinear inward current in the mutant and none in the wild type (Fig. 2e), similar to gating pore currents (I_{gp}) observed previously for mutations of the outermost gating charges of the $Na_V1.2$ channel IIS4 voltage sensor[22].

The gating pore currents conducted by R666G were much smaller than the central pore Na^+ current. Overexpression of $Na_V1.4$ channels to allow accurate recording of gating pore current usually results in central pore currents that are too large for accurate voltage clamp control in the absence of TTX. However, in favourable cases, we were able to accurately record both gating pore current and central pore current in the same oocyte. A typical example (Fig. 2f) shows that 8 μA of central pore current at −10 mV corresponds to about 80 nA of I_{gp} at −140 mV. As a more physiological comparison, the central pore current at the peak of the action potential (4 μA at +30 mV) is 80-fold greater than the gating pore current at the resting membrane potential (50 nA at −90 mV; Fig. 2f). Although the gating pore current is only about 1.25% of the central pore current, it would be open constantly at the resting membrane potential, whereas the central pore would open for only 1–2 ms during action potentials.

We determined the ion selectivity of the R666G gating pore current for monovalent cations by substituting selected cations for Na^+ in the extracellular solution and measuring the nonlinear component of leak current in the presence of 1 μM TTX to block the central pore (Fig. 3). Surprisingly, even the large organic cation *N*-methyl-D-glucamine ($NMDG^+$) was detectably permeable through this gating pore, as revealed by the nonlinear current increasing towards more negative membrane potentials (Fig. 3a, open squares). For a quantitative comparison of permeability for different monovalent cations, I_{gp} was first measured with 120 mM $NMDG^+$ as the only permeant extracellular monovalent cation. Subsequently, an equal concentration of Na^+, K^+, Cs^+, Li^+ or tetraethylammonium (TEA^+) was added to the recording chamber, and gating pore currents were measured again (Fig. 3a–c). The rank order for the ion selectivity of the gating pore was $Cs^+ \approx K^+ > Na^+ \approx Li^+ \gg TEA^+ \approx NMDG^+$, after correction for the reduced driving force for K^+ resulting from its high internal concentration (Fig. 3c). The R666G gating pore discriminates approximately twofold between Na^+ and K^+ (Fig. 3c), but at the resting membrane potential of a skeletal muscle cell, near the equilibrium potential for K^+ conductance, essentially all gating pore current would be inward movement of Na^+.

Divalent cations block the gating pore (Fig. 3d). Ba^{2+} (6 mM) decreased I_{gp} conducted by Na^+ by 55 ± 9% at −140 mV, which is consistent with a K_d of 4.9 mM, whereas Zn^{2+} (6 mM) completely inhibited gating pore current, indicating a much higher affinity. Complete block by Zn^{2+} strengthens the identification of I_{gp} as a distinct hyperpolarization-activated component of leak current caused by the R666G mutation. Increasing Ca^{2+} concentration from 1.8 mM to 5.9 mM caused a small but significant (27 ± 7%) decrease in I_{gp}, indicating that Ca^{2+} is a weak blocker of I_{gp} (Fig. 3d). Halving the extracellular concentration of Ca^{2+} had no effect on I_{gp}, indicating that Ca^{2+} is not measurably permeant (Fig. 3d). These results suggest that Ca^{2+} leakage through the R666G gating pore is unlikely to contribute to the physiological effects of this mutation.

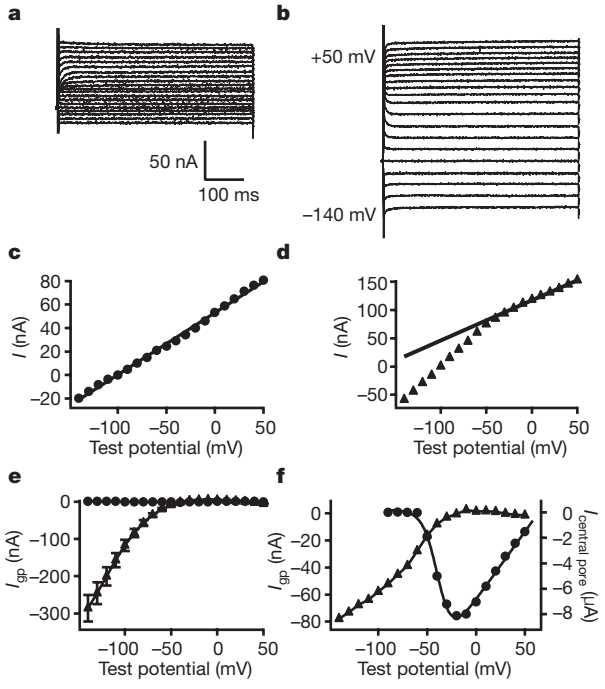

Figure 2 | Gating pore Na^+ currents for HypoPP mutant R666G channels. **a**, **b**, Representative gating pore Na^+ currents in oocytes expressing $Na_v1.4$ (**a**) and R666G (**b**) channels in response to voltage steps ranging from −140 mV to +50 mV without leak subtraction after the blocking of the central pore with 1 μM TTX. **c**, **d**, Relationship of leak current to voltage for $Na_v1.4$ (**c**) or R666G (**d**) channels. **e**, Mean nonlinear component of ionic current for R666G (triangles, $n = 37$) and wild-type (circles, $n = 10$; error bars smaller than symbols) channels. **f**, Comparison of central pore (circles, right axis) and gating pore (triangles, left axis) Na^+ currents in a representative oocyte before and after the addition of 1 μM TTX. Error bars denote s.e.m.

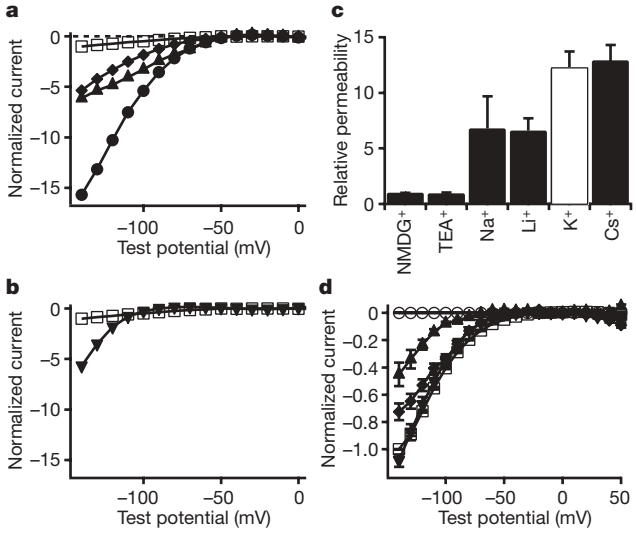

Figure 3 | Ion selectivity of R666G gating pore currents. **a**, **b**, Gating pore currents in representative oocytes were first measured in 120 mM $NMDG^+$ (open squares) and after the addition of Na^+ (triangles), Li^+ (diamonds), or Cs^+ (circles, **a**) or K^+ (inverted triangles, **b**) to the external solution to give a final concentration of 48 mM. Currents are normalized relative to the $NMDG^+$ current at −140 mV in a given oocyte. **c**, Cation selectivity of the gating pore in R666G relative to $NMDG^+$. Data are corrected for ion concentration; those for K^+ (white bar) are corrected for the reduced driving force due to elevated cytosolic K^+ concentration. **d**, Effects of divalent cations on I_{gp}. I_{gp} was recorded with 120 mM Na^+ and 1.8 mM Ca^{2+} in the external solution (squares, $n = 9$) and after the addition of 4.8 mM Ca^{2+} (diamonds, $n = 5$), 6 mM Ba^{2+} (upright triangles, $n = 5$) or 6 mM Zn^{2+} (circles, $n = 4$), or diluting the Ca^{2+} concentration to 0.9 mM (inverted triangles, $n = 4$). Error bars denote s.e.m.

A total of four mutations at only two positions in $Na_V1.4$ channels have been shown to cause HypoPP with complete penetrance: R663H, R666G, R666H and R666S (refs 9, 10, 24). To determine whether gating pore current is a general feature of HypoPP mutations, we tested $Na_V1.4$ channels with the HypoPP mutations R666H and R663H. Both of these mutations conducted a substantial hyperpolarization-activated gating pore current, similar to R666G (Fig. 4). The presence of gating pore current for all three of the HypoPP mutants studied here, including mutations at both relevant positions in the amino acid sequence of $Na_V1.4$ channels, provides strong evidence for an essential role of gating pore current in HypoPP.

Our results show that removal of the positively charged side chain of a gating-charge-carrying arginine residue by the R663H, R666G and R666H mutations creates a gating pore that is measurably permeant to large cations such as $NMDG^+$ and substantially more permeant to the physiological cations Na^+ and K^+. The ion conductance of these gating pores is activated at negative membrane potentials, at which the S4 voltage sensor would be in its most inward position. The effect of these three naturally occurring mutations in $Na_V1.4$ channels therefore resembles those of previous site-directed mutations of the outermost gating charge in $Na_V1.2$ and Shaker K^+ channels[21,22]. Depolarization is likely to move these outermost gating charges towards the extracellular surface of the membrane, out of the narrow point in the gating pore, as a consequence of the conformational change that initiates the activation of these channels[19]. The mutant gating pore would therefore act as a hyperpolarization-activated cation leak in HypoPP skeletal muscle cells. This cation leak would substantially increase resting membrane conductance and Na^+ influx into HypoPP skeletal muscle fibres. These gain-of-function effects would contribute substantially to the dominant inheritance, depolarization, reduced rate of rise and amplitude of the action potential, cytopathology and episodic paralysis correlated with decreased serum K^+ that are the hallmarks of HypoPP[9]. Moreover, a scan of known mutations in other ion channelopathies reveals numerous examples that would be predicted to cause gating pore current (Supplementary Table 1), indicating that gating pore current might contribute significantly to many ion channelopathies. The effects of gating pore current on the pathophysiology of HypoPP and its potential role in other ion channelopathies are considered in more detail in the Supplementary Material.

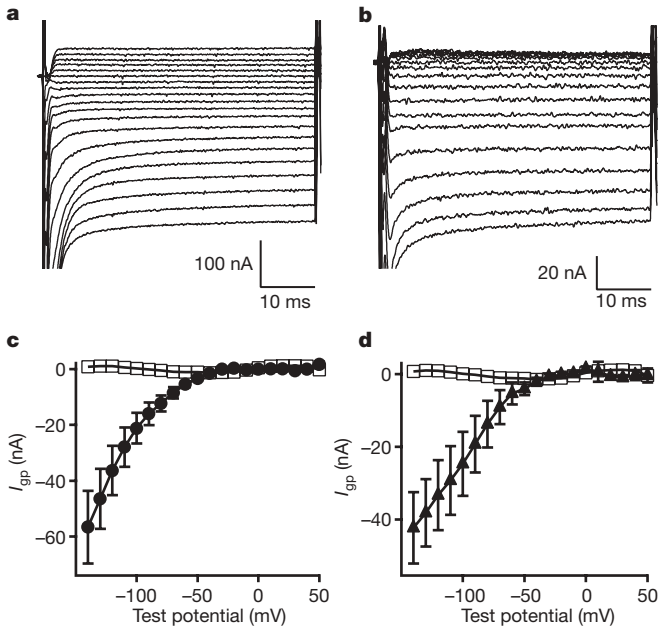

Figure 4 | Gating pore Na^+ current in R663H and R666H HypoPP mutants. **a**, **b**, Representative gating pore Na^+ currents in oocytes expressing R663H (**a**) and R666H (**b**) channels. **c**, **d**, Averaged gating pore currents after linear leak subtraction for R663H (**c**; circles, $n = 8$) and R666H (**d**; triangles, $n = 8$). Results for wild-type $Na_v1.4$ (**c**, **d**; squares, $n = 10$) are reproduced from Fig. 2e. Error bars denote s.e.m.

METHODS

Site-directed mutants in $Na_V1.4$ channels were constructed by polymerase-chain-reaction mutagenesis of a subclone encoding the IIS4 segment and surrounding region of the channel and insertion of the mutant segment into the full-length complementary DNA encoding $Na_V1.4$ as described in Supplementary Methods. RNA encoding wild-type or mutant $Na_V1.4$ plus wild-type β_1 subunits was transcribed *in vitro* and expressed in *Xenopus* oocytes as described in Supplementary Methods. The $Na_V1.4$ channels expressed were analysed with the cut-open oocyte voltage clamp as described[23] (see Supplementary Methods). Gating pore currents were measured in the presence of 1 μM TTX to block the central pore current.

Received 30 November 2006; accepted 15 January 2007.

1. Ashcroft, F. M. From molecule to malady. *Nature* **440,** 440–447 (2006).
2. Venance, S. L. *et al.* The primary periodic paralyses: diagnosis, pathogenesis and treatment. *Brain* **129,** 8–17 (2006).
3. Barchi, R. L. Protein components of the purified sodium channel from rat skeletal sarcolemma. *J. Neurochem.* **36,** 1377–1385 (1983).
4. Trimmer, J. S. *et al.* Primary structure and functional expression of a mammalian skeletal muscle sodium channel. *Neuron* **3,** 33–49 (1989).
5. Isom, L. L. *et al.* Primary structure and functional expression of the beta 1 subunit of the rat brain sodium channel. *Science* **256,** 839–842 (1992).
6. Catterall, W. A. From ionic currents to molecular mechanisms: The structure and function of voltage-gated sodium channels. *Neuron* **26,** 13–25 (2000).
7. Cannon, S. C. Pathomechanisms in channelopathies of skeletal muscle and brain. *Annu. Rev. Neurosci.* **29,** 387–415 (2006).
8. Struyk, A. F., Scoggan, K. A., Bulman, D. E. & Cannon, S. C. The human skeletal muscle Na channel mutation R669H associated with hypokalemic periodic paralysis enhances slow inactivation. *J. Neurosci.* **20,** 8610–8617 (2000).
9. Jurkat-Rott, K. *et al.* Voltage-sensor sodium channel mutations cause hypokalemic periodic paralysis type 2 by enhanced inactivation and reduced current. *Proc. Natl Acad. Sci. USA* **97,** 9549–9554 (2000).
10. Bendahhou, S., Cummins, T. R., Griggs, R. C., Fu, Y. H. & Ptacek, L. J. Sodium channel inactivation defects are associated with acetazolamide-exacerbated hypokalemic periodic paralysis. *Ann. Neurol.* **50,** 417–420 (2001).
11. Kuzmenkin, A. *et al.* Enhanced inactivation and pH sensitivity of sodium channel mutations causing hypokalaemic periodic paralysis type II. *Brain* **125,** 835–843 (2002).
12. Armstrong, C. M. Sodium channels and gating currents. *Physiol. Rev.* **61,** 644–682 (1981).
13. Bezanilla, F. The voltage sensor in voltage-dependent ion channels. *Physiol. Rev.* **80,** 555–592 (2000).
14. Catterall, W. A. Voltage-dependent gating of sodium channels: correlating structure and function. *Trends Neurosci.* **9,** 7–10 (1986).
15. Catterall, W. A. Molecular properties of voltage-sensitive sodium channels. *Annu. Rev. Biochem.* **55,** 953–985 (1986).
16. Guy, H. R. & Seetharamulu, P. Molecular model of the action potential sodium channel. *Proc. Natl Acad. Sci. USA* **508,** 508–512 (1986).
17. Horn, R. Coupled movements in voltage-gated ion channels. *J. Gen. Physiol.* **120,** 449–453 (2002).
18. Gandhi, C. S. & Isacoff, E. Y. Molecular models of voltage sensing. *J. Gen. Physiol.* **120,** 455–463 (2002).
19. Yarov-Yarovoy, V., Baker, D. & Catterall, W. A. Voltage sensor conformations in the open and closed states in ROSETTA structural models of K^+ channels. *Proc. Natl Acad. Sci. USA* **103,** 7292–7297 (2006).
20. Starace, D. M. & Bezanilla, F. A proton pore in a potassium channel voltage sensor reveals a focused electric field. *Nature* **427,** 548–553 (2004).
21. Tombola, F., Pathak, M. M. & Isacoff, E. Y. Voltage-sensing arginines in a potassium channel permeate and occlude cation-selective pores. *Neuron* **45,** 379–388 (2005).
22. Sokolov, S., Scheuer, T. & Catterall, W. A. Ion permeation through a voltage-sensitive gating pore in brain sodium channels having voltage sensor mutations. *Neuron* **47,** 183–189 (2005).
23. Stefani, E. & Bezanilla, F. Cut-open oocyte voltage-clamp technique. *Methods Enzymol.* **293,** 300–318 (1998).
24. Bulman, D. E. *et al.* A novel sodium channel mutation in a family with hypokalemic periodic paralysis. *Neurology* **53,** 1932–1936 (1999).

Supplementary Information is linked to the online version of the paper at www.nature.com/nature.

Acknowledgements We thank E. M. Sharp for technical assistance in molecular biology. This work was funded by research grants from the National Institutes of Health and the Muscular Dystrophy Association to W.A.C.

Author Information Reprints and permissions information is available at www.nature.com/reprints. The authors declare no competing financial interests. Correspondence and requests for materials should be addressed to W.A.C. (wcatt@u.washington.edu).

LETTERS

Chemical rescue of cleft palate and midline defects in conditional GSK-3β mice

Karen J. Liu[1,2*†], Joseph R. Arron[1*†], Kryn Stankunas[3], Gerald R. Crabtree[1,3,4] & Michael T. Longaker[2,5]

Glycogen synthase kinase-3β (GSK-3β) has integral roles in a variety of biological processes, including development, diabetes, and the progression of Alzheimer's disease[1–4]. As such, a thorough understanding of GSK-3β function will have a broad impact on human biology and therapeutics. Because GSK-3β interacts with many different pathways, its specific developmental roles remain unclear[5]. We have discovered a genetic requirement for *GSK-3β* in midline development. Homozygous null mice display cleft palate, incomplete fusion of the ribs at the midline and bifid sternum as well as delayed sternal ossification. Using a chemically regulated allele of *GSK-3β* (ref. 6), we have defined requirements for GSK-3β activity during discrete temporal windows in palatogenesis and skeletogenesis. The rapamycin-dependent allele of *GSK-3β* produces GSK-3β fused to a tag, FRB* (FKBP/rapamycin binding), resulting in a rapidly destabilized chimaeric protein. In the absence of drug, *GSK-3β*$^{FRB*/FRB*}$ mutants appear phenotypically identical to *GSK-3β*$^{-/-}$ mutants. In the presence of drug, GSK-3βFRB* is rapidly stabilized, restoring protein levels and activity[6]. Using this system, mutant phenotypes were rescued by restoring endogenous GSK-3β activity during two distinct periods in gestation. This technology provides a powerful tool for defining windows of protein function during development.

Common congenital birth defects such as cleft palate, which affects roughly one in 2,000 births and is associated with approximately 400 known human syndromes, have multifactorial genetic and environmental causes[7]. Mouse genetic models provide insight into the complex biological interactions that go awry during development to produce human disease. However, existing genetic methods, which depend primarily on deletion of target genes, provide limited temporal resolution. To improve studies of embryonic development, we have devised a strategy combining pharmacologic and genetic manipulation of developmentally relevant genes. The advantage of pharmacologic intervention is that, by targeting at the protein level, gene function can be rapidly and reversibly controlled. Recent applications of small molecules to developmental studies include the use of cyclopamine to define the roles of Hedgehog signalling[8] in development and cancer, and cyclosporine to characterize calcineurin function during angiogenesis and neurogenesis[9,10]. Chemical genetic approaches have also identified new biologically active small molecules[11–13]. However, isolating a specific inhibitor of a target of choice can be prohibitively laborious and expensive. To circumvent this difficulty, we have developed a generalized technology for making highly specific drug-dependent alleles using a destabilizing tag (FRB*) and we have applied it to *GSK-3β* (ref. 6). The 89 amino acid FRB* domain is thermally unstable. Fusion to FRB* transfers this instability and reduces the melting temperature of the target protein. Thus, FRB*-tagged proteins are also unstable and rapidly degraded. Instability of the chimaeric protein is reversed by rapamycin binding to the FRB* domain[6] (Supplementary Fig. 1a–c).

GSK-3β has regulatory roles in many developmentally important molecular pathways, including Wnt, NFAT, Hedgehog and insulin signalling[2]. *GSK-3β* homozygous null mice had previously been reported to die during mid-gestation owing to liver degeneration[5]. We found, to our surprise, that *GSK-3β*$^{-/-}$ mice survived gestation and died perinatally. All of these mice had a complete cleft of the secondary palate (Fig. 1c); the observed phenotypic range is shown ($n = 17$, Fig. 1e). In mice, palatal development occurs between stages e12.5–e15 and is a process in which the bilateral maxillary processes descend vertically from the maxilla. Subsequently, the palatal shelves rotate horizontally, meet at the midline, and fuse by the time of e15 (schematized in coronal cross-sections in Fig. 1a). Clefts of the secondary palate result from an inability of the palatal shelves to differentiate, grow, rotate or fuse[14]. Mice homozygous for the FRB*-tagged

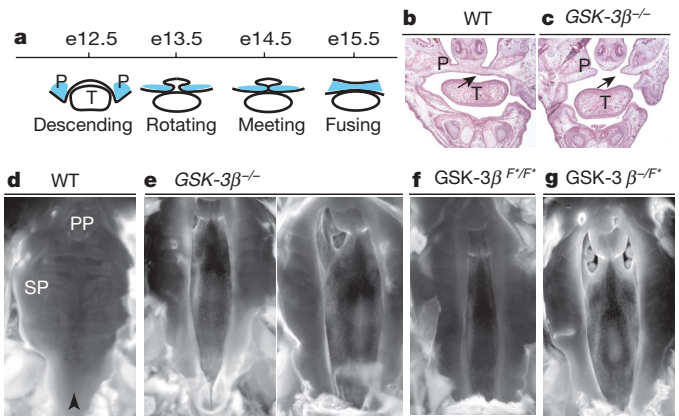

Figure 1 | *GSK-3β* mutants have cleft palates. **a**, Schematic of palate fusion in coronal cross-section; palate closure occurs between e12.5 and e15.5. At e12.5, palatal shelves (P, blue) grow downward from the maxillary processes, lateral to the tongue (T). Palatal shelves have rotated and elevated above the tongue by stage e13.5, extended towards the midline at e14.5, and fused by e15.5. **b–e**, Palate closure. **b**, Palatal shelves (black arrow) are fully fused in e16.5 wild-type (WT) mice (coronal cross-sections, stained with haematoxylin and eosin). **c**, In *GSK-3β*$^{-/-}$ mice, palatal shelves (black arrow) have rotated but do not meet at the midline. **d**, Palates are fully fused in e18.5 wild-type mice. The roof of the mouth is pictured (anterior at top of image). PP, primary palate; SP, secondary palate; midline marked with black arrowhead. **e–g**, *GSK-3β*$^{-/-}$ (**e**), *GSK-3β*$^{FRB*/FRB*}$ (**f**) and *GSK-3β*$^{-/FRB*}$ (**g**) mice have cleft palates; **e** shows representatives of the range of clefts observed. (F* is FRB*.)

[1]The Department of Pathology, [2]The Stanford Institute for Stem Cell Biology and Regenerative Medicine, [3]Department of Developmental Biology, [4]Howard Hughes Medical Institute, and the [5]Division of Plastic and Reconstructive Surgery, Department of Surgery, Stanford University School of Medicine, Palo Alto, California 94305, USA. †Present addresses: Department of Craniofacial Development, King's College London, London SE1 9RT, UK (K.J.L.); Department of Immunology Diagnostics, Genentech, 1 DNA Way, South San Francisco, California 94080, USA (J.R.A.).
*These authors contributed equally to this work.

allele, *GSK-3β*$^{FRB^*/FRB^*}$ ($n = 58$), all had identical palate defects to null mice (Fig. 1f), as did 22 out of 23 *trans*-heterozygotes (*GSK-3β*$^{-/FRB^*}$, $n = 23$, Fig. 1g). At birth, all mutants were present at roughly mendelian ratios (*GSK-3β*$^{-/-}$, 22% or 45/203; *GSK-3β*$^{FRB^*/FRB^*}$, 28% or 82/288; *GSK-3β*$^{-/FRB^*}$, 26% or 23/90). We did not observe any cleft palates in wild type or heterozygous littermates (*GSK-3β*$^{+/+}$, $n = 167$; *GSK-3β*$^{+/FRB^*}$, $n = 149$; *GSK-3β*$^{+/-}$, $n = 115$).

Because many signalling pathways regulated by GSK-3 affect osteogenesis[15,16], we stained cartilage with alcian blue and ossified bone with alizarin red. The three classes of mutants (*GSK-3β*$^{-/-}$, *GSK-3β*$^{FRB^*/FRB^*}$ and *GSK-3β*$^{-/FRB^*}$) displayed comparable arrays of defects in skeletal development and ossification. We observed a number of anomalies including delayed ossification of the skull, ear bones and cranial base (K.J.L. and M.T.L., unpublished observations). In the present study, we focus on sternal fusion and ossification. Sternal development occurs later in gestation than palate fusion. The sternal body develops from two mesenchymal bars that migrate ventrally during development, meet and fuse at the midline (e13.5 to e16.5). Subsequently, ossification centres (marked in red to mimic alizarin red staining of bone) arise at the points of contact between the ribs and the sternum[17] (schematic in Fig. 2a; developmental progression of ossification shown in wild-type animals in Fig. 2b). In contrast to wild-type animals (Fig. 2b), in *GSK-3β*$^{-/-}$ mice, the sternal bars were frequently bifurcated and the appearance of ossification centres was markedly delayed (Fig. 2d). Often there were holes in the xiphoid cartilage (asterisk, Fig. 2d). *GSK-3β*$^{FRB^*/FRB^*}$ and *GSK-3β*$^{-/FRB^*}$ were identical to *GSK-3β*$^{-/-}$ with regard to the sternal phenotype (Fig. 2d, e and data not shown). The delay in ossification was most obvious at early stages; by e18.5, mutants sometimes showed levels of ossification comparable to wild-type, although often in aberrant locations (compare Fig. 2d, e to Fig. 2b, c). We examined cell proliferation and death, which are known to be important in palatal fusion[18]. There was a mild but statistically insignificant increase in cell proliferation in mutant animals (Supplementary Fig. 2a). Neither the palatal nor sternal defects seemed to result from aberrant cell death: both wild-type and mutant animals showed minimal cell death (Supplementary Fig. 2f, g and data not shown).

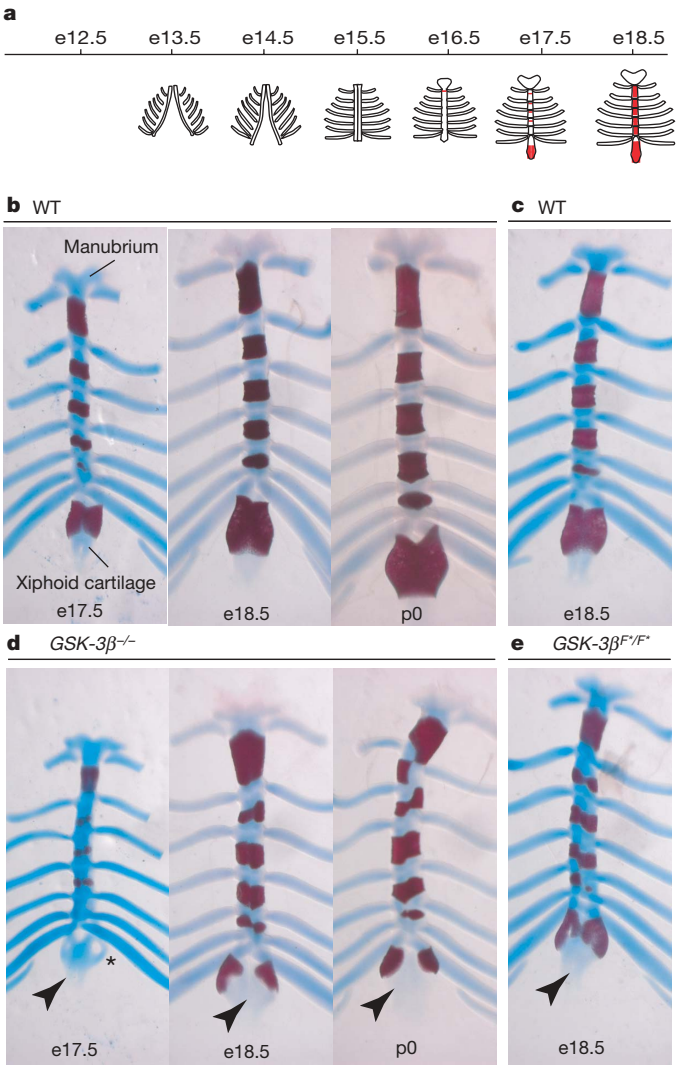

Figure 2 | *GSK-3β* mutants show bifid sternum and delayed sternal ossification. **a**, Schematic of sternal fusion: sternal bars form as two cartilaginous processes medial to the ribs. Sternal bars migrate towards the midline (from e13.5 on), and meet and fuse to form the sternum (by e16.5). Ossification (marked in red to depict alizarin red staining) occurs craniocaudally and continues after birth. **b**, In wild-type animals the sternum is fused by e17.5; ossification centres appear in a stereotypical fashion and progress after birth. Representative animals are shown from e17.5 through birth. Animals in **b** are littermates of those shown in corresponding columns in **d**. Alizarin red stains ossified bone; alcian blue stains cartilage. **c**, Wild-type (e18.5); littermate control for **e**. **d**, *GSK-3β*$^{-/-}$ mutants display aberrant fusion of the sternebrae resulting in nearly completely bifid sterna. Xiphoid cartilage (black arrowheads) often has holes (asterisk). **e**, *GSK-3β*$^{FRB^*/FRB^*}$ mutants phenocopy *GSK-3β*$^{-/-}$ mutants.

Having confirmed that in the absence of drug treatment the FRB*-tagged allele of *GSK-3β* mimics the phenotypes of a conventional knockout, we set out to rescue GSK-3β activity during the critical periods of palatogenesis and skeletogenesis. In the presence of rapamycin or rapamycin analogues, FRB*-tagged proteins dimerize with endogenous FK506 binding proteins (FKBPs), thus stabilizing the fusion protein and restoring protein levels and activity (Supplementary Fig. 1a–c)[6]. Because the FRB*-tag was inserted as a knock-in to the *GSK-3β* locus, any protein activity restored by drug treatment results from expression encoded by the endogenous locus and reflects endogenous expression and activity, both temporally and spatially. In the absence of drug treatment, there is minimal protein expression and activity[6].

Teratogenicity had previously been described in mouse embryos treated with rapamycin during early gestation stages (up to e10.5)[19]. Forty-eight hour drug treatments from e13.5 onward bypassed the period of rapamycin sensitivity and wild-type embryos showed no overt phenotypic abnormalities (Supplementary Fig. 1g) or skeletal defects. As a further control, all phenotypic analysis was performed by comparison with littermate controls as well as conventional knockout animals (*GSK-3β*$^{-/-}$) treated with rapamycin, and treated animals showed no phenotypic abnormalities beyond those observed in knockout animals. However, it is important to note the possibility that rapamycin has effects on other tissues not examined in this study.

We wanted to ensure that any rapamycin-dependent rescue of *GSK-3β* mutant phenotypes correlated with accessibility of the drug *in utero*, with the perdurance of rapamycin after the final treatment, and with stabilization of GSK-3β. From each litter treated, we harvested brain, liver and placental samples for pharmacokinetic and protein analysis. In brain samples harvested seven hours after the last dose administered, rapamycin was detectable (data not shown) and GSK-3βFRB* was clearly stabilized (Supplementary Fig. 1d). Although residual rapamycin was detected in embryos 15–27 h after the final dose (data not shown), we were unable to detect stabilization of GSK-3βFRB* 15 h after the last dose (Supplementary Fig. 1e) indicating that GSK-3βFRB* stabilization was reversed after drug treatment was stopped. Thus, we can achieve a high degree of temporal precision of protein stabilization during specific stages of embryonic development.

Our results demonstrate that GSK-3βFRB* was stabilized by maternal rapamycin treatment (Supplementary Fig. 1d, f). We

did not observe developmental defects in untreated heterozygotes, indicating that 50% of wild type protein was sufficient for proper embryogenesis. This led us to predict that stabilizing a portion of the pool of GSK-3β (Supplementary Fig. 1d) might be enough to rescue the mutant phenotype and would provide a temporal mapping of GSK-3β requirements during embryogenesis.

In *GSK-3β* mutants, the palatal shelves clearly descended and rotated but did not meet and fuse at the midline (Fig. 1c). Therefore, we predicted that rescue of cleft palate would require stabilization of GSK-3βFRB* at or around e14.5 (Fig. 1a). We dosed pregnant dams with rapamycin (5 mg kg^{-1} every 12 h for a total of 4 doses) in two-day windows beginning at e13.5–e15.0 and up to e16.5–e18.0. Indeed, administration of rapamycin at the earliest time points tested (e13.5–e15.0) rescued palatogenesis completely in 56% (5/9) and partially in 11% (1/9) of treated *GSK-3β*$^{FRB*/FRB*}$ embryos (Fig. 3b, c). Wild-type animals treated with rapamycin closed their palates normally (Fig. 3a). *GSK-3β*$^{-/-}$ embryos were not rescued by parallel drug treatment (Fig. 3c; 0/2 rescued). Consistent with our hypothesis that GSK-3β is required during a critical early step in palate morphogenesis, we saw no restoration of palate closure when treating during two-day windows beginning e14.5, e15.5 or e16.5 (Fig. 3c; 0/23 rescued). This identifies the essential developmental window for GSK-3β in palatogenesis between e13.5 to e15.0.

We next examined the sternal phenotype in rapamycin-treated animals. To ensure that rapamycin had no effect on skeletal development, we first examined treated wild-type animals by alcian blue and alizarin red staining and determined that normal sternal development was unaffected (Fig. 4a, c, e and g). As shown in Fig. 2b–e, mutant animals had bifurcated sternebrae and delayed sternal ossification. We predicted that GSK-3β might be required for both fusion and ossification, or it might be involved only in fusion, implying that the delay in ossification was secondary to a fusion defect. Using drug treatments, we defined the critical period for GSK-3β in sternal development as e15.5 to e17.0 (Fig. 4a, b). This is consistent with the onset of ossification occurring at e17 and continuing after birth[17]. *GSK-3β*$^{FRB*/FRB*}$ animals treated during this period of gestation displayed an onset of ossification (Fig. 4b, i; 7/7 rescued) comparable with littermate controls. Many also displayed fully fused sterna (4/7 rescued) and those that did not had only minor caudal clefts (3/7 partially rescued). Treatment at the earliest time point (e13.5–e15.0) failed to restore either sternal fusion or ossification (Fig. 4f), whereas embryos treated from e14.5 to e16.0 showed some improvement in sternal ossification, but not to the level observed with e15.5 to e17.0 (Fig. 4h, i). Our data suggest that although there was a correlation between the degree of sternal fusion and the onset of ossification, full ossification did not require complete fusion of the sternum (compare e14.5–e16 treatment with e15.5–e17 treatment, Fig. 4i). Again, in comparison, *GSK-3β*$^{-/-}$ mice treated for the same period with rapamycin had the full loss-of-function phenotype (Fig. 4d, 0/2 rescued). This result maps GSK-3β function to a temporal window consistent with a role for GSK-3β function in sternal fusion and onset of ossification between e15.5 and e17.0.

The range of rescue seen is likely to be due to variation in the stabilization of GSK-3βFRB*. These differences may be due to inconsistency of drug penetrance resulting from differences in transplacental blood flow related to embryo position in the uterine horns[20]. There is also inherent variability in the timing of organogenesis from embryo to embryo and from litter to litter, as seen in the range of palatal (Fig. 1) and sternal (Fig. 2) phenotypes observed in untreated mutant embryos.

Although GSK-3β functions had previously been studied using conventional gene targeting strategies, an observation of early lethality precluded a more careful analysis of GSK-3β's roles in later development. We did not observe the reported early lethality phenotype, and comparison of the drug-dependent conditional allele with the existing knockout allele has allowed us to identify novel developmental roles for GSK-3β and confirmed the specificity of the conditional allele. In the future, combining traditional knockout alleles with promoter-regulated FRB*-tagged transgenics or conditional knock-ins of FRB*-tags will allow additional spatial and temporal refinement of our studies. Drug-dependent rescue of developmental defects will provide a powerful tool to study GSK-3β requirements postnatally and allow us to learn more about GSK-3's roles in development and disease. Finally, our data showing the feasibility of small-molecule-based chemical genetics strategies have prospective clinical implications. New approaches to rescuing selected developmental defects require detailed knowledge of timing and levels of protein expression; our studies provide an improved method for defining these experimental conditions *in vivo*.

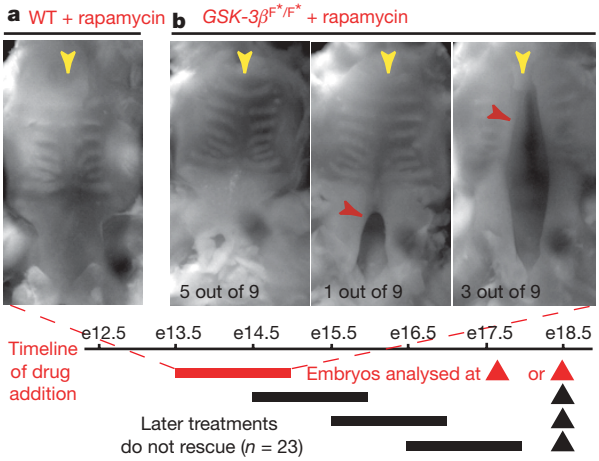

c

Untreated	Cleft	Partial	Closed
GSK-3β$^{-/-}$	17	0	0
GSK-3β$^{F*/F*}$	58	0	0
GSK-3β$^{-/F*}$	22	0	1
(only includes e17.5 to p0)			
Phenotypes of rapamycin-treated animals			
GSK-3β$^{F*/F*}$			
e13.5–e15	3	1	5
e14.5–e16	4	0	0
e15.5–e17	16	0	0
e16.5–e18	3	0	0
GSK-3β$^{-/-}$			
e13.5–e15	2	0	0
Vehicle-treated animals			
GSK-3β$^{F*/F*}$	6	0	0

Figure 3 | Drug-dependent rescue of cleft palate *GSK-3β*$^{FRB*/FRB*}$ mice *in utero*. Embryos were treated with four doses of rapamycin at 5 mg kg^{-1} *in utero* at the indicated time points. Animals were euthanized at e18.5 and scored for palate closure. **a**, Palates are fully fused in wild-type littermates treated with rapamycin. Midlines are marked with yellow arrowheads. **b**, Rapamycin treatment *in utero* from e13.5 to e15 rescues palatogenesis in *GSK-3β*$^{FRB*/FRB*}$ embryos. Full rescue observed in 5/9, 1/9 showed a small cleft in the posterior part of the palate (middle panel, red arrowhead) and 3/9 were not rescued. Solid bar in timeline below indicates period of rapamycin treatment; triangle indicates gestational age at harvest. Red bar corresponds with pictured experiments. Treatment at later time points did not rescue cleft palate (indicated by black bars, $n = 23$). **c**, Distribution of cleft palate in mutant animals. *GSK-3β*$^{-/-}$, *GSK-3β*$^{FRB*/FRB*}$ and *GSK-3β*$^{-/FRB*}$ mutants had complete clefts of the secondary palate (97/98 animals). *In utero* treatment of *GSK-3β*$^{FRB*/FRB*}$ embryos (e13.5–e15.0) rescued cleft palate, whereas later treatments did not. Neither *GSK-3β*$^{-/-}$ animals nor animals treated with vehicle (300 μl of injection solution—10% polyethylene glycol 400, 17% Tween-80 in H_2O) were rescued.

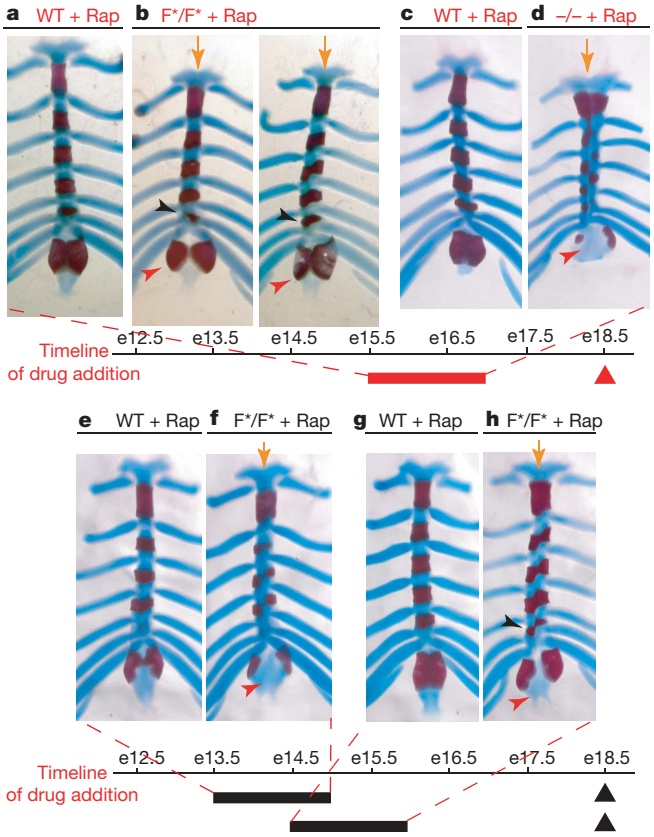

i

Untreated	Bifid	Fused	Delay
GSK-3β$^{-/-}$	14/16	2/16	11/16
e17.5	3/3	0/3	2/3
e18.5	5/7	2/7	6/7
p0	6/6	0/6	3/6
GSK-3β$^{-/F*}$	11/11	0/11	3/11
e17.5	4/4	0/4	2/4
e18.5	1/1	0/1	1/1
p0	6/6	0/6	2/6
GSK-3β$^{F*/F*}$	6/8	2/8	6/8
e18.5	1/1	0/1	1/1
p0	5/7	2/7	5/7

+ Rapamycin	Bifid	Fused	Delay
GSK-3β$^{F*/F*}$			
e13.5–e15	4/4	0/4	4/4
e14.5–e16	4/4	0/4	1/4
e15.5–e17	3/7	4/7	0/7
e16.5–e18	1/3	2/3	2/3
GSK-3β$^{-/-}$			
e15.5–e17	2/2	0/2	2/2
Vehicle-treated animals			
GSK-3β$^{-/-}$	2/2	0/2	2/2

Figure 4 | Reversal of sternal defects in chemically sensitive *GSK-3β* embryos. Embryos were treated *in utero* with four doses of rapamycin (5 mg kg^{-1} every 12 h) as indicated, euthanized at e18.5, stained with alizarin red (ossified bone) and alcian blue (cartilage) and scored. In each case, mutant animals were compared with the littermate controls shown. **a**, **c**, **e**, **g**, Sternal defects in wild-type embryos are unaffected by treatment with rapamycin *in utero*. Timing of treatments is indicated by schematics. **b**, *GSK-3β*$^{FRB*/FRB*}$ mutants treated with rapamycin from e15.5 to e17.0 showed improved sternal fusion and ossification. Note the fused sternebrae (midline marked by orange arrow), robust ossification (fifth ossification centre, black arrowhead) and some rescue of ossification of the xiphoid cartilage (red arrowhead). **d**, Treatment of *GSK-3β*$^{-/-}$ embryos with rapamycin at e15.5 to e17.0 failed to rescue the mutant phenotype. **f**, Treatment of *GSK-3β*$^{FRB*/FRB*}$ embryos from e13.5 to e15.0 failed to rescue sternal bifurcation. **h**, Treatment of *GSK-3β*$^{FRB*/FRB*}$ embryos from e14.5 to e16.0 failed to rescue sternal bifurcation, although the delay in ossification is not as severe (1/4 was delayed). Fifth ossification centre, black arrowhead. **i**, Distribution of sternal defects in mutant animals. Many *GSK-3β*$^{-/-}$, *GSK-3β*$^{FRB*/FRB*}$ and *GSK-3β*$^{-/FRB*}$ mutants showed bifid sternebrae. Some animals also exhibited delayed onset of ossification. In untreated animals, totals are listed by genotype followed by breakdown according to gestational age. In rapamycin treated animals, all animals were scored at e18.5; gestational age listed indicates beginning of *in utero* rapamycin treatment. Vehicle controls were treated from e15.5 to e17.0.

METHODS

Mice. Generation of drug-dependent *GSK-3β*^{FRB*} mice was described previously[6]. These mice will be made available at the Jackson Laboratory (JAX stock number JR6824, strain GSK3b$^{tm1Grc/J}$). Conventional mutant alleles of *GSK-3* (*GSK-3β*$^{-/+}$) were a gift from J. Woodgett and have been described previously[5]. All of the experiments shown were performed in outbred CD-1 mice; however, we found the same cleft palate phenotype in the original *GSK-3β*$^{-/-}$ and *GSK-3β*$^{FRB*/FRB*}$ mice and observed neither hepatic defects nor mid-gestational lethality. Alcian blue and alizarin red staining of bones and cartilage were performed according to established protocols.

Drug treatments. Rapamycin (sirolimus) was resuspended in a stock solution at 20 mg ml^{-1} in N,N-dimethylacetamide (DMA) and stored at –20 °C until use. Pregnant dams were treated with subcutaneous injections every 12 h during the time periods indicated. Each injection consisted of 5 mg kg rapamycin^{-1} diluted in 200 µl of injection vehicle (10% polyethylene glycol 400, 17% Tween-80). For vehicle controls, animals were injected with 200 µl of injection vehicle (every 12 h either for two days or continuously from e13.5 to e18.5) and displayed no phenotypic abnormalities.

Received 4 August; accepted 27 December 2006.
Published online 11 February 2007.

1. Cohen, P. & Frame, S. The renaissance of GSK3. *Nature Rev. Mol. Cell Biol.* **2,** 769–776 (2001).
2. Frame, S. & Cohen, P. GSK3 takes centre stage more than 20 years after its discovery. *Biochem. J.* **359,** 1–16 (2001).
3. Doble, B. W. & Woodgett, J. R. GSK-3: tricks of the trade for a multi-tasking kinase. *J. Cell Sci.* **116,** 1175–1186 (2003).
4. Jope, R. S. & Johnson, G. V. The glamour and gloom of glycogen synthase kinase-3. *Trends Biochem. Sci.* **29,** 95–102 (2004).
5. Hoeflich, K. P. *et al.* Requirement for glycogen synthase kinase-3β in cell survival and NF-κB activation. *Nature* **406,** 86–90 (2000).
6. Stankunas, K. *et al.* Conditional protein alleles using knockin mice and a chemical inducer of dimerization. *Mol. Cell* **12,** 1615–1624 (2003).
7. Murray, J. C. & Schutte, B. C. Cleft palate: players, pathways, and pursuits. *J. Clin. Invest.* **113,** 1676–1678 (2004).
8. Chen, J. K., Taipale, J., Cooper, M. K. & Beachy, P. A. Inhibition of Hedgehog signaling by direct binding of cyclopamine to Smoothened. *Genes Dev.* **16,** 2743–2748 (2002).
9. Graef, I. A., Chen, F., Chen, L., Kuo, A. & Crabtree, G. R. Signals transduced by Ca^{2+}/calcineurin and NFATc3/c4 pattern the developing vasculature. *Cell* **105,** 863–875 (2001).
10. Graef, I. A. *et al.* Neurotrophins and netrins require calcineurin/NFAT signaling to stimulate outgrowth of embryonic axons. *Cell* **113,** 657–670 (2003).
11. Peterson, R. T. *et al.* Chemical suppression of a genetic mutation in a zebrafish model of aortic coarctation. *Nature Biotechnol.* **22,** 595–599 (2004).
12. Peterson, R. T., Link, B. A., Dowling, J. E. & Schreiber, S. L. Small molecule developmental screens reveal the logic and timing of vertebrate development. *Proc. Natl Acad. Sci. USA* **97,** 12965–12969 (2000).
13. Liu, J. *et al.* A small-molecule agonist of the Wnt signaling pathway. *Angew. Chem. Int. Ed.* **44,** 1987–1990 (2005).
14. Sharpe, P. M. & Ferguson, M. W. Mesenchymal influences on epithelial differentiation in developing systems. *J. Cell Sci.* **10** (suppl.), 195–230 (1988).
15. Karsenty, G. & Wagner, E. F. Reaching a genetic and molecular understanding of skeletal development. *Dev. Cell* **2,** 389–406 (2002).
16. Krishnan, V., Bryant, H. U. & Macdougald, O. A. Regulation of bone mass by Wnt signaling. *J. Clin. Invest.* **116,** 1202–1209 (2006).
17. Chen, J. M. Studies on the morphogenesis of the mouse sternum. I. Normal embryonic development. *J. Anat.* **86,** 373–386 (1952).
18. Ito, Y. *et al.* Conditional inactivation of *Tgfbr2* in cranial neural crest causes cleft palate and calvaria defects. *Development* **130,** 5269–5280 (2003).
19. Hentges, K. E. *et al.* FRAP/mTOR is required for proliferation and patterning during embryonic development in the mouse. *Proc. Natl Acad. Sci. USA* **98,** 13796–13801 (2001).
20. Flake, A. W., Villa, R. L., Adzick, N. S. & Harrison, M. R. Transamniotic fetal feeding. II. A model of intrauterine growth retardation using the relationship of "natural runting" to uterine position. *J. Pediatr. Surg.* **22,** 816–819 (1987).

Supplementary Information is linked to the online version of the paper at www.nature.com/nature.

Acknowledgements We thank M. S. Dionne for critical reading of the manuscript; M. S. Dionne, M. M. Winslow, J. E. Gestwicki, J. H. Bayle, S. C. Kao and members of the Longaker and Crabtree laboratories for invaluable discussions; and J. Woodgett for the gift of *GSK-3β* knockout mice. K.J.L and M.T.L. are supported by the NIH, M.T.L. is also supported by the Oak Foundation and J.R.A. is a fellow of the Berry Foundation.

Author Information Reprints and permissions information is available at www.nature.com/reprints. The authors declare no competing financial interests. Correspondence and requests for materials should be addressed to K.J.L. (karen.liu@kcl.ac.uk) or M.T.L. (longaker@stanford.edu).

LETTERS

In vivo imaging of germinal centres reveals a dynamic open structure

Tanja A. Schwickert[1], Randall L. Lindquist[1], Guy Shakhar[3]†, Geulah Livshits[1], Dimitris Skokos[1], Marie H. Kosco-Vilbois[4], Michael L. Dustin[3] & Michel C. Nussenzweig[1,2]

Germinal centres are specialized structures wherein B lymphocytes undergo clonal expansion, class switch recombination, antibody gene diversification and affinity maturation. Three to four antigen-specific B cells colonize a follicle to establish a germinal centre and become rapidly dividing germinal-centre centroblasts that give rise to dark zones[1–4]. Centroblasts produce non-proliferating centrocytes that are thought to migrate to the light zone of the germinal centre, which is rich in antigen-trapping follicular dendritic cells and CD4$^+$ T cells[5–7]. It has been proposed that centrocytes are selected in the light zone on the basis of their ability to bind cognate antigen[5–8]. However, there have been no studies of germinal-centre dynamics or the migratory behaviour of germinal-centre cells *in vivo*. Here we report the direct visualization of B cells in lymph node germinal centres by two-photon laser-scanning microscopy in mice. Nearly all antigen-specific B cells participating in a germinal-centre reaction were motile and physically restricted to the germinal centre but migrated bi-directionally between dark and light zones. Notably, follicular B cells were frequent visitors to the germinal-centre compartment, suggesting that all B cells scan antigen trapped in germinal centres. Consistent with this observation, we found that high-affinity antigen-specific B cells can be recruited to an ongoing germinal-centre reaction. We conclude that the open structure of germinal centres enhances competition and ensures that rare high-affinity B cells can participate in antibody responses.

To examine germinal-centre B-cell behaviour in real time, we visualized the inguinal lymph nodes of live mice by two-photon laser-scanning microscopy (TPLSM)[9–11]. Germinal centres were induced by immunizing with ovalbumin (OVA) and boosting with OVA conjugated to 4-hydroxy-3-nitrophenylacetyl (NP–OVA). Green fluorescent protein (GFP)-expressing NP-specific B cells[12,13] were transferred into immunized mice one day before the boost, resulting in an average frequency of 0.2% NP-specific B cells (Fig. 1a; see also Supplementary Figs 1–4). As an internal control we also transferred naive polyclonal wild-type B cells that expressed cyan fluorescent protein (CFP)[14] 1 day before imaging. Although this control population contains some NP-specific B cells, they are rare and would not have time to expand in the 24 h between transfer and imaging. Germinal centres were visualized by injecting mice with follicular dendritic cell (FDC)-M1 labelled with Alexa-633 or -546 (Supplementary Fig. 5)[15]. FDC-M1, but not isotype control antibody (Supplementary Fig. 5), labels mature FDCs and tingible-body macrophages, both of which are thought to capture antigens in germinal centres[16]. Because the FDC-M1 antibody might, in theory, interfere with the germinal-centre reaction, we also imaged in the absence of FDC-M1 injection but found no difference in any of the parameters measured (Supplementary Fig. 6 and Supplementary Video 1).

TPLSM revealed that CFP$^+$ and GFP$^+$ B cells were highly motile (Fig. 1b–e), whereas plasma cells in the medulla and FDC-M1-labelled FDCs and tingible-body macrophages were sessile (Supplementary Videos 1 and 2). In the absence of the specific antigen boost (NP–OVA), GFP$^+$ NP-specific and CFP$^+$ polyclonal wild-type B cells were distributed throughout the B-cell follicle and moved at equivalent speeds (Fig. 1c, e; see also Supplementary Video 3)[17–19]. B cells proliferate in the dark zone of the germinal centre and are believed to be selected by antigen trapped in immune complexes in the light zone[6,7]. The light zone is proximal to the lymph node capsule, contains more FDCs (Supplementary Fig. 5), and is less densely packed with lymphoid cells. Although both B-cell types were in large part excluded from the dark zone of the OVA-specific germinal centres, they were frequently found in the FDC-rich light zone (Fig. 1c, left panels; see also Supplementary Fig. 5 and Supplementary Video 3). We conclude that in the absence of specific antigen both NP-specific and control polyclonal B cells continually pass through the FDC-rich light zone.

Boosting with NP–OVA did not alter the shape or behaviour of the CFP$^+$ control B cells (Fig. 1e; see also Supplementary Videos 4 and 5). In contrast, GFP$^+$ NP-specific B cells became physically restricted to the germinal centre. The specific cells had a significantly decreased speed compared to control populations and showed a twofold increase in cell volume (Fig. 1e; see also Supplementary Videos 4 and 5). They showed a reduced confinement index, higher average turning angles and a lower average displacement rate than the CFP$^+$ control B cells (Fig. 1e, all P-values <0.001). As a result, GFP$^+$ NP-specific germinal-centre B cells appeared to roam within the confines of the germinal centre. Antigen-specific B cells spent more time pausing than CFP$^+$ control B cells, but only a small percentage of cells paused for an extended period of time (Fig. 1e). The plot of mean displacement versus the square root of time was linear between 1 and 2.5 min$^{1/2}$ in the presence and absence of NP–OVA, indicating a random walk on short timescales (Fig. 1d)[18,20]. In the absence of NP, the motility coefficient[18], a measure of the region scanned, was equivalent for GFP$^+$ NP-specific germinal-centre B cells and CFP$^+$ control B cells (Fig. 1d, left panel). In contrast, after NP–OVA boosting, the motility coefficient decreased from 30 $\mu m^2\ min^{-1}$ to 13 $\mu m^2\ min^{-1}$ for GFP$^+$ NP-specific germinal-centre B cells (Fig. 1d, right panel). We conclude that antigen-specific germinal-centre B cells are restricted to the region of the germinal centre where they move with a lower average velocity and greater confinement than follicular B cells.

To investigate the impact of the germinal-centre polarity on B-cell migration, the germinal centre was divided into dark and light zones

[1]Laboratory of Molecular Immunology, and [2]Howard Hughes Medical Institute, The Rockefeller University, New York, New York 10021, USA. [3]Program in Molecular Pathogenesis and Department of Pathology, Skirball Institute of Biomolecular Medicine, New York University School of Medicine, New York, New York 10016, USA. [4]NovImmune SA, 64 avenue de la Roseraie, 1211 Geneva 4, Switzerland. †Present address: Department of Immunology, Weizmann Institute of Science, Rehovot 76100, Israel.

(Fig. 2a; see also Supplementary Methods). Over a 30-min period we found that 8% of the cells migrated from the dark zone to the light zone and 5% in the opposite direction (Fig. 2b). When corrected for the higher B-cell density in the dark zone, the relative traffic between the two compartments was nearly indistinguishable (Fig. 2b, bottom panel). This was confirmed by analysing the net displacement vector for all B cells in germinal centres irrespective of their initial position (Supplementary Fig. 7). The magnitude of the displacement vector was less than a cell diameter for the wild-type control (5 μm) and NP-specific germinal-centre B cells (6 μm), suggesting no major directional bias in the presence or absence of specific antigen (Fig. 2b; see also Supplementary Fig. 7). In addition, we found no evidence of directional migration of germinal-centre B cells by random walk analysis (Fig. 1d). We estimate that there is full exchange between compartments in less than 18 h, supporting a model of germinal-centre selection that involves multiple rounds of proliferation and selection[6,7,21].

Comparing the behaviour of GFP$^+$ NP-specific germinal-centre B cells in dark and light zones, we found only a slight increase in the arrest coefficient of dark-zone cells, as might be expected for cells

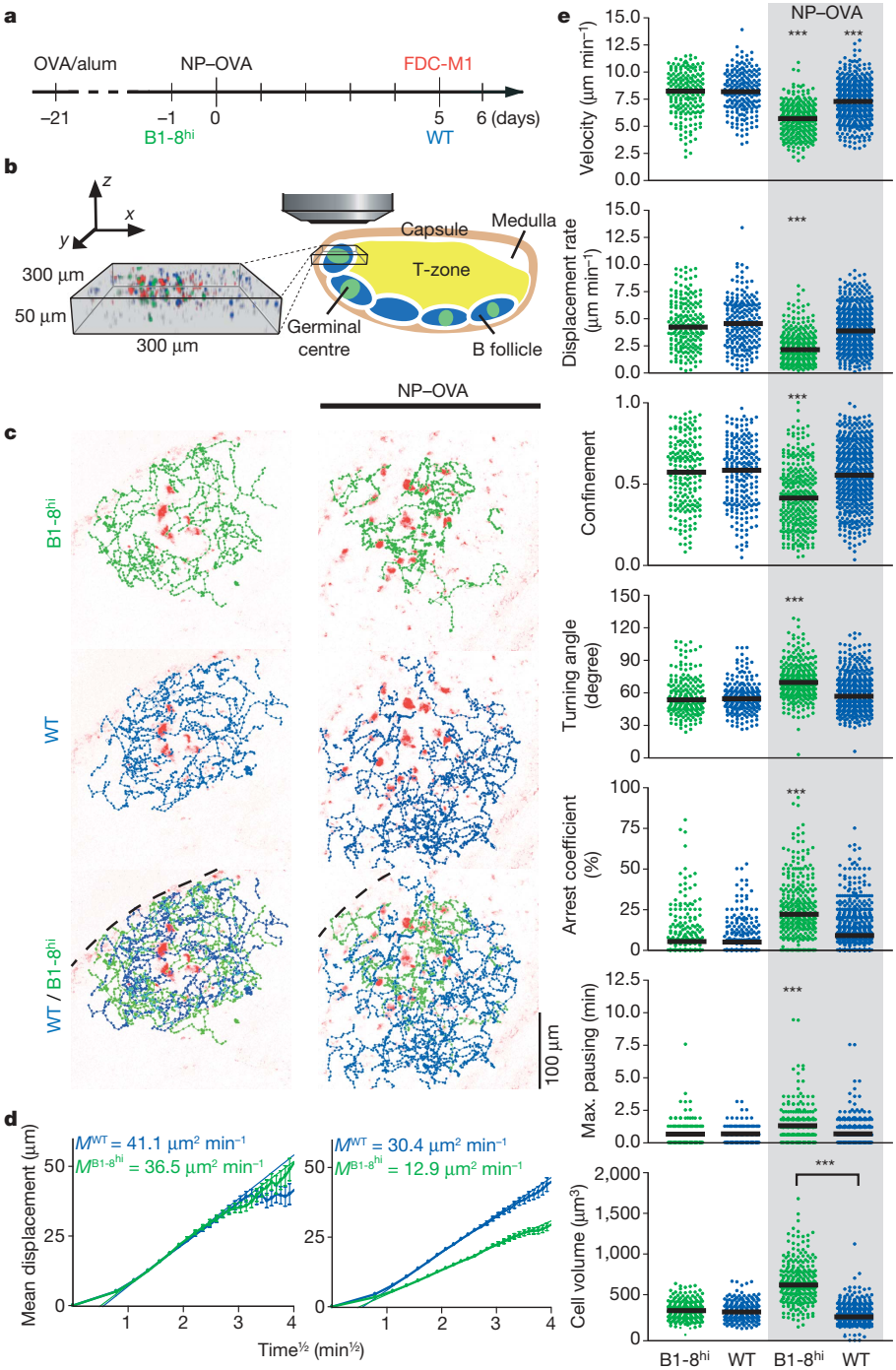

Figure 1 | Germinal centre and naive B-cell behaviour. a, Timeline. **b**, Imaged region and dimensions. **c**, z-Projection of FDC-M1 cells (red) superimposed on B1-8^{hi} (green, top row) and control (blue, middle row) B cell tracks. Tracks with (right) and without (left) NP are shown. The dashed line represents the lymph node capsule. **d, e**, Analysis of wild-type and B1-8^{hi} B cells with (right: wild type, 534 cells; B1-8^{hi}, 311 cells) and without (left: wild type, 212 cells; B1-8^{hi}, 200 cells) NP (three experiments). **d**, Random walk analysis in the absence (left) and presence of NP (right). Error bars represent standard error. **e**, Statistical analysis. Each data point represents a single cell and black bars indicate mean values. Significant differences are marked (triple asterisk, $P < 0.001$).

undergoing cell division (Fig. 2c). To characterize further the interaction between germinal-centre B cells and FDC-M1$^+$ cells, we analysed contacts between FDC-M1$^+$ cells and either GFP$^+$ NP-specific or CFP$^+$ control B cells (Fig. 3a, b). We found that CFP$^+$ control B cells in secondary follicles contact FDC-M1$^+$ cells every 1.8 h (±0.44 h; on average 29.3% of the CFP$^+$ control cells contacted FDC-M1$^+$ cells during the 30-min time-lapse sequences, based on two independent experiments and three time-lapse movies, Supplementary Video 5). However, control B cells (Supplementary Video 6) did not maintain contact with the FDC-M1$^+$ cells for as long as GFP$^+$ NP-specific germinal-centre B cells (Fig. 3c, 2.3 versus 3.5 min, $P < 0.0001$, Supplementary Video 7). During these contacts, GFP$^+$ antigen-specific germinal-centre B cells slowed, on average, from 7 μm min^{-1} to 5.6 μm min^{-1} (Fig. 3d, $P < 0.001$) and remained in contact with the FDC-M1$^+$ cells while migrating along their cell bodies and dendrites, stopping only briefly (Fig. 3a, b, compare maximal pausing time in Fig. 1e). Thus, B cells actively participating in a germinal-centre reaction crawl along FDC-M1$^+$ cells and through a dense FDC network (Supplementary Video 5), making multiple, transient contacts.

The observation that germinal centres are open structures continually visited by naive follicular B cells indicated that occasional antigen-specific B cells in this population might recognize cognate antigen in the germinal centre and join a pre-existing germinal centre. In our system, germinal centres are well established by 6 days after the NP–OVA boost (Supplementary Fig. 4) and therefore GFP$^+$ NP-specific B cells transferred 6 or 9 days after boosting would have the opportunity to join pre-existing germinal centres (Fig. 4a; see also Supplementary Fig. 8). Whereas GFP$^+$ NP-specific germinal-centre B cells transferred before the boost produced germinal centres that were composed nearly exclusively of the transferred cells (Fig. 4b), transfer 6 or 9 days after boosting produced predominantly mixed germinal centres (Fig. 4b). To examine the role of affinity in germinal-centre joining, we transferred high-affinity anti-NP-specific B cells (B1-8^{hi}) into wild-type, B1-8^{lo} (low-affinity heavy-chain knock-in[12]), or B1-8^{hi}

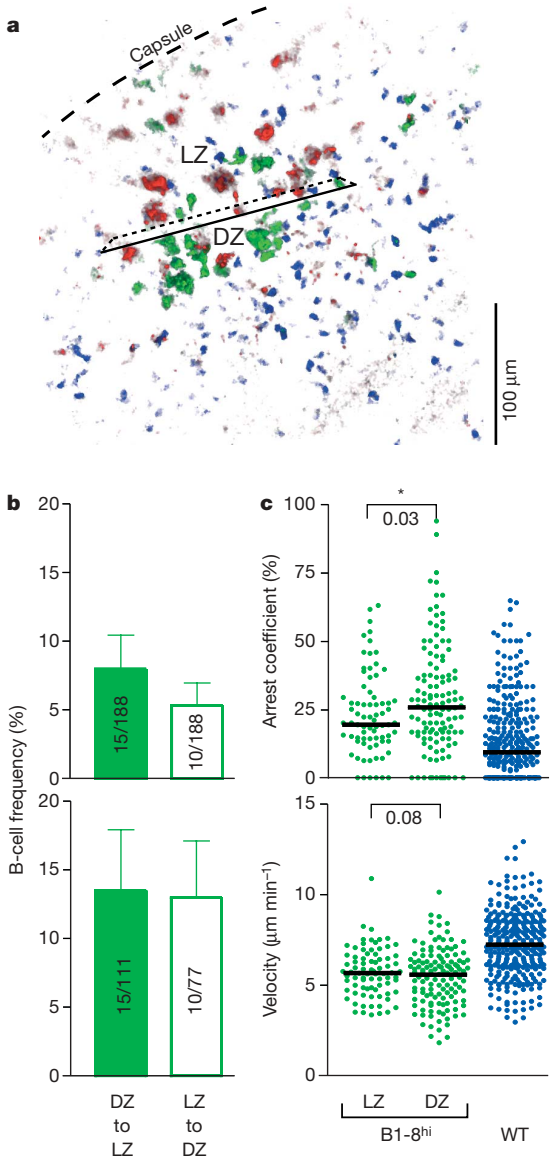

Figure 2 | B-cell behaviour in germinal-centre light and dark zones. **a**, Time-lapse image showing germinal-centre light and dark zones (LZ and DZ, respectively). **b**, Top: percentage of cells moving from the light zone to the dark zone (8%, $n = 188$) and the reverse (5%, $n = 188$) during 30 min. Bottom: number of cells migrating from dark zone to light zone as a percentage of dark zone cells ($n = 111$) and light zone to dark zone as a percentage of light zone cells ($n = 77$). Error bars, standard error. **c**, Arrest coefficients (top) and velocity (bottom) for NP-specific B1-8^{hi} cells in the dark zone and light zone (green), and for control B cells (blue) (two-tailed *t*-test: arrest coefficient $P = 0.03$; velocity $P = 0.08$). The velocity is representative for all other migratory parameters shown in Fig. 1e. Data are from four time-lapse movies from three experiments.

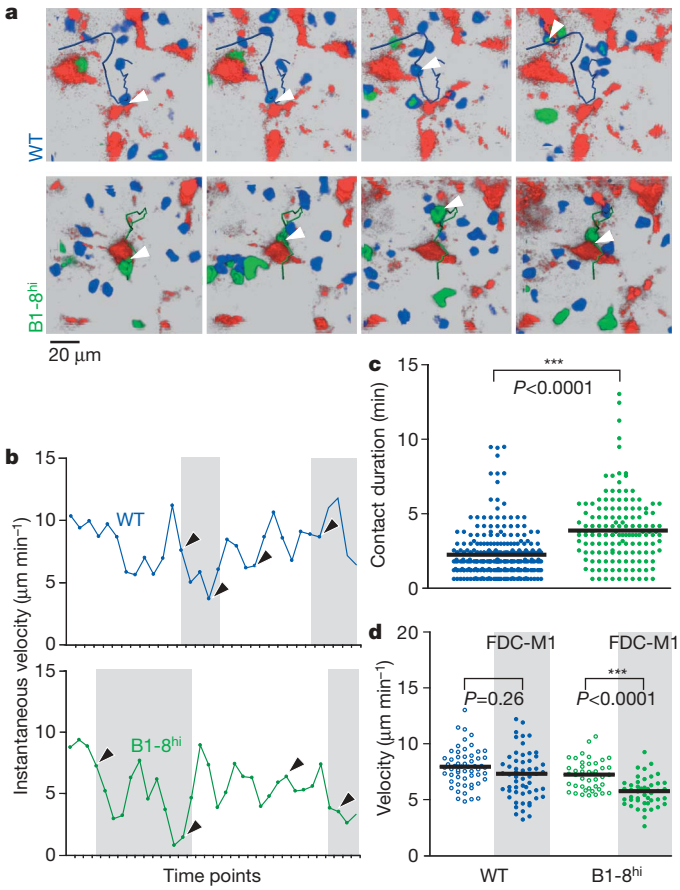

Figure 3 | Contacts between B cells and FDC-M1$^+$ cells. **a**, Still images showing tracks and contacts between FDC-M1$^+$ cells, NP-specific B cells (bottom, green) and naive B cells (top, blue). White arrowheads indicate the position of the tracked cell. Red shows FDC-M1$^+$ cells. **b**, Instantaneous velocity. Contact duration is indicated by grey shading; black arrows correspond to time points in the still images of **a**. The *x* axis indicates time in units of 37 seconds. **c**, Contact between FDC-M1$^+$ and control (blue) or germinal-centre B cells (green). Each dot represents a contact ($P < 0.0001$, unpaired two-tailed *t*-test). **d**, Velocity of control and germinal-centre B cells in contact with FDC-M1$^+$ cells (grey shading) or not (wild type, $P = 0.26$; B1-8^{hi}, $P < 0.0001$; paired *t*-test). Data are from two experiments and three movies.

mice immunized with Ova and boosted with NP-OVA 6 days before transfer (Fig. 4c). In B1-8^{lo} recipients all germinal centres examined were mixed (that is, transferred B1-8^{hi} and endogenous B cells) and in wild-type recipients 19 out of 21 germinal centres were mixed (Fig. 4d, middle and left panel). In contrast, we found only endogenous B cells in B1-8^{hi} recipients (Fig. 4d, right panel). Thus, B cells only joined germinal centres when they had a competitive advantage in antigen-binding affinity (Fig. 4d). We conclude that germinal-centre seeding is an ongoing process and that only B cells with a competitive advantage in antigen-binding affinity can join a pre-existing germinal-centre reaction.

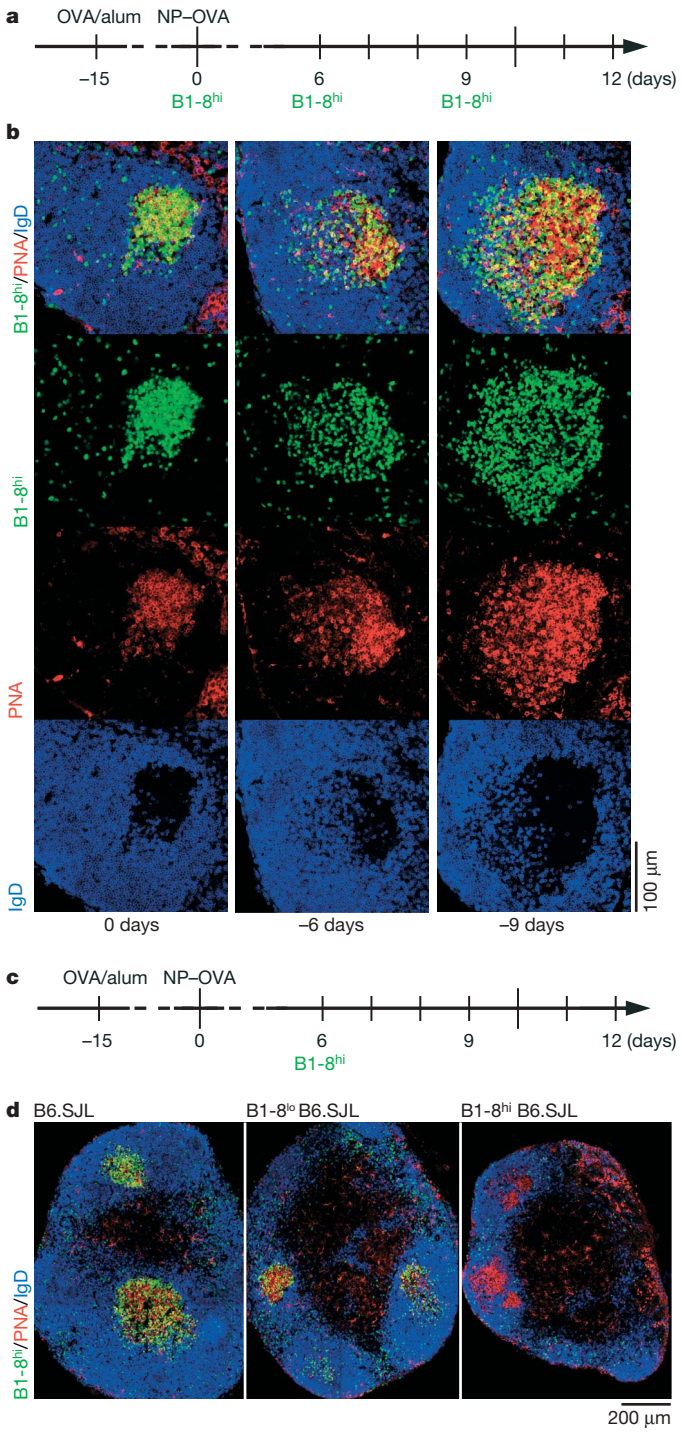

Figure 4 | Ongoing seeding of germinal centres. a,c, Timeline. **b**, Lymph nodes 6 days after B1-8^{hi} B-cell (green) transfer. Peanut agglutinin (PNA) (red) and IgD (blue) label germinal-centre and naive B cells, respectively. When cells were transferred with the boost (0 days), 22 out of 25 germinal centres consisted entirely of transferred cells (two experiments). When cells were transferred 6 or 9 days after the boost, 47 out of 54 germinal centres were mixed (six experiments). **d**, As in **b**. In B1-8^{lo} mice, all 25 germinal centres were mixed (transferred and endogenous B cells, three experiments); in wild-type mice, 19 out of 21 germinal centres were mixed (four experiments); and in B1-8^{hi} mice, all 18 germinal centres consisted entirely of endogenous B cells (three experiments).

B-cell clonal expansion in the germinal centre is accompanied by affinity maturation, a process that requires positive selection of cells that express high-affinity antigen receptors and negative selection of those that damage or lose their receptors as a result of somatic hypermutation[6,7]. Our experiments show that the germinal centre is a highly dynamic environment and that germinal-centre B cells differ from other B cells and plasmablasts in speed, confinement and association with FDC-M1^{+} cells. In contrast to naive B and T cells, which stop moving when they initially encounter high-affinity antigens presented by conventional dendritic cells, germinal-centre B cells simply slow down and crawl along the FDC-M1^{+} cells but rarely stop for prolonged periods[10,11,22–24]. We speculate that selection of germinal-centre B cells is governed by multiple dynamic interactions.

Naive B cells are long-lived cells that migrate randomly through lymph node follicles for 12–18 h before circulating to other lymph-node follicles[25]. We estimate that the probability that a follicular B cell will interact with an antigen-trapping cell before leaving a germinal-centre-containing follicle is 99.9%, and this may be an underestimate because not all cell processes were visible by TPLSM. Indeed, analysis of follicles in non-immunized mice indicates that B cells are always in contact with the processes of stromal cells[26]. Because germinal centres persist for 2–3 weeks, and B cells circulate through many different nodes during this time, a large fraction of all B cells will scan any given germinal centre. Dynamic scanning of antigen-trapping cells by naive B cells was not anticipated by previous studies that focused on specific antigens or antibody genes[1,27,28]. However, scanning is consistent with single-cell analysis of human germinal centres, which found numerous B cells with unmutated and unrelated antibody genes in two tonsillar germinal centres[29]. Scanning would increase competition for antigen and contribute to the stringency of affinity maturation, while providing a dynamic explanation for the phenomenon of epitope spreading[30]. In addition, scanning ensures that a large fraction of the B-cell repertoire is exposed to antigen trapped in germinal centres and that rare high-affinity B cells not initially recruited into the germinal-centre reaction might have the opportunity to participate in the antibody response.

METHODS

Mice. Immunoglobulin heavy-chain knock-in C57BL6 (B6) mice (B1-8^{hi} or B1-8^{lo} (ref. 12)) were bred to B6-GFP (ref. 13) or B6.SJL mice. B6 and B6.SJL mice were purchased from Jackson Laboratories.

Immunization and cell transfer. B6 recipients were injected intraperitoneally with 100 µg OVA (Seikagaku) precipitated in alum (2:1, Pierce). Three to five weeks later mice were boosted with 150 µg soluble NP(17)–OVA (Biosearch Technology) subcutaneously. For imaging, either 10^7 B1-8^{hi} or 2–5 $\times$ 10^6 B1-8^{hi} λ B cells (CD43 and CD90 depleted) were transferred intravenously 1 day before boosting. One day before imaging, 3 $\times$ 10^7 polyclonal CFP-expressing B cells[14] were transferred and 25 µg of FDC-M1 conjugated to Alexa-633/546 was injected subcutaneously. Germinal centres were imaged 6 days after NP–OVA boost.

Immunohistochemistry. Cryostat sections of lymph nodes were fixed and stained as described previously[11]. The following antibodies were used: anti-B220-A647 (RA3-6B2, Caltag), anti-IgD (11-26), anti-CD45.1-FITC (A20, eBioscience), PNA-biotin (Vector), FDC-M1 (4C11, provided by S. Burton), FDC-M2 (209, ImmunoKontact), anti-GFP-A488, anti-fluorescein-A488 (Molecular Probes), rat IgG2b (G15-337), anti-CD35-biotin (8C12), anti-CD45.1-biotin (A20, BD Pharmingen), anti-CD68-bio (FA-11, Serotec) anti-rat-Cy3, anti-rat-Cy5, anti-rabbit-Cy3, anti-rabbit F(ab′)$_2$-Cy3, SA-Cy3, SA-Cy5 (Jackson Immunoresearch Laboratories). FDC-M1 was labelled with the Alexa-546 or -633 labelling kit (Molecular Probes).

Confocal microscopy. Confocal images were acquired on a Zeiss LSM 510 system with 488-, 543- and 633-nm excitation line (Rockefeller University

Bio-Imaging Facility). Z-stack (three planes, 3-μm z-steps) images were obtained with a C-Apochromat ×40 (NA 1.2, water-immersion) or a Plan-Apochromat ×20 (NA 0.75) objective.

Intra-vital two-photon microscopy. Mice were anaesthetized and maintained normothermic as described[11]. Microsurgically exposed inguinal lymph nodes were imaged using a Bio-Rad Radiance multiphoton microscope fitted with a Tsunami pulsed laser (Spectraphysics) tuned to 870 nm. For fluorescent protein detection, band-pass filters optimized for CFP (480/30) and YFP (540/30) were used.

Additional detailed methods can be found in Supplementary Information.

Received 13 December 2006; accepted 10 January 2007.
Published online 31 January 2007.

1. Jacob, J., Kelsoe, G., Rajewsky, K. & Weiss, U. Intraclonal generation of antibody mutants in germinal centres. *Nature* **354,** 389–392 (1991).
2. Jacob, J. & Kelsoe, G. *In situ* studies of the primary immune response to (4-hydroxy-3-nitrophenyl)acetyl. II. A common clonal origin for periarteriolar lymphoid sheath-associated foci and germinal centers. *J. Exp. Med.* **176,** 679–687 (1992).
3. Kroese, F. G., Wubbena, A. S., Seijen, H. G. & Nieuwenhuis, P. Germinal centers develop oligoclonally. *Eur. J. Immunol.* **17,** 1069–1072 (1987).
4. Hanna, M. G. Jr. An autoradiographic study of the germinal center in spleen white pulp during early intervals of the immune response. *Lab. Invest.* **13,** 95–104 (1964).
5. Nossal, G. J., Ada, G. L., Austin, C. M. & Pye, J. Antigens in immunity. 8. Localization of 125-I-labelled antigens in the secondary response. *Immunology* **9,** 349–357 (1965).
6. MacLennan, I. C. Germinal centers. *Annu. Rev. Immunol.* **12,** 117–139 (1994).
7. Rajewsky, K. Clonal selection and learning in the antibody system. *Nature* **381,** 751–758 (1996).
8. Liu, Y. J. *et al.* Mechanism of antigen-driven selection in germinal centres. *Nature* **342,** 929–931 (1989).
9. Miller, M. J., Wei, S. H., Cahalan, M. D. & Parker, I. Autonomous T cell trafficking examined *in vivo* with intravital two-photon microscopy. *Proc. Natl Acad. Sci. USA* **100,** 2604–2609 (2003).
10. Mempel, T. R., Henrickson, S. E. & Von Andrian, U. H. T-cell priming by dendritic cells in lymph nodes occurs in three distinct phases. *Nature* **427,** 154–159 (2004).
11. Lindquist, R. L. *et al.* Visualizing dendritic cell networks *in vivo*. *Nature Immunol.* **5,** 1243–1250 (2004).
12. Shih, T. A., Roederer, M. & Nussenzweig, M. C. Role of antigen receptor affinity in T cell-independent antibody responses *in vivo*. *Nature Immunol.* **3,** 399–406 (2002).
13. Schaefer, B. C., Schaefer, M. L., Kappler, J. W., Marrack, P. & Kedl, R. M. Observation of antigen-dependent $CD8^+$ T-cell/dendritic cell interactions *in vivo*. *Cell. Immunol.* **214,** 110–122 (2001).
14. Hadjantonakis, A. K., Macmaster, S. & Nagy, A. Embryonic stem cells and mice expressing different GFP variants for multiple non-invasive reporter usage within a single animal. *BMC Biotechnol.* **2,** 11 (2002).
15. Kosco, M. H., Pflugfelder, E. & Gray, D. Follicular dendritic cell-dependent adhesion and proliferation of B cells *in vitro*. *J. Immunol.* **148,** 2331–2339 (1992).
16. Szakal, A. K., Kosco, M. H. & Tew, J. G. A novel *in vivo* follicular dendritic cell-dependent iccosome-mediated mechanism for delivery of antigen to antigen-processing cells. *J. Immunol.* **140,** 341–353 (1988).
17. Okada, T. *et al.* Antigen-engaged B cells undergo chemotaxis toward the T zone and form motile conjugates with helper T cells. *PLoS Biol.* **3,** e150 (2005).
18. Miller, M. J., Wei, S. H., Parker, I. & Cahalan, M. D. Two-photon imaging of lymphocyte motility and antigen response in intact lymph node. *Science* **296,** 1869–1873 (2002).
19. Han, S. B. *et al.* Rgs1 and Gnai2 regulate the entrance of B lymphocytes into lymph nodes and B cell motility within lymph node follicles. *Immunity* **22,** 343–354 (2005).
20. Sumen, C., Mempel, T. R., Mazo, I. B. & von Andrian, U. H. Intravital microscopy: visualizing immunity in context. *Immunity* **21,** 315–329 (2004).
21. Oprea, M. & Perelson, A. S. Somatic mutation leads to efficient affinity maturation when centrocytes recycle back to centroblasts. *J. Immunol.* **158,** 5155–5162 (1997).
22. Fleire, S. J. *et al.* B cell ligand discrimination through a spreading and contraction response. *Science* **312,** 738–741 (2006).
23. Qi, H., Egen, J. G., Huang, A. Y. & Germain, R. N. Extrafollicular activation of lymph node B cells by antigen-bearing dendritic cells. *Science* **312,** 1672–1676 (2006).
24. Shakhar, G. *et al.* Stable T cell–dendritic cell interactions precede the development of both tolerance and immunity *in vivo*. *Nature Immunol.* **6,** 707–714 (2005).
25. Fossum, S., Smith, M. E. & Ford, W. L. The recirculation of T and B lymphocytes in the athymic, nude rat. *Scand. J. Immunol.* **17,** 551–557 (1983).
26. Bajenoff, M. *et al.* Stromal cell networks regulate lymphocyte entry, migration, and territoriality in lymph nodes. *Immunity* **25,** 989–1001 (2006).
27. Jacob, J., Przylepa, J., Miller, C. & Kelsoe, G. *In situ* studies of the primary immune response to (4-hydroxy-3-nitrophenyl)acetyl. III. The kinetics of V region mutation and selection in germinal center B cells. *J. Exp. Med.* **178,** 1293–1307 (1993).
28. Liu, Y. J., Zhang, J., Lane, P. J., Chan, E. Y. & MacLennan, I. C. Sites of specific B cell activation in primary and secondary responses to T cell-dependent and T cell-independent antigens. *Eur. J. Immunol.* **21,** 2951–2962 (1991).
29. Kuppers, R., Zhao, M., Hansmann, M. L. & Rajewsky, K. Tracing B cell development in human germinal centres by molecular analysis of single cells picked from histological sections. *EMBO J.* **12,** 4955–4967 (1993).
30. Deshmukh, U. S., Bagavant, H., Lewis, J., Gaskin, F. & Fu, S. M. Epitope spreading within lupus-associated ribonucleoprotein antigens. *Clin. Immunol.* **117,** 112–120 (2005).

Supplementary Information is linked to the online version of the paper at www.nature.com/nature.

Acknowledgements We thank E. Besmer, M. Zimmer and members of the Nussenzweig laboratory for comments on the manuscript. This work was supported by the Schering Foundation (T.A.S.), a Medical Scientist Training Program grant (R.L.L.), the Rothchild Foundation (G.S.), Fondation de Recherche Medicale (D.S.), and the NIH (M.C.N. and M.L.D.). M.C.N. is an investigator of the Howard Hughes Medical Institute.

Author Information Reprints and permissions information is available at www.nature.com/reprints. The authors declare competing financial interests: details accompany the full-text HTML version of the paper at www.nature.com/nature. Correspondence and requests for materials should be addressed to M.L.D. (mikeroscope@nyc.rr.com) or M.C.N. (nussen@rockefeller.edu).

LETTERS

Specific role of mitochondrial electron transport in blood-stage *Plasmodium falciparum*

Heather J. Painter[1], Joanne M. Morrisey[1], Michael W. Mather[1] & Akhil B. Vaidya[1]

The origin of all mitochondria can be traced to the symbiotic arrangement that resulted in the emergence of eukaryotes in a world that was exclusively populated by prokaryotes[1–3]. This arrangement, however, has been in continuous genetic flux: the varying degrees of gene loss and transfer from the mitochondrial genome in different eukaryotic lineages seem to signify an ongoing 'conflict' between the host and the symbiont. Eukaryotic parasites belonging to the phylum Apicomplexa provide an excellent example to support this view. These organisms contain the smallest mitochondrial genomes known[4,5], with an organization that differs among various genera; one genus, *Cryptosporidium*, seems to have lost the entire mitochondrial genome[6,7]. Here we show that erythrocytic stages of the human malaria parasite *Plasmodium falciparum* seem to maintain an active mitochondrial electron transport chain to serve just one metabolic function: regeneration of ubiquinone required as the electron acceptor for dihydroorotate dehydrogenase, an essential enzyme for pyrimidine biosynthesis. Transgenic *P. falciparum* parasites expressing *Saccharomyces cerevisiae* dihydroorotate dehydrogenase, which does not require ubiquinone as an electron acceptor[8], were completely resistant to inhibitors of mitochondrial electron transport. Maintenance of mitochondrial membrane potential, however, was essential in these parasites, as indicated by their hypersensitivity to proguanil, a drug that collapsed the membrane potential in the presence of electron transport inhibitors. Thus, acquisition of just one enzyme can render mitochondrial electron transport nonessential in erythrocytic stages of *P. falciparum*.

Apicomplexan parasites contain two cytoplasmic organelles endowed with their own genomes—a mitochondrion and a plastid[9,10]. The mitochondrial DNA (mtDNA) encodes just three components of the electron transport chain and scrambled fragments of ribosomal RNA[5,11], thus the mitochondrion requires the import of hundreds of nuclear-encoded proteins not just to serve the physiological functions but also for the upkeep of its separate genetic system. In *P. falciparum*, biochemical data indicate that the mitochondrion is not a source of ATP[12]; furthermore, the genome does not seem to encode critical subunits of the F_oF_1 ATP synthase[13,14]. Yet, the mitochondrial electron transport chain is critical for parasite survival: inhibition of the cytochrome bc_1 complex (Complex III) is the mode of action for a currently used antimalarial drug, atovaquone[15,16]. The parasite encodes at least five mitochondrial dehydrogenases (a rotenone-insensitive NADH dehydrogenase, glycerol 3-phosphate dehydrogenase, dihydroorotate dehydrogenase, succinate dehydrogenase and malate-quinone oxidoreductase); all five enzymes generate reduced coenzyme Q (CoQ), which in turn is re-oxidized by Complex III, feeding the electron transport chain[14] . Dihydroorotate dehydrogenase (DHOD), the fourth enzyme in the pyrimidine biosynthetic pathway, is essential for malaria parasites' survival because they cannot salvage pyrimidines[17]. Although most eukaryotes possess a mitochondrially located, membrane-anchored type 2 DHOD that uses CoQ as the electron acceptor, many bacteria encode a soluble DHOD that is independent of CoQ, using fumarate as the electron acceptor[8] (type 1A, see Fig. 1a). The yeast *S. cerevisiae* seems to have acquired the type 1A DHOD, possibly through a lateral gene transfer from a prokaryote[18]. We cloned the yeast DHOD gene under the control of a constitutive *P. falciparum* promoter in a shuttle vector[19] that permitted generation of stably transfected parasites using the antifolate WR99210 as a selective agent (see Supplementary Fig. 1). To assess the expression of the transgene, it was fused to a gene encoding green fluorescent protein (GFP). As shown in Fig. 1b, RNA encoding DHOD–GFP was detectable by northern blot hybridization and the fluorescent protein could be detected in the cytosol of the transfected parasites, but not in the mitochondria (Fig. 1c). The fusion DHOD–GFP protein was enzymatically active as judged by its ability to rescue a DHOD null *S. cerevisiae* strain, allowing growth under conditions requiring *de novo* pyrimidine biosynthesis (see Supplementary Fig. 2).

We examined the transgenic *P. falciparum* for their susceptibility to atovaquone in a standard 48 h growth inhibition assay measuring ^{3}H-hypoxanthine incorporation. Whereas the parental parasites were fully susceptible to atovaquone with a midpoint inhibition concentration (IC_{50}) of about 1 nM, the transgenic parasites were not inhibited by even the highest concentrations (2,250 nM) of atovaquone (Fig. 2a). Transgenic parasites expressing GFP alone or fused to unrelated genes were equally susceptible to atovaquone as the parental parasites (data not shown), ruling out the possibility that the resistance was due to the expression of GFP or the transfection

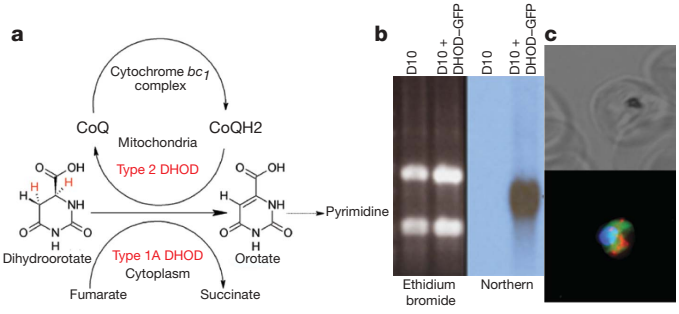

Figure 1 | Transgenic *P. falciparum* expressing *S. cerevisiae* DHOD. **a**, Oxidation of dihydroorotate by Type 1A and Type 2 DHOD is carried out in different cellular locations using different electron acceptors. **b**, The transgene is expressed as a 2.7 kilobase RNA as judged by a northern blot probed with *S. cerevisiae* DHOD DNA. D10 is the parental parasite and D10 + DHOD–GFP is the transgenic parasite line. **c**, The yeast DHOD is localized to the cytoplasm of the transgenic parasite. A phase contrast image of an intraerythrocytic parasite (top), and a confocal image (bottom) of the same parasite showing Mitotracker (red), GFP tag (green) and nuclear (blue) staining.

[1]Center for Molecular Parasitology, Department of Microbiology and Immunology, Drexel University College of Medicine, Philadelphia, Pennsylvania 19129, USA.

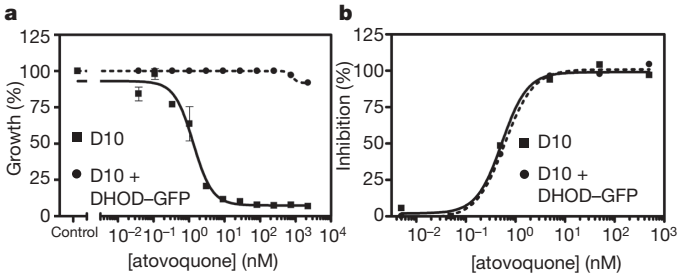

Figure 2 | Transgenic parasites are resistant to atovaquone. a, Parasite growth was assessed by ^{3}H-hypoxanthine incorporation when exposed to varying concentrations of drug for 48 h. The parental D10 line was highly susceptible whereas the transgenic D10 + DHOD–GFP was fully resistant to the compound ($\chi^2 = 1.36 \times 10^4$; $P < 0.0001$). Error bars indicate ± s.e.m. ($n = 3$). **b**, The profiles of inhibition by atovaquone of the cytochrome bc_1 complex activity of mitochondria isolated from the parental (D10) and transgenic (D10 + DHOD–GFP) parasites were indistinguishable from each other ($P > 0.999$), showing that the resistance of the transgenic parasites to atovaquone was not due to the resistance of Complex III.

process itself. Because atovaquone resistance in *P. falciparum* can arise quickly both *in vivo* and *in vitro* through point mutations in the mtDNA-encoded cytochrome *b* (ref. 20), we amplified and sequenced this gene from the DHOD-transgenic parasites, but failed to detect any mutations. To examine the possibility that the resistance may be due to mutations elsewhere in the genome, we isolated mitochondria from the parental and transgenic parasites to assess atovaquone inhibition of the Complex III activity and found it to be equally susceptible to atovaquone in both cases (Fig. 2b). We further assessed the susceptibility of the transgenic parasites to other electron transport inhibitors, such as antimycin and myxothiazol, that act at sites different from atovaquone, and found the parasites to be resistant to all these compounds at concentrations > 1,000-fold higher than the IC_{50} for the parental parasites (Table 1). These results suggest that the cytosolic bypass provided by DHOD was sufficient to serve the critical pyrimidine biosynthetic pathway, and that the erythrocytic stages of such parasites became independent of mitochondrial electron transport. At this point, it remains to be tested whether non-erythrocytic life cycle stages of *P. falciparum* could also be rendered independent of mitochondrial electron transport solely through a cytosolic bypass for pyrimidine synthesis. Our results validate the parasite DHOD being investigated as an attractive drug target[21]. On the other hand, the ability of DHOD-transgenic parasites to survive mitochondrial electron transport inhibition suggests that other CoQ-requiring mitochondrial dehydrogenases, such as the single-subunit NADH dehydrogenase and malate-quinone oxidoreductase, are not essential for the growth of erythrocytic stages of *P. falciparum*, and thus not likely to be attractive drug targets.

In the antimalarial drug registered as Malarone, atovaquone is combined with a synergistic partner, proguanil, which we have previously shown to act by lowering the concentration at which atovaquone collapses mitochondrial membrane potential in a rodent malaria model[22]. Proguanil is a prodrug that is converted by a human cytochrome P450 to cycloguanil, which inhibits the parasite dihydrofolate reductase. The synergistic action of proguanil, however, is due to its prodrug form; cycloguanil does not show synergy with atovaquone[22]. We assessed the susceptibility of DHOD-transgenic parasites to proguanil in both the presence and absence of atovaquone. As shown in Fig. 3a, proguanil alone had similar IC_{50} values, ~55 μM, for both the transgenic and parental parasites. Remarkably, when 100 nM atovaquone was included in the medium for the transgenic parasites, the IC_{50} for proguanil was reduced 1,000-fold to 45 nM. Inclusion of 1 μM proguanil decreased the IC_{50} of atovaquone from 1.3 nM to 0.23 nM in the wild-type parasites, but from > 2,250 nM to 0.68 nM in the transgenic parasites (Fig. 3b and Table 1). Similar reductions in IC_{50} values were also seen in the transgenic parasites exposed to 1 μM proguanil and varying concentrations of antimycin and myxothiazol, which by themselves were ineffective against the transgenic parasites (Table 1). These results suggest that proguanil affects a mitochondrial function that becomes essential only when mitochondrial electron transport is inhibited. Maintenance of electropotential across the mitochondrial inner membrane is a critical function of the electron transport chain[23]. When we examined the transgenic parasites treated with atovaquone, mitochondrial membrane potential, as judged by accumulation of a lipophilic cationic compound (Mitotracker) within the mitochondria, was not eliminated, a phenomenon also observed in parental parasites (Fig. 3c). However, the combination of atovaquone and proguanil seemed to be highly effective in collapsing mitochondrial membrane potential. Mitochondrial membrane potential collapse was observable within 15 min of treatment with atovaquone plus proguanil, with 75% of the parasites losing the potential in 2 h of treatment (see Supplementary Fig. 3). Mitotracker staining in these parasites was diffused all throughout the parasite cytoplasm because the intact plasma membrane electropotential[24] drove Mitotracker

Table 1 | Growth inhibition of parental and transgenic *P. falciparum*

Parasite Strain	Proguanil (1 μM)	IC_{50} (nM)			
		Atovaquone	Myxothiazol	Antimycin	Chloroquine
D10	−	1.3	37.2	129.4	87.0
D10	+	0.23	14.9	71.45	62.6
D10 + DHOD–GFP	−	>2,250	>3,300	>33,300	62.1
D10 + DHOD–GFP	+	0.68	21.9	67.44	62.7

The growth of parental (D10) and transgenic (D10 + DHOD–GFP) parasites exposed to various inhibitors was examined by assessing ^{3}H-hypoxanthine incorporation. Midpoint inhibition concentrations (IC_{50}) of the compounds in the absence and presence of 1 μM proguanil were determined.

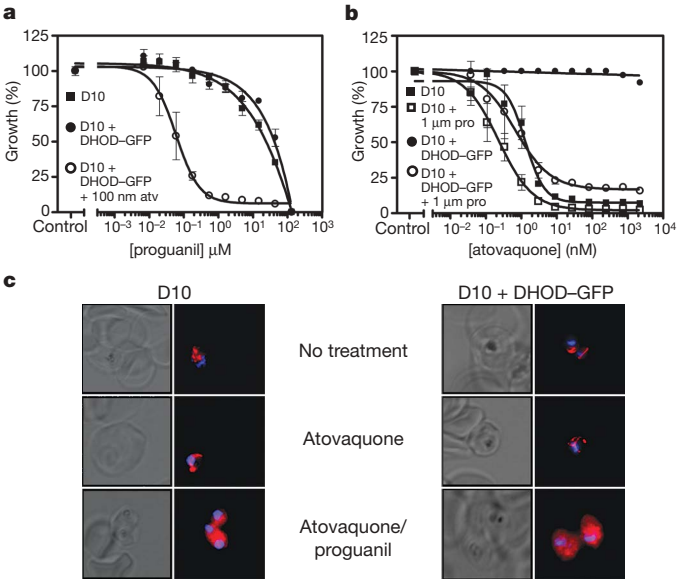

Figure 3 | Extreme hypersensitivity of the transgenic parasites to atovaquone/proguanil combination. a, Both the parental and transgenic parasites showed comparable responses to proguanil. Inclusion of 100 nM of atovaquone reduced the proguanil IC_{50} by 1,000-fold in transgenic parasites ($P < 0.0001$). **b**, Inclusion of 1 μM proguanil reduced the IC_{50} of atovaquone by about sixfold in the parental parasites, but by > 3,300-fold in the transgenic parasites ($P < 0.0001$). Error bars indicate ± s.e.m. ($n = 3$). **c**, Mitochondrial membrane potential assessed by the accumulation of Mitotracker is maintained in both the parental and transgenic parasites incubated for 24 h with 100 nM atovaquone. Incubation with atovaquone and proguanil eliminated mitochondrial membrane potential; cytoplasmic accumulation of the probe is driven by the plasma membrane potential of the parasite[23].

accumulation inside the parasite, but the lack of mitochondrial membrane potential precluded its concentration within the mitochondria. These results suggest a proguanil-sensitive pathway for generating mitochondrial membrane potential in malaria parasites that is independent of the electron transport chain.

In many eukaryotes, when electron transport is rendered nonfunctional, mitochondrial membrane potential can be maintained for a period by the reverse action of F_oF_1 ATP synthase using ATP hydrolysis to pump protons[23]. This may be unlikely in *P. falciparum* because mitochondrial ATP synthesis appears to be absent[12], and a complete F-type ATP synthase does not seem to be present[13,14]. Yet, genes encoding parts of the F_1 domain of the enzyme complex, especially the α and β subunits that possess the ATPase activity, are clearly present in *Plasmodium*. Even in *Cryptosporidium*, a genus that has lost mtDNA in its entirety, genes encoding α and β subunits of ATP synthase as well as an ATP/ADP translocator seem to be still maintained. Interestingly, *Cryptosporidium* does not depend on *de novo* pyrimidine biosynthesis, having acquired pyrimidine salvage enzymes through apparent lateral gene transfers[25]. A vestigial mitochondrial structure continues to be maintained in *Cryptosporidium*[26], most probably to serve the generation, assembly and transport of iron–sulphur clusters, an essential pathway that requires electropotential across the inner mitochondrial membrane[27]. We propose that this electropotential is established through a combined action of the matrix-located F_1 sector of ATP synthase and the membrane-located ATP/ADP transporter (see Supplementary Fig. 4 for a model). In our proposal, ATP will be hydrolysed by the ATP synthase and ADP^{3-} generated will be exchanged for ATP^{4-} by the ATP/ADP transporter, resulting in a net negative charge gain for the matrix, thereby establishing the membrane potential, which after all requires the movement of but a few ions across the membrane[23]. A similar means to establish mitochondrial membrane potential has been suggested in *Saccharomyces*[28] and *Trypanosoma*[29] that lack mtDNA. Because the electron transport chain in *P. falciparum* is dominant in establishing the membrane potential, the alternative (proguanil-sensitive) pathway becomes apparent only when electron transport is inhibited. On the other hand, the lack of mtDNA, and thus the electron transport chain, in *Cryptosporidium* makes the alternative pathway for generating membrane potential the only route available. By providing a means to acquire independence from the electron transport chain for membrane potential generation in DHOD-transgenic *P. falciparum*, we may have experimentally achieved a condition that *Cryptosporidium* seems to have achieved through evolution.

The loss of the mitochondrial genome seems to have occurred in many single cell eukaryotes[30]. At the evolutionary scale, Apicomplexan parasites appear to be in the process of minimizing mitochondrial contributions to their physiology. In erythrocytic stages of *P. falciparum*, mitochondrial electron transport can be rendered unnecessary by acquisition of just one metabolic enzyme. It would seem that the only function of mtDNA, which is the provision of a few subunits of the electron transport chain, could be made superfluous by lateral gene transfers that bypass the need for electron transport. The system described here now provides means to investigate what other metabolic adjustments need to be made for the optimal functioning of an organism lacking mitochondrial electron transport.

METHODS

Detailed methods and procedures are provided in Supplementary Information.

Transgene construction. The plasmid pHHMC*/3R0.5 was used as the vector[19]. Genes encoding GFP and *S. cerevisiae* DHOD were PCR amplified, and cloned as a translational fusion into the unique *Bst*B1 and *Xho*I sites of the vector, placing the transcription of the fused gene under the control of a *P. falciparum Hsp86* promoter, yielding the plasmid pHHyDHOD–GFP. The plasmid contains a human dihydrofolate reductase gene as a WR99210-selectable marker.

Parasite culture and transfection. *P. falciparum* clone D10 and its transgenic derivative were cultured in human erythrocytes at 5% hematocrit in RPMI1640 medium containing 0.5% Albumax. Transfection was carried out through electroporation of the purified pHHyDHOD–GFP plasmid into ring stages of *P. falciparum* using a BioRad GenePulser.

Growth inhibition assays. Parasite growth as measured by ^{3}H-hypoxanthine incorporation was assessed by incubation with various doses of inhibitors over a 48 h period.

Parasite mitochondrial isolation and biochemical assay. Mitochondria from parental and transgenic *P. falciparum* trophozoite stages were isolated by a method that employed nitrogen cavitation of parasites, magnetic hemozoin removal and differential centrifugation. See Supplementary Information for details. Cytochrome bc_1 complex activity was assessed by reduction of cytochrome *c* using a synthetic ubiquinol as the electron donor. Inhibition of this activity by atovaquone was assayed at various concentration of the inhibitor.

Microscopic localization and membrane potential assessment. The localization of the DHOD–GFP was carried out by immunofluorescence using an anti-GFP antibody. Membrane potential was assessed by accumulation of MitoTracker (Molecular Probes) as described in Supplementary Information. Confocal microscopic images were obtained with an Olympus system and deconvoluted using SlideBook software.

Received 10 October 2006; accepted 5 January 2007.

1. Martin, W. & Müller, M. The hydrogen hypothesis for the first eukaryote. *Nature* **392,** 37–41 (1998).
2. Embley, T. M. & Martin, W. Eukaryotic evolution, changes and challenges. *Nature* **440,** 623–630 (2006).
3. Lane, N. *Power, Sex, Suicide: Mitochondria and the Meaning of Life* (Oxford Univ. Press, New York, 2005).
4. Vaidya, A. B. & Arasu, P. Tandemly arranged gene clusters of malarial parasites that are highly conserved and transcribed. *Mol. Biochem. Parasitol.* **22,** 249–257 (1987).
5. Vaidya, A. B., Akella, R. & Suplick, K. Sequences similar to genes for two mitochondrial proteins and portions of ribosomal RNA in tandemly arrayed 6-kilobase-pair DNA of a malarial parasite. *Mol. Biochem. Parasitol.* **35,** 97–107 (1989).
6. Xu, P. *et al.* The genome of *Cryptosporidium hominis*. *Nature* **431,** 1107–1112 (2004).
7. Abrahamsen, M. S. *et al.* Complete genome sequence of the apicomplexan, *Cryptosporidium parvum*. *Science* **304,** 441–445 (2004).
8. Nagy, M., Lacroute, F. & Thomas, D. Divergent evolution of pyrimidine biosynthesis between anaerobic and aerobic yeasts. *Proc. Natl Acad. Sci. USA* **89,** 8966–8970 (1992).
9. Wilson, R. J. & Williamson, D. H. Extrachromosomal DNA in the Apicomplexa. *Microbiol. Mol. Biol. Rev.* **61,** 1–16 (1997).
10. Wilson, R. J. Progress with parasite plastids. *J. Mol. Biol.* **319,** 257–274 (2002).
11. Vaidya, A. B., Lashgari, M. S., Pologe, L. G. & Morrisey, J. Structural features of *Plasmodium* cytochrome b that may underlie susceptibility to 8-aminoquinolines and hydroxynaphthoquinones. *Mol. Biochem. Parasitol.* **58,** 33–42 (1993).
12. Fry, M., Webb, E. & Pudney, M. Effect of mitochondrial inhibitors on adenosinetriphosphate levels in *Plasmodium falciparum*. *Comp. Biochem. Physiol. B* **96,** 775–782 (1990).
13. Gardner, M. J. *et al.* Genome sequence of the human malaria parasite *Plasmodium falciparum*. *Nature* **419,** 498–511 (2002).
14. Vaidya, A. B. & Mather, M. W. A. Post-genomic view of the mitochondrion in malaria parasites. *Curr. Top. Microbiol. Immunol.* **295,** 233–250 (2005).
15. Fry, M. & Pudney, M. Site of action of the antimalarial hydroxynaphthoquinone, 2-[trans-4-(4′-chlorophenyl) cyclohexyl]-3-hydroxy-1,4-naphthoquinone (566C80). *Biochem. Pharmacol.* **43,** 1545–1553 (1992).
16. Vaidya, A. B. in *Malaria: Parasite biology, Pathogenesis, and Protection* (ed. Sherman, I. W.) 355–368 (ASM Press, Washington DC, 1998).
17. Gutteridge, W. E., Dave, D. & Richards, W. H. Conversion of dihydroorotate to orotate in parasitic protozoa. *Biochim. Biophys. Acta* **582,** 390–401 (1979).
18. Gojkovic, Z. *et al.* Horizontal gene transfer promoted evolution of the ability to propagate under anaerobic conditions in yeasts. *Mol. Genet. Genomics* **271,** 387–393 (2004).
19. O'Donnell, R. A. *et al.* A genetic screen for improved plasmid segregation reveals a role for Rep20 in the interaction of *Plasmodium falciparum* chromosomes. *EMBO J.* **21,** 1231–1239 (2002).
20. Vaidya, A. B. & Mather, M. W. Atovaquone resistance in malaria parasites. *Drug Resist. Updat.* **3,** 283–287 (2000).
21. Baldwin, J. *et al.* High-throughput screening for potent and selective inhibitors of *Plasmodium falciparum* dihydroorotate dehydrogenase. *J. Biol. Chem.* **280,** 21847–21853 (2005).
22. Srivastava, I. K. & Vaidya, A. B. A mechanism for the synergistic antimalarial action of atovaquone and proguanil. *Antimicrob. Agents Chemother.* **43,** 1334–1339 (1999).
23. Nicholls, D. G. & Ferguson, S. J. *Bioenergetics 3* (Academic Press, London, 2002).
24. Allen, R. J. & Kirk, K. The membrane potential of the intraerythrocytic malaria parasite *Plasmodium falciparum*. *J. Biol. Chem.* **279,** 11264–11272 (2004).
25. Striepen, B. *et al.* Gene transfer in the evolution of parasite nucleotide biosynthesis. *Proc. Natl Acad. Sci. USA* **101,** 3154–3159 (2004).
26. Keithly, J. S., Langreth, S. G., Buttle, K. F. & Mannella, C. A. Electron tomographic and ultrastructural analysis of the *Cryptosporidium parvum* relict mitochondrion,

its associated membranes, and organelles. *J. Eukaryot. Microbiol.* **52,** 132–140 (2005).
27. Lill, R. & Muhlenhoff, U. Iron–sulfur-protein biogenesis in eukaryotes. *Trends Biochem. Sci.* **30,** 133–141 (2005).
28. Giraud, M. F. & Velours, J. The absence of the mitochondrial ATP synthase delta subunit promotes a slow growth phenotype of rho- yeast cells by a lack of assembly of the catalytic sector F_1. *Eur. J. Biochem.* **245,** 813–818 (1997).
29. Schnaufer, A., Clark-Walker, G. D., Steinberg, A. G. & Stuart, K. The F_1-ATP synthase complex in bloodstream stage trypanosomes has an unusual and essential function. *EMBO J.* **24,** 4029–4040 (2005).
30. van der Giezen, M. & Tovar, J. Degenerate mitochondria. *EMBO Rep.* **6,** 525–530 (2005).

Supplementary Information is linked to the online version of the paper at www.nature.com/nature.

Acknowledgements We thank our colleagues within the Center for Molecular Parasitology, especially J. Burns and B. Bergman, for discussions, advice, and general cheer; K. Henry for providing yeast strains; and B. A. Palfey (University of Michigan) for communicating that the Type 1A DHOD is not inhibited by proguanil. This work was supported by grants from the National Institute of Allergy and Infectious Diseases to A.B.V.

Author Information Reprints and permissions information is available at www.nature.com/reprints. The authors declare no competing financial interests. Correspondence and requests for materials should be addressed to A.B.V. (avaidya@drexelmed.edu).

LETTERS

Transferrin receptor 1 is a cellular receptor for New World haemorrhagic fever arenaviruses

Sheli R. Radoshitzky[1]*, Jonathan Abraham[2]*, Christina F. Spiropoulou[3], Jens H. Kuhn[1,4], Dan Nguyen[2], Wenhui Li[1], Jane Nagel[1], Paul J. Schmidt[5], Jack H. Nunberg[6], Nancy C. Andrews[5], Michael Farzan[1] & Hyeryun Choe[2]

At least five arenaviruses cause viral haemorrhagic fevers in humans. Lassa virus, an Old World arenavirus, uses the cellular receptor α-dystroglycan to infect cells[1]. Machupo, Guanarito, Junin and Sabia viruses are New World haemorrhagic fever viruses that do not use α-dystroglycan[2]. Here we show a specific, high-affinity association between transferrin receptor 1 (TfR1) and the entry glycoprotein (GP) of Machupo virus. Expression of human TfR1, but not human transferrin receptor 2, in hamster cell lines markedly enhanced the infection of viruses pseudotyped with the GP of Machupo, Guanarito and Junin viruses, but not with those of Lassa or lymphocytic choriomeningitis viruses. An anti-TfR1 antibody efficiently inhibited the replication of Machupo, Guanarito, Junin and Sabia viruses, but not that of Lassa virus. Iron depletion of culture medium enhanced, and iron supplementation decreased, the efficiency of infection by Junin and Machupo but not Lassa pseudoviruses. These data indicate that TfR1 is a cellular receptor for New World haemorrhagic fever arenaviruses.

Arenaviruses are enveloped, single-stranded, bisegmented RNA viruses[3]. The family Arenaviridae consists of a single genus (Arenavirus), which includes at least 23 recognized viruses[4]. Arenaviruses have been classified into two antigenically and geographically distinct groups, the Lassa–lymphocytic choriomeningitis serocomplex ('Old World arenaviruses') and the Tacaribe serocomplex ('New World arenaviruses'). Five arenaviruses are known to cause acute viral haemorrhagic fever in humans, with case-fatality rates as high as 30%. Lassa virus (LASV) is an Old World arenavirus that causes Lassa fever. Machupo (MACV), Guanarito (GTOV), Junin (JUNV) and Sabia (SABV) viruses are New World arenaviruses that cause Bolivian, Venezuelan, Argentinian and Brazilian haemorrhagic fever, respectively. LASV, MACV, GTOV and JUNV have been classified as National Institute of Allergy and Infectious Diseases Category A Priority Pathogens, in part because of their lethality and significant potential for misuse[4,5].

The arenaviral entry protein GP is processed into two subunits, GP1 and GP2 (ref. 6). Like other class 1 fusion proteins, GP1 is thought to mediate association with a cellular receptor[7]. After internalization of the virus to an acidified endosomal compartment, GP2 undergoes a conformational change that promotes fusion of the viral and cellular membranes[7–9]. We characterized a series of MACV GP1 truncation variants, fused at their carboxy termini to the Fc domain of human IgG1 (Fig. 1a). Only full-length MACV GP1 (residues 59–258) and a single truncation variant, GP1Δ (residues 79–258), efficiently bound MACV-permissive Vero African green monkey kidney cells, whereas GP1 variants expressing residues 102–258, 121–258, 59–170 or 59–205 did not (Supplementary Fig. 1a). GP1Δ bound Vero cells saturably and more efficiently than GP1 (Fig. 1b). GP1Δ, but not the receptor-binding domains of Lake Victoria marburgvirus or severe acute respiratory syndrome (SARS) coronavirus entry proteins, precipitated from Vero cells a protein of 95 kDa under reducing conditions, and approximately 200 kDa under non-reducing conditions (Fig. 1c). Mass-spectrometric analysis identified this protein as TfR1 (CD71). MACV GP1 efficiently bound a Chinese hamster ovary (CHO) cell line stably expressing human TfR1 (CHO-hTfR1)[10] but did not bind parental CHO cells, confirming a high-affinity association between MACV GP1 and human TfR1 (Fig. 1d).

We then sought to identify cell lines that were non-permissive to infection by a murine retrovirus pseudotyped with MACV GP. Consistent with previous studies[11,12] was our observation that murine NIH 3T3 cells and baby hamster kidney (BHK-S) and CHO cell lines were relatively non-permissive to MACV pseudovirus and did not bind MACV GP1. Vero, rhesus macaque LLC-MK2, and human HeLa and 293T cell lines efficiently bound GP1 and were permissive to MACV-GP-mediated infection (not shown). Consistent with the binding study in Fig. 1d was our observation that CHO-hTfR1 cells, but not parental CHO cells, were efficiently infected by MACV pseudoviruses, whereas LASV and lymphocytic choriomeningitis virus (LCMV) pseudoviruses infected CHO-hTfR1 and parental cells comparably (Fig. 2a). We investigated the ability of an anti-human TfR1 antibody and a control anti-HLA (anti-human leukocyte antigen) antibody to inhibit infection mediated by MACV and LASV GP proteins. Both antibodies efficiently bound HeLa and 293T cells (Fig. 2b, upper panels) but only the anti-human TfR1 antibody inhibited infection by MACV pseudovirus (Fig. 2b, lower panels). The anti-human TfR1 antibody had no effect on LASV pseudovirus infection. Together, these data indicate that TfR1 is a necessary receptor for MACV.

To determine whether TfR1 contributed to infection by other New World arenaviruses, we investigated infection by JUNV pseudovirus, as well as replication of infectious arenaviruses. Infection of CHO-hTfR1 cells by JUNV, but not LASV, pseudovirus was substantially more efficient than infection of parental CHO cells (Fig. 3a). Like MACV pseudovirus, JUNV pseudovirus infection of 293T cells was inhibited by anti-human TfR1 antibody (Fig. 3b). Replication of infectious MACV, GTOV, JUNV and SABV in 293T cells was markedly inhibited by anti-human TfR1 antibody, but not by anti-HLA antibody (Fig. 3c). Nearly identical results were obtained with HeLa cells (not shown). These data indicate that TfR1 is an obligate receptor for each of these New World haemorrhagic fever arenaviruses,

[1]Department of Microbiology and Molecular Genetics, Harvard Medical School, New England Primate Research Center, Southborough, Massachusetts 01772, USA. [2]Pulmonary Division, Children's Hospital, Department of Pediatrics, Harvard Medical School, Boston, Massachusetts 02115, USA. [3]Special Pathogens Branch, Centers for Disease Control and Prevention, Atlanta, Georgia 30333, USA. [4]Department of Biology, Chemistry, Pharmacy, Freie Universität Berlin, 14195 Berlin, Germany. [5]Division of Hematology/Oncology, Children's Hospital, Department of Pediatrics, Harvard Medical School, Boston, Massachusetts 02115, USA. [6]Montana Biotechnology Center, The University of Montana, Missoula, Montana 59812, USA.
*These authors contributed equally to this work.

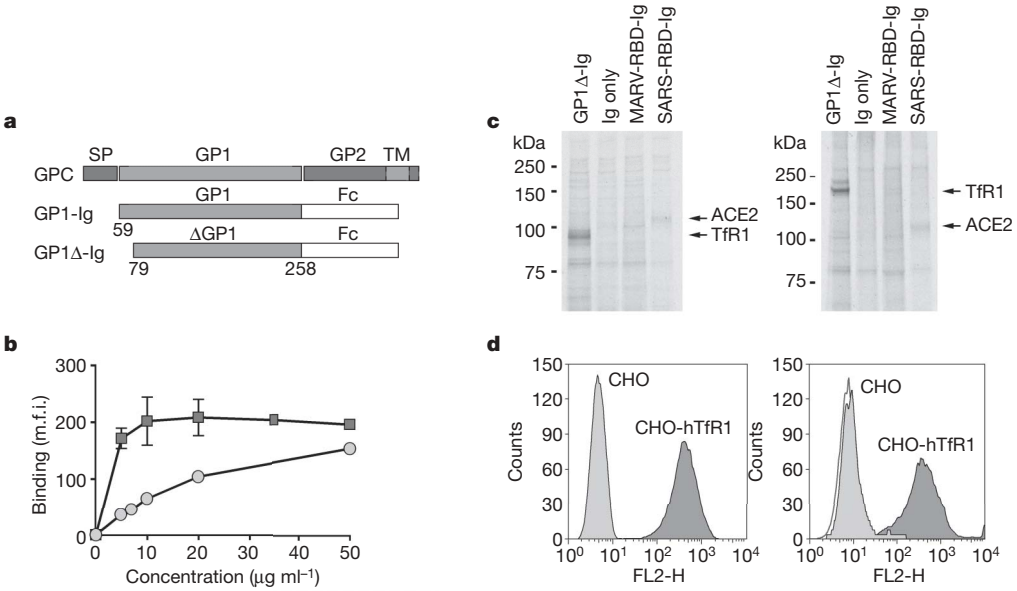

Figure 1 | MACV GP1 and GP1Δ efficiently bind TfR1. **a**, Schematic representation of MACV glycoprotein precursor (GPC), GP1-Ig and GP1Δ-Ig. Locations of the signal peptide (SP), the GP1 and GP2 domains and the transmembrane domain (TM) are indicated. **b**, Vero cells analysed by flow cytometry with the use of the indicated concentrations of purified GP1-Ig (circles) or GP1Δ-Ig (squares). m.f.i., mean fluorescence intensity. Error bars indicate standard deviation. **c**, Vero cells were metabolically labelled, incubated with GP1Δ-Ig or the indicated control Ig-fusion proteins, lysed, immunoprecipitated, and analysed by SDS–PAGE under reducing (left) or non-reducing (right) conditions. **d**, Binding of anti-human TfR1 antibody (left) and MACV GP1-Ig (right) to CHO (light grey) or CHO-hTfR1 (dark grey) cells analysed by flow cytometry. The unfilled curve in the right-hand panel is secondary antibody alone.

despite the diversity of their GP1 proteins, but are consistent with previous studies indicating that these viruses use a common cellular receptor[11,12].

Transferrin receptor 2 (TfR2) is similar (54% identity) to TfR1 and binds transferrin. We examined its role in MACV, GTOV or JUNV GP-mediated entry. Infection by MACV, JUNV, LASV, GTOV or

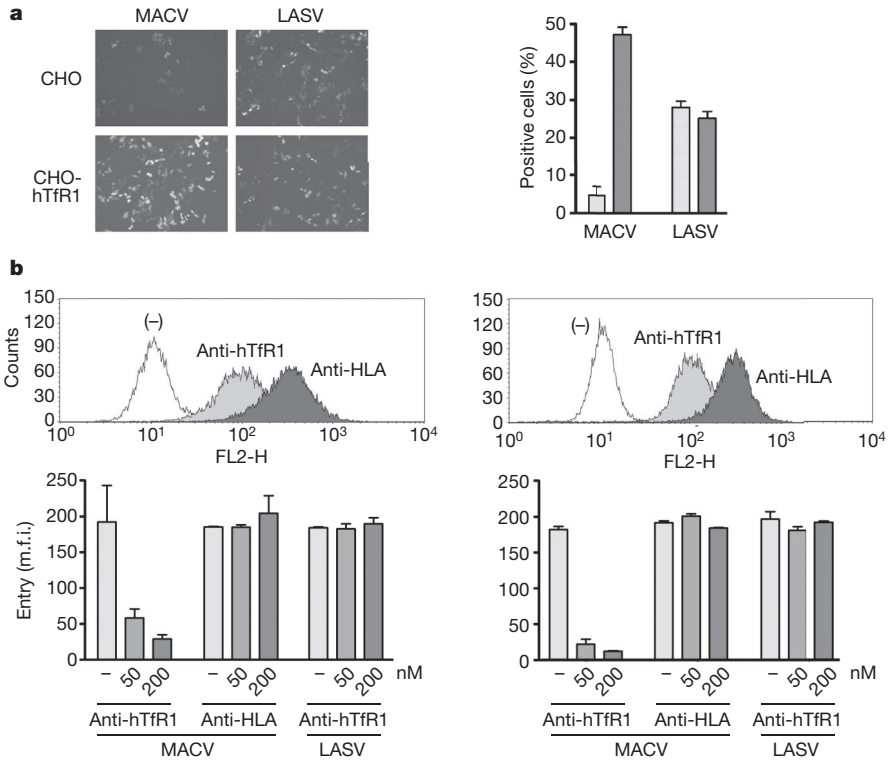

Figure 2 | MACV pseudovirus entry depends on human TfR1. **a**, Parental CHO or CHO-hTfR1 cells were incubated with MACV or LASV pseudoviruses expressing GFP. Infection level was assessed two days later by flow cytometry. Left: fluorescent micrographs of infected cells. Right: results of flow cytometric analysis of the same cells; light grey bars, CHO; dark grey bars, CHO-hTfR1. **b**, Top: analysis of HeLa cells (left) and 293T cells (right) with anti-human TfR1 and anti-HLA-A,B,C antibodies. Bottom: infection of these cells incubated with the MACV or LASV pseudoviruses in the presence of the indicated concentrations of antibodies, measured as GFP fluorescence. m.f.i., mean fluorescence intensity. Error bars indicate standard deviation.

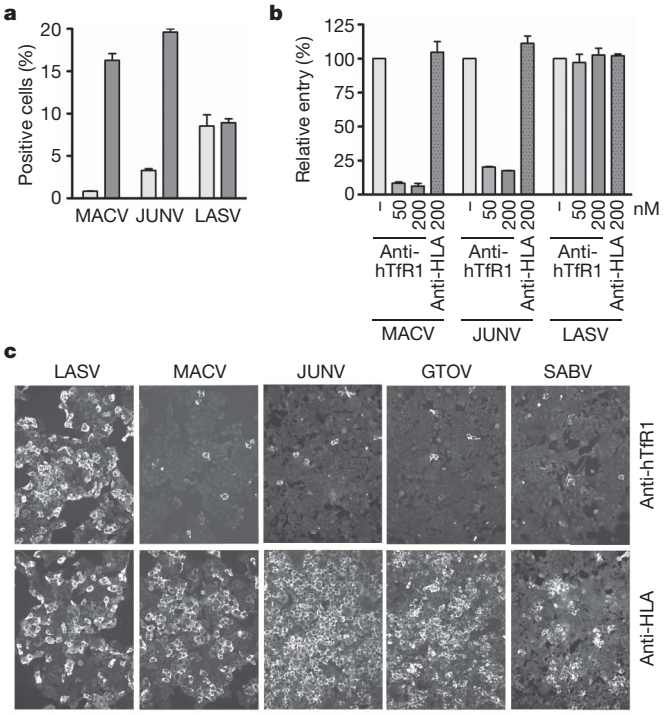

Figure 3 | JUNV, GTOV and SABV use human TfR1. **a**, CHO cells (light grey bars) and CHO-hTfR1 cells (dark grey bars) were incubated with indicated pseudoviruses, and infection level was assessed two days later by flow cytometry. **b**, 293T cells were incubated with the indicated concentrations of anti-human TfR1 or control antibody, pseudoviruses were added, and infection was measured as described for Fig. 2b. **c**, 293T cells were incubated in the presence of the indicated antibody at 200 nM, infectious viruses were added, and incubation was continued for 24 h. Cells were washed, fixed and stained as described in Methods. Error bars indicate standard deviation.

LCMV pseudoviruses was not enhanced by the introduction of human TfR2 in CHO or BHK cells (Fig. 4a) despite its efficient expression (Supplementary Fig. 1b). LCMV has been proposed to use a receptor in addition to α-dystroglycan[11], but no enhancement of LCMV pseudovirus entry was observed in the presence of human TfR1, indicating that this alternative receptor is not human TfR1. Transferrin is present at micromolar concentrations in human plasma[13]. We investigated whether iron-bound (holo) transferrin, which binds TfR1 with high affinity, or apo-transferrin, which does not, could modulate the infection of MACV pseudoviruses. Holo-transferrin did not interfere with the binding of MACV-GP1 or LASV-GP1 to 293T cells (not shown). Neither holo-transferrin nor apo-transferrin interfered with or enhanced infection with MACV pseudoviruses (Fig. 4b). Soluble TfR1 is also found in plasma at concentrations of about 20 nM, and up to 150 nM in anaemic individuals[14]. Soluble TfR1 inhibited the infection of 293T cells by JUNV and, to a smaller extent, MACV pseudoviruses (Fig. 4c). No inhibition of LASV pseudovirus infection was observed.

Depletion of iron in culture medium or *in vivo* has been shown to upregulate the cell-surface or tissue expression of TfR1 (refs 15–17). We investigated the effect of iron depletion on MACV, JUNV and LASV GP-mediated infection. JUNV pseudovirus more efficiently infected 293T cells and SLK human endothelial cells preincubated with the iron chelator deferoxamine (Fig. 5a), used clinically to treat iron toxicity[18]. However, treatment with deferoxamine consistently had a more modest effect on MACV pseudovirus infection. The basis of the lower sensitivity of MACV pseudovirus infection to deferoxamine is not clear, but it may indicate a role for an additional factor, limiting in these assays, in the entry of MACV. LASV infection was unaffected by deferoxamine at all concentrations. We also investigated the ability of excess iron to modulate GP-mediated infection. Ferric ammonium citrate, which downregulates TfR1 (ref. 19), efficiently inhibited MACV and JUNV pseudovirus infection but not that of LASV or LCMV. These data show that iron concentrations can modulate the efficiencies of MACV and JUNV infection.

Collectively our data indicate that TfR1 is a necessary cellular receptor for the four New World arenaviruses that cause haemorrhagic fevers in humans. Several properties of TfR1 indicate its possible role in arenaviral replication and disease. It is rapidly and constitutively endocytosed to an acidic compartment, which is consistent with the pH dependence of arenavirus entry[8]. It is expressed ubiquitously, and at high levels on activated or rapidly dividing cells, including macrophages and activated lymphocytes, major targets of

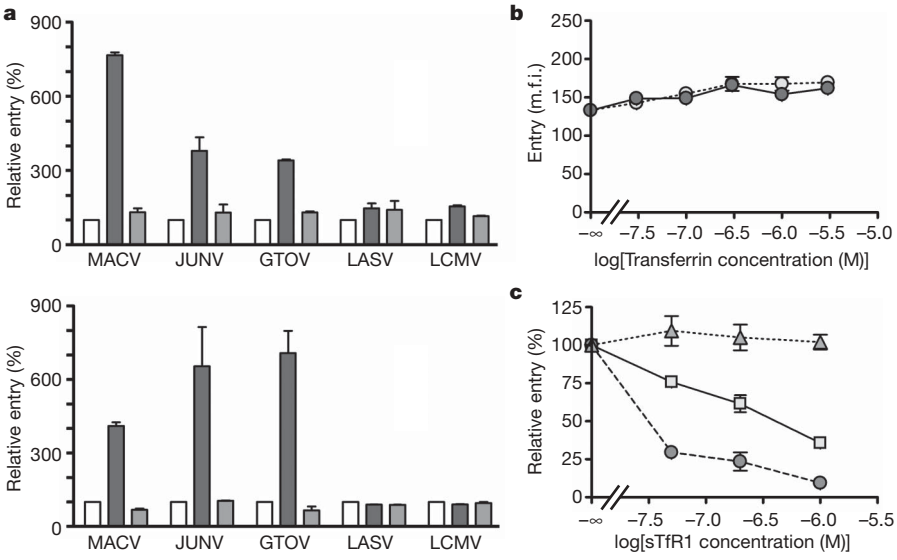

Figure 4 | Soluble human TfR1, but not transferrin or human TfR2, modulates New World arenavirus infection. **a**, CHO cells (top) and BHK cells (bottom) were transfected with plasmids expressing human TfR1 (dark grey bars) or TfR2 (light grey bars) or with vector alone (white bars), and incubated with the indicated pseudoviruses. Entry was measured as in Fig. 2a. **b**, 293T cells were incubated for 1 h with MACV pseudovirus produced in serum-free medium and with the indicated amounts of human apo-transferrin (white circles) or holo-transferrin (grey circles) and then washed; the infection level was assessed two days later. **c**, 293T cells were infected for 1 h with LASV (triangles), MACV (squares) or JUNV (circles) preincubated with increasing concentrations of soluble human TfR1 for 30 min. Cells were washed, and GFP fluorescence was measured two days later. Error bars indicate standard deviation.

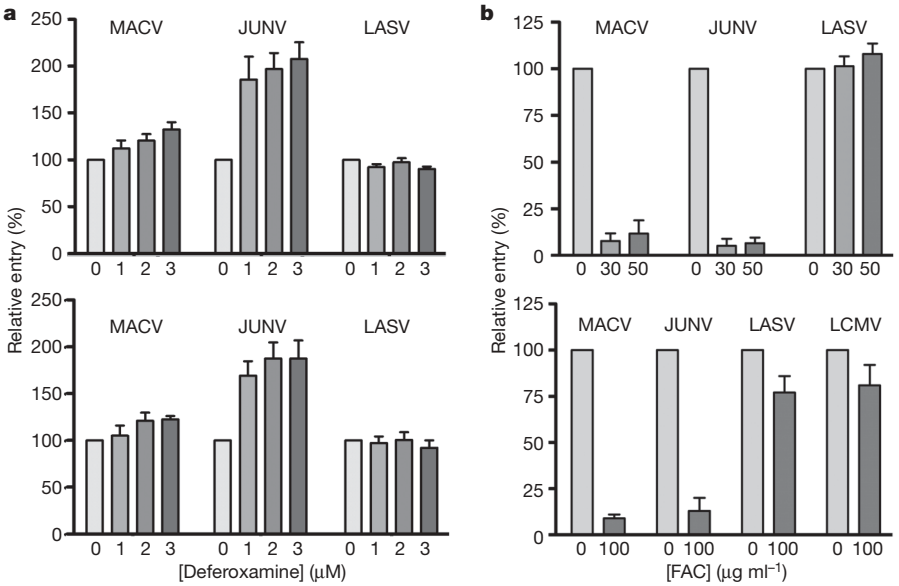

Figure 5 | Iron concentration modulates MACV and JUNV pseudovirus entry. a, Human fibroblast 293T cells (top) or endothelial SLK cells (bottom) were incubated in cell culture medium containing 10% fetal bovine serum and the indicated amounts of deferoxamine. After 24 h, cells were infected with the indicated pseudoviruses at 4 °C. Cells were washed, complete medium was added, and infection level was assessed by GFP fluorescence. Entry is normalized to that of VSV pseudovirus. Results are shown as means ± s.d. for five experiments for both cell lines. **b**, Human fibroblast 293T cells (top) or epithelial HeLa cells (bottom) were incubated for 1 h with the indicated concentrations of ferric ammonium citrate (FAC) at 37 °C, infected with the indicated pseudovirus containing FAC. Cells were washed 1 h later and infection level was assessed by GFP fluorescence two days later. Error bars indicate standard deviation.

arenaviral infection[20,21]. TfR1 is also highly expressed on endothelial cells[22,23], which are thought to be central to the pathogenesis of haemorrhagic fever[24]. TfR1 upregulation on immune cells activated in response to infection may accelerate viral replication in these cells and may in part explain the higher lethality of New World haemorrhagic fevers compared with Lassa fever. Some of these properties may also be useful to canine and feline parvoviruses and to mouse mammary tumour virus, animal viruses that also use TfR1 (refs 25, 26).

It is well established that cytosolic iron regulates TfR1 expression[16]. We show here that infection mediated by the JUNV GP was increased by depleting the culture medium of iron. These data raise the possibility that iron deficiency might therefore enhance susceptibility to or the severity of Argentine haemorrhagic fever in particular. However, soluble TfR1, which we have shown to inhibit MACV and JUNV GP-mediated infection, is also elevated in iron-deficient animals and can be found in anaemic individuals at concentrations that may inhibit JUNV replication[14]. Further studies will be necessary to clarify the role of iron deficiency as a risk factor in haemorrhagic fevers caused by New World arenaviruses. Our data also raise the possibility that iron supplementation may be useful in moderating these haemorrhagic fevers, because ferric ammonium citrate, which is used to treat anaemia in humans, markedly inhibited infection mediated by MACV and JUNV GP molecules.

Our studies suggest another approach to the treatment of, or prophylaxis for, New World haemorrhagic fevers, namely with a humanized anti-human TfR1 antibody. Several anti-human TfR1 antibodies have been developed and are currently under investigation as anti-tumour therapeutics[21]. Some of these antibodies, like the antibody used in this study, do not compete with transferrin, indicating that an anti-TfR1 antibody can limit arenaviral replication in an infected individual without interfering with iron metabolism. If so, such antibodies may be employed to limit a natural or intentional outbreak of New World haemorrhagic fever.

METHODS

Cells and plasmids. Vero cells (African green monkey kidney epithelial; CCL-81; ATCC), 293T cells (human kidney epithelial; CRL-11268; ATCC), HeLa 229 cells (human cervical epithelial; CCL-2.1; ATCC) and 3T3-Swiss cells (mouse embryo fibroblast; CCL-92; ATCC) were grown in DMEM medium; LLC-MK2 cells (rhesus monkey kidney epithelial; CCL-7; ATCC) in medium 199; BHK-21 cells (Chinese hamster kidney fibroblast; CCL-10; ATCC) and EJG cells (bovine capillary endothelial; CRL-8659; ATCC) in minimal essential medium (Eagle); SLK cells (human endothelial; NIH AIDS Research & Reference Regent Program) in RPMI medium; CHO cells (Chinese hamster ovary epithelial) in F12 medium; CHO-hTfR1 cells (a gift from T. McGraw) in F12 medium containing 400 μg ml^{-1} G418. All cell lines were grown in 10% fetal bovine serum.

MACV GPC coding sequence (residues 1–496 of Carvallo strain) was built from overlapping oligonucleotides by PCR and cloned into a pcDNA3.1 expression plasmid. MACV GP1-Ig was generated by PCR amplification of GP1 codons 59–258 and cloning into a previously described pcDM8-based plasmid expressing the CD5 signal sequence and the Fc region of human IgG1 (ref. 27). Truncation variants of GP1-Ig were generated by a modified QuickChange method (Stratagene). JUNV (MC2), GTOV (VINH-9551) and LASV (Josiah) GPC have been described previously[28,29], as have SARS-RBD-Ig and MARV-RBD-Ig (ref. 30). LCMV (Armstrong) GPC-expressing plasmid was provided by J. de la Torre. Coding regions of human TfR1 and TfR2 were cloned into pCAGGS expression plasmid. Human TfR2 gene was provided by M. Wessling-Resnick. Soluble human TfR1 (residues 121–760) with an amino-terminal Myc tag was cloned into the modified pcDM8 plasmid described above.

Immunoprecipitation and flow cytometry. Ig-fusion proteins used for immunoprecipitation and flow cytometry were produced in SFM II medium (Invitrogen) from 293T cells transfected with the appropriate plasmids. Ig-fusion proteins, bound to Protein A–Sepharose, were eluted in 3 M $MgCl_2$ and dialysed against PBS. Anti-human TfR1 (clone M-A712) and anti-HLA-A,B,C (clone G46-2.6) were purchased from BD Biosciences, and anti-human TfR2 (9F8-1C11) was purchased from Cell Sciences. Goat anti-human and anti-mouse secondary antibodies, conjugated with phycoerythrin, were purchased from Jackson Immunological Laboratories. Flow cytometry was performed in PBS containing 2% goat serum, except in experiments with apo-transferrin and holo-transferrin (Sigma), which were performed in 1% BSA.

To identify GP1Δ-Ig-binding proteins, Vero cells were labelled with [^{35}S]-Express (New England Nuclear) for one day, scraped in the presence of a protease inhibitor cocktail (Sigma), incubated on ice with GP1Δ-Ig for 1 h, lysed in 1% decyl maltopyranoside (Anatrace), precipitated with Protein–A Sepharose (Pfizer-Pharmacia) and analysed by SDS–polyacrylamide-gel electrophoresis (SDS–PAGE). For mass-spectrometric analysis, immunoprecipitates were prepared in a similar manner from unlabelled cells. Coomassie-stained SDS–PAGE bands were excised and then digested in trypsin; tryptic fragments were

identified by tandem mass spectrometry (LTQ-FT; ThermoElectron) and the SEQUEST algorithm.

Pseudovirus infection. Pseudoviruses were produced from 293T cells by transfecting at 1:1:1 ratio of plasmids expressing murine leukaemia virus *gag/pol*, arenaviral GP and pQCXIX transduction vector (BD Biosciences) expressing enhanced green fluorescent protein (EGFP), as described previously[30]. Virus-containing culture supernatant was harvested two days later, and filtered through 0.45-μm filter disks. Anti-human TfR1 and anti-HLA-A,B,C antibodies were dialysed against PBS. Cells were incubated with each of these antibodies at the indicated concentrations for 30 min at 37 °C. Pseudoviruses were added, cells were washed 16 h after infection, and entry level was measured by flow cytometry. To study the effect of tranferrin on viral entry, pseudoviruses were produced in serum-free medium (FreeStyle; Invitrogen). The role of human TfR2 was assessed in BHK cells transfected with pCAGGS-human TfR2 plasmid complexed with Lipofectamine 2000 (Invitrogen). Transfected cells were infected the next day, and the infection level was assessed two days later.

To study the role of iron in arenaviral infection, cells were incubated in complete medium containing indicated concentrations (1–3 μM) of the iron chelator deferoxamine (Sigma) for 24 h, or ferric ammonium citrate (30–100 $\mu g\,ml^{-1}$) for 1 h. Cells were cooled on ice and infected with pseudoviruses by centrifugation (2,000*g*) at 4 °C for 30 min. Cells were washed, and GFP expression level was assessed 24 h (293T and HeLa cells) or 48 h (SLK cells) after infection.

Antibody inhibition of infectious arenaviruses. All infections of 293T and HeLa cells with LASV (Josiah), MACV (Carvallo), JUNV (XJ-13) GTOV (VINH-9551) or SABV were performed in the BSL-4 laboratory at the Special Pathogens Branch, Centers for Disease Control and Prevention, Atlanta. Infections and immunofluorescence staining were performed as described previously[12]. HeLa and 293T cells were grown on gelatin-treated glass coverslips, preincubated for 30 min with the indicated antibody at 200 nM, and then infected with virus at a multiplicity of infection of 0.1–1.0. At 24 h after infection, cells were washed, fixed with 3% formaldehyde, permeabilized with 0.1% Triton X-100 and incubated with mouse hyperimmune sera specific for New World or Old World arenaviruses. Cells were then washed and incubated with fluorescein isothiocyanate-conjugated secondary antibody.

Received 4 November; accepted 18 December 2006.
Published online 7 February 2007.

1. Cao, W. *et al.* Identification of α-dystroglycan as a receptor for lymphocytic choriomeningitis virus and Lassa fever virus. *Science* **282,** 2079–2081 (1998).
2. Spiropoulou, C. F., Kunz, S., Rollin, P. E., Campbell, K. P. & Oldstone, M. B. New World arenavirus clade C, but not clade A and B viruses, utilizes α-dystroglycan as its major receptor. *J. Virol.* **76,** 5140–5146 (2002).
3. Oldstone, M. B. Arenaviruses. I. The epidemiology molecular and cell biology of arenaviruses. Introduction. *Curr. Top. Microbiol. Immunol.* **262,** v–xii (2002).
4. Charrel, R. N. & de Lamballerie, X. Arenaviruses other than Lassa virus. *Antiviral Res.* **57,** 89–100 (2003).
5. Borio, L. *et al.* Hemorrhagic fever viruses as biological weapons: medical and public health management. *J. Am. Med. Assoc.* **287,** 2391–2405 (2002).
6. Buchmeier, M. J., Southern, P. J., Parekh, B. S., Wooddell, M. K. & Oldstone, M. B. Site-specific antibodies define a cleavage site conserved among arenavirus GP-C glycoproteins. *J. Virol.* **61,** 982–985 (1987).
7. Kunz, S., Borrow, P. & Oldstone, M. B. Receptor structure, binding, and cell entry of arenaviruses. *Curr. Top. Microbiol. Immunol.* **262,** 111–137 (2002).
8. Castilla, V. & Mersich, S. E. Low-pH-induced fusion of Vero cells infected with Junin virus. *Arch. Virol.* **141,** 1307–1317 (1996).
9. Burns, J. W. & Buchmeier, M. J. Protein–protein interactions in lymphocytic choriomeningitis virus. *Virology* **183,** 620–629 (1991).
10. McGraw, T. E., Greenfield, L. & Maxfield, F. R. Functional expression of the human transferrin receptor cDNA in Chinese hamster ovary cells deficient in endogenous transferrin receptor. *J. Cell Biol.* **105,** 207–214 (1987).
11. Reignier, T. *et al.* Receptor use by pathogenic arenaviruses. *Virology* **353,** 111–120 (2006).
12. Rojek, J. M., Spiropoulou, C. F. & Kunz, S. Characterization of the cellular receptors for the South American hemorrhagic fever viruses Junin, Guanarito, and Machupo. *Virology* **349,** 476–491 (2006).
13. Kasvosve, I. & Delanghe, J. Total iron binding capacity and transferrin concentration in the assessment of iron status. *Clin. Chem. Lab. Med.* **40,** 1014–1018 (2002).
14. Raya, G., Henny, J., Steinmetz, J., Herbeth, B. & Siest, G. Soluble transferrin receptor (sTfR): biological variations and reference limits. *Clin. Chem. Lab. Med.* **39,** 1162–1168 (2001).
15. Anderson, G. J., Powell, L. W. & Halliday, J. W. Transferrin receptor distribution and regulation in the rat small intestine. Effect of iron stores and erythropoiesis. *Gastroenterology* **98,** 576–585 (1990).
16. Andrews, N. C., Fleming, M. D. & Levy, J. E. Molecular insights into mechanisms of iron transport. *Curr. Opin. Hematol.* **6,** 61–64 (1999).
17. Templeton, D. M. & Liu, Y. Genetic regulation of cell function in response to iron overload or chelation. *Biochim. Biophys. Acta* **1619,** 113–124 (2003).
18. Mattia, E., Rao, K., Shapiro, D. S., Sussman, H. H. & Klausner, R. D. Biosynthetic regulation of the human transferrin receptor by desferrioxamine in K562 cells. *J. Biol. Chem.* **259,** 2689–2692 (1984).
19. Ward, J. H., Kushner, J. P. & Kaplan, J. Regulation of HeLa cell transferrin receptors. *J. Biol. Chem.* **257,** 10317–10323 (1982).
20. Oldstone, M. B. Arenaviruses. II. The molecular pathogenesis of arenavirus infections. Introduction. *Curr. Top. Microbiol. Immunol.* **263,** V–XII (2002).
21. Daniels, T. R., Delgado, T., Rodriguez, J. A., Helguera, G. & Penichet, M. L. The transferrin receptor, part I: Biology and targeting with cytotoxic antibodies for the treatment of cancer. *Clin. Immunol.* **121,** 144–158 (2006).
22. Soda, R. & Tavassoli, M. Liver endothelium and not hepatocytes or Kupffer cells have transferrin receptors. *Blood* **63,** 270–276 (1984).
23. Jefferies, W. A. *et al.* Transferrin receptor on endothelium of brain capillaries. *Nature* **312,** 162–163 (1984).
24. Peters, C. J. & Zaki, S. R. Role of the endothelium in viral hemorrhagic fevers. *Crit. Care Med.* **30,** S268–S273 (2002).
25. Parker, J. S., Murphy, W. J., Wang, D., O'Brien, S. J. & Parrish, C. R. Canine and feline parvoviruses can use human or feline transferrin receptors to bind, enter, and infect cells. *J. Virol.* **75,** 3896–3902 (2001).
26. Ross, S. R., Schofield, J. J., Farr, C. J. & Bucan, M. Mouse transferrin receptor 1 is the cell entry receptor for mouse mammary tumor virus. *Proc. Natl Acad. Sci. USA* **99,** 12386–12390 (2002).
27. Li, W. *et al.* Angiotensin-converting enzyme 2 is a functional receptor for the SARS coronavirus. *Nature* **426,** 450–454 (2003).
28. York, J. & Nunberg, J. H. Role of the stable signal peptide of Junin arenavirus envelope glycoprotein in pH-dependent membrane fusion. *J. Virol.* **80,** 7775–7780 (2006).
29. Kunz, S., Rojek, J. M., Perez, M., Spiropoulou, C. F. & Oldstone, M. B. Characterization of the interaction of lassa fever virus with its cellular receptor α-dystroglycan. *J. Virol.* **79,** 5979–5987 (2005).
30. Wong, S. K., Li, W., Moore, M. J., Choe, H. & Farzan, M. A 193-amino acid fragment of the SARS coronavirus S protein efficiently binds angiotensin-converting enzyme 2. *J. Biol. Chem.* **279,** 3197–3201 (2004).

Supplementary Information is linked to the online version of the paper at www.nature.com/nature.

Author Information Reprints and permissions information is available at www.nature.com/reprints. The authors declare no competing financial interests. Correspondence and requests for materials should be addressed to H.C. (hyeryun.choe@childrens.harvard.edu).

LETTERS

The molecular organization of cypovirus polyhedra

Fasséli Coulibaly[1], Elaine Chiu[1], Keiko Ikeda[2], Sascha Gutmann[3], Peter W. Haebel[4], Clemens Schulze-Briese[3], Hajime Mori[5] & Peter Metcalf[1]

Cypoviruses and baculoviruses are notoriously difficult to eradicate because the virus particles are embedded in micrometre-sized protein crystals called polyhedra[1,2]. The remarkable stability of polyhedra means that, like bacterial spores, these insect viruses remain infectious for years in soil. The environmental persistence of polyhedra is the cause of significant losses in silkworm cocoon harvests but has also been exploited against pests in biological alternatives to chemical insecticides[3,4]. Although polyhedra have been extensively characterized since the early 1900s[5], their atomic organization remains elusive[6]. Here we describe the 2 Å crystal structure of both recombinant and infectious silkworm cypovirus polyhedra determined using crystals 5–12 micrometres in diameter purified from insect cells. These are the smallest crystals yet used for *de novo* X-ray protein structure determination[7]. We found that polyhedra are made of trimers of the viral polyhedrin protein and contain nucleotides. Although the shape of these building blocks is reminiscent of some capsid trimers, polyhedrin has a new fold and has evolved to assemble *in vivo* into three-dimensional cubic crystals rather than icosahedral shells. The polyhedrin trimers are extensively cross-linked in polyhedra by non-covalent interactions and pack with an exquisite molecular complementarity similar to that of antigen–antibody complexes. The resulting ultrastable and sealed crystals shield the virus particles from environmental damage. The structure suggests that polyhedra can serve as the basis for the development of robust and versatile nanoparticles for biotechnological applications[8] such as microarrays[9] and biopesticides[4].

Cypoviruses (cytoplasmic polyhedrosis virus, CPV) are members of the Reoviridae, a virus family with characteristic icosahedral subviral particles that function as small 'replication machines' transcribing viral messenger RNAs from internal, segmented double-stranded RNA templates in the cytoplasm of infected cells[10]. CPVs are the only known members of the Reoviridae where the virus particles are protected by polyhedra, each of which contains several thousand CPV particles[1,2,6,11,12].

In the extracellular environment, virus particles embedded in polyhedra survive dehydration, freezing and enzymatic degradation[6]. In addition, we found that polyhedra tolerate chemical treatments that would denature most proteins, including incubation in concentrated urea, acid and detergents, and still maintain their ordered crystalline organization (see Table 1). In contrast, polyhedra dissolve readily when exposed to pH values higher than 10.5 (ref. 6). The molecular basis of the remarkable stability of these *in vivo* crystals and how they are primed for disassembly in the alkaline mid-gut of insect larvae is unknown.

We developed methods for analysing polyhedra suspended in thin layers of cryoprotectant using low X-ray background micromesh mounts[13] and were able to observe single-crystal diffraction using the MD2 diffractometer at the X06SA beamline at the Swiss Light Source. Over 300 microcrystals purified from insect cells were tested to determine the atomic structure of CPV polyhedra to a resolution of 2 Å. To our knowledge, this is the first report of the atomic structure of functional intracellular crystals[14].

The micrometre-sized polyhedra are the relevant biological assemblies and thus the polyhedrin protein functions as a three-dimensional crystal, rather than as a single molecule or oligomer (Supplementary Fig. S1). A typical 2 μm crystal (Fig. 1a) has 200 body-centred cubic unit cells along each edge and contains several thousand virus particles. With a cell edge of 103 Å, the unit cells of polyhedra are far smaller than a 720 Å diameter icosahedral CPV particle. Electron microscopy revealed that virus particles are uniformly distributed in polyhedra and occupy holes in the lattice in place of at least 150 unit cells[1] (Fig. 1a, right panel). We have determined the atomic structures of polyhedra with and without CPV particles and also of polyhedra where the virus particles are replaced by a protein kinase through fusion with the polyhedra-targeting sequence of the CPV turret protein. These crystals all diffract beyond 2.5 Å and are isomorphous with unit cell dimensions differing by less than 0.2 Å (Table 2). No significant difference was observed and the refined structures are essentially identical. These observations demonstrate that cargoes of strikingly different molecular weights can be stably incorporated into polyhedra without disrupting the overall order of the crystalline lattice.

Polyhedra are made from trimeric building blocks of the 28 kDa polyhedrin protein interlocked into a tight scaffold generated by the amino-terminal α-helix. The fold of polyhedrin has the shape of a left hand with the thumb and index finger outstretched. The index finger is an N-terminal α-helix (H1) which extends from the fist formed by a compact three-layer β sandwich core. This sandwich is made up of two β-sheets of six S1 and three S2 anti-parallel strands (Fig. 1b). The topology of the S1–S2 sandwich (IBADGF-CHE) is akin to the canonical 'jelly-roll' found in many viral capsid proteins (BIDG-CHEF), although the exchange between strands A and I is novel. The third layer (S3) is formed by the carboxy-terminal part of the protein and consists of a β-hairpin preceded by a short α-helix. S3 packs against the concave face of S1, forming a deep groove above S1 in the orientation shown in Fig. 1b. The central sandwich is flanked by additional helices with the H3 helix and adjacent loops forming a clamp-like protrusion above S1–S2 represented as the little finger in Fig. 1b. The thumb is an amphipathic helix (H4) located next to the three-fold axis. The H1 helix, S1/S3 groove, clamp and H4 helix are all involved in the higher organization of polyhedra.

The polyhedrin trimers are composed of a central barrel in which the sandwich domains are held together by a bundle of H4 helices and the three clamps (Fig. 1c, d). They are formed mainly through hydrophobic interactions with over 25% (3,800 $Å^2$) of the total surface of a polyhedrin molecule buried in the trimer interfaces (Supplementary Fig. S2). The trimers have three-fold crystallographic symmetry so that one polyhedrin molecule constitutes the asymmetric unit of the crystal. Polyhedrin has a similar central β-sandwich and overall

[1]School of Biological Sciences, University of Auckland, 1010, New Zealand. [2]Protein Crystal Corporation, Osaka 541-0053, Japan. [3]Swiss Light Source at Paul Scherrer Institute, Villigen 5232, Switzerland. [4]Altana Pharma AG, Konstanz 78467, Germany. [5]Kyoto Institute of Technology, Kyoto 606-8585, Japan.

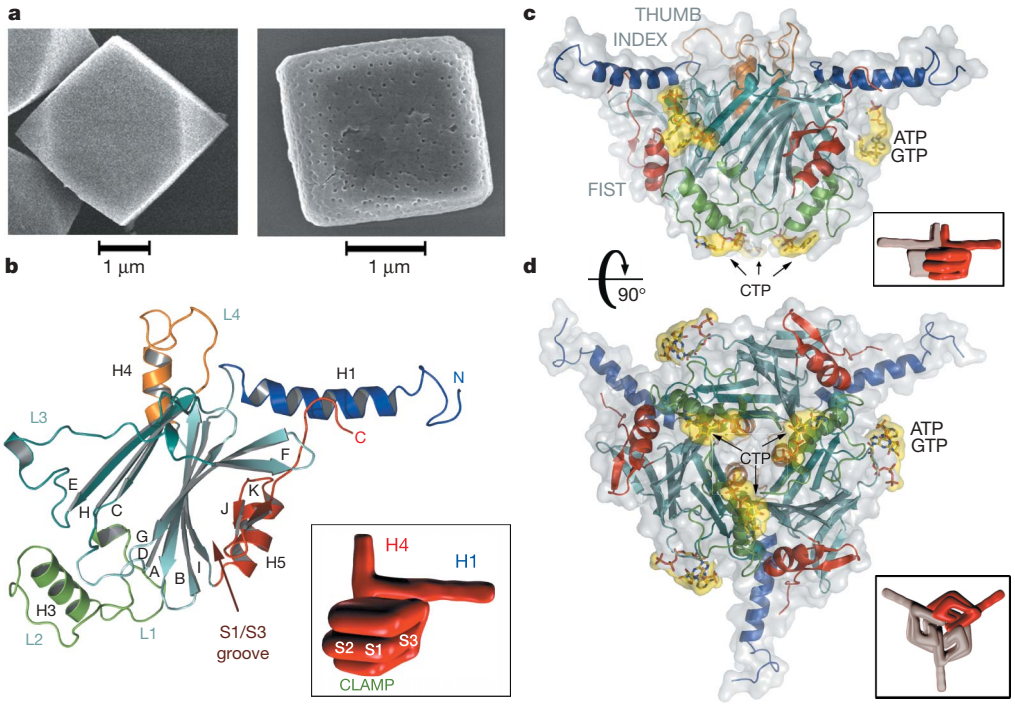

Figure 1 | Compact trimers are the building blocks of polyhedra. **a**, Scanning electron micrographs of recombinant (left) and infectious (right) polyhedra. Both crystals are made up of densely packed 103 Å unit cells (Figs 2 and 3) but the indentations on the surface of infectious polyhedra are due to virus particles which replace blocks of at least 150 unit cells. **b**, Polyhedrin has the shape of a left hand (inset). The finger (H1, blue), thumb (H4, orange), fist (S1–S2, cyan and S3, red) and clamp (H3, green) all contribute to the organization of polyhedra. **c**, **d**, The polyhedrin trimer in two orthogonal views with bound nucleotides shown in a yellow surface. The insets represent trimer models with one of the subunits highlighted in red.

trimeric shape to capsid proteins of double-stranded RNA viruses such as VP7 of bluetongue virus[15], Mu1 of reovirus[16] or VP2 of birnavirus[17]. However, the quaternary arrangement in the trimer is different from these viral capsid proteins and polyhedrin trimers are organized into a three-dimensional body-centred cubic lattice, rather than an icosahedral shell.

The next level of organization in polyhedra is a tetrahedral cluster of four trimers at the centre of the *I*23 unit cell. All 12 polyhedrin molecules in this tetrahedral cluster are oriented with the thumbs pointing away from the centre of the cell and are linked together predominantly by interactions between the clamp regions (Fig. 2a). Two of these tetrahedral clusters constitute the unit cell of the crystal, which is repeated a few hundred times along each axis to form micrometre-sized cubic polyhedra. The tetrahedral clusters are tightly cross-linked in polyhedra, by noncovalent interactions mainly mediated by the H1 helices (Fig. 2b, c). For instance, H1 helices protruding

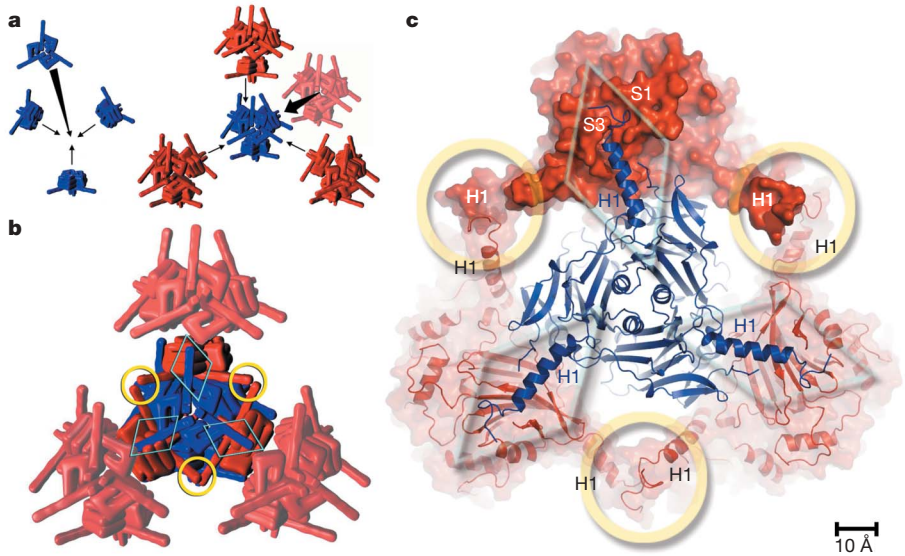

Figure 2 | Polyhedra are built around a tight scaffold of H1 helices. **a**, Four polyhedrin trimers assemble around each lattice point of polyhedra to form a central tetrahedral cluster (blue hands). These clusters then pack tightly to form the body-centred cubic crystal. **b**, **c**, Schematic and molecular models of the crystal packing along the three-fold axis of a trimer. The eight trimers of one *I*23 unit cell are highlighted in **b**. Two of the non-covalent interactions cross-linking trimers in polyhedra are shown as diamonds (finger–fist interactions) and circles (finger–finger interactions).

from the tetrahedral clusters dock into the S1/S3 grooves of trimers of surrounding clusters (finger–fist interactions in Fig. 2). These are the most extended and intimate crystal contacts stabilizing polyhedra. Moreover, a bundle of H1 helices around crystallographic dyads further strengthens the crystal through long-range interactions between tetrahedral clusters (finger–finger interactions in Fig. 2).

The stability of polyhedra stems from an extensive network of interactions connecting the trimers and shielding over 70% of the polyhedrin surface from solvent. In polyhedra, each polyhedrin contacts eighteen other molecules, more than in any other protein crystal with the same *I*23 symmetry (the average is 7.7). Some of these interactions are comparable in their exquisite chemical and shape complementarity to antigen–antibody complexes[18] (surface complementarity factor[19] is 0.70 for polyhedra and 0.64–0.68 for immune complexes). In particular, the H1 helix is central to the architecture of polyhedra, as is evident from the extensive crystal contacts it mediates, with three-quarters of its surface involved in intimate contacts with four neighbouring trimers (Supplementary Fig. S2).

The dense packing of polyhedrin molecules also results in one of the lowest solvent contents reported for protein crystals (19%). It is interrupted only by narrow channels between unit cells, along and perpendicular to the crystallographic dyads, and by closed cavities around each lattice point, at the centre of the tetrahedral clusters (Fig. 3). The axial channels are narrow and blocked by H1 helices, and the extensions of the cavity along the three-fold axes of the crystal are blocked by H4 helices (Supplementary Fig. S3). Polyhedra thus form a sealed matrix, shielding embedded virus particles from the external environment.

Interestingly, we found nucleotides at strategic places in both recombinant and infectious polyhedra. These nucleotides were determined to be ATP, GTP and CTP by mass spectrometry. Stacked ATP and GTP molecules are bound at the interface between four tetrahedral clusters and a CTP molecule interacts with each of the twelve symmetry-related clamp regions lining the central cavity (Fig. 1c, d, Fig. 3b and Supplementary Fig. S3). The specific interactions found at these two nucleotide binding sites near symmetry axes suggest that the nucleotides bind during crystallization and may

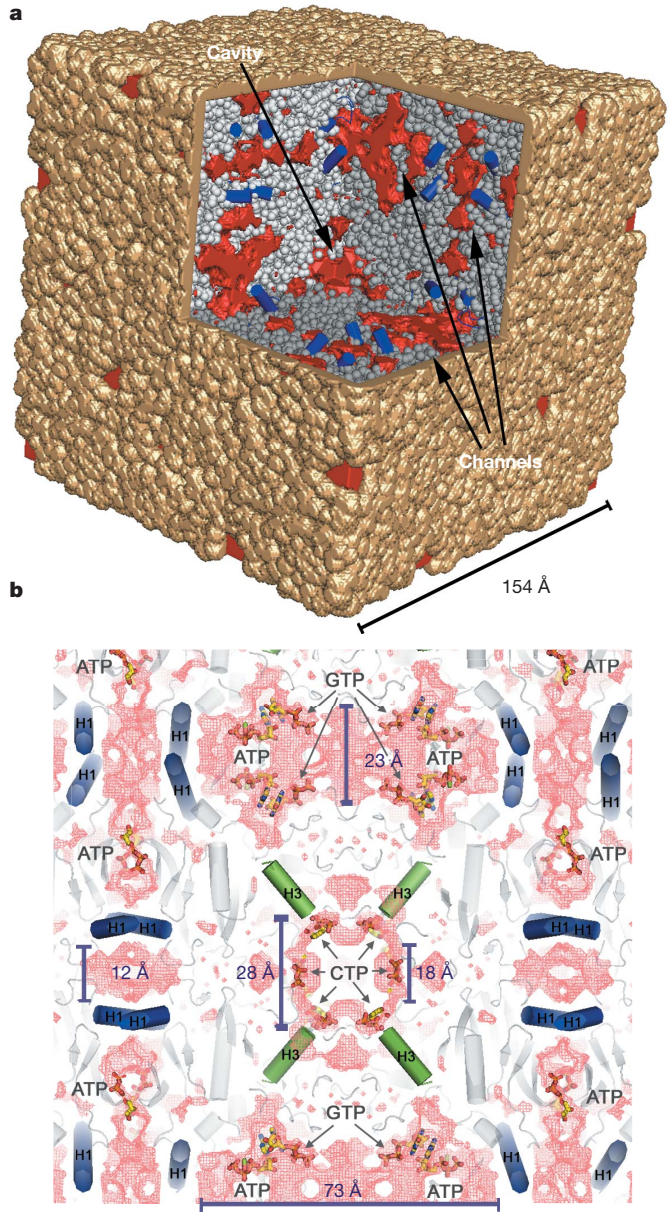

Figure 3 | Polyhedra are dense and sealed microcrystals containing nucleotides. **a**, The continuous protein matrix of the unit cell is represented as a brown surface and grey spheres. The dense packing leaves only narrow solvent channels and a central cavity (red surface) blocked by H1 helices (blue cylinders). These blocks are repeated along the lattice, interrupted by the presence of virus particles. **b**, Mesh representation of the solvent channels and the central cavity. The ATP and GTP molecules located in the channels and the CTP molecules bound in the central cavity are represented as sticks. H1 and H3 helices are shown as blue and green cylinders respectively.

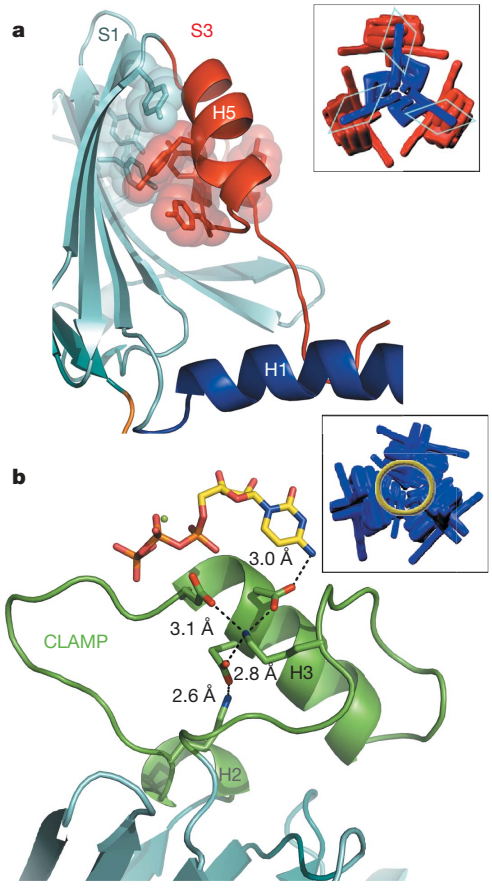

Figure 4 | Proposed mechanism for the release of virus particles. Unpaired buried negative charges are introduced at pH > 10.5 in a tyrosine cluster found between S1 and S3 (**a**) and in a chain of salt bridges (residues K69–E82–K99–D81–D78) of the clamp (**b**). These regions, circled in the insets, are important in the packing of polyhedra and we propose that their disruption leads to dissolution of the crystal and release of the virus particles in the alkaline mid-gut of larvae.

Table 1 | Stability of polyhedra

	Incubation time	Diffraction
Chaotropic agents		
8 M urea	2 days	Yes
Detergents		
10% SDS	2 days	Yes
Acids		
20% acetic acid, pH 1.9	2 days	Yes
1 M HCl	2 days	No
Bases		
20 mM NaH_2CO_3, pH 10.5	<1 min	Dissolved
10 mM PBS, pH 11.0	<1 min	Dissolved
Solvent		
100% ethanol	30 min	Yes
Physical stress		
Dehydration*	24 h	Yes
Freeze–thaw	-	Yes
90 °C	16 h	No

* Polyhedra in water were left to dry on a micromesh mount at relative humidity of 50% and frozen in liquid nitrogen without rehydration or cryoprotectant.

Table 2 | Data collection and refinement statistics (molecular replacement)

	Infectious	Kinase-containing
Data collection		
Cell dimensions $a = b = c$ (Å)	102.78	102.74
Resolution (Å)	20–1.98 (2.05–1.98)	20–2.45 (2.54–2.45)
R_{sym} or R_{merge}	0.14 (0.50)	0.13 (0.35)
$I/\sigma I$	13.9 (4.3)	12.6 (3.7)
Completeness (%)	99.0 (100)	99.9 (99.4)
Redundancy	7.2 (7.3)	8.2 (3.5)
Refinement		
Resolution (Å)	18.76–1.98	18.8–2.45
Number of reflections	11,348	6,092
R_{work}/ R_{free}	0.093/0.154	0.112/0.221
Number of atoms		
Protein	2,056	2007
Ligand/ion	92/3	92/3
Water	286	137
B-factors		
Protein	11.4	20.6
Ligand/ion	41.5/27.1	54.7/45.5
Water	26.3	21.5
r.m.s. deviations		
Bond lengths (Å)	0.013	0.016
Bond angles (°)	1.490	1.680

The space group for all data sets is *I*23. The number of crystals merged to obtain a complete data set is indicated in parentheses for the following data sets: infectious (3) and kinase-containing (5). The highest-resolution shell is shown in parentheses.

play a part in controlling the formation of polyhedra in the cytoplasm. Once polyhedra are formed, the nucleotides are trapped in the crystal and were observed in crystals stored for three years in water.

These ligands have not been described previously to our knowledge; they suggest that polyhedra can be modified to carry other small molecules such as drugs or fluorescent probes. Unlike existing virus-like nanoparticles[8], these nanocontainers are easy to manipulate because of their size and strength, and accommodate a wide range of cargoes, as shown here and in novel microarrays[9] or promising biopesticides[4].

Another attractive feature of these nanocontainers is the possibility that the cargo can be released at alkaline pH. Despite their striking stability even at pH 2, polyhedra are primed for disassembly and dissolve readily above pH 10.5, releasing the virus particles in the alkaline mid-gut of larvae after ingestion. The difference in stability between low and high pH values suggests that loss of hydrogen bonds and salt bridges is not sufficient to account for the dissolution of the crystals. Instead, we propose a virus-release mechanism in which deprotonation of a buried cluster of tyrosines ($pK_a \approx 10.1$) leads to partial unfolding of S3 and loss of the S1/S3 grooves, destabilizing the crystal because of their critical role in binding H1 helices (Fig. 4). We also propose that disruption of a network of salt bridges at high pH destabilizes the clamps by the introduction of unpaired buried charges and the loss of crucial inter-trimer and nucleotide-binding interactions (Fig. 4).

Finally, polyhedrin forms unique intracellular crystals and has no close structural homologues. However the polyhedrin of a nucleopolyhedrovirus (NPV, *Baculoviridae*) assembles into a body-centred cubic lattice with dimensions similar to those of CPV polyhedra[20,21]. This protein is also predicted to have a long N-terminal helix comparable to the H1 helix which forms the scaffold of CPV polyhedra[21]. The architecture of polyhedra may therefore be shared by members of the *Reoviridae* and *Baculoviridae* families despite considerable evolutionary distance and fundamental differences in the life cycles of these viruses. Whether CPV and NPV polyhedra converged to a common architecture from different proteins or were derived from a common ancestor remains an intriguing question.

Table 3 | Data collection, phasing and refinement statistics (recombinant polyhedra)

	Native	$KAuCN_2$	KI/I_2	$AgNO_3$	Se-Met
Data collection					
Cell dimensions $a = b = c$ (Å)	102.96	103.11	102.36	102.92	103.00
Resolution (Å)	14.5–2.1 (2.17–2.10)	18.8–2.8 (2.9–2.8)	24.1–2.8 (2.9–2.8)	24.3–2.6 (2.69–2.60)	18.8–2.6 (2.69–2.6)
R_{sym} or R_{merge}	0.13 (0.43)	0.13 (0.26)	0.13 (0.28)	0.14 (0.30)	0.15 (0.32)
$I/\sigma I$	7.6 (2.6)	7.5 (4.0)	12.7 (6.7)	12.1 (4.7)	13.1 (6.9)
Completeness (%)	97.9 (98.2)	96.9 (96.6)	95.4 (98.2)	98.7 (97.1)	97.8 (99.6)
Redundancy	3.6 (2.6)	2.6 (2.6)	5.8 (5.6)	5.3 (3.4)	7.3 (7.0)
Refinement					
Resolution (Å)	14.5–2.1				
Number of reflections	9,434				
R_{work}/ R_{free}	0.129/0.196				
Number of atoms					
Protein	2,007				
Ligand/ion	92/3				
Water	141				
B-factors					
Protein	17.3				
Ligand/ion	56.6/42.3				
Water	27.0				
r.m.s. deviations					
Bond lengths (Å)	0.012				
Bond angles (°)	1.378				

The space group for all data sets is *I*23. The number of crystals merged to obtain a complete data set is indicated in parentheses for the following data sets: native (2), $KAuCN_2$ (2), KI/I_2 (3), $AgNO_3$ (4) and Se-Met (2). The highest-resolution shell is shown in parentheses.

METHODS

Polyhedra expression and characterization. Expression and purification of recombinant and wild-type *Bombyx mori* CPV polyhedra in insect cells were carried as described elsewhere[22]. Polyhedra containing the human death-associated protein kinase 3 (DAPK3-kinase, known as ZIP-kinase) (Genbank accession number AK074799) fused to an N-terminal fragment of the CPV turret protein were produced as previously described[9]. Scanning electron microscopy was performed on Pt-coated samples. Mass spectrometry analyses confirmed the presence of ribonucleotide triphosphates in purified polyhedra and showed that acetylation of the N-terminal alanine is the only polyhedrin post-translational modification.

Structure determination. Crystals were spread on MicroMesh mounts[13] leaving a thin film of 50% ethylene glycol and data were collected at 120 K on the MD2 diffractometer of the X06SA beamline (Swiss Light Source) with a strongly attenuated beam focused onto the crystal. Data were processed with Denzo/Scalepack[23] in space group *I*23 and data sets from two to four crystals were merged because of severe radiation damage. Successful heavy-atom soaks were performed on recombinant polyhedra at high concentrations, usually half-saturation in appropriate buffer. Heavy-atom sites for four isomorphous derivatives including selenomethionine-substituted crystals were found by SHELX[24] and refined at 2.6 Å using SHARP[25]. The structures of recombinant and infectious polyhedra and of polyhedra containing the ZIP-kinase were refined at resolutions of 2.1 Å, 1.98 Å and 2.45 Å, respectively, using Refmac5[26]. The final models are essentially identical. The structure of infectious polyhedra is of high crystallographic quality for such small crystals ($R = 9.3\%$, $R_{free} = 15.4\%$ to 1.98 Å, Tables 2 and 3) and all residues lie in the allowed region of the Ramachandran plot[27].

Model analysis and illustrations. The oligomeric and crystal contact interfaces were characterized with AREAIMOL from CCP4[28] and the PISA[29] server at the European Bioinformatics Institute. Solvent cavities and channels were analysed with VOIDOO[30] (Uppsala Software Factory). Illustrations were prepared with PyMOL v0.99 (DeLano Scientific; http://www.pymol.org).

Received 29 November 2006; accepted 31 January 2007.

1. Belloncik, S. & Mori, H. in *The Insect Viruses* (eds Miller, L. K. & Ball, L. A.), 337–369 (Plenum, New York, 1998).
2. Miller, L. K. *The Baculoviruses* (Plenum, New York, 1997).
3. Summers, M. D. Milestones leading to the genetic engineering of baculoviruses as expression vector systems and viral pesticides. In *Advances in Virus Research* (eds Bonning, B. C., Maramorosch, K. & Shatkin, A. J.), Ch. 68, 3–73 (Academic Press, New York, 2006).
4. Chang, J. H. *et al.* An improved baculovirus insecticide producing occlusion bodies that contain *Bacillus thuringiensis* insect toxin. *J. Invertebr. Pathol.* **84,** 30–37 (2003).
5. Glaser, R. W. & Chapman, J. W. The nature of the polyhedral bodies found in insect cells. *Biol. Bull.* **30,** 367–390 (1916).
6. Rohrmann, G. F. Polyhedrin structure. *J. Gen. Virol.* **67,** 1499–1513 (1986).
7. Riekel, C., Burghammer, M. & Schertler, G. Protein crystallography microdiffraction. *Curr. Opin. Struct. Biol.* **15,** 556–562 (2005).
8. Douglas, T. & Young, M. Viruses: making friends with old foes. *Science* **312,** 873–875 (2006).
9. Ikeda, K. *et al.* Immobilization of diverse foreign proteins in viral polyhedra and potential application for protein microarrays. *Proteomics* **6,** 54–66 (2006).
10. Fields, B. N., Knipe, D. M., Howley, P. M. & Griffin, D. E. *Field's Virology* (Lippincott Williams & Wilkins, Philadelphia, 2001).
11. Zhang, H. *et al.* Visualization of protein-RNA interactions in cytoplasmic polyhedrosis virus. *J. Virol.* **73,** 1624–1629 (1999).
12. Hill, C. L. *et al.* The structure of a cypovirus and the functional organization of dsRNA viruses. *Nature Struct. Mol. Biol.* **6,** 565–568 (1999).
13. Thorne, R. E., Stum, Z., Kmetko, J., O'Neill, K. & Gillilan, R. Microfabricated mounts for high-throughput macromolecular cryocrystallography. *J. Appl. Cryst.* **36,** 1455–1460 (2003).
14. Doye, J. P. K. & Poon, W. C. K. Protein crystallization *in vivo*. *Curr. Opin. Colloid Interf. Sci.* **11,** 40–46 (2006).
15. Grimes, J., Basak, A. K., Roy, P. & Stuart, D. The crystal structure of bluetongue virus VP7. *Nature* **373,** 167–170 (1995).
16. Liemann, S., Chandran, K., Baker, T. S., Nibert, M. L. & Harrison, S. C. Structure of the reovirus membrane-penetration protein, Mu1, in a complex with its protector protein, Sigma3. *Cell* **108,** 283–295 (2002).
17. Coulibaly, F. *et al.* The birnavirus crystal structure reveals structural relationships among icosahedral viruses. *Cell* **120,** 761–772 (2005).
18. Wodak, S. J. & Janin, J. Structural basis of macromolecular recognition. *Adv. Protein Chem.* **61,** 9–73 (2002).
19. Lawrence, M. C. & Colman, P. M. Shape complementarity at protein/protein interfaces. *J. Mol. Biol.* **234,** 946–950 (1993).
20. Fujiwara, T. *et al.* Xray diffraction studies of the polyhedral inclusion bodies of nuclear and cytoplasmic polyhedrosis viruses. *Appl. Entomol. Zool. Jpn* **19,** 402–403 (1984).
21. Anduleit, K. *et al.* Crystal lattice as biological phenotype for insect viruses. *Protein Sci.* **14,** 2741–2743 (2005).
22. Mori, H. *et al.* Expression of *Bombyx mori* cytoplasmic polyhedrosis virus polyhedrin in insect cells by using a baculovirus expression vector, and its assembly into polyhedra. *J. Gen. Virol.* **74,** 99–102 (1993).
23. Otwinowski, Z. & Minor, W. Processing of X-ray diffraction data collected in oscillation mode. In *Methods in Enzymology* (eds Carter, C. W. & Sweet, R. M.) Ch. 276, 307–326 (Academic Press, New York, 1997).
24. Schneider, T. R. & Sheldrick, G. M. Substructure solution with SHELXD. *Acta Crystallogr. D* **58,** 1772–1779 (2002).
25. de La Fortelle, E. & Bricogne, G. Maximum-likelihood heavy-atom parameter refinement for multiple isomorphous replacement and multiwavelength anomalous diffraction methods. In *Methods in Enzymology* (eds Carter, C. W. & Sweet, R. M.) Ch. 276, 472–494 (Academic Press, New York, 1997).
26. Murshudov, G. N., Vagin, A. A. & Dodson, E. J. Refinement of macromolecular structures by the maximum-likelihood method. *Acta Crystallogr. D* **53,** 240–255 (1997).
27. Lovell, S. C. *et al.* Structure validation by Cα geometry: ϕ, ψ and Cβ deviation. *Proteins* **50,** 437–450 (2003).
28. Collaborative Computational Project, Number 4. The CCP4 suite: programs for protein crystallography. *Acta Crystallogr. D* **50,** 760–763 (1994).
29. Krissinel, E. & Henrick, K. Detection of protein-assemblies in crystals. In *Lecture Notes in Computer Science* (ed. Berthold, M. R.) Ch. 3695, 163–174 (Springer, Berlin/Heidelberg, 2005).
30. Kleywegt, G. J. & Jones, T. A. Detection, delineation, measurement and display of cavities in macromolecular structures. *Acta Crystallogr. D* **50,** 178–185 (1994).

Supplementary Information is linked to the online version of the paper at www.nature.com/nature. A figure summarizing the main result of this paper is available as Supplementary Fig. S1.

Acknowledgements We are very grateful for support from E. N. Baker. We thank R. E. Thorne for providing MicroMesh mounts; J. Taylor, A. Mitra and colleagues at SBS for critically reading the manuscript; and M. Middleditch, C. Hobbis, R. Graves, R. Bunker, A. Wagner, E. Pohl and J. Diez for experimental help. S.G. is funded by the Swiss NCCR Structural Biology and E.C. by a TEAC Bright Futures doctoral scholarship. This work was supported by the NZ FRST (F.C.), the UARC (P.M.), the Maurice Wilkins Centre for Molecular Biodiscovery (E.C.) and grants for Regional Consortium Research Development Work from the Kansai Bureau of METI (K.I. and H.M.), from CREST by JST (H.M.) and a JSPS Invitation Fellowship for Research in Japan (P.M.).

Author Information Structures of polyhedrins from infectious, recombinant and kinase-containing polyhedra have been deposited in the Protein Data Bank with accession codes 2OH5, 2OH6 and 2OH7. Reprints and permissions information is available at www.nature.com/reprints. The authors declare no competing financial interests. Correspondence and requests for materials should be addressed to P.M. (peter.metcalf@auckland.ac.nz).

CORRIGENDUM

doi:10.1038/nature05642

Genetically modified *Plasmodium* parasites as a protective experimental malaria vaccine

A. K. Mueller, M. Labaied, S. Kappe & K. Matuschewski

Nature 433, 164–176 (2005)

It has been drawn to *Nature*'s attention that A.K. M., S. K. and K. M. were named as inventors on a patent application relevant to this work (patent number WO 2005/063991) in 2004, which should therefore have been formally declared as a competing financial interest. The authors' non-profit institutions filed for patent protection to promote the development and distribution of malaria vaccines to people in need worldwide, in accordance with a global access strategy[1].

1. Chen, I. Thinking big about global health. *Cell* 124, 661–663 (2006).

CORRIGENDUM

doi:10.1038/nature05640

Deletion of active ADAMTS5 prevents cartilage degradation in a murine model of osteoarthritis

Sonya S. Glasson, Roger Askew, Barbara Sheppard, Brenda Carito, Tracey Blanchet, Hak-Ling Ma, Carl R. Flannery, Diane Peluso, Kim Kanki, Zhiyong Yang, Manas K. Majumdar & Elisabeth A. Morris

Nature 434, 644–648 (2005)

It has been drawn to *Nature*'s attention that E.A.M. and S.S.G. filed a patent application relevant to this work (patent number WO 2006/0004066) under the Patent Cooperation Treaty in 2004, which should therefore have been declared as a competing financial interest.

ERRATUM

doi:10.1038/nature05581

Chronic polyarthritis caused by mammalian DNA that escapes from degradation in macrophages

Kohki Kawane, Mayumi Ohtani, Keiko Miwa, Takuji Kizawa, Yoshiyuki Kanbara, Yoshichika Yoshioka, Hideki Yoshikawa & Shigekazu Nagata

Nature 443, 998–1002 (2006)

In this Letter, the units of the *y*-axis for Fig. 3d should be picograms, not micrograms. The label should read 'TNF-α in serum (pg ml^{-1})'.

CORRIGENDUM

doi:10.1038/nature05639

A Mesozoic gliding mammal from northeastern China

Jin Meng, Yaoming Hu, Yuanqing Wang, Xiaolin Wang & Chuankui Li

Nature 444, 889–893 (2006)

Of the binomen *Volaticotherium antiquus* established for a Mesozoic gliding mammal discovered from northeastern China, the termination of the trivial name should have a neuter suffix to agree with the gender of the generic name[1]. The species name is therefore corrected to *Volaticotherium antiquum*.

1. International Commission on Zoological Nomenclature. *International Code of Zoological Nomenclature* 4th edn (International Trust for Zoological Nomenclature, The Natural History Museum, London, 1999).

ERRATUM

doi:10.1038/nature05646

Fish can infer social rank by observation alone

Logan Grosenick, Tricia S. Clement & Russell D. Fernald

Nature 445, 429–432 (2007)

In the print version of this Letter, the significance level for hypothesis testing was incorrect for the 'first-choice' results (line 19 on page 430) and should be 0.05 instead of 0.01. The online PDF and HTML versions are correct.

ADDENDUM

doi:10.1038/nature05607

Artificial 'spin ice' in a geometrically frustrated lattice of nanoscale ferromagnetic islands

R. F. Wang, C. Nisoli, R. S. Freitas, J. Li, W. McConville, B. J. Cooley, M. S. Lund, N. Samarth, C. Leighton, V. H. Crespi & P. Schiffer

Nature 439, 303–306 (2006)

During the field treatment of the samples prior to measurement, the magnetic field was switched in polarity with each step down in magnitude while the sample was being rotated within the magnetic field. A more detailed description of the field treatment can be found in ref. 1.

1. Wang, R. F, *et al.* Demagnetization protocols for frustrated interacting nanomagnet arrays. *J. Appl. Phys.* (in the press); preprint at ⟨http://arxiv.org/abs/cond-mat/0702084⟩ (2007).

CORRIGENDUM

doi:10.1038/nature05642

Genetically modified *Plasmodium* parasites as a protective experimental malaria vaccine

A. K. Mueller, M. Labaied, S. Kappe & K. Matuschewski

Nature 433, 164–176 (2005)

It has been drawn to *Nature*'s attention that A.K. M., S. K. and K. M. were named as inventors on a patent application relevant to this work (patent number WO 2005/063991) in 2004, which should therefore have been formally declared as a competing financial interest. The authors' non-profit institutions filed for patent protection to promote the development and distribution of malaria vaccines to people in need worldwide, in accordance with a global access strategy[1].

1. Chen, I. Thinking big about global health. *Cell* 124, 661–663 (2006).

CORRIGENDUM

doi:10.1038/nature05640

Deletion of active ADAMTS5 prevents cartilage degradation in a murine model of osteoarthritis

Sonya S. Glasson, Roger Askew, Barbara Sheppard, Brenda Carito, Tracey Blanchet, Hak-Ling Ma, Carl R. Flannery, Diane Peluso, Kim Kanki, Zhiyong Yang, Manas K. Majumdar & Elisabeth A. Morris

Nature 434, 644–648 (2005)

It has been drawn to *Nature*'s attention that E.A.M. and S.S.G. filed a patent application relevant to this work (patent number WO 2006/0004066) under the Patent Cooperation Treaty in 2004, which should therefore have been declared as a competing financial interest.

ERRATUM

doi:10.1038/nature05581

Chronic polyarthritis caused by mammalian DNA that escapes from degradation in macrophages

Kohki Kawane, Mayumi Ohtani, Keiko Miwa, Takuji Kizawa, Yoshiyuki Kanbara, Yoshichika Yoshioka, Hideki Yoshikawa & Shigekazu Nagata

Nature 443, 998–1002 (2006)

In this Letter, the units of the *y*-axis for Fig. 3d should be picograms, not micrograms. The label should read 'TNF-α in serum (pg ml^{-1})'.

CORRIGENDUM

doi:10.1038/nature05639

A Mesozoic gliding mammal from northeastern China

Jin Meng, Yaoming Hu, Yuanqing Wang, Xiaolin Wang & Chuankui Li

Nature 444, 889–893 (2006)

Of the binomen *Volaticotherium antiquus* established for a Mesozoic gliding mammal discovered from northeastern China, the termination of the trivial name should have a neuter suffix to agree with the gender of the generic name[1]. The species name is therefore corrected to *Volaticotherium antiquum*.

1. International Commission on Zoological Nomenclature. *International Code of Zoological Nomenclature* 4th edn (International Trust for Zoological Nomenclature, The Natural History Museum, London, 1999).

ERRATUM

doi:10.1038/nature05646

Fish can infer social rank by observation alone

Logan Grosenick, Tricia S. Clement & Russell D. Fernald

Nature 445, 429–432 (2007)

In the print version of this Letter, the significance level for hypothesis testing was incorrect for the 'first-choice' results (line 19 on page 430) and should be 0.05 instead of 0.01. The online PDF and HTML versions are correct.

ADDENDUM

doi:10.1038/nature05607

Artificial 'spin ice' in a geometrically frustrated lattice of nanoscale ferromagnetic islands

R. F. Wang, C. Nisoli, R. S. Freitas, J. Li, W. McConville, B. J. Cooley, M. S. Lund, N. Samarth, C. Leighton, V. H. Crespi & P. Schiffer

Nature 439, 303–306 (2006)

During the field treatment of the samples prior to measurement, the magnetic field was switched in polarity with each step down in magnitude while the sample was being rotated within the magnetic field. A more detailed description of the field treatment can be found in ref. 1.

1. Wang, R. F, *et al.* Demagnetization protocols for frustrated interacting nanomagnet arrays. *J. Appl. Phys.* (in the press); preprint at ⟨http://arxiv.org/abs/cond-mat/0702084⟩ (2007).

CORRIGENDUM

doi:10.1038/nature05642

Genetically modified *Plasmodium* parasites as a protective experimental malaria vaccine

A. K. Mueller, M. Labaied, S. Kappe & K. Matuschewski

Nature 433, 164–176 (2005)

It has been drawn to *Nature*'s attention that A.K. M., S. K. and K. M. were named as inventors on a patent application relevant to this work (patent number WO 2005/063991) in 2004, which should therefore have been formally declared as a competing financial interest. The authors' non-profit institutions filed for patent protection to promote the development and distribution of malaria vaccines to people in need worldwide, in accordance with a global access strategy[1].

1. Chen, I. Thinking big about global health. *Cell* 124, 661–663 (2006).

CORRIGENDUM

doi:10.1038/nature05640

Deletion of active ADAMTS5 prevents cartilage degradation in a murine model of osteoarthritis

Sonya S. Glasson, Roger Askew, Barbara Sheppard, Brenda Carito, Tracey Blanchet, Hak-Ling Ma, Carl R. Flannery, Diane Peluso, Kim Kanki, Zhiyong Yang, Manas K. Majumdar & Elisabeth A. Morris

Nature 434, 644–648 (2005)

It has been drawn to *Nature*'s attention that E.A.M. and S.S.G. filed a patent application relevant to this work (patent number WO 2006/0004066) under the Patent Cooperation Treaty in 2004, which should therefore have been declared as a competing financial interest.

ERRATUM

doi:10.1038/nature05581

Chronic polyarthritis caused by mammalian DNA that escapes from degradation in macrophages

Kohki Kawane, Mayumi Ohtani, Keiko Miwa, Takuji Kizawa, Yoshiyuki Kanbara, Yoshichika Yoshioka, Hideki Yoshikawa & Shigekazu Nagata

Nature 443, 998–1002 (2006)

In this Letter, the units of the *y*-axis for Fig. 3d should be picograms, not micrograms. The label should read 'TNF-α in serum (pg ml^{-1})'.

CORRIGENDUM

doi:10.1038/nature05639

A Mesozoic gliding mammal from northeastern China

Jin Meng, Yaoming Hu, Yuanqing Wang, Xiaolin Wang & Chuankui Li

Nature 444, 889–893 (2006)

Of the binomen *Volaticotherium antiquus* established for a Mesozoic gliding mammal discovered from northeastern China, the termination of the trivial name should have a neuter suffix to agree with the gender of the generic name[1]. The species name is therefore corrected to *Volaticotherium antiquum*.

1. International Commission on Zoological Nomenclature. *International Code of Zoological Nomenclature* 4th edn (International Trust for Zoological Nomenclature, The Natural History Museum, London, 1999).

ERRATUM

doi:10.1038/nature05646

Fish can infer social rank by observation alone

Logan Grosenick, Tricia S. Clement & Russell D. Fernald

Nature 445, 429–432 (2007)

In the print version of this Letter, the significance level for hypothesis testing was incorrect for the 'first-choice' results (line 19 on page 430) and should be 0.05 instead of 0.01. The online PDF and HTML versions are correct.

ADDENDUM

doi:10.1038/nature05607

Artificial 'spin ice' in a geometrically frustrated lattice of nanoscale ferromagnetic islands

R. F. Wang, C. Nisoli, R. S. Freitas, J. Li, W. McConville, B. J. Cooley, M. S. Lund, N. Samarth, C. Leighton, V. H. Crespi & P. Schiffer

Nature 439, 303–306 (2006)

During the field treatment of the samples prior to measurement, the magnetic field was switched in polarity with each step down in magnitude while the sample was being rotated within the magnetic field. A more detailed description of the field treatment can be found in ref. 1.

1. Wang, R. F, *et al.* Demagnetization protocols for frustrated interacting nanomagnet arrays. *J. Appl. Phys.* (in the press); preprint at ⟨http://arxiv.org/abs/cond-mat/0702084⟩ (2007).

CORRIGENDUM

doi:10.1038/nature05642

Genetically modified *Plasmodium* parasites as a protective experimental malaria vaccine

A. K. Mueller, M. Labaied, S. Kappe & K. Matuschewski

Nature 433, 164–176 (2005)

It has been drawn to *Nature*'s attention that A.K. M., S. K. and K. M. were named as inventors on a patent application relevant to this work (patent number WO 2005/063991) in 2004, which should therefore have been formally declared as a competing financial interest. The authors' non-profit institutions filed for patent protection to promote the development and distribution of malaria vaccines to people in need worldwide, in accordance with a global access strategy[1].

1. Chen, I. Thinking big about global health. *Cell* 124, 661–663 (2006).

CORRIGENDUM

doi:10.1038/nature05640

Deletion of active ADAMTS5 prevents cartilage degradation in a murine model of osteoarthritis

Sonya S. Glasson, Roger Askew, Barbara Sheppard, Brenda Carito, Tracey Blanchet, Hak-Ling Ma, Carl R. Flannery, Diane Peluso, Kim Kanki, Zhiyong Yang, Manas K. Majumdar & Elisabeth A. Morris

Nature 434, 644–648 (2005)

It has been drawn to *Nature*'s attention that E.A.M. and S.S.G. filed a patent application relevant to this work (patent number WO 2006/0004066) under the Patent Cooperation Treaty in 2004, which should therefore have been declared as a competing financial interest.

ERRATUM

doi:10.1038/nature05581

Chronic polyarthritis caused by mammalian DNA that escapes from degradation in macrophages

Kohki Kawane, Mayumi Ohtani, Keiko Miwa, Takuji Kizawa, Yoshiyuki Kanbara, Yoshichika Yoshioka, Hideki Yoshikawa & Shigekazu Nagata

Nature 443, 998–1002 (2006)

In this Letter, the units of the *y*-axis for Fig. 3d should be picograms, not micrograms. The label should read 'TNF-α in serum (pg ml^{-1})'.

CORRIGENDUM

doi:10.1038/nature05639

A Mesozoic gliding mammal from northeastern China

Jin Meng, Yaoming Hu, Yuanqing Wang, Xiaolin Wang & Chuankui Li

Nature 444, 889–893 (2006)

Of the binomen *Volaticotherium antiquus* established for a Mesozoic gliding mammal discovered from northeastern China, the termination of the trivial name should have a neuter suffix to agree with the gender of the generic name[1]. The species name is therefore corrected to *Volaticotherium antiquum*.

1. International Commission on Zoological Nomenclature. *International Code of Zoological Nomenclature* 4th edn (International Trust for Zoological Nomenclature, The Natural History Museum, London, 1999).

ERRATUM

doi:10.1038/nature05646

Fish can infer social rank by observation alone

Logan Grosenick, Tricia S. Clement & Russell D. Fernald

Nature 445, 429–432 (2007)

In the print version of this Letter, the significance level for hypothesis testing was incorrect for the 'first-choice' results (line 19 on page 430) and should be 0.05 instead of 0.01. The online PDF and HTML versions are correct.

ADDENDUM

doi:10.1038/nature05607

Artificial 'spin ice' in a geometrically frustrated lattice of nanoscale ferromagnetic islands

R. F. Wang, C. Nisoli, R. S. Freitas, J. Li, W. McConville, B. J. Cooley, M. S. Lund, N. Samarth, C. Leighton, V. H. Crespi & P. Schiffer

Nature 439, 303–306 (2006)

During the field treatment of the samples prior to measurement, the magnetic field was switched in polarity with each step down in magnitude while the sample was being rotated within the magnetic field. A more detailed description of the field treatment can be found in ref. 1.

1. Wang, R. F, *et al.* Demagnetization protocols for frustrated interacting nanomagnet arrays. *J. Appl. Phys.* (in the press); preprint at ⟨http://arxiv.org/abs/cond-mat/0702084⟩ (2007).

CORRIGENDUM

doi:10.1038/nature05642

Genetically modified *Plasmodium* parasites as a protective experimental malaria vaccine

A. K. Mueller, M. Labaied, S. Kappe & K. Matuschewski

Nature 433, 164–176 (2005)

It has been drawn to *Nature*'s attention that A.K. M., S. K. and K. M. were named as inventors on a patent application relevant to this work (patent number WO 2005/063991) in 2004, which should therefore have been formally declared as a competing financial interest. The authors' non-profit institutions filed for patent protection to promote the development and distribution of malaria vaccines to people in need worldwide, in accordance with a global access strategy[1].

1. Chen, I. Thinking big about global health. *Cell* 124, 661–663 (2006).

CORRIGENDUM

doi:10.1038/nature05640

Deletion of active ADAMTS5 prevents cartilage degradation in a murine model of osteoarthritis

Sonya S. Glasson, Roger Askew, Barbara Sheppard, Brenda Carito, Tracey Blanchet, Hak-Ling Ma, Carl R. Flannery, Diane Peluso, Kim Kanki, Zhiyong Yang, Manas K. Majumdar & Elisabeth A. Morris

Nature 434, 644–648 (2005)

It has been drawn to *Nature*'s attention that E.A.M. and S.S.G. filed a patent application relevant to this work (patent number WO 2006/0004066) under the Patent Cooperation Treaty in 2004, which should therefore have been declared as a competing financial interest.

ERRATUM

doi:10.1038/nature05581

Chronic polyarthritis caused by mammalian DNA that escapes from degradation in macrophages

Kohki Kawane, Mayumi Ohtani, Keiko Miwa, Takuji Kizawa, Yoshiyuki Kanbara, Yoshichika Yoshioka, Hideki Yoshikawa & Shigekazu Nagata

Nature 443, 998–1002 (2006)

In this Letter, the units of the *y*-axis for Fig. 3d should be picograms, not micrograms. The label should read 'TNF-α in serum (pg ml^{-1})'.

CORRIGENDUM

doi:10.1038/nature05639

A Mesozoic gliding mammal from northeastern China

Jin Meng, Yaoming Hu, Yuanqing Wang, Xiaolin Wang & Chuankui Li

Nature 444, 889–893 (2006)

Of the binomen *Volaticotherium antiquus* established for a Mesozoic gliding mammal discovered from northeastern China, the termination of the trivial name should have a neuter suffix to agree with the gender of the generic name[1]. The species name is therefore corrected to *Volaticotherium antiquum*.

1. International Commission on Zoological Nomenclature. *International Code of Zoological Nomenclature* 4th edn (International Trust for Zoological Nomenclature, The Natural History Museum, London, 1999).

ERRATUM

doi:10.1038/nature05646

Fish can infer social rank by observation alone

Logan Grosenick, Tricia S. Clement & Russell D. Fernald

Nature 445, 429–432 (2007)

In the print version of this Letter, the significance level for hypothesis testing was incorrect for the 'first-choice' results (line 19 on page 430) and should be 0.05 instead of 0.01. The online PDF and HTML versions are correct.

ADDENDUM

doi:10.1038/nature05607

Artificial 'spin ice' in a geometrically frustrated lattice of nanoscale ferromagnetic islands

R. F. Wang, C. Nisoli, R. S. Freitas, J. Li, W. McConville, B. J. Cooley, M. S. Lund, N. Samarth, C. Leighton, V. H. Crespi & P. Schiffer

Nature 439, 303–306 (2006)

During the field treatment of the samples prior to measurement, the magnetic field was switched in polarity with each step down in magnitude while the sample was being rotated within the magnetic field. A more detailed description of the field treatment can be found in ref. 1.

1. Wang, R. F, *et al.* Demagnetization protocols for frustrated interacting nanomagnet arrays. *J. Appl. Phys.* (in the press); preprint at ⟨http://arxiv.org/abs/cond-mat/0702084⟩ (2007).

CORRIGENDUM

doi:10.1038/nature05642

Genetically modified *Plasmodium* parasites as a protective experimental malaria vaccine

A. K. Mueller, M. Labaied, S. Kappe & K. Matuschewski

Nature 433, 164–176 (2005)

It has been drawn to *Nature*'s attention that A.K. M., S. K. and K. M. were named as inventors on a patent application relevant to this work (patent number WO 2005/063991) in 2004, which should therefore have been formally declared as a competing financial interest. The authors' non-profit institutions filed for patent protection to promote the development and distribution of malaria vaccines to people in need worldwide, in accordance with a global access strategy[1].

1. Chen, I. Thinking big about global health. *Cell* 124, 661–663 (2006).

CORRIGENDUM

doi:10.1038/nature05640

Deletion of active ADAMTS5 prevents cartilage degradation in a murine model of osteoarthritis

Sonya S. Glasson, Roger Askew, Barbara Sheppard, Brenda Carito, Tracey Blanchet, Hak-Ling Ma, Carl R. Flannery, Diane Peluso, Kim Kanki, Zhiyong Yang, Manas K. Majumdar & Elisabeth A. Morris

Nature 434, 644–648 (2005)

It has been drawn to *Nature*'s attention that E.A.M. and S.S.G. filed a patent application relevant to this work (patent number WO 2006/0004066) under the Patent Cooperation Treaty in 2004, which should therefore have been declared as a competing financial interest.

ERRATUM

doi:10.1038/nature05581

Chronic polyarthritis caused by mammalian DNA that escapes from degradation in macrophages

Kohki Kawane, Mayumi Ohtani, Keiko Miwa, Takuji Kizawa, Yoshiyuki Kanbara, Yoshichika Yoshioka, Hideki Yoshikawa & Shigekazu Nagata

Nature 443, 998–1002 (2006)

In this Letter, the units of the *y*-axis for Fig. 3d should be picograms, not micrograms. The label should read 'TNF-α in serum (pg ml^{-1})'.

CORRIGENDUM

doi:10.1038/nature05639

A Mesozoic gliding mammal from northeastern China

Jin Meng, Yaoming Hu, Yuanqing Wang, Xiaolin Wang & Chuankui Li

Nature 444, 889–893 (2006)

Of the binomen *Volaticotherium antiquus* established for a Mesozoic gliding mammal discovered from northeastern China, the termination of the trivial name should have a neuter suffix to agree with the gender of the generic name[1]. The species name is therefore corrected to *Volaticotherium antiquum*.

1. International Commission on Zoological Nomenclature. *International Code of Zoological Nomenclature* 4th edn (International Trust for Zoological Nomenclature, The Natural History Museum, London, 1999).

ERRATUM

doi:10.1038/nature05646

Fish can infer social rank by observation alone

Logan Grosenick, Tricia S. Clement & Russell D. Fernald

Nature 445, 429–432 (2007)

In the print version of this Letter, the significance level for hypothesis testing was incorrect for the 'first-choice' results (line 19 on page 430) and should be 0.05 instead of 0.01. The online PDF and HTML versions are correct.

ADDENDUM

doi:10.1038/nature05607

Artificial 'spin ice' in a geometrically frustrated lattice of nanoscale ferromagnetic islands

R. F. Wang, C. Nisoli, R. S. Freitas, J. Li, W. McConville, B. J. Cooley, M. S. Lund, N. Samarth, C. Leighton, V. H. Crespi & P. Schiffer

Nature 439, 303–306 (2006)

During the field treatment of the samples prior to measurement, the magnetic field was switched in polarity with each step down in magnitude while the sample was being rotated within the magnetic field. A more detailed description of the field treatment can be found in ref. 1.

1. Wang, R. F, *et al.* Demagnetization protocols for frustrated interacting nanomagnet arrays. *J. Appl. Phys.* (in the press); preprint at ⟨http://arxiv.org/abs/cond-mat/0702084⟩ (2007).

naturejobs

THE CAREERS MAGAZINE FOR SCIENTISTS

Robert Lang is a master of metamorphosis. He has folded sheets of paper into cuckoo clocks, nuns, inflatable bunnies and three-dimensional likenesses of Jimmy Carter and Darth Vader. The California physicist has also transformed his career in applied lasers into the full-time pursuit of origami — the 400-year-old Japanese art of folding paper (see www.langorigami.com).

For Lang, origami helped him cope with his day-to-day pressures, and his advancement in it mirrors his scientific progression. He folded his way through a master's in electrical engineering at Stanford, and designed more than 50 pieces — including a hermit crab, a mouse in a mousetrap, an ant and a skunk — as a way to relieve stress during his PhD dissertation at the California Institute of Technology.

Along the way, he has managed to affect both physics and origami, according to a recent article in *The New Yorker*. He has altered origami by coming up with computer-based models for ever-more-sophisticated fold patterns, as well as pioneering the use of lasers to score paper according to his complex designs. And he has changed physics by lending origami methods to other disciplines that faced vexing spatial-relations puzzles — from designing a foldable pouch for medical instruments that could be opened without contaminating the sterile tools inside, to a mesh device that could be implanted via a tube, but that on release would enfold and support the heart.

His full-time embrace of professional origami came about by necessity as much as creativity. During the dot-com collapse earlier this decade, Lang's duties at computer components company JDS Uniphase in San Jose shifted from overseeing research to eliminating jobs, cutting pay and closing plants. So he figured out a way to turn his creative passion into a profession.

Lang's story says a lot about how creativity and hobbies can inform both science itself and careers within it. I'm not suggesting that all researchers should leave the bench to follow their hobbies full-time, whether they be scrimshaw, macramé or gnome collecting. But Lang's profession shows that transformation — in the way we think about both scientific problems and career paths — is always a possibility.

Paul Smaglik, *Naturejobs* editor

CONTACTS
Editor: Paul Smaglik
Assistant Editor: Gene Russo

European Head Office, London
The Macmillan Building,
4 Crinan Street,
London N1 9XW, UK
Tel: +44 (0) 20 7843 4961
Fax: +44 (0) 20 7843 4996
e-mail: naturejobs@nature.com

European Sales Manager:
Andy Douglas (4975)
e-mail: a.douglas@nature.com
Business Development Manager:
Amelie Pequignot (4974)
e-mail: a.pequignot@nature.com
***Nature*events:**
Claudia Paulsen Young
(+44 (0) 20 7014 4015)
e-mail: c.paulsenyoung@nature.com

France/Switzerland/Belgium:
Muriel Lestringuez (4994)
UK/Ireland/Italy/RoW:
Nils Moeller (4953)
Scandinavia/Spain/Portugal:
Evelina Rubio-Morgan (4973)
Germany/Austria/The Netherlands:
Reya Silao (4970)
Online Job Postings:
Matthew Ward (+44 (0) 20 7014 4059)

Advertising Production Manager:
Stephen Russell
To send materials use London address above.
Tel: +44 (0) 20 7843 4816
Fax: +44 (0) 20 7843 4996
e-mail: naturejobs@nature.com
***Naturejobs* web development:**
Tom Hancock
***Naturejobs* online production:**
Catherine Alexander

US Head Office, New York
75 Varick Street,
9th Floor,
New York,
NY 10013-1917
Tel: +1 800 989 7718
Fax: +1 800 989 7103
e-mail: naturejobs@natureny.com

US Sales Manager: Peter Bless

Japan Head Office, Tokyo
Chiyoda Building,
2-37 Ichigayatamachi,
Shinjuku-ku,
Tokyo 162-0843
Tel: +81 3 3267 8751
Fax: +81 3 3267 8746

Asia-Pacific Sales Manager:
Ayako Watanabe
e-mail: a.watanabe@natureasia.com

CORBIS

Getting in the frame

Prospective grant applicants were like "vultures circling around the European Union's money pots", joked one participant at the German launch event this January of the Seventh Research Framework Programme (FP7). Hunger for funding was palpable during this meeting, which attracted some 1,600 researchers. That's hardly surprising: as national funding stagnates in most countries, more and more scientists are pinning their hopes on money from the European Union (EU).

The world's biggest research-funding programme is both a blessing and a curse, depending on one's viewpoint and experiences. Some scientists enthuse about the fruitfulness of EU-wide research collaboration, whereas others roll their eyes when thinking about tortuous application procedures and Byzantine project-management requirements.

The European Commission will, during the next seven years, channel research grants worth more than €50 billion (US$65 billion) through FP7. As always, researchers are hoping that the bureaucracy involved will be less overwhelming this time around. And as always, the commission has promised that it will be. But when scientists at the launch, in Bonn, asked programme administrators what elements would get easier, the disappointing answer was: "Not many."

One of the biggest criticisms of the Sixth Framework Programme was its emphasis on collaborative projects carried out by consortia with participants from different countries. The size, scope and internal organization of projects can vary from field to field and from topic to topic. And each consortium must have at least three research organizations or individual scientists, each from a different member state or associated country. The grant reviewers are not free to decide whether there are enough participants from enough countries; these criteria are laid down in the rules.

The overall guidelines for FP7 collaborative projects remain largely the same, despite these criticisms. The commission, for its part, is increasingly frustrated by scientists' complaints about the programme, which nonetheless is hugely over-subscribed. Success rates of grant applications in some areas of the previous framework programme, such as cancer research, were as low as 15% (see *Nature* **424,** 605; 2003).

The conditions for framework funding are complex and the competition is tough, says **Nora Eichinger**. But many find the prize is worth the effort.

OLDENBURG UNIV.

Wired: one of Volker Mellert's volunteers.

"We have somehow slipped into a scapegoat's role," says Richard Escritt, director of inter-institutional and legal matters for the framework programme. The widespread feeling that the commission won't specify precisely enough what it expects is unfounded, he says: detailed descriptions of criteria and guides for applicants are easily available. "The most important message is: keep it short!" he said at the launch. Applicants should strive for clarity when describing their ideas and make sure that proposals match the 'personality' and content of the programme. Unstructured and over-ambitious — hence implausible — ideas are unlikely to be accepted, another experienced evaluator said.

Deciphering the framework

EU-funded research does have clear socio-economic objectives. The foremost goal of the framework programmes is not to support curiosity-driven research, but to increase the EU's economic competitiveness and improve the living and working conditions of its almost 500 million citizens.

This special personality of the programmes has, in the past, deterred some of the best scientists in Europe. Many others struggle to understand the objectives and requirements, which they say have an annoying tendency to change from one programme to the next.

Like its predecessors, FP7 is divided into different categories, in this case headlined 'cooperation', 'ideas', 'people' and 'capacities'. These broad categories refer to the specific objectives of EU research policies, from funding of multinational research that is too intricate and costly to be carried out at national level, to the training and mobility of young researchers, to capacity building and support of research infrastructures. 'Ideas' refers to the new European Research Council (ERC), a quasi-autonomous agency that will fund basic, investigator-driven research.

But the core of FP7 is the €32-billion cooperation programme, which will support interdisciplinary research collaboration on ten themes. The largest are 'information and communication technologies', 'health'

and 'transport'. For the first time in the framework's 25-year history, there is also a €623-million budget for social sciences, economic sciences and humanities. At the Bonn event, interest in this new area was so strong that an information workshop had to be repeated.

The first calls for proposals in all themes were issued in December. Sequencing the human 'meta-genome' — the genomes of bacteria living in and on the human body — is a typical large project in the health theme, for example. Leading European groups, from academy and industry, are expected to participate. But it will take months of grant writing and evaluation before contracts can be negotiated and the consortium can start work.

Grappling with grant proposals

Meanwhile, it has become a widespread practice to hire grant-writing experts to do the paperwork. Indeed, EU grant-writing for scientific and industrial customers has almost become a profession in itself.

There are good reasons for seeking expert advice. Experienced evaluators say that applications are often rejected because they don't meet formal requirements or aren't fully formed, and grand proposals are not described concisely. Many interesting ideas don't make the cut simply because grant proposals are being written too hastily, they say.

Even professional grant writers find it hard to penetrate the jungle of FP7 language and requirements. "The effort involved in writing EU proposals is enormous," says Martin Wyrwich, who specializes in writing grant applications. "One of the problems is that the programme is so damn political."

Managing the multimillion-euro consortia that have dominated the previous framework programme, and will form the core of FP7, can be a thankless job. Volker Mellert, a physicist at the University of Oldenburg in Germany, can tell a tale or two about what it means to be project coordinator. From 2001 to 2005 he was responsible for an EU project aimed at improving the comfort and well-being of aircraft passengers and crews. The consortium of acoustics experts, aircraft engineers and physicians studied the impact of noise, humidity and pressure conditions. Their findings are being used to improve passenger aircraft design. But Mellert would rather not do it again. "Project coordination is extremely time-consuming," he says.

Some scientists show sympathy for the commission's standpoint. "Scientists are often too focused on their test-tubes," says a Germany-based scientist who doesn't want to be named. "But EU projects involve an awful lot of money. We do have to justify what we are doing with it, and of course there has to be tight project management." Big money naturally involves paperwork, accountability and public outreach, he adds.

"Scientists are often too focused on their test-tubes. But EU projects involve an awful lot of money: there has to be tight project management."

Some of the scientists in Bonn were not only keen to learn about simplified applications procedures, but to find partners too. "If you don't carefully choose a good group you may end up with less grant money and more management work," says one cancer researcher.

Many participants complain that the projects have become too big to be efficiently managed, and that responsibility is spread among too many people. Some fear that the very size of the consortia and the large number of scientists involved creates the risk that some members could behave irresponsibly when it comes to administration, data exchange or publishing ethics.

But not everything about the framework is considered complex and unwieldy. The creation of the ERC has been applauded throughout Europe for its promise to support individual bottom-up research grants on the sole criterion of excellence. The Marie Curie Actions are lauded too, having helped countless young scientists gain experience outside their home countries, with little red tape. They have lifted a lot of bureaucracy, says Daniel Funeriu, a chemist at the Technical University of Munich.

"The initial experience was a bit tough," says Funeriu, who leads a Marie Curie excellence team. On arrival in Munich he spent several months on organizational issues, and the university had to create a new position, 'EU visiting scientist', as his salary and responsibilities didn't fit the profile of any existing position in the German science system. But the Curie programme alleviates many of the problems — such as work permits, insurance and low pay — that young visiting scientists in Europe tend to have in common, he says.

Marie Curie excellence grants are for research teams working on cutting-edge and interdisciplinary research in an EU state or associated country. Fellowships are much sought-after, with a success rate of around 10%.

Intellectual freedom

Funeriu now works with his ten-strong team on enzyme microassays, seeking novel enzyme inhibitors that could help treat diseases. The EU grant provides the intellectual freedom that young scientists need, he says. And the Technical University, like many other large universities in Europe, has set up a bureau that deals with special problems arising from EU grants.

But as success rates are likely to be frustratingly low in all FP7 programmes, including the ERC, applicants should be prepared for disappointment. One particularly unlucky scientist in Bonn talked with gallows humour about his enduring lack of funding success. Aware of his "well-proven project-killer qualities", he said that in future he would only agree to collaborations with colleagues he particularly dislikes.

It remains to be seen whether the newest framework will placate scientists, nurture research and untangle bureaucratic constraints more than previous efforts. The only certainty is that European scientists will still compete for part of the large pot of money — and complain about both the process and the results. ■

Nora Eichinger is a former intern in *Nature*'s Munich office.

http://cordis.europa.eu/fp7/home_en.html

R. HAAS

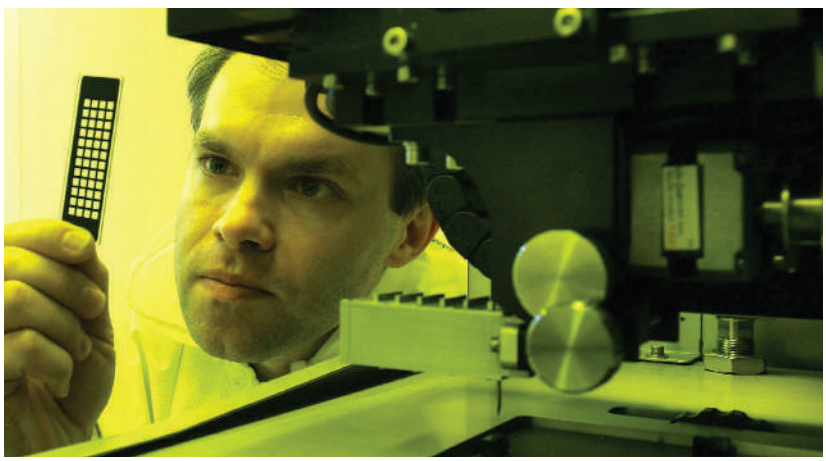

Daniel Funeriu believes that Europe's Marie Curie programme has proved worthwhile.

NATURE|Vol 446|1 March 2007

MOVERS

Tim de Zeeuw, director-general, European Southern Observatory, Garching, Germany

2003–07: Director, Leiden Observatory, Leiden, the Netherlands
1993–2007: Director, Netherlands Research School for Astronomy (NOVA), Leiden, the Netherlands
1990–2007: Professor of theoretical astronomy, Leiden University, the Netherlands

While fighting the third-year PhD blues at Leiden University in the Netherlands, Tim de Zeeuw, a student in theoretical astronomy, came across an intriguing problem. Until then, galaxies were assumed to have similar elliptical shapes. "But new observations at the time showed the shapes were not as symmetric as scientists once thought," he says. Over three years, he worked with astronomer Martin Schwarzschild, based at Princeton University, New Jersey, who was developing numerical models to describe one particular galaxy shape. In 1982, de Zeeuw offered an explanation for the full orbital structure and variety of observed motions for the entire range of possible galaxy shapes — complementing Schwarzschild's approach. The experience spurred him to seek more new observations that led to interesting problems.

He later went to the Institute for Advanced Study in Princeton, New Jersey, to do theoretical work detailing the structure of galaxies. Next he and his wife, astrophysicist Ewine van Dishoeck, moved to the California Institute of Technology. In 1990 they accepted offers from Leiden University, where de Zeeuw helped to create a research school, NOVA, from existing astronomy departments. Now proud of the school's success, he admits that "you never know with new initiatives — whether to go for it and put the energy in or not". As director of NOVA, de Zeeuw secured ten years' funding from the Netherlands Ministry of Education, Culture and Science. He also served on advisory committees for the Hubble Space Telescope — a pivotal move that fostered excellent relations with US scientists.

In the mid-1990s, he helped garner international support to build a replacement instrument for the William Herschel Telescope in the Canary Islands, which was earmarked for retirement. Dubbed SAURON, the instrument surveys spectra across galaxies to study galaxy formation. That experience spurred de Zeeuw to design other instruments.

From September, he will be director-general of the European Southern Observatory (ESO). "Tim's international experience puts him in a good position to lead the ESO, a European organization that operates globally," says Richard Wade, president of the ESO council.

His first challenge will be to complete the Atacama Large Millimetre Array (ALMA) in Chile on time and on budget. By fostering new opportunities to learn about the formation of stars and planets, ALMA could be as transformational as the Hubble telescope, says de Zeeuw. ■

Virginia Gewin

BRICKS & MORTAR

Hub of alternative energy

The Energy Biosciences Institute isn't built yet, but it is already transforming the field of renewable energy and creating new research positions for scientists. The US$500-million agreement was announced on 8 February by energy giant BP with the University of California, Berkeley, the Lawrence Berkeley National Laboratory (LBNL) and the University of Illinois at Urbana-Champaign.

At least 25 research groups — comprising some 200 scientists, technicians, postdocs and graduate students — will need a broad range of expertise. Interest is already high, and recruitment will begin later this year. Topics include synthetic biology, plant genetic engineering, functional genomics, microbiology, biochemistry and even carbon sequestration in a comprehensive, carbon-neutral approach to biofuel development.

"This is like the Manhattan Project for bioenergy," says one of the project's coordinators Jay Keasling. Lee Lynd, a biofuels expert at Dartmouth College in Hanover, New Hampshire, estimates that the project roughly doubles the cumulative investment in energy biotechnology worldwide.

One focus will be on developing energy-producing crops. Berkeley wants to hire seven new faculty members, particularly in plant-based research, says Keasling. The main thrust for Illinois will be feedstock development of potential energy crops, including switch grass, and assessing their environmental impact. It plans to fund at least three faculty positions as well as the 30–45 postdocs and postgraduate support staff supported by BP. Participants at Illinois will use the new Institute for Genomic Biology, designed for cross-disciplinary research.

"One of the reasons BP wanted to do this is the lack of trained scientists in biofuels development," says Fleming Graham, deputy director of the LBNL. But some have met BP's involvement with scepticism (see *Nature* **445,** 688; 2007). "When a university and a national lab get involved with a big company, sometimes hackles can be raised," acknowledges Graham, although he adds that the response so far has largely been positive.

The Energy Biosciences Institute is likely to have a strong influence on future biofuels development. Meanwhile, Graham and others are already seeking federal funding for a separate, six-partner Joint Bioenergy Institute, in the hope of making California's Bay Area the world leader in fundamental energy research. ■

Virginia Gewin

POSTDOC JOURNAL

On resilience

If doing cutting-edge research is like running a marathon, then in the field of molecular biology, DNA cloning — inserting known sequences of DNA into an organism to amplify them — is the equivalent of tying your shoelaces. A basic skill that you learn as an undergraduate, DNA cloning is usually the starting point for getting more complex experiments up and running. This procedure is a familiar routine. So when I recently encountered a problem it was like falling over my own two feet. I was surprised and embarrassed.

Getting my momentum back was a process. First there was denial: "This can't be happening." Then came anger: "*$#!#*&%! protocol!" Bargaining and abject begging followed: "Please, just let this experiment work…" Next came depression: "I'm never going to finish this project — my career is over." And, finally, acceptance settled in: "It's time to re-evaluate my strategy and to move on."

I had to get back on track after being thrown off course by this unexpected obstacle. Despite a slightly bruised ego, I picked myself up, dusted myself down and kept going, and my resilience paid off. Relief and redemption came in the form of small bacterial colonies. Back on my feet, I'm up and running once again. ■

Maria Thelma Ocampo-Hafalla is a research fellow at Cancer Research UK's London Research Institute.

The inside track from academia and industry

Temporary display

If you look on short-term employment as a way of window shopping, you could get a bargain.

Martin Lang

SCENE: A pavement café in a bustling European capital. A forlorn German scientist stares into her coffee. An American friend arrives and sits down.

AMERICAN
Hey, what's up? You're looking pretty stressed.

GERMAN
I've lost my job. It was such a great position, too: full-time, supposedly secure. I'd been there years. So now I'm looking for something similar — but I'm getting nowhere. All I can find are short-term slots. I just can't imagine working for six months, and then having to look for another job, and then another — and maybe having to move to another city.

AMERICAN
You make it sound like torture — but it's actually not a bad life. Sure, it might not always be convenient, but then, what is? Temping exposes you to a host of different companies and it helps you to learn new skills.

GERMAN
Hmm. You might be right — in theory. But I'd still rather have the stability of a permanent position. I want to stay put until I retire.

AMERICAN
To be honest, those days are over. It just doesn't happen any more. If the choice is between staying unemployed and trying something different, why not give temping a try?

This brief encounter is fictional — but it reflects accurately the views I have heard from both sides of the Atlantic when it comes to short-term contracts. To some, the idea of sacrificing the alleged security of a 'permanent' position for the life of a temp is a wholly unappealing prospect. But such feelings need to be informed by a healthy dose of reality.

There is no point mourning a job market that has been undergoing dramatic change for several years. It's even less useful to stick your head in the sand and convince yourself that you'll soon get a permanent job if you are in a sector where there are few such opportunities. So if you're not tied down with family and financial commitments, why not make use of your freedom to exploit the temporary job market?

Both employers and employees are constantly reacting to changes caused by globalization, new technology and shifting scientific and political fortunes. Temporary employment is one reaction to these changes. It is accepted in most sectors as a way to keep staffing levels responsive to fluctuating needs. But to PhD scientists in some parts of the world, the idea of temporary employment can, as in our story, elicit a negative response.

The term 'temp' can also carry negative connotations. "We would never trust a temp in this responsible position," a drug company in Germany once said in a discussion about its staffing needs. What was it afraid of? Transfer of knowledge to someone who was just passing through? Didn't the company rely on its employees' skills and qualifications? And didn't it expect employees to be flexible and have a broad knowledge of different scientific fields? Or was the firm not prepared to pay adequate salaries for the appropriate skills?

In many countries, such as Britain or the United States, temporary employment in the scientific industry is far more common than on the European mainland. Although hiring a very qualified scientist on a temporary basis may mean higher short-term labour costs, these arrangements are accepted by both employer and the employee.

Some trepidation about temporary employment is natural — particularly in cultures that value permanent jobs, and among people with financial commitments. But the philosophy behind such posts can make employers wary. What if they get stuck with someone whose skills are only useful for a certain period? What if the new person is simply not a 'good fit'? In many European countries, employees are protected from losing their jobs in such circumstances.

Temporary posts offer an alternative, with benefits to both the employee and the employer. For companies that are cautious about bringing in high-level staff permanently, it gives them an opportunity to see the scientists in action, before they make a more long-term commitment. In my experience, just over half of temping positions result in such offers.

For the employee, such positions offer more than just six months' salary. They provide an opportunity to gain new skills and to experience work in different organizations. Many firms offer placements in different parts of the world, thus allowing scientists their geographical preferences — something that can be hard when seeking an academic position. In fact, scientists seeking temporary work may actually have more choice over location than those in long-term posts.

The biggest benefit to both sides, of course, occurs when the temp's skill set meshes with the long-term needs of the company and the temporary employee has the chance to become permanent. Both the company and the employee understand each other, eliminating fears from both sides about being 'a good fit' for each other. Temporary employment in the scientific industry allows scientists and companies to try each other on for size. ■

Martin Lang is recruitment consultant for Kelly Scientific Resources in Cologne, Germany.

Group Leaders

The CRUK Cambridge Research Institute is a major new Cancer Institute located in an outstanding scientific research and clinical research environment. The aim of the Institute is to carry out world class basic research and to take the results to practical clinical application. 15 research groups of an eventual 30 are now in place. The Institute is core funded by Cancer Research UK, providing substantial stable support to group leaders, including competitive personal salaries and dedicated research posts, a core funded pool of clinical and non clinical PhD studentships, annual running costs and access to state-of-the-art core facilities.

We wish to recruit outstanding group leaders at all stages of their careers (tenure and tenure-track), in any area of basic or applied cancer research. We particularly welcome applicants at tenure-track level, with interests in specific epithelia including lung, prostate, and breast; in epigenetics; in "experimental medicine" based clinical studies and in drug development; in epidemiology and in computational biology.

Further information about the Institute, the Cambridge research environment and the application process can be found at (www.cambridgecancer.org.uk; www.hutchison-mrc.cam.ac.uk; www.addenbrookes.org.uk/serv/clin/oncol/oncology1.html). Each application must consist of a CV (no longer than 3 pages), names and contact details of 3 referees, a publication list, a summary of past research (1 page) and plans for the next 5 years (2 pages). Applications that fail to conform to these guidelines will not be considered. Shortlisting followed by invitations to visit CRI for interview, including a seminar, will take place within 6-8 weeks of this advertisement.

For further details, to apply online or register for email alerts please visit https://jobs.cancerresearchuk.org/

Alternatively please send in two copies of both your covering letter and CV to:
Cancer Research UK, PO Box 123, Lincoln's Inn Fields, London WC2A 3PX
Please quote reference number 6101 on all correspondence.

Closing date: 30th March 2007.

CANCER RESEARCH UK

Registered charity no 1089464

97743R

Meteorological Scientist

REF: VN-07/02

Formed in 1986 and comprising 20 European member states, EUMETSAT's role is to establish, operate and exploit European meteorological satellite systems. Data from these systems are essential for precise and accurate weather forecasting; they also assist global observation and climatological programmes and directly benefit national economies by enabling marine, agricultural, aviation and other industries to plan and act more effectively.

EUMETSAT's geostationary satellite programmes include the continuation of the current Meteosat system with a Meteosat Second Generation (MSG). The first MSG satellite was launched in August 2002, to provide continuity and improvement of the service well into the next decade. The second MSG satellite was launched in 2005 and the third MSG satellite at the nominal end of life of MSG-1. Preparation is under way for a fourth MSG satellite.

In addition to these two geostationary systems, an entirely new Low Earth Orbit (LEO) system has been developed within the framework of the EUMETSAT Polar System (EPS) programme. EPS will provide the operational meteorological satellite service delivering earth observation data for extraction of meteorological and climate monitoring products from 2007.

Within a matrix structure, the Meteorological Scientist will support current and future programmes of EUMETSAT in the analysis and development of satellite calibration methods leading to improved and consistent calibration among different instruments. The emphasis will be on Meteosat Second Generation and the MetOp satellites instruments. The post holder will also support future EUMETSAT programmes with specifications of instrument characterisation and calibration. She/he will support the development of a Global Satellite Inter-calibration System (GSICS), whose goal is to make the calibration of current instruments consistent. This in turn will enhance the benefit of satellites for the Global Earth Observation System of Systems (GEOSS) and the Global Monitoring for Environment and Security (GMES).

The candidate for the post will have a University degree in physics, remote sensing, meteorology or equivalent. He/she should have experience in remote sensing techniques and a very good knowledge of the physics of atmospheric radiative transfer covering the solar, thermal infrared and the micro-wave region of the spectrum. A good understanding of applications in meteorology and climate will be considered an advantage. Strong skills in a high-level computer language (e.g. Fortran or C) are essential. Ability to work in a matrix structure within EUMETSAT and to cooperate with international partners are also prerequisites. The official languages of EUMETSAT are English and French. Candidates must be able to work effectively in one of these languages and also have a working knowledge of the other.

Based in Darmstadt, the post is offered on an initial four-year contract. Further information on the position and salary details can be found on the EUMETSAT web site: www.eumetsat.int.

To apply, please send your CV in English or French with covering letter, quoting reference VN 07/02, to EUMETSAT, Mr. J. K. Myatt, Head of Personnel, Postfach 10 05 55, 64205 Darmstadt, Germany, or recruitment@eumetsat.int.

Please note that only applications from nationals of one of the EUMETSAT Member States can be considered and that applications will not be returned.

Closing date: 16 March 2007.

Member states: Austria, Belgium, Croatia, Denmark, Germany, Finland, France, Greece, Ireland, Italy, Luxembourg, The Netherlands, Norway, Portugal, Slovakia, Spain, Sweden, Switzerland, Turkey and the United Kingdom.

EUMETSAT

Europe's Meteorological Satellite Organisation

Organisation Européenne de Satellites Météorologiques

W97667R

PENELOPE

"Evolution of Protein Interaction Networks" 8 Ph.D. and 5 Postdoctoral Positions

Penelope is a Marie Curie Research Training Network with four years duration (www.penelope.crg.es). Seven leading European Institutions have joined this ambitious project to promote fruitful training of early stage and experienced researchers.

The scientific goal of **Penelope** is to unravel the evolution of protein networks in Eukaryotes with the example of the interplay between the Src Homology 3 (SH3) domains, their host proteins and their binding partners. The study will focus on four different yeasts, which encompass up to a thousand million years of evolution: *Saccharomyces cerevisiae*, *Candida albicans*, *Ashbya gossypi*i and *Schizosaccharomyces pombe*.

Penelope will involve an astounding multidisciplinary approach. Researchers will have the opportunity to receive theoretical and practical training in several different disciplines of biology such as genetics, biochemistry, structural biology, advanced light microscopy, genomics, and systems biology, through exchanges and workshops in the participating laboratories. The successful candidates will receive an attractive salary, travel, mobility, and relocation allowances. Applications from women are highly encouraged. A limited number of non-EU members may be considered. Citizens and long-term residents of European countries may not apply for their home country institutions.

- **The Carlsberg Laboratory, Copenhagen**: 2 Ph.D. positions.
- **Academic Medical Center, Amsterdam**: 2 Ph.D. and 1 Postdoctoral position.
- **Biozentrum, Basel**: 1 Ph.D. and 1 Postdoctoral position.
- **GMGM, CNRS, Strasburg**: 1 Ph.D. and 1 Postdoctoral position.
- **Institute of Biochemistry and Biophysics, Warsaw**: 1 Ph.D. position.
- **EMBL-Hamburg Unit**: 1 Ph.D. and 1 Postdoctoral position.
- **EMBL-Heidelberg Unit**: 1 Postdoctoral position

Applicants should send a presentation letter, curriculum vitae and two letters of recommendation to **Dr. Michela Bertero (michela.bertero@crg.es)**, indicating two or more institutes of preference. For further information, please visit the Penelope web site, **http://penelope.crg.es**

W97598R

HUMBOLDT-UNIVERSITÄT ZU BERLIN

The Faculty of Mathematics and Natural Sciences I, Institute of Biology at Humboldt-Universität zu Berlin (HU) invites applications from scientists with experience in research and teaching for a

Full Professorship (W3) for Theoretical Biophysics

to commence by April 1, 2008.

We will consider applicants with an established track record in any aspect of Theoretical Biophysics though preference may be given to applicants whose research complements existing research in the department. The Professor is expected to demonstrate a strong commitment to excellence in teaching 'Theoretical Biophysics' in undergraduate and graduate programs for biology and biophysics students. The successful candidate is expected to participate in existing international research projects such as the International Research Training Group 'Genomics and Systems Biology of Molecular Networks' (GK 1360), and the Collaborative Research Centres (SFB 555 'Complex non-linear Processes', SFB 618 'Theoretical Biology: Robustness, Modularity and evolutionary Design of living Systems', SFB 740 'From Molecules to Modules: Organisation and dynamics of functional units in cells') and the Interdisciplinary Centre for Biophysics and Bioinformatics at the HU.
Applicants must meet the legal requirements for appointments of professors in accordance with § 100 of the "Berliner Hochschulgesetz". Habilitation or documented evidence of equivalent scientific qualifications is required.

HU is an equal opportunity employer, committed to the advancement of individuals without regard to race, colour, religion, sex, age, national origin, ethnicity, disability or any other protected status. HU seeks to increase the proportion of female faculty members. Thus qualified women are particularly encouraged to apply.

Applications should include a curriculum vitae, lists of publications and previously taught courses, a statement of research and teaching interests, and up to five selected publications and are to be sent with above reference number **PR/005/07** within 4 weeks to: Humboldt-Universität zu Berlin, Dekan der Mathematisch-Naturwissenschaftlichen Fakultät I, Prof. Dr. Christian Limberg, Unter den Linden 6, 10099 Berlin.

97730R

Max Planck Institute for Neurological Research

MAX-PLANCK-GESELLSCHAFT

with Klaus-Joachim-Zülch-Laboratories
of the Max Planck Society and the Faculty of Medicine
of the University of Cologne
Director Prof. Dr. D. Yves von Cramon

University of Cologne

Medical Faculty
Dean Prof. Dr. Joachim Klosterkötter

The Max-Planck-Institute for Neurological Research invites applications for a Group Leader position

Selbständige Nachwuchsgruppe der Max-Planck-Gesellschaft (Independent Junior Research Group)

The Max Planck Institute for Neurological Research and the Medical Faculty of the University of Cologne has opening for a Group Leader position, funding for a research group (Selbständige Nachwuchsgruppe der Max-Planck-Gesellschaft / Independent Junior Research Group) dedicated to neurological and oncological research. While there is no particular restriction on the research area, there is the expectation that the successful candidate has a particular expertise in molecular imaging.

Currently, the following technologies / methods are available at the Institute: **human brain PET and MRT, animal PET and animal MRT, optical imaging, autoradiography, electron microscopy, histology, immunohistochemistry and invasive imaging / neuromonitoring.** In 2007, a **combined human brain PET-MR System** will be installed.

Cologne and its rich scientific environment in North-Rhine-Westphalia provide many opportunities of interactions with the University of Cologne and the Universities in the region, including the teaching of courses.

The Group Leader position and funding is guaranteed for five years with the possibility of extension.

The Max Planck Society and the University of Cologne aim to increase the representation of women and therefore explicitly encourage applications from female scientists.

Deadline for applications is March 28, 2007. For further details and the application procedure please visit www.nf.mpg.de/careers.

W97256R

MAX-PLANCK-GESELLSCHAFT
Generalverwaltung

The Max Planck Society for the Advancement of Science, Germany's largest non-profit research organisation, is inviting applications for two positions in its Department of Research Policy/International Relations. The successful applicants should be qualified scientific experts who will work in the areas of research analysis and foresight at the Administrative Headquarters of the Max Planck Society in Munich. The positions are open immediately.

Two positions for Scientific Experts for Research Analysis and Foresight with a focus on Life Sciences/Medicine or on Physics/Material Sciences

Job Description
In order to provide support to the scientific governing bodies of the Max Planck Society and to contribute to internal interdisciplinary discussions, the successful candidate should be able to identify and explore the challenges and opportunities of scientific development across disciplines and their societal implications. Primary duties will include:

- Analysis and evaluation of thematic developments of internationally peer-reviewed scientific literature with a major focus on life sciences and cognition sciences/medicine, or on chemistry, physics, material sciences and computer science
- Evaluation of international foresight studies and strategies
- Compilation of news and reports about important scientific publications
- Close networking with Max Planck researchers and their partners, as well as regular participation in international conferences
- Assisting in the establishment and maintenance of an internal online information platform for all Max Planck Society scientists.

Candidate Profile
The ideal candidate must possess outstanding scientific qualifications and experience, strong language skills as well as a keen interest in keeping abreast of modern research developments, the ability to recognise trends at an early stage and to report on them in a cross-disciplinary manner. He or she must be highly motivated to work in an innovative team and to try out new forms and methods of analysis and presentation of scientific results.

Requirements

- A doctoral degree in life sciences, medicine or pharmaceuticals, or a doctoral degree in physics, chemistry, material sciences or astronomy
- Extensive knowledge of the interdisciplinary developments in modern research, combined with enthusiasm for presenting such developments
- Very good analytical skills and a particular talent for quickly summarising complex scientific contexts in a concise and accessible manner
- Suitable candidates must enjoy working with people, and possess very good language skills in both German and English
- High level of self-motivation and initiative
- Experience in working with web-based tools and databases

Our Offer
Depending on previous experience and type of responsibilities, we offer a salary up to group 14 within the public service pay scale (TVöD) as well as various social benefits. For candidates changing to the position directly from civil service employment, we offer a salary up to salary group A14 of the Federal Salary Law. The workplace is situated in the heart of Munich and easily accessible through public transportation. Willingness to travel frequently is a must. This position is initially limited to two years.

As an equal opportunity employer, the Max Planck Society seeks to increase the percentage of female employees in areas where they are under-represented. Qualified women are therefore strongly encouraged to apply. The Max Planck Society is also committed to employing more individuals with disabilities. We therefore actively encourage individuals with disabilities to apply.

Applicants are requested to send their application with indication of the earliest starting date to our Department of Central Services.

We look forward to hearing from you.

Max-Planck-Gesellschaft
zur Förderung der Wissenschaften e. V.
Zentrale Dienste, Kennziffer 11/07
Postfach 10 10 62, D-80084 München
E-Mail: HR@gv.mpg.de, www.mpg.de

W97740R

Post Doctoral Scientists x 2

Cell Biology/Molecular Biology

We develop innovative solutions and automation in the fields of cell biology, molecular biology and protein science. Our systems are adopted by major pharmaceutical companies, biotechnology companies and research organisations worldwide.

Two new research positions are being created for highly motivated scientists with post-doctoral experience. The positions will be based at our laboratories in New Milton UK, but with significant external collaboration and travel. Preference will be given to candidates with a demonstrable understanding of cellular processes, and a proven ability in implementing innovative cell biology/molecular biology techniques. Candidates should be enthusiastic and capable of thinking and working independently. Flexibility and creativity, coupled with excellent communication and time-management skills are essential. The appointed persons will be good team players, and will become a committed part of our Research & Development team.

We offer a competitive salary, commensurate with experience, plus BUPA.

If you have the skills and experience required for this challenging role, please email your CV and covering letter, stating why you are interested in this job, your current salary and notice period to sharon.barton@genetix.com before the closing date of 16 March 2007.

Applicants must have the legal right to work in the UK.

Genetix
Take the lead

97841R

www.genetix.com

Information and Public Relations Liaison

incf International Neuroinformatics Coordinating Facility

The INCF is an international organization established through a collaborative effort of 12 OECD member countries. The mission of the INCF is to coordinate and facilitate the development of database and web applications for neuroscience data, analytical tools, and modeling and simulation capabilities pertaining to nervous system functions.

INCF is setting up local offices in 12 countries and is now recruiting a talented science writer and communicator for a position as Scientific Information and Public Relations Liaison at our international central office in Stockholm, Sweden.

Your mission and responsibilities will include promoting the INCF on an international basis to scientific and public communities, contact with the press, development of material and articles for web sites, brochures and journals, and communication with INCF National Nodes concerning the promotion of their activities.

The successful applicant should have excellent social skills and the ability to naturally attract people's attention and translate complex issues to a language that is commonly understood.

Please refer to* www.incf.org *for further information about INCF, the position, and how to apply.

W97764R

Research Into Ageing

Research into Ageing Funding Opportunities

Research into Ageing is a charity supporting biomedical research into the biology of ageing, and diseases and disabilities associated with older people (excluding cancer). Applicants may be any nationality, but the research must be carried out in the UK. The following awards are currently available:

Research Fellowships; providing personal support for postdoctoral scientists plus research expenses for three years in the first instance, deadline **1 May 2007** for outline applications.

Clinical Research Fellowships; The British Geriatrics Society and Research into Ageing are delighted to announce the availability of a clinical research training fellowship to members of the BGS with an NTN in Geriatric Medicine. Funding is for a period up to three years and should not exceed £250,000. Deadline for outline applications is **1 May 2007**.

PhD Studentships; outline applications from prospective supervisors are invited by **1 May 2007**.

Small Incontinence Awards; to provide support for up to £50,000 for research into urinary or faecal incontinence. Deadline **13 July 2007**.

Discipline Hopping Awards; support for up to £50,000 for established researchers not in the ageing field to investigate and develop ideas, skills and collaborations into ageing. Deadline **1 May 2007**.

New Investigator Awards; to provide short-term flexible funding up to £50,000 for researchers at the start of their first academic appointment. Deadline **13 July 2007**.

Project Grants; available to established (lecturer and above) researchers with a strong track record in ageing research. Project grants are available up to £225,000 over 3 years. Deadline **1 May 2007**.

Further information about the research funded by Research into Ageing, eligibility and how to apply, and application forms is available at our web-site www.ageing.org

Research into Ageing, 207-221 Pentonville Road, London N1 9UZ. Email: grants@ageing.org

Research into Ageing is a special trust within Help the Aged.
Research into Ageing is a Registered Charity No. 277468
Help the Aged is a Registered Charity No. 272786.

BRITISH GERIATRICS SOCIETY

97770R

HELP THE AGED WE WILL™

Trip Hazard

Career paths can be precarious. Stride confidently with insider-knowledge from *Naturejobs*.

naturejobs

HELMHOLTZ ASSOCIATION

The Helmholtz Association of German Research Centres is seeking excellent young scientists and engineers as leaders for

20 Helmholtz Young Investigators Groups

in six Research Fields:
Energy, Earth and Environment,
Health, Key Technologies,
Structure of Matter,
Transport and Space

The Helmholtz Association is Germany's largest organisation for scientific research and development. The 15 Research Centres united in the Association have a staff of 25,700 and an annual budget of about 2,3 billion euros. They perform top-rate research in strategic programmes and thus contribute to solving grand challenges which face society, science and industry.
The Association's potential for realising these ambitious objectives lies in the excellence of its personnel, its world-class large-scale facilities and excellent scientific infrastructure and its experience in researching systems of great complexity.
The Young Investigators Groups will promote and further strengthen collaborations between the Helmholtz Centres and universities.

Eligibility: Individuals who have earned a doctoral degree within the last six years and have achieved a superior record of accomplishment during their doctoral and postdoctoral research.

Award:
- Group leader position, salary BAT Ia/Ib or TVL/TVöD 14/15,
- Adequate laboratory space,
- Funds for laboratory set-up and operation,
- Positions for post-docs, graduate students and technical staff.

Duration: 5 years with a peer evaluation.

Perspective: Permanent employment, if evaluation attests excellence of group leaders.

Application:
Step 1 Candidates contact the Helmholtz Centre of their choice with a CV, publication list and a letter of intent
Step 2 The formal applications have to be handed in by the chairman of the executive board of the Centre.

For further details and application information:
www.helmholtz.de/yig

Deadlines: For applicants: **4 May, 2007**
For Helmholtz Centres: **30 June, 2007**

The Helmholtz Association is an equal opportunity employer and is committed to increasing the percentage of women in group leader positions.

Contact: berit.dannenberg@helmholtz.de

AWI · DESY · dkfz. · DLR · FZ Jülich · GFZ Potsdam · GKSS Forschungszentrum · gsf · GSI · Helmholtz Centre for Infection Research · HMI · IPP · MDC Berlin-Buch · Helmholtz Centre for Environmental Research – UFZ

W97141R

DIRECTOR

Applications are invited for the Directorship of the Marine Biological Association (MBA) of the UK, an independent charity and Learned Society established in 1884 to promote scientific research into all aspects of life in the sea and to disseminate the knowledge gained. The MBA is grant-aided by the Natural Environment Research Council (NERC). The MBA receives substantial grant and contract income from a wide range of other sources.

The Director must have a proven ability to initiate, stimulate and conduct innovative research and provide the scientific leadership to promote a diverse and creative environment. He or she will be expected to continue an active research programme. The MBA will be contributing to the NERC-funded "Oceans 2025" programme with the other UK marine research centres funded for 2007 – 2012.

The Director will require excellent management skills, and the energy and ability to promote the Association and its activities both nationally and internationally. These include educational and knowledge transfer programmes. The Director will also act as Secretary to the distinguished Council that governs the affairs of the Association and runs the Learned Society.

The appointment will be at Professorial level. A joint permanent position with the University of Plymouth will be available. Secondments for five years from other organisations are also encouraged. The starting date should be by Autumn 2007, but is negotiable. **The salary will be commensurate with age and experience within the range £45,000-£65,000 per annum,** and the terms and conditions of employment will be analogous to those of universities (including USS).

Applications, together with full CV, list of publications and the names of three persons willing to act as referees, should be sent by e-mail (sec@mba.ac.uk) with a hard copy by post marked "CONFIDENTIAL" to:

Mr Jon Parr, Operations & Infrastructure Manager, Marine Biological Association of the UK, The Laboratory, Citadel Hill, Plymouth PL1 2PB, UK.

Applications will close on 5th April 2007.

Further particulars on the position can be obtained from Mr Parr at the above address, (tel: +44 (0)1752 633331) via e-mail (sec@mba.ac.uk) or from the MBA website (www.mba.ac.uk)

97591R

Eberhard Karls
Universität
Tübingen

The **Faculty of Biology** of the Eberhard-Karls-University Tübingen invites applications for the position of

Full Professor (W3) in „Evolutionary Biology of Vertebrates"

available from 1st of April 2008.

The successful applicant will pursue an internationally high-ranking research agenda in the field of organismal zoology, preferably with a focus on vertebrates. Teaching obligations cover all aspects of zoology, with emphasis on vertebrate evolution. Close collaborations with the interfacultary teaching and research platform „Evolution and Ecology Forum" EvE are expected. EvE integrates organismal biology in Tübingen and offers cooperation with the faculties of Biology and Geosciences and the Max-Planck-Institute for Developmental Biology. The position includes management of the zoological collection and the limnological field station „Federsee".

A formal requirement for appointment is a „Habilitation" or equivalent level of scientific and academic teaching qualifications.

The University of Tübingen is committed to strengthen the proportion of women in research and teaching and strongly encourages applications of qualified female scientists.

If this is a candidate's first professorship, the appointment is limited to three years initially, with tenure being granted after positive evaluation. Exceptions can be made for foreign applicants or candidates from the private industry. Tenure does not require another appointment procedure.

Disabled applicants with equal qualification will be considered with higher preference.

Please send your application letter including CV, certificates, list of publications and a summary of teaching experience by 10th of April 2007 to

Dekanat für Biologie der Universität Tübingen
Auf der Morgenstelle 28 · 72076 Tübingen · Germany

W97522R

Klinikum der
Johann Wolfgang Goethe-Universität
Frankfurt am Main

Cardiovascular Physiology

The position of a

postdoctoral research associate position

is available in the Cardiovascular Physiology Institute to investigate signalling by the angiotensin converting enzyme in different pathological disease models. The position is initially for 24 months but there is possibility for renewal for an additional 36 months.

The successful candidate should have experience in translational research and surgical intervention, have worked with various mouse models of cardiovascular disease and be able to assume responsibility for breeding programmes and genotyping etc. He/she will join a dynamic and multi-national team of internationally recognised and well funded scientists.

The Johann Wolfgang Goethe University Frankfurt has the policy of raising the proportion of women in academic positions and therefore encourage applications from women with the necessary qualification.

Under German law disabled applicants with full qualifications are to be preferred.

Applicants should submit a cover letter and full CV, including the names of two referees to

Prof. Dr. Ingrid Fleming, Institut für Kardiovaskuläre Physiologie, Johann Wolfgang Goethe-Universität, Theodor-Stern-Kai 7, 60590 Frankfurt, fleming@em.uni-frankfurt.de.

W97348R

Klinikum der
Johann Wolfgang Goethe-Universität
Frankfurt am Main

Cardiovascular Physiology

The position of a

senior postdoctoral/ research associate position

is available in the Cardiovascular Physiology Institute to investigate the role of monocyte cytochrome P450 enzymes in vascular biology. The position is initially for 24 months but there is possibility for renewal for an additional 36 months.

The successful candidate should have a wide range of cell biology, biochemistry and molecular biology techniques as well as translational research and surgical intervention, and have worked with various mouse models of cardiovascular disease. He/she will join a dynamic and multi-national team of internationally recognised and well funded scientists.

The Johann Wolfgang Goethe University Frankfurt has the policy of raising the proportion of women in academic positions and therefore encourage applications from women with the necessary qualification.

Under German law disabled applicants with full qualifications are to be preferred.

Applicants should submit a cover letter and full CV, including the names of two referees to
Prof. Dr. Ingrid Fleming, Institut für Kardiovaskuläre Physiologie, Johann Wolfgang Goethe-Universität, Theodor-Stern-Kai 7, 60590 Frankfurt fleming@em.uni-frankfurt.de.

W97349R

MD/PHD PROGRAM IN MOLECULAR MEDICINE

The Paracelsus Medical University offers a PhD progam in "Molecular Medicine" (accredited by the Austrian Accreditation Council) to health professionals who have graduated from Medical School. Research projects during this PhD program focus on metabolic diseases and atherosclerosis, musculoskeletal diseases, oncology, immunological diseases and those related to allergies as well as neurological and psychiatric diseases.

Prerequisites for admission are graduation from medical school and basic knowledge of the German language. The Paracelsus Medical University admits 10 students to the program who should finish the course of studies within 3 years, graduating with a PhD. The deadline for applications is May 31st, 2007, the program begins on October 1st, 2007.

Please send application materials (CV and application letter) to:
Paracelsus Medizinische Privatuniversität | Strubergasse 21, A-5020 Salzburg
Email: phd@pmu.ac.at | Phone: +43 (0)662 / 44 2002-1221

PARACELSUS
MEDIZINISCHE PRIVATUNIVERSITÄT

W97386R

Please refer to our homepage for further information: **www.pmu.ac.at**

International PhD-Program "Cell Communication in Health and Disease" - CCHD 2007

Starting October 2007

Application deadline: April 30, 2007

At the Medical University of Vienna, **CCHD**, a PhD Program in biomolecular Medicine supported by the Austrian Science Fund (FWF), has been established. The program offers cutting-edge education in the fields of **Neurobiology, Vascular Biology, Immunology, and Inflammation Research** and integrates basic, applied, and clinical sciences, as well as a huge spectrum of experimental techniques.

Admitted PhD students will receive funding for at least three years including support to visit international conferences and specialized workshops. Applicants must hold a final degree in the diploma studies of Medicine, Dentistry, or in any scientific/technical subject-related diploma studies (such as Cell or Molecular Biology) by the commencing term of the program.

Further information on research topics and courses, as well as application forms are available at:
www.phd-cchd.at
Applications must be submitted by e-mail to
phd_cchd@meduniwien.ac.at

www.meduniwien.ac.at

CHD FWF Der Wissenschaftsfonds. MEDICAL UNIVERSITY OF VIENNA

W97435R

John Innes Centre

INDEPENDENT RESEARCH FELLOWSHIPS

The John Innes Centre (JIC), Norwich, UK is a world leading centre of excellence in plant and microbial sciences based on the Norwich Research Park. We are inviting applications from outstanding researchers who either hold, or wish to apply for Independent Research Fellowships, to attend a Conference at the JIC on 4/5 June 2007. At the meeting you will be able to present a talk about your proposed area of research and to discuss your proposals, the development of your group and your future career plans in depth with senior JIC Scientists.

After the Conference we will select and mentor outstanding candidates in writing Fellowship applications and/or offer the opportunity to move existing Fellowships to the JIC.

Further details and particulars can be found at
http://www.jic.ac.uk/corporate/opportunities/vacancies/fellows.htm

Please e-mail a 2-page summary of your research plan, a copy of your CV and arrange for three letters of recommendation to be emailed to dawn.barrett@bbsrc.ac.uk by Friday 20th April 2007.

97460R

The John Innes Centre is a registered charity (No223852) grant-aided by the Biotechnology and Biological Sciences Research Council and is an Equal Opportunities Employer.

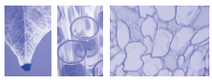

www.cardiff.ac.uk/jobs

CARDIFF UNIVERSITY
PRIFYSGOL CAERDYDD

Centre Manager for the Cardiff Neurosciences Centre

Cardiff School of Medicine

Cardiff University invites applications from a creative person with a strong scientific background for the post of manager of the newly established Cardiff Neurosciences Centre (CNC). CNC has been established to coordinate and expand Cardiff University's flourishing centre of excellence in Neurosciences and has the broad aim of understanding the functioning of the brain in health and disease. CNC will be a "virtual" centre comprised of academics from across the University. Expertise in neuroscience spans a number of schools (particularly Medicine, Biosciences, Psychology and Optometry) and covers many areas of neuroscience (see www.cardiff.ac.uk).

The Centre will promote interdisciplinary activity and provide administrative support for the Centre's academics in developing emerging collaborative ventures and putting together proposals for funding. The Directorship of the Centre will be rotated between the Centre's main participating schools. In the first instance, the Director will be Professor Mike Owen of the School of Medicine. You should be a good team worker with a degree in neuroscience or related area and experience of project management and leadership. This post is fixed term for 3 years.

Salary: £33799 - £39160 per annum

Informal enquiries can be made to Professor Mike Owen, email: owenmj@cardiff.ac.uk

To work for an employer that values and promotes equality of opportunity, visit www.cardiff.ac.uk/jobs telephone + 44 (0) 29 2087 4017 or email vacancies@cardiff.ac.uk for an application form quoting vacancy number 115.

Closing date: 23 March 2007

97681R

Paul Getty III Chair in Epilepsy

Institute of Psychiatry

at The Maudsley

Following a generous donation from Paul Getty III, a Chair in Epilepsy has been created within the Institute of Epileptology, based on the Denmark Hill Campus of King's College London. Research and treatment in epilepsy have been internationally-leading on this campus for more than 50 years. You will join the Department of Clinical Neuroscience at the Institute of Psychiatry and will be offered a contract as an Honorary Consultant Neurologist in King's College Hospital NHS Foundation Trust, which provides the largest regional Neuroscience service in the UK.

We are seeking to appoint an internationally recognised leader in laboratory-based experimental epilepsy research to this prestigious new post.

Starting salary in the range £70,822 pa to £95,831 pa (inclusive of £2,162 pa London Allowance), depending on qualifications and experience.

To obtain further particulars and further information about the Institute, please see our website at http://www.iop.kcl.ac.uk/vacancies or alternatively email vacancies@iop.kcl.ac.uk Applications, in the form of a CV (including details of four referees), covering letter and equal opportunities statement, should be emailed to this address or posted to the address given in the further particulars. Informal contact will be welcome and should be directed to Professor Christopher Shaw on +44 207 848 5183 or chris.shaw@iop.kcl.ac.uk

Please quote reference number 07/A04 in all correspondence. Closing date for applications 8th March 2007.

KING'S College LONDON

Equality of opportunity is College policy

University of London

97350R

UNIVERSITEIT GENT

Nine full-time research professorships

After more than twenty years of uninterrupted growth, Ghent University is now one of the most important institutions of higher education and research in the Low Countries.

Every year, Ghent University attracts over 28,000 students, with a foreign student population of over 2,200 EU and non-EU citizens, and employs over 6,000 staff.

Ghent University offers a broad range of study programmes in all academic and scientific areas. With a view to foster cooperation in research and to offer a pluralist community service, a wide range of research groups, centres and institutes have been established over the years.

The following positions are vacant, starting from October 1, 2007:

- Faculty of Arts and Philosophy: a position in the rank of Lecturer, Senior Lecturer or Full Professor in the field of Archaeometry.
- Faculty of Law: a position as Full Professor in the field of Law and Technology (either in commercial law, intellectual property rights, civil law, public law, international private and commercial law, criminal law or criminology).
- Faculty of Sciences: a position in the rank of Lecturer, Senior Lecturer or Full Professor in the field of Experimental Subatomic Physics.
- Faculty of Medicine and Health Sciences: a position in the rank of Full Professor or Senior Full Professor in the field of Health Economics.
- Faculty of Veterinary Medicine: a position in the rank of Lecturer, Senior Lecturer or Full Professor in the field of Gene Therapy.
- Faculty of Psychology and Educational Sciences: a position in the rank of Lecturer, Senior Lecturer, Full Professor or Senior Full Professor in the field of Philosophy of Education.
- Faculty of Bioscience Engineering: a position in the rank of Full Professor or Senior Full Professor in the field Bioresources Processing.
- Faculty of Pharmaceutical Sciences: a position in the rank of Lecturer, Senior Lecturer or Full Professor in the field of Alternative in Vitro Toxicity Testing.
- Faculty of Political and Social Sciences: a position as Full Professor in the field of Sociology.

The rank that will be granted depends on the specific profile of the selected candidate.

Deadline for submission of applications: **15 March 2007.**

For more detailed information on these vacancies, please visit the URL: **https:/webster.ugent.be/vacatures/ZAP/research.html**

W97601R

Nuffield Department of Surgery

UNIVERSITY OF OXFORD

MRC Research Studentship

The Nuffield Department of Surgery was rated 5* in the 2001 HEFCE Research Assessment, has a well-established training programme for research students and has laboratories equipped with state-of-the-art facilities.

Applications are now invited for an MRC research studentship starting October 2007 in one of the following areas:

- Optimisation of Human Islet Isolation
- Developmental Biology of the Pancreas
- The Importance of Early Innate Immune Response in Rejection and Tolerance
- Dendritic Cell Immunotherapies for Cancer
- A Quality Improvement Approach to the Reduction of Errors on Surgical Wards

Applicants must be citizens of the European Community, with a first degree in the biological sciences, should be self-motivated and able to work both independently and as part of a research team.

Further information, including outlines of the available projects, may be obtained from the Assistant Administrator on rhian.perridge@nds.ox.ac.uk or Tel: (01865) 220532 or are available from the NDS website: http://www.surgery.ox.ac.uk/about/jobvacancies/studentship/

Formal application by CV and covering letter, including the names and full contact details of two academic referees, should be sent to The Research Administrator, Nuffield Department of Surgery, University of Oxford, Level 6, John Radcliffe Hospital, Headington, Oxford OX3 9DU. Applications must quote reference NDSA/216/07. Closing date for receipt of applications is Friday, 23rd March at 5.00pm.

The University is an Equal Opportunities Employer.

www.ox.ac.uk/jobs

97745R

THE UNIVERSITY OF WARWICK

Department of Biological Sciences

Research Fellow

Ecology and Epidemiology

£24,402 - £31,840 pa **Ref: 59370-027**

Fixed Term Contract for up to a maximum of 3 years

Warwick is one of Britain's leading universities with an enviable reputation for educational opportunities, first rate research and its commitment to the local community.

The University Values Diversity

You will undertake research in order to support the study of the epidemiology and population dynamics of *Theileria annulata* infection. The post is funded by the Wellcome Trust as part of an international collaboration of field and laboratory studies.

You will be fully qualified (PhD or MSc) with proven aptitude in veterinary epidemiology, mathematical modelling and statistical analysis.

Informal enquiries: Professor Graham Medley at graham.medley@warwick.ac.uk

Application packs are available from Personnel Services on 024 7652 3685 (24 hour answerphone), by email: recruit@warwick.ac.uk, our website below or www.jobs.ac.uk/warwick. An application form MUST be completed if you wish to apply for this post.

Closing date: 23 March 2007

97757R

www.warwick.ac.uk/jobs

Roche

Pharmaceuticals

Project Leader in Vascular Biology

Who we are:
At Roche, we believe passionately in what we do, and that our products make a difference in people's lives. We are a successful business that can offer exciting career opportunities to you, both locally and internationally, in a supportive and rewarding culture. We know that our people are responsible for our success and we value our employees, aiming to create a work environment where feeling valued, respected and empowered is a daily experience.

Headquartered in Basel, Switzerland, Roche is one of the world's leading research-focused healthcare groups in the fields of pharmaceuticals and diagnostics. As a supplier of innovative products and services for the early detection, prevention, diagnosis and treatment of disease, the Group contributes on a broad range of fronts to improving people's health and quality of life. Roche is a world leader in diagnostics, the leading supplier of medicines for cancer and transplantation and a market leader in virology.

The Position:
You will lead a multidisciplinary team of technicians and associate scientists with a proven track record in drug discovery and basic research. The team's mission is to identify and evaluate potential drug targets in vascular inflammation, in the pursuit of truly novel medicines for atherosclerosis.

Who you are:
You have a PhD and/or MD and a strong background in drug discovery, with at least five years' experience in pharmaceutical research and significant experience in atherothrombosis research. Your area of expertise is physiology/pharmacology, with a strong background in animal models of atherosclerosis. Successful research on mechanisms of atherosclerotic lesion instability is documented by your excellent publication record. Previous exposure to therapeutic approaches using apolipoproteins or apolipoprotein mimetics would be an advantage.

You should also have experience in working with high-profile scientific leaders and be able to represent Roche at scientific meetings and in academic and industry consortia. Previous experience in working in cost-effective, cross-functional, interdisciplinary groups in a matrix organisation and the ability to work in a goal-oriented manner within strict time constraints are additional pre-requisites for this position.

If you are interested in this position please apply online at:
http://careers.roche.com, Job ID 3395 and attach full supporting documentation (CV, diplomas).

W97375R

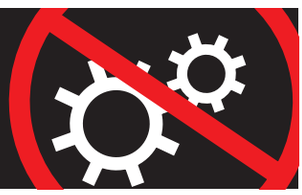

www.nottingham.ac.uk/hr

The University of Nottingham

School of Pharmacy
Division of Drug Delivery & Tissue Engineering

Lecturer in Drug Delivery

The School of Pharmacy at the University of Nottingham wishes to appoint a new Lecturer in Drug Delivery within the Division of Drug Delivery and Tissue Engineering. The Division has a broad range of research interests including the design of bioresponsive polymers, pharmaceutical nanotechnologies, biopharmaceuticals delivery, oral drug delivery and tissue engineering. The activities of the School of Pharmacy in this area of research include a new prestigious Doctoral Training Centre in Targeted Therapeutics funded jointly by EPSRC and AstraZeneca. Applications/enquiries are welcome from candidates who can complement our skills or take the Division/School into new areas of pharmaceutical science, particularly in biopharmaceuticals formulation, cellular fate of delivery systems and intracellular trafficking.

The successful candidate will be expected to contribute to and develop research programmes that will maintain the School's world-class research reputation. They will also contribute to the teaching of the MPharm degree course. Candidates should have a record of high quality publications in an appropriate field of research.

Salary will be within the range £29,138 - £39,160 pa, depending on qualifications and experience (salary can progress to £45,397 pa, subject to performance).

Informal enquiries may be addressed to Dr C Alexander, tel: 0115 846 7678 or Email: Cameron.Alexander@Nottingham.ac.uk.

For more details and/or to apply on-line please access: http://jobs.nottingham.ac.uk/RUB859S/ or contact the Human Resources Department, The University of Nottingham, King's Meadow Campus, Lenton Lane, Nottingham NG7 2NR. Tel: 0115 951 3262. Fax: 0115 951 5205. **Please quote ref. RUB/859S. Closing date: 23 March 2007. Interview date: 26 April 2007.**

97688R

University of Southampton

School of Biological Sciences

Research Fellow: Database and Bioinformatics Specialist Plant and Environment Group

£24,402 - £30,013 Ref: 0818-07-M

(starting salary £24,402)

Employed in a thriving laboratory interested in all aspects of tree biology and particularly genomics, genetics and environmental biology of the model genus Populus, you will undertake the bioinformatics tasks associated with the development of the 'Laboratory without Walls for Ecosystem Genomics' (LWEG) within the 6th Framework Network of Excellence, EVOLTREE (www.evoltree.org).

You will be leading the integration of databases from diverse biological data enabling wide access via a users' web browser and web services. You will have been working within the bioinformatics field and have a sound grasp of PHP/MySQL programming.

This full-time post will run for one year in the first instance with the expectation of extension during the lifetime of the EVOLTREE Network of Excellence up to March 2010.

The post is available immediately. Informal enquiries may be made to Professor Gail Taylor (g.taylor@soton.ac.uk).

To find out more about us and the roles we have on offer visit www.jobs.soton.ac.uk and apply on-line. Alternatively tel 023 8059 2750. The closing date for this position is 16 March 2007 at 12pm. Please quote reference number 0818-07-M on all correspondence.

97691R

www.jobs.soton.ac.uk

UNIVERSITÉ DE GENÈVE

UNIL | Université de Lausanne

ÉCOLE POLYTECHNIQUE FÉDÉRALE DE LAUSANNE

THE UNIVERSITIES OF GENEVA (UNIGE) AND LAUSANNE (UNIL), THE ECOLE POLYTECHNIQUE FEDERALE DE LAUSANNE (EPFL), AND THE UNIVERSITY HOSPITALS OF GENEVA (HUG) AND LAUSANNE (CHUV) OFFER

9 PhD Fellowships

to work in laboratories covering a large spectrum of topics from molecular to cognitive Neuroscience.

Lemanic Neuroscience PhD Fellowships
starting in September 2007
Geneva & Lausanne, Switzerland

More information about the application, selection procedure, Doctoral Program and potential host laboratories may be obtained at this address:

www.lemanic-neuroscience.ch/phd-fellowships

Candidates with Masters or equivalent degrees are invited to submit their application on line **before April 15th 2007.**

W97012R

THE ROYAL SOCIETY

Royal Society Industry Fellowships 2007

The Industry Fellowship Scheme aims to foster knowledge transfer and exchange between academia and industry. The Fellowships provide the chance for scientists with permanent positions in industry and academia (or not-for-profit research organisations) to work for up to two years (full-time) or 4 years (part-time) in the other sector. The personal and corporate links forged will provide a foundation for future collaborative development.

The fellowships are jointly funded with EPSRC, BBSRC, NERC, Rolls-Royce plc and Astra Zeneca Ltd.

Each Fellowship offers:

- salary costs for the fellow (non FeC) and research expenses of up to £2000 per year;
- funding for up to two years full-time or four years part-time enabling the holder to maintain links with their employing institution during the fellowship;
- the opportunity to network with other Royal Society Research Fellows and to participate in various professional development activities run by the Royal Society.

Closing Date: **20 April 2007**

Applications must be submitted online on the Royal Society's electronic Grants Application and Processing (e-GAP) system (https://e-gap.royalsoc.ac.uk, or via the e-GAP logo on the front page of the Royal Society's web site.

For further information, visit www.royalsoc.ac.uk/funding or email ukgrants@royalsoc.ac.uk

97512R

the University of Twente is looking for

Assistant Professor Regenerative Medicine

at the Institute for Biomedical Technology, 1,0 fte

The successful candidate will be responsible for the development of a research line within the chair Tissue Regeneration of Prof. Dr. Clemens van Blitterswijk. The candidate must demonstrate leadership qualities oriented to supervising researchers and must have demonstrated the ability to attract research funding from governmental and corporate funding sources. The candidate is expected to have extensive international contacts, helping to set up joint research programs, and must have a track record in the relevant research area, as demonstrated by refereed publications and presentations on national and international platforms.

The assistant professor will contribute to the bachelor and master programs in Biomedical Engineering and Technical Medicine. In due course the candidate is expected to participate in the regular managerial tasks within the Faculty and the University. We are recruiting an assistant professor fitting one of the following profiles

- Biomaterials
- Ceramics
- Bioprocess Technology

We offer a top level research and academic environment with excellent opportunities for personal development. The work is highly interdisciplinary and the atmosphere in the group as well at the institute is collegial and collaborative. The University offers, after a trial period of one year, a permanent full time position as an Assistant Professor according to the qualifications. The university offers a competitive salary of maximum € 4761,- gross per month. For more detailed information you can contact the head of the group, Prof. Dr. C.A. van Blitterswijk, phone +31-53 4893400, email: C.A.vanBlitterswijk@utwente.nl. Interested candidates are invited to send, by email, an application letter, resume, and publication list before March 22th, to University of Twente, Faculty of Science and Technology, attn. to Mrs. Drs. M.D. Hilderink, head of the department Human Resources Faculty of Science and Technology, e-mail PenO@tnw.utwente.nl.

University of Twente
The Netherlands

W97775R

Marie Curie Research Institute Oxted, Surrey, UK

Postdoctoral Scientist
Cytoskeletal Organisation Laboratory

Salary range £26,274 - £32,313

The Marie Curie Research Institute (MCRI) is an internationally renowned cancer research institute funded by Marie Curie Cancer Care, one of the largest independent cancer charities in the world. The Institute supports both basic and translational research programmes investigating the molecular and cellular basis of cancer and the development of new therapeutic approaches. The Institute is equipped to a high standard with all laboratories supported by centralised service units. We are located in an extremely pleasant rural environment with easy access to London.

Applications are invited for a Postdoctoral Fellowship in the new MCRI Cytoskeletal Organisation Laboratory headed by Dr. Anne Straube. The project will focus on the role of the microtubule cytoskeleton during cellular differentiation.

Applicants should be highly motivated, enthusiastic individuals, should have, or expect to obtain, a PhD in cell biology, biochemistry or related subject area and be able to demonstrate expertise in molecular biology, protein biochemistry and imaging techniques. The successful candidate will be offered a 3 year fixed-term contract for a full-time Research Training Fellowship.

Informal enquiries are welcome and should be made directly to Dr. A. Straube (a.straube@mcri.ac.uk).

Applications including a concise description of research experiences and interests, a full CV and the names and addresses of three referees should be submitted to: Julie Curtis, Marie Curie Research Institute, The Chart, Oxted, Surrey RH8 0TL, UK.

Closing Date: 15th April 2007.

The Marie Curie Research Institute is committed to equal opportunities in employment

97802R

MARIO NEGRI
ISTITUTO DI RICERCHE FARMACOLOGICHE

The Istituto di Ricerche Farmacologiche "*Mario Negri*" (http://www.marionegri.it/) is one of the largest private no-profit foundation in Europe with two campuses in Milano and Bergamo. The areas of scientific interest covered range from *Neurosciences*, *Biochemistry and Molecular Biology*, *Oncology*, *Cardiovascular Medicine*, *Nephrology*, *Immunology of Transplantation and Rare Diseases* to *Environmental Toxicology and Population Health*. By July 2007 our Institute in Milano will move to a new location. The new campus will triplicate in size relative to our current premises with increased research facilities, state-of-the-art technology and emphasis on in vivo models in various areas of bio-medicine and pharmacology. With this new operation, we want to strengthen our traditional areas of research and pursue new and promising avenues.

We are looking for talented European scientists with an excellent scientific record and currently working outside EU to apply for the first call of the

"ERC-STARTING RESEARCH INDEPENDENT GRANT"

funds, within the frame of the FP7 program "***IDEAS***".

Contact addresses: **egarattini@marionegri.it**
lesti@marionegri.it

W97787R

Imperial College London

100 years of living science 100

Lecturer in Computer Aided Drug Design

Department of Chemistry
Salary: From £37,740

Imperial College is ranked in the top ten universities of the world, according to the 2006 Times Higher Education Supplement league tables.

We are seeking to recruit a motivated and enthusiastic Lecturer of the highest calibre in the area of computer aided drug design. The appointed candidate will be provided with a unique opportunity to further drug discovery and development in a major academic centre of excellence.

You will have research interests and experience in synthetic organic or medicinal chemistry and/or industrial experience in a major pharmaceutical research or biotech company.

You will be expected to establish and develop a research programme of international standing on the structure-based design of novel inhibitors of enzymes and designated protein/protein interactions including protein homology modeling, virtual screening, de novo design, pharmacophore discovery and development, docking studies and related methods.

You will also be expected to contribute to the undergraduate and postgraduate teaching of the department.

Imperial College is one of Europe's leading teaching and research institutions and the Department of Chemistry is a 5* department of the Faculty of Natural Sciences, based at the South Kensington Campus.

(http://www.imperial.ac.uk/physicalsciences)

The post will be permanent and full-time and is available immediately.

Informal enquiries may be directed to the Head of Synthetic Chemistry, Professor AGM Barrett, agmb@imperial.ac.uk,

Further particulars and an application form can be obtained from the following website: http://www3.imperial.ac.uk/employment/academic/ns200725as

Completed applications forms, with an up to date CV showing relevant experience, listing publications, describing research interests and plans for future research should be sent to Ms C Oriel, c.oriel@imperial.ac.uk PA to Head of Department, Department of Chemistry, Imperial College London, South Kensington campus, London SW7 2AZ. Electronic submission preferred. Please quote ref: Lecturer in CADD on all correspondence.

Closing date: 9 March 2007.

Valuing diversity and committed to equality of opportunity

97748R

2 Posts: Lecturer & Postdoctoral Research Worker

Department of Neuroscience - Centre for the Cellular Basis of Behaviour

Institute of Psychiatry

at The Maudsley

We would like to invite applications for the post of lecturer in the Neurobiology of Mental Health and the post of Postdoctoral Research Worker in Neural Stem Cell Research.

The Lecturer in the Neurobiology of Mental Health will develop a novel research program in the area of molecular mechanisms of learning and memory. The post holder will also contribute to teaching and administration duties within the Department. The appointee will have a proven track record of research productivity, as demonstrated by high impact publications.

The successful candidate will have a PhD in biochemistry, molecular biology or neuroscience. They will have postdoctoral experience and extensive experience with behavioural studies of learning and memory. They should also be familiar with biochemical methods and mouse molecular genetic approaches. They should be self-motivated with a commitment to gaining independent research funding and have some experience of supervision and teaching of research students.

Starting salary in the range £32,314 pa to £40,771 pa (inclusive of £2,323 pa London Allowance), depending on qualifications and experience.

The Postdoctoral Research Worker will work on a project funded by the European Commission Framework V to develop neural stem cells for the treatment of spinal cord injury. They will be part of a team led by Dr Sandrine Thuret and Professor Jack Price studying stem cell repair mechanisms in the central nervous system.

The successful candidate will have a PhD in Neuroscience or a related discipline. He/she will have experience in neural cell culture and preferably some experience in gene manipulation and gene expression analysis.

Starting salary in the range £23,175 pa to £26,439 pa (inclusive of £2,323 pa London Allowance), depending on qualifications and experience.

To obtain further particulars and further information about the Institute, please see our website at http://www.iop.kcl.ac.uk/vacancies or alternatively email vacancies@iop.kcl.ac.uk Applications, in the form of a CV (including details of two referees), covering letter and equal opportunities statement, should be emailed to this address or posted to the address given in the further particulars. Please quote reference number 07/A07 for the Lecturer post and reference number 07/R16 for the Postdoctoral Research Worker post in all correspondence.
Closing date for applications: 21st March 2007.
Only candidates shortlisted for interview will be contacted.

KING'S College LONDON

University of London

Equality of opportunity is College policy

97687R

*icrea
Institució Catalana de Recerca i Estudis Avançats

CATALAN INSTITUTION FOR RESEARCH AND ADVANCED STUDIES

Senior Research Positions 2007

ICREA announces the opening of 25 senior research positions in different fields.

Minimum requirements are a Ph.D. degree obtained before May 2003, preferably with four years of international exposure at the doctoral and/or post-doctoral level. However, **only those candidates with an outstanding research record and excellent leadership capabilities will be considered.**

Successful applicants will have a **permanent contract** with ICREA and will work at universities, research centres and other cooperating institutions in Catalonia. Salaries will be in line with those paid at Catalan universities.

ICREA research professors will be subject to an evaluation of research progress and general performance after a three-year period, and subsequently every five years. A positive evaluation will lead to a salary increase.

For further details visit **www.icrea.eu**

Junior – Academia Research Contracts 2007

ICREA announces the opening of 15 junior – academia research contracts in different fields.

Minimum requirements are a Ph.D. degree obtained before May 2005, preferably with two years of international exposure at the doctoral and/or post-doctoral level. Applicants should be around 34 years old at the time of their application, although consideration will be given to older candidates in special circumstances.

Successful applicants will have a **five-year contract** with ICREA and will work at universities, research centres and other cooperating institutions in Catalonia. Salaries will be at the level of a first-year professor *(Professor Titular)* in the Catalan public university system.

ICREA researchers will be evaluated after their contracts have been in effect for four years. Researchers whose performance is outstanding may be eligible for a permanent ICREA senior position at the end of their five-year contract. The number of such positions will be limited.

For further details visit **www.icrea.eu**

Applications and deadline

Applications for both calls must be submitted electronically via ICREA's website **www.icrea.eu** The website provides all the information needed to apply. **Deadlines:** Senior Call – 20 April 2007 · Junior - Academia Call – 27 April 2007.

***ICREA** is a foundation jointly sponsored by the Ministry of Innovation, Universities and Enterprises of the Government of Catalonia *(Generalitat de Catalunya)* and by the Catalan Research and Innovation Foundation. ICREA's main goal is to support high-level research in Catalonia by creating new research positions.

W97574R

SCRI
living technology

POST DOCTORAL RESEARCHER

SCRI is Scotland's leading Institute for research on plants and their interactions with the environment, particularly in managed eco-systems. Our mission is to conduct excellent research in plant and environmental sciences. Our vision is to deliver innovative products, knowledge and services that enrich the life of the community and address the public goods of sustainability and high quality, healthy food.

Applications are invited for a highly motivated post-doc to join SCRI, to study regulated gene expression controlling flower development. The work in Gordon Simpson's lab focuses on the regulation of gene expression in the control of the floral transition.

The main objectives are to :

- characterize the molecular basis by which the RNA binding protein, FPA, controls flowering time and
- characterize novel Arabidopsis and barley mutants affecting flowering.

This post requires the individual to conduct research into the molecular basis of regulated gene expression controlling flowering, by designing and conducting experiments involving molecular biology and molecular genetics methods to characterise mutants.

Candidates must be highly motivated, capable of independent work and have a PhD. Previous experience with Arabidopsis, gene expression analysis or molecular genetics would be an advantage. The successful candidate should be highly organized and be able to work as part of an interactive team.

This position is working in a lab which is jointly supported by **Dundee University College of Life Sciences** and the **Scottish Crop Research Institute**. This interaction combines a stimulating research environment with state-of-the-art plant growth facilities.

This position has approved funding for 3 years.

Informal enquiries about the position should be directed to Dr Gordon Simpson (g.g.simpson@dundee.ac.uk) **(DO NOT SEND APPLICATIONS TO THIS EMAIL ADDRESS)**

Covering letter and CV including the names and addresses of 2 referees should be sent to, Human Resources Office, SCRI, Invergowrie, Dundee, DD2 5DA, quoting the reference REF GGB/6 or by email to jkeith@scri.ac.uk Closing Date 30 March 2007.

The Institute is an equal opportunities employer.

97784R

Department of Pharmacology

UNIVERSITY OF OXFORD

BBSRC MSc Studentships

The Department of Pharmacology are pleased to announce that four one year BBSRC MSc studentships are available for 2007/08 on the MSc in Pharmacology. This is an exciting opportunity to receive funding for a well established MSc. Further details of the course can be found at: http://www.pharm.ox.ac.uk/gso/msc/index_html

Oxford is an excellent centre to pursue an intensive programme which will cover pharmacology from gene to organism, combining fundamental pharmacological principles with essential practical training including that for a Home Office personal licence. The Department has research groups at the international forefront of Pharmacology with the research groups taking the lead in outstanding innovative research. This course is of value to those within or wishing to embark upon a career in the pharmaceutical industry as well as in academic research which is a central aim of this programme.

Students will receive training in research methods and undertake an individual investigative practical project. Leading pharmaceutical companies support the course and will provide additional specialist lectures and tutorials.

Entry requirements are a 2:1 minimum (or equivalent) in a scientific subject. Overseas candidates are not eligible for these Studentships, and the award varies according to eligibility for UK and EU students as follows:

- Fees and a maintenance award for UK students
- Fees only for EU nationals

A Guide to Studentship Eligibility can be found at:
http://www.bbsrc.ac.uk/funding/training/eligibility.pdf

Prospective candidates should contact the Graduate Studies Office in the Department, quoting 'Taught MSc', for further details. Tel: 44 1865 271646; E-mail: graduate.studies@pharm.ox.ac.uk; Post: Dept of Pharmacology, University of Oxford, Mansfield Road, Oxford OX1 3QT, UK.

Those interested in these studentships should apply by 30th March 2007. Applicants should already have been offered places on the MSc in Pharmacology by the Department or should be in the competition for the course via graduate admissions at time of application.

97751R

ulm university universität
uulm

In the **Section for Sports- and Rehabilitation Medicine,** Center for Internal Medicine II, the following non permanent positions are available for the muscle research lab:

The muscle research lab focuses on the adaptation of skeletal muscle to physical training and stress, i.e. muscle structural proteins, stress proteins and cellular mechanisms. New projects will focus on the effects of ageing, physical inactivity and metabolism on muscle sarcopenia.

PhD position (Wissenschaftlicher Mitarbeiter)

full-time, 3 years, extension possible.

Experience in standard techniques of biochemistry and molecular biology are expected which includes excellent knowledge of and skills in gel electrophoresis, characterization of proteins, immunohistochemistry, cell biology, primary cell culture systems and animal models. We are looking for individuals while promoting and developing the scientific projects of the lab ideas.

PhD-Student (Doktorand)

half-time position, 3 years

We seek for a qualified, highly motivated PhD student with a master/diploma degree in biology, biochemistry or related life sciences. The candidate should be familiar with standard molecular biology.

The candidates are expected to have good communication and writing skills and to work constructively in a multi-disciplinary team.

The University of Ulm invites qualified women to apply. In case of equal qualification and job performance, women are considered in favor if not good reasons in the person of the competitor preponderate. Applications from qualified handicapped people are favorably considered.

Applications (English/German) must include a full CV, summary of the doctoral, master/diploma thesis, and name and address of two references and should be submitted by mail within two weeks to:
Universitätsklinikum Ulm, Herrn Professor Dr. J. M. Steinacker,
Sektion Sport- und Rehabilitationsmedizin, Klinik für Innere Medizin II,
89070 Ulm, Tel.: +49-731-500-45300, Fax: +49-731-500-45303,
email: juergen.steinacker@uniklinik-ulm.de,
website: http://www.uni-ulm.de/sportmedizin

W97683R

University of Mannheim

For the international, EU-funded project SOMAPS on research about body perception the following positions at the University of Mannheim are offered:

At the Otto-Selz-Institute for Applied Psychology:

1 PhD position (EG 13; before 0.5 BAT IIa)

for at first a duration of 2 years (extension possible).

Applications are requested until March, 12th 2007 to: Prof. Dr. Rupert Hölzl, Professur für Klinische und Biologische Psychologie, Universität Mannheim, 68131 Mannheim.

At the Institute for Computational Medicine (ICM, www.icm-mannheim.org)
two positions in the field of MR imaging research are offered:

1 PhD position (EG 13; before 0.5 BAT IIa)
1 Postdoc position (EG 13; before BAT IIa)

for a duration of three years each.

Applications with the usual documents are requested until March, 12th 2007 to:
Dr. Daniel Gembris, Institut für Computerunterstützte Medizin (ICM) und Lehrstuhl für Informatik V, Universität Mannheim, B6, 23-29B, D-68131 Mannheim.

W97696R

the Beatson
institute for cancer research

Postdoctoral Scientists

(Two posts, 3 year fixed-term contract)

Starting Salary from £25k

The newly formed Urology Research Group at the Beatson Institute for Cancer Research is seeking two postdoctoral researchers to study the role of aberrant signalling in prostate carcinogenesis. We have recently discovered the significance of Sprouty2 and MKK5/ERK5 pathways in prostate cancer. The successful candidates will study the molecular basis of these and other relevant signalling network. Studies will involve microarray analysis, protein-protein interaction and real time imaging techniques.

The Beatson Institute is one of the UK's leading cancer research centres. It is core funded by Cancer Research UK and supports cutting edge research into the molecular mechanisms of cancer development. The Beatson Institute provides an outstanding research environment, underpinned by state-of-the-art core services and advanced technologies. A new research facility, due for completion this year will allow significant expansion of the Institute over the next few years.

Applications with CV and names of two referees should be sent to Professor Hing Leung, The Beatson Institute for Cancer Research, Garscube Estate, Switchback Road, Bearsden, Glasgow G61 1BD, Scotland (fax: 0141 942 6521) or by email to h.leung@beatson.gla.ac.uk.

Closing date for applications: Thursday 15th March 2007

CANCER RESEARCH UK

Charity no: SC006106

97689R

Institute of Food Research

Clostridium botulinum Researcher

A position is available for a post-doctoral molecular biologist (with microbiology expertise) in the *Clostridium botulinum* research team led by Prof. Mike Peck at the Institute of Food Research. A principal target of our research is to extend understanding of the genetic basis for the physiological response of *C. botulinum* to environmental stress. The appointed researcher will work on projects concerned with the development and validation of novel molecular methods to detect and characterise *C. botulinum* and other pathogens, and with assessing the effect of environmental factors on growth and toxin formation by *C. botulinum*.

Experience in molecular microbiology and microbiology, willingness to work in a team, familiarity with handling hazardous pathogens, and communication skills are required. Experience with *C. botulinum* or other spore-forming bacteria, or in anaerobic microbiology would be of benefit, but are not essential. (More details can be found on our web site: http://www.ifr.ac.uk/).

For an informal discussion please contact Prof Mike Peck +44 (0)1603 255251; e-mail: Mike.Peck@bbsrc.ac.uk. Starting salary will be in the range £24,200 to £27,200 per annum depending on qualifications and experience.

For an application form please contact the Human Resources Office, Norwich BioScience Institutes, Colney, Norwich, NR4 7UH, UK or Email: nbi.recruitment@bbsrc.ac.uk quoting post reference number 1702. Indefinite contract (initially funded to 31/12/08).

Closing Date: 22 March 2007

An equal opportunities employer

ifr
Institute of Food Research,
Norwich Research Park,
Colney, Norwich. NR4 7UA

www.ifr.bbsrc.ac.uk

97726R

brighton & sussex medical school

5 Postdoctoral Research Fellow Positions

Fixed-term **£20,852 - £31,211 pa**

3 Postgraduate Studentships

As a relatively new medical school, Brighton and Sussex Medical School is now at the stage of developing postgraduate degrees and creating posts for Postdoctoral Research Fellows to drive its dynamic programme of research in several areas forward. For this reason, in its second phase of strategic planning, BSMS is seeking to recruit 5 Postdoctoral positions, each of 3 years duration, and additionally is offering 3 Postgraduate Studentships.

The 5 projects attracting these posts are:

1. 'The role of superantigens in induction of post-infective autoimmunity' **Ref: 673**

This post is within a research group with diverse interests covering the clinical and laboratory investigation of immune responses to bacterial infection, particularly focusing on the role of bacterial superantigens. The post-holder will work primarily on a project looking at superantigen-induced T-cell self-reactivity and will be required to design, supervise and perform experiments involving *ex-vivo* stimulation of human T-cells, measurement of proliferation and functional cellular responses, the generation of T-cell lines and mapping of T-cell epitopes.

Informal enquiries to: Dr Martin Llewelyn, Senior Lecturer in Infectious Diseases, m.j.llewelyn@bsms.ac.uk

2. 'Exploration of associations between the phenotypic manifestations of infectious disease, and the later onset of autoimmune disease, using large primary care databases' **Ref: 674**

The specific purpose of the first phase of this postdoctoral fellowship is to explore the relationship between *phenotypic manifestations of infectious disease, and the later onset of autoimmune disease.* The Fellowship has been developed in order to provide experience in the analysis of large, complex routine clinical datasets. An interest in the potential applications of pattern recognition and related techniques from computer science in this field will be particularly welcome.

Informal enquiries to: Dr Jackie Cassell, Senior Lecturer in Clinical Epidemiology, j.cassell@bsms.ac.uk

3. 'Understanding and overcoming radioresistance in glioma stem cells' **Ref: 675**

An opportunity for a Postdoctoral Scientist to investigate the molecular mechanisms underlying the radioresistance of glioma stem cells with a view to identifying specific therapeutic targets. The project will focus on the interplay between DNA repair pathways and cell cycle checkpoints and will be based in the Genome Damage and Stability Centre in the University of Sussex.

Informal enquiries to: Dr Anthony Chalmers, Senior Lecturer in Clinical Oncology, a.j.chalmers@sussex.ac.uk

4. 'A programme of research focused on exploring the psychophysiological correlates of symptom expression in psychiatric and neuropsychiatric patient groups' **Ref: 676**

The post provides an opportunity for a Neuroscientist to develop research skills within a programme focused on exploring psychophysiological correlates of symptom expression in psychiatric and neuropsychiatric patient groups. Central to these investigations will be autonomic psychophysiology in conjunction with functional, structural and metabolic brain imaging within the Clinical Imaging Sciences Centre (CISC) at the University of Sussex campus at Falmer. Neurosciences are identified within the Medical School's core research areas.

Informal enquiries to: Professor Hugo Critchley, Chair in Psychiatry, h.critchley@bsms.ac.uk

5. 'Quantitative MRI measurements' **Ref: 677**

Novel parameters for detecting subtle disease, invisible by conventional MRI, will include measurement of Magnetisation Transfer (including estimation of bound macromolecular proton fraction), diffusion tensor imaging, T_1, and subtle Gd leakage. Imaging reproducibility, as measured by scan-rescan, will be measured, modeled and optimised using mathematical and numerical techniques. Clinical applications will include measuring Normal-Appearing Brain Tissue in HIV, Lupus and other neurological diseases. Dynamic Contrast-Enhanced Gd imaging will be used in oncology (prostrate cancer), rheumatoid arthritis, and liver blood flow, where correlations with CT will be made.

Informal enquiries to: Professor Paul Tofts, Chair in Imaging Physics, p.s.tofts@bsms.ac.uk

Research Fellows

Applicants wishing to discuss the Postdoctoral positions informally should contact the supervisors directly via email. Similarly, further particulars of the projects can be obtained from the supervisors.

Closing date for applications: 22 March 2007

Please quote the post reference number(s) in your application.

Application details for the 5 Postdoctoral positions are available from and should be returned to the Human Resources Division, Sussex House, University of Sussex, Falmer, Brighton BN1 9RH. Tel: (01273) 678706, fax: (01273) 877401, email: recruitment@sussex.ac.uk. Details of the posts can be found via the Medical School, (www.bsms.ac.uk), University of Sussex (http://www.sussex.ac.uk/jobs) and University of Brighton (www.bton.ac.uk/vacancies/) websites.

The studentships will be in the fields of:

1. 'Regulation of RNA stability during Drosophila spermatogenesis'
Enquiries to: Dr Sarah Newbury, Senior Lecturer in Cell Biology, s.newbury@bsms.ac.uk

2. 'Measurements of cognitive and MRI changes in acute and chronic SLE (Lupus, or Systemic Lupus Erythematosus)'
Enquiries to: Professor Paul Tofts, Chair in Imaging Physics, p.s.tofts@bsms.ac.uk

3. 'A clinical and molecular study of birch pollen immunotherapy for the oral allergy syndrome'
Enquiries to: Professor Anthony Frew, Consultant in Respiratory Medicine, anthony.frew@bsuh.nhs.uk

Studentships

Applicants wishing to discuss the Studentships informally should contact the supervisors directly via email. Similarly, further particulars of the projects can be obtained from the supervisors.

Please quote relevant project title.

Application details for the 3 Studentships are available from http://www.bsms.ac.uk/postgraduate/studentships.htm Completed application forms should be sent to the Unit Administrator, Medical Research Building, Brighton & Sussex Medical School, Biology Road, Brighton BN1 9PS. Tel: 01273 877889, fax: 01273 877884, email: j.wellington@bsms.ac.uk Details of the posts can be found via the Medical School, (www.bsms.ac.uk) website.

97755R

UNIVERSITY of GLASGOW

FACULTY OF MEDICINE – DIVISION OF IMMUNOLOGY, INFECTION AND INFLAMMATION

Chair

Salary: within professional range, subject to negotiation. Ref 13069/HRS/A1.

Senior Lecturer/Lecturer

£41,544 – £46,758/£34,793 – £40,335 Ref 12931/HRV/A1.

Immunology, Infection and Inflammation is a Division of the Medical Faculty at the University of Glasgow and was rated 5* in the last RAE. A new state of the art facility, the Glasgow Biomedical Research Centre, has just been completed in which research groups from this and cognate disciplines are being brought together to create a centre of excellence integrating structural, cellular and clinical sciences. Current research in the Division focuses on immunoregulation, signaling, chemokines, mucosal immunology, in vivo and molecular immunology. Rheumatology, respiratory medicine and infectious diseases are also active areas of research. We are currently seeking applications from people at Lecturer to Professorial level with expertise in any area of basic cellular or molecular immunology complementary to the existing research strengths of the Division, or individuals with strong backgrounds in other aspects of fundamental immunology and/or translational research, are welcome (www.gla.ac.uk/immunology/index.htm). In addition you will be able to demonstrate some or all of the following depending on your experience and the post being applied for: an excellent record of publications, evidence of independence with the ability to raise significant grant funding, supervision of PhD students, and a willingness to participate in undergraduate teaching.

Interested candidates should contact Professor F Y Liew (Head of Division) – f.y.liew@clinmed.gla.ac.uk or Tel: 0141 330 8411.

For an application pack, please see our website or write quoting appropriate reference and indicating whether you wish to be considered for a Lecturer, Senior Lecturer or Professorial position, to the Recruitment Section, Human Resources Department, University of Glasgow, Glasgow G12 8QQ. Closing date: 23 March 2007.

DIVISION OF CANCER SCIENCES AND MOLECULAR PATHOLOGY

Research Assistant (full or part time)

£23,002 – £25,889 pro rata

You will take forward a research project studying genes involved in regulating tumour growth in malignant melanoma and its precursor lesions. You will have a good biomedical degree (or equivalent) in an appropriate discipline and a minimum of two years' experience in basic molecular biology including primer design, DNA extraction, PCR, cloning and sequencing. Microscopy experience is preferable. This post is available for six months full time, or up to one year (depending on part time hours).

Letters of application, including a CV, the names, postal and e-mail addresses and fax numbers of two academic referees, should be sent to: Dr Fiona Roberts, c/o Department of Pathology, Western Infirmary, University of Glasgow, Glasgow G12 8QQ quoting Ref 12977/DPV/A3. Closing date: 23 March 2007.

The University is committed to equality of opportunity in employment.

www.gla.ac.uk

UNIVERSITY of GLASGOW

97727R

UNIVERSITY OF LIVERPOOL

School of Biological Sciences

Centre for Cell Imaging

Two Postdoctoral Researchers

£27,465 pa

The Centre for Cell Imaging (CCI) is a £4m state-of-the-art facility for live cell imaging, equipped for time-lapse luminescence and fluorescence cell microscopy. Training will be provided in advanced microscopy and you will join a well funded multidisciplinary research team. Both posts are funded by the BBSRC for up to three years.

Post 1: **This is an exciting opportunity for an innovative molecular cell biologist. You will develop and apply novel multiparameter imaging technology to quantify dynamic biological processes in single cells for the systems biology analysis of mammalian cell signalling. You will develop new integrated fluorescence and luminescence technology that builds on a world-class record of innovation in the Centre for Cell Imaging. A relevant PhD is essential and knowledge of microscopy and recombinant DNA techniques would be advantageous. Quote Ref: B/965/N**

Post 2: This is an exciting opportunity for a cell biologist to perform high throughput cell imaging. You will identify how small molecule chemical agents can specifically modulate the dynamics and function of the NF-kappaB signalling pathway in living cells. This will be done by developing and applying novel delivery of chemical libraries. A relevant PhD is essential and knowledge of cell imaging would be advantageous. Quote Ref: B/966/N

Closing date for both posts: 23 March 2007

For full details, or to request an application pack, visit www.liv.ac.uk/university/jobs.html or e-mail: jobs@liv.ac.uk Tel 0151 794 2210 (24 hr answerphone) Please quote ref in all enquiries.

COMMITTED TO DIVERSITY AND EQUALITY OF OPPORTUNITY

97728R

JESUS COLLEGE OXFORD

John Houghton Research Fellowship in Sustainable Energy

Jesus College, Oxford, invites applications for the first John Houghton Research Fellowship in Sustainable Energy, tenable for two years from 1st October 2007 or as soon as possible thereafter, with the possibility of renewal for a third and final year. The Fellowship is open to researchers in the natural sciences or engineering who are likely to be at an early to mid stage in their academic career. This exciting new position, sponsored by Sir John Houghton and The Shell Foundation, is designed to form a link between basic research and its application in providing sustainable solutions to energy supply in developing countries in Africa and/or Asia and to build capacity there.

The starting salary will be in the region of either £27,000 p.a. including a housing allowance, or £22,000 p.a. plus free accommodation in a furnished College flat. An annual research grant of up to £8,750, free lunch and dinner in College, and membership of the USS pension scheme are also offered.

Further information on the Fellowship may be found at www.jesus.ox.ac.uk or obtained from the Principal's Secretary, Jesus College, Oxford OX1 3DW (helen.gee@jesus.ox.ac.uk), to whom applications should be sent by Friday 27 April 2007.

The College and the University are Equal Opportunities Employers.

97753R

DEPARTMENT OF BIOLOGICAL SCIENCES

Lecturer in Biological Sciences

The post is available from 1 September 2007, or as soon as possible thereafter. Applications are particularly welcome from candidates with interests in using gene expression and developmental biology techniques in the study of evolutionary and environmental questions. However, applicants with interests in other fields will be given full consideration. You will be expected to participate in teaching environmental physiology/eco-physiology/environmental genomics, as part of our popular range of degree programmes (Biology, Marine & Freshwater Biology, Aquatic Zoology). You should have a strong record of publication in high-profile journals.

Informal enquiries should be directed to the head of department, Dr Jörg Hardege (tel. +44(0) 1482 465187; email: j.d.hardege@hull.ac.uk) or the Director of Research, Professor George Turner (email: g.f.turner@hull.ac.uk).

Salary range £33,465 - £38,772 pa.

For an application pack, tel: (01482) 465557 (textphone for applicants with a hearing/speech impairment: 01482 466851), fax: (01482) 466660, or email: science-recruitment@hull.ac.uk (quoting ref. FS23).

Closing date: 29 March 2007.

For online information see www.hull.ac.uk

We promote diversity in employment and welcome applications from all sections of the community.

THE UNIVERSITY OF HULL

97690R

scri
living technology

RESEARCH SCIENTISTS

Salary Range £24,200 to £27,200

(or up to £33,450 for exceptional candidates)

SCRI is Scotland's leading Institute for research on plants and their interactions with the environment, particularly in managed eco-systems. Our mission is to conduct excellent research in plant and environmental sciences. Our vision is to deliver innovative products, knowledge and services that enrich the life of the community and address the public goods of sustainability and high quality and healthy food.

We invite applications for six new research scientists to strengthen and extend our expertise in key areas. Each of the successful candidates will be expected to develop and execute work that will complement ongoing research at SCRI and to advance the science in the areas described. Initially the research will be supported from funds within the Institute but it is expected that the appointees will obtain external funding to sustain their research in the future.

The successful candidates will have PhDs and a proven track record of working in the areas described as shown by their publication record. They will also demonstrate excellent communications skills and will be capable of developing their own field of research through collaborations and by attracting external funding.

RHIZOSPHERE SCIENTIST Ref EPI/2/07

The postholder will be expected to contribute to SCRI's research on plant mineral nutrition and water use efficiency. The work will focus on genetic and environmental factors that enhance resource-use efficiency in cropping systems via processes in the rhizosphere.

MATHEMATICAL PHYTOLOGIST Ref EPI/3/07

The postholder will be responsible for the development and realisation of computer models for resource capture by plants incorporating the effects of genetics. This work will contribute to the scientific objectives of SCRI by identifying plant genetic and environmental factors, and their interactions, that improve resource-use efficiency as well as establishing models and methods for predicting plant types and management practices that enhance productivity, resilience and biodiversity through predictive functional-structural modelling.

MOLECULAR BACTERIOLOGIST Ref PP/3/07

The postholder will contribute to SCRI's research on plant-bacterial interactions and will be expected to develop work contributing to two new areas of research. This includes investigating the role of plants on the survival of human and enterobacterial pathogens in the environment, and/or investigating threats posed by the possible arrival and establishment of non-indigenous bacterial plant pathogens into the UK, with a particular emphasis on climate change as a key factor in the process.

BIOLOGICAL CHEMIST Ref QHN/2/07

The postholder will be expected to oversee the metabolomics effort at SCRI and to develop and advance this area of work. It is expected that the primary focus of the individual's research will be metabolomics in relation to the biosynthesis of, and post-harvest changes in, taste and health related secondary plant metabolites in potato and fruit.

PLANT BIOINFORMATICIST Ref GEN/5/07

This position will be expected to develop, execute and manage a bioinformatics-led research programme focusing on the analysis of genomic and genotypic data. The principal focus will be on barley and/or potato and will fully exploit comparative genetics information from model species.

MOLECULAR GENETICIST Ref GEN/6/07

The postholder will develop and ultimately lead a programme of research focusing on the potato traits that are of increasing importance as a result of climate change, particularly in relation to water use and/or nutrient uptake. It is expected that the individual will develop strong associations with breeders, physiologists, statisticians and bioinformaticists in order to establish a vibrant, interactive and contemporary research programme.

Further information on all the posts is available on our website www.scri.ac.uk/HR/jobs.htm or by contacting the HR office on 01382 568561.

Applications for these posts must include a curriculum vitae (resume), a covering letter, an outline research plan and details of 3 referees capable of providing informed comment on research potential. Applications should be sent to the HR Office, SCRI, Invergowrie, Dundee DD2 5DA by Friday, 23rd March 2007, quoting the appropriate reference number.

The Institute is an equal opportunities employer.

97685R

The Bloomsbury Colleges PhD Studentships

The Bloomsbury Colleges are a consortium of six University of London colleges comprising Birkbeck, Institute of Education, Royal Veterinary College, London School of Hygiene & Tropical Medicine, School of Oriental and African Studies and The School of Pharmacy.

The consortium is offering ten PhD studentships, each of three years duration, to start October 2007. The studentships will cover course fees (at the usual level for UK and EU studentships) and a student stipend. (Studentships where the Institute of Education is the lead college will cover the full fee for non-EU students plus a stipend). They will encompass a wide range of topics spanning the biomedical and social sciences and humanities, reflecting the diversity of disciplines represented in the consortium.

The studentships available are as follows:

Biological, Veterinary & Pharmaceutical Sciences

- Development of models of human intestinal epithelium to study how infection by Campylobacter jejuni causes diarrhoeal disease.
- Relationship between medication error and patient harm due to adverse drug effects.
- Antibacterial compounds from locusts.
- The physicochemical characterisation and optimisation of a new cost affordable amphotericin B medicine.
- Investigations into Acg and other putative nitrosoreductases, key proteins in the dormancy phase of tuberculosis.
- Modification of bacterial surface polysaccharide as a novel therapy for Streptococcus suis meningitis and septicaemia in the pig.
- Poultry movement networks in Vietnam and their impact on the spread and control of Highly Pathogenic Avian Influenza (HPAI) H5N1 infection.

Education, Social Sciences & Humanities

- Strengthening open, distance and flexible learning systems to increase education access and attainment for young people living in high HIV prevalance areas in Malawi.
- Development NGOs and human rights education.
- A history of the origins and uses of the 1946 and 1958 British Cohort Studies (1945 - 1981).

Further details are available from www.bloomsbury.ac.uk/studentships.

Closing Date: 29th March 2007.

97351R

ETH

Eidgenössische Technische Hochschule Zürich
Swiss Federal Institute of Technology Zurich

POSITIONS FOR GROUP LEADERS, POSTDOCS AND Ph.D CANDIDATES

The ETH Institute for Chemical- and Bio-Engineering has several vacancies for competitive group leaders (Oberassistenten), postdocs and Ph.D. candidates, who will foster novel research initiatives in gene therapy, drug discovery, host-pathogen crosstalk, tissue engineering and biopharmaceutical manufacturing.

Successful candidates are highly skilled in standard molecular, cell biology and in vivo techniques, have a command of state-of-the-art transduction technologies and have advanced skills in cultivating primary cells.

We expect applicants to have ambition to pursue an academic career or initiate technology transfer activities; applicants for group leader and postdoc positions should also have an outstanding publication record.

All applicants should send two hardcopies of your application, including CV, publication list, and two letters of recommendation, and applicants for group leader and postdoc positions should also send a three-year research plan to:

Prof. Dr. Martin Fussenegger, c/o Mrs. Marcia Schoenberg,
ETH Institute for Chemical- and Bio-Engineering,
ETH Hoenggerberg, HCI F117, Wolfgang-Pauli-Strasse 10,
CH-8093 Zurich, Switzerland.

W97684R

UCD DUBLIN

A University to match your ambitions

College of Life Sciences

UCD School of Biomolecular and Biomedical Sciences

Lecturers (5 posts)

The UCD School of Biomolecular and Biomedical Science hosts scientists from a range of academic disciplines including Biochemistry, Microbiology, Pharmacology, Neuroscience, Molecular Biology and Genetics. Such diversity of expertise facilitates interdisciplinary scholarship and research and provides the School with a unique platform for the study and integration of knowledge of biological systems at molecular, cellular and whole organism levels. The School is highly research intensive with international standing in the areas of Neuroscience, Infection and Immunity, Developmental Biology, Cancer, Structural Biology and Bio-catalysis and Diabetes. It offers postgraduate training and research opportunities in these major areas with Ph.D. students constituting a significant and valued presence in the School. The School offers undergraduate programmes in Biochemistry, Biochemistry and Molecular Biology, Microbiology, Pharmacology, Neuroscience and Genetics. Staff in the School also make significant contribution to teaching programmes in Medicine, Nursing Studies and Agriculture.

Applications are invited from suitably qualified individuals [Ph.D. or equivalent] who have a proven record of research activity in one of these disciplines in one of the School's areas of interest.

The School wishes to recruit five Lecturers in the following disciplines:

Lecturer in Biochemistry (2)	**Ref: 002785**
Lecturer in Pharmacology (2)	**Ref: 002784**
Lecturer in Microbiology	**Ref: 002783**

Salary: **€33,894 - €79,476 p.a.**

Appointment on scale will commensurate with experience and qualifications.

Closing date: April 20th, 2007

www.ucd.ie/vacancies

Further particulars and application procedures for these posts are available at **www.ucd.ie/vacancies** or from UCD Personnel.
UCD Personnel, University College Dublin, Belfield, Dublin 4, Ireland.
Tel: 00-353-1-716 1412; Fax: 00-353-1-2692472

UCD is an equal opportunities employer.

W97746R

Ireland's education capital

University College Dublin
An Coláiste Ollscoile,
Baile Átha Cliath

www.cam.ac.uk/jobs/

Post-Doctoral Research Associate

Vascular/Apoptosis Research

Department of Medicine, Division of Cardiovascular Medicine

£24,402 - £31,840 pa

Applications are invited for a vacant post-doctoral research associate post funded by the award of a British Heart Foundation project grant for 3 years. The research associate will join an established group of investigators studying the regulation and consequences of smooth muscle cell apoptosis and cell proliferation (see Nature Med 2006;12(9):1075-1080, Circ Res 96, 667-74 (2005)). A minimum of 3 years post-doctoral experience is required.

For further details please contact Professor M R Bennett on 44 (0)1223 331504/5 or mrb@mole.bio.cam.ac.uk

Completed applications forms, Parts 1 and 3 only (available from http://www.admin.cam.ac.uk/offices/personnel/forms/pd18/pd18.doc) including a CV with the names of two referees should be sent to Professor Martin Bennett, Addenbrooke's Centre for Clinical Investigation, Level 6, Box 110, Addenbrooke's Hospital, Hills Road, Cambridge CB2 2QQ or emailed to cju22@medschl.cam.ac.uk Closing date: 22 March 2007. Only short listed candidates will be contacted.

Cambridge University aims to achieve the highest quality in teaching and research.

Addenbrooke's Hospital is a no-smoking area.

UNIVERSITY OF CAMBRIDGE

The University offers a range of benefits including attractive pension schemes, professional development, family friendly policies, health and welfare provision, and staff discounts. The University is committed to equality of opportunity.

97680R

Oxford Centre for Diabetes, Endocrinology and Metabolism

UNIVERSITY OF OXFORD

Diabetes UK Research Studentship

Project Title: Comprehensive assessment of the role of phosphate tensin homologue deleted on chromosome 10 (PTEN) in insulin secretion in humans using a combined molecular genetic and cell biological approach.
Supervisors: Dr Anna L Gloyn & Professor Patrik Rorsman

The successful student will have the opportunity to work on an exciting project which combines the use of human molecular genetics and cellular and molecular biology to characterise the role of PTEN in insulin secretion and pancreatic beta-cell dysfunction.

This project offers an excellent portfolio of basic scientific skills and techniques in islet cellular and molecular biology and human genetics. State-of-the-art facilities are available in the laboratories of both Dr Gloyn and Professor Rorsman for molecular genetic and cell biological techniques.

The studentship is available for a 3 year period. The Diabetes UK Research Studentship provides a stipend of £13,000/year. Diabetes UK only provides University Composition Fees for home students. For more details on how the University currently defines 'home' students please visit: http://www.admin.ox.ac.uk/postgraduate/finance/clas.shtml. Informal enquires about this studentship are encouraged. Please contact Dr Anna Gloyn (anna.gloyn@drl.ox.ac.uk). For further information on the research of Dr Gloyn and Prof Rorsman please visit www.ocdem.com.

Further information can be obtained by contacting the Personnel Administrator, OCDEM, Churchill Hospital, Headington, Oxford OX3 7LJ, by calling (01865) 857214, or by emailing ocdem.personnel@ndm.ox.ac.uk to whom applications, including a CV with the names and contact details of two referees and a short statement of research interests, should be sent. Please remember to quote reference number H7-07-001-AG in all correspondence. The deadline for applications is Friday 23rd March 2007 and interviews will be held on Thursday 12th April 2007.

The University is an Equal Opportunities Employer.

www.ox.ac.uk/jobs

97752R

Lecturers/Senior Lecturers in Clinical & Biomedical Sciences (6 posts)

The Peninsula Medical School is the fastest growing medical school in the UK and has an impressive track record in research and teaching. The success of the School has been confirmed by the award of a significant expansion in undergraduate medical student numbers and also by the establishment, following a national competition, of the Peninsula Dental School, the first new dental school in the UK for over 30 years.

As a consequence of this major expansion in our activities, the Peninsula Medical School (now known as the Peninsula College of Medicine and Dentistry) is seeking to appoint 6 substantive academic posts at the level of Lecturer/ Senior Lecturer. Individuals are sought with outstanding track records in research, teaching and scholarship.

Applicants research will align with the School's research areas namely Diabetes, Metabolism and Vascular Diseases, Ageing, Public Health, Inflammation, Neurosciences or Medical Education and may cover any aspect from basic science to clinical research, research synthesis, bioinformatics or policy. The School encourages and supports translational research.

You will contribute at an internationally competitive level to the research agenda of the School's Institute of Biomedical and Clinical Science and will contribute to teaching/learning in one of the following areas: Human Function, Human Structure, Pharmacology & Therapeutics, Pathological Processes or Biochemical Basis of Health and Disease.

You will be appointed at either Lecturer or Senior Lecturer level depending on prior experience. Academics will be involved equally in teaching and research. A PhD in a relevant discipline and teaching experience in higher education is essential. Consideration will be given to applicants whose expertise is in the field of teaching and scholarship rather than in science research.

In addition to this, those applicants wishing to apply for a Senior Lectureship will be expected to have a proven track record of peer-reviewed publications and grant awards from recognised bodies; will be able to evidence international conference contributions and will have management experience.

The School will appoint to either a University of Exeter or University of Plymouth contract. You will be based at the Exeter or Plymouth School campus and will be expected to travel between sites when necessary.

Salary for Lecturer appointment will be on scale £28,290 to £34,793 pa with accelerated incrementation (University of Exeter) or £27,465 to £39,160 (University of Plymouth). Salary for Senior Lecturer appointment will be on scale £34,793 to £46,758 pa (University of Exeter), or £40,335 to £46,758 (University of Plymouth).

For an informal discussion please contact Professor Angela Shore on (01392) 403091, or e-mail angela.shore@pms.ac.uk although applications should be made in accordance with the details shown below.

For an application pack please email jobs@pms.ac.uk or see the job vacancies section of the PMS website www.pms.ac.uk or telephone (01752) 437448 quoting reference no: EO93/PMS.

Closing date: 14th March 2007

Interviews will be held on Monday 2nd April 2007 in Exeter, Devon.

Equal opportunities employer

PENINSULA
MEDICAL SCHOOL
UNIVERSITIES OF EXETER & PLYMOUTH

97754R

The University of Manchester

MANCHESTER 1824

AquaTRAIN Marie Curie Research Training Network on Geogenic Chemicals in Groundwaters and Soils

Early Stage Researchers
(Postgraduate Research Assistants) **Ref: EPS/053/07**

Experienced Researchers
(Postdoctoral Research Assistants) **Ref: EPS/054/07**

Competitive salaries offered

AquaTRAIN is inviting applications for 12 Early Stage Researcher posts (all of which may lead to the award of a PhD or European PhD) and for 3 experienced Researcher (Postdoctoral Research Assistant) posts.

AquaTRAIN, a consortium of 15 leading European Universities and Research Institutes, has been awarded a maximum of €3,150,000.00 by the European Commission to set up a Marie Curie Research Training Network to foster a better understanding of geogenic chemicals (e.g. arsenic, selenium, manganese) and of the microbiological controls on their mobility, an essential step towards the development of novel remediation and protection technologies.

AquaTRAIN will provide a group of 15 researchers with a rich and challenging interdisciplinary learning environment which will incorporate the biogeochemical processes controlling the cycling of chemicals in groundwater/soil systems, protection and remediation technologies, the biochemistry of chemical uptake in humans through the food chain, and the human health and environmental consequences of trace geogenic chemicals in groundwaters and soils. This will be provided through a joint innovative research and training programme involving individual training plans, mentoring, network-wide training workshops with invited international experts and strong links with other European and international research and training projects. ERs will be expected to play a prominent role in network management and transfer of knowledge activities.

For each post, further details, including Scientists-in-Charge and location of host institutions, may be downloaded from the AquaTRAIN website http://www.AquaTRAIN.eu/

Competitive starting salaries are offered under the conditions of the Marie Curie Research Training Networks scheme. In addition generous travel, mobility and career exploration allowances are offered.

Appointments will be overall for 36 months (13 posts) or 30 months (2 posts). For a number of ESR posts, further funding has also been independently secured to enable the researcher to complete a four year PhD programme, where this is necessary.

Applications from women candidates are particularly encouraged.

Informal enquiries should be made to the particular Scientist-in-Charge of the relevant research post. Alternatively general academic enquiries can be made to AquaTRAIN Co-ordinator, Dr David Polya, SEAES, The University of Manchester, UK. Tel: + 44 (0) 161 275 3818; fax: + 44 (0) 161 306 9361.

Applications should include a full CV and the contact details of three academic referees and be submitted by 15 March 2007 via the AquaTRAIN website http://www.AquaTRAIN.eu/

Please follow closely the instructions on the website.

These posts are funded under the European Commission Sixth Framework Programme (2002-2006), Marie Curie Actions - Human Resources Mobility Activity Area, Research Training Networks.

The University will actively foster a culture of inclusion and diversity and will seek to achieve true equality of opportunity for all members of its community.

www.manchester.ac.uk/jobs

97776R

UniS

University of Surrey
Postgraduate Medical School (PGMS)

Salary: Circa £31,000 per annum depending on skills and experience
Ref: 5794

Postdoctoral Research Fellow in Immunology (RA1A/RA11)

The Oncology department, based within the Postgraduate Medical School (PGMS), is responsible for carrying out pioneering research into the development and evaluation of novel cancer therapies. Working within the 5*A rated Postgraduate Medical School, adjacent to the Royal Surrey County Hospital, this post will be involved in research work in tumour immunology, and particularly cancer immunotherapy using dendritic cells.

Able to effectively work as part of a team that thrives on mutual support, you will develop the next generation of dendritic cell vaccines for cancer patients. This includes optimising immunogens and adjuvants as well evaluating this approach in synergy with chemotherapy, viral therapy and modulation of regulatory T cell function. You will be expected to write grant proposals, to communicate effectively with funding bodies and potential collaborators and to take responsibility for the day-to-day management of your own research activities, the dissemination, presentation and publication of research findings. In return, the University offers a generous holiday entitlement, an attractive pension scheme, a comprehensive training and development portfolio and subsidised gym membership.

This full-time appointment is initially available until 31st July 2010.

Informal enquiries about this exciting new post are welcome and should be made to Professor Hardev Pandha Tel: 01483 688602, email: h.pandha@surrey.ac.uk

To apply please visit our website www.surrey.ac.uk click on 'Working at UniS' or contact Linda Sharp on 01483 684559, linda.sharp@surrey.ac.uk

Benefits package includes relocation provision, final salary pension, childcare assistance and leisure facilities.

Closing Date: Wednesday 21st March 2007.

We acknowledge, understand and embrace diversity

97760R

www.surrey.ac.uk/vacancies

W97367L

Oslo University
Department of Biology
Associate Professor (Førsteamanuensis)
The post includes the administrative leadership (management) of Finse research center. The manager is expected to administrate the various activities, including practical and economical responsibilities, and expects to develop university courses and research projects in his/her field of science and to supervise MSc and PhD students at the station.

Contact
Snr Executive Officer Bente Schjoldager
Tel. + 47 22 85 47 04
http://www.uio.no/

W97365L

University of Oslo
Biology (Mycology)
Associate Professor (Førsteamanuensis)
We are seeking a person with research expertise in mycology with focus on fungal molecular ecology and evolution. The person appointed must be able to participate in teaching, supervision and examination work at all levels within the fields of mycology, molecular ecology, molecular evolution, and biosystematics.

Contact
Snr Executive Officer Bente Schjoldager
Tel. + 47 22 85 47 04
http://www.uio.no/

Gobierno de La Rioja
www.larioja.org

Rioja Salud
CIBIR

LA RIOJA BIOMEDICAL RESEARCH CENTRE

Call for Candidates

CENTRO DE INVESTIGACION BIOMEDICA DE LA RIOJA (CIBIR)

A new Biomedical Research Centre, CIBIR, is being created by the Government of La Rioja (Spain) to perform biomedical investigation both at the basic and applied levels. The new Centre will be located in Logroño nearby the major Hospital in the area.

The aims of this Centre are: To develop high quality biomedical research, with a strong but non-exclusive focus on oncology research and to facilitate technology transfer in keeping with current clinical and R&D priorities.

Call for Candidates

The CIBIR is seeking, for the Department of Oncological Research, highly motivated scientists at the following levels:

- **Group Leaders (Ref. GL)**
- **Senior and Junior Research Scientists (Ref. RS)**
- **Senior Laboratory Technicians (Ref. LT)**

Applications must include a detailed CV and synopsis of research experience. Fluent Spanish and English are required. A summary of proposed research line is also required and shall be exposed, only for GL applications.

See the complete basis of this call on: **www.fundacionriojasalud.org**

Apply by e-mail to: **cibir@riojasalud.es** or to our postal address: **Fundación Rioja Salud, Av. Portugal 7. 6th floor. Logroño (Spain) c.p. 26001,** quoting the corresponding reference on all correspondence. All enquiries and applications will be treated confidentially.

Visit our Web site (**www.riojasalud.es/institucion/cibir**) to learn more about our Centre and for additional available positions.

W97768R

School of Medical Sciences

Research Fellow

A suitably qualified postdoctoral research scientist, you will be part of a project investigating the transcriptional systems that control the expression of tachykinins in the amygdala where they play a role in the modulation of fear and anxiety.The objectives of the project are to understand how these transcriptional systems operate and how they may contribute to susceptibility to depression and chronic anxiety.

You must have a PhD in a biological/medical science or a related discipline, or an MSc in a similar area plus the appropriate level of skills and experience which indicate the ability to carry out the duties and responsibilities of a post-doctoral role. Experience of tissue culture, immunohistochemistry, pharmacology and molecular biology is essential, while experience of transgenic analysis, comparative genomics, EMSA, ChIP assays and RNA expression analysis is desirable, although training in these techniques will be provided as required.

This three-year project is funded by the Wellcome Trust and the salary shall be paid at the appropriate point of the University's pay and grading structure (£26,915 – £28,554 per annum).

Informal enquiries to Dr MacKenzie (tel: 01224 555893, e-mail: mbi167@abdn.ac.uk).

Online application forms and further particulars are available from www.abdn.ac.uk/jobs Alternatively telephone (01224) 272727 (24 hour answering service) quoting reference number YMB131R for an application pack.

Closing date: 29 March 2007.

Promoting Diversity and Equal Opportunities throughout the University

1495
UNIVERSITY OF ABERDEEN

97778R

Several **PHD AND POSTDOCTORAL POSITIONS** are available at the **Technical University Munich**, within the **Marie Curie Excellence Team** led by **Dr. Daniel P. Funeriu**.

Research will be performed in the fields of chemical biology, biochemistry, biophysics, surface chemistry, organic chemistry, microarray technology and are associated with highly competitive financial conditions. Excellent candidates with cross-disciplinary training are particularly welcomed and we highly encourage applications from female candidates.

One of the PhD students will be enrolled in the International Graduate School of Science and Engineering **www.igsse.de** English is a requirement, German and French are a bonus. The positions will remain open until suitable candidates will be recruited.

Please submit your application to **daniel.funeriu@ch.tum.de** including a CV, letter of intent and a scientific career development plan.

W97731R

THE KAY KENDALL LEUKAEMIA FUND
SENIOR RESEARCH FELLOWSHIP

The Kay Kendall Leukaemia Fund invites applications from outstanding biomedical scientists for a five-year senior research fellowship to study any aspect of leukaemia. The research will typically address one or more questions relating to the epidemiology, aetiology, pathogenesis, diagnosis or treatment of leukaemia or a closely allied malignancy. Applicants may be of any nationality and should intend to work in an appropriate institution in the UK. The appointment will be made on either clinical or non-clinical payscales as appropriate, and will normally be taken up within 6 months of the award. The fellowship will cover the cost of salaries for five years for the fellow and may support up to two assistants together with costs of laboratory consumables but will not contribute to departmental overheads.

The application (by electronic mail as well as one hard copy) should be received on or before 4 May 2007. It must include a scientific proposal of up to 10 single-spaced pages (excluding references, costings and CV), and a statement from the departmental chairman or laboratory director that he/she is prepared to make available all appropriate facilities if the applicant is successful.

Further information can be obtained from the website www.kklf.org.uk or contact

THE KAY KENDALL LEUKAEMIA FUND
Allington House (1st Floor), 150 Victoria Street
London SW1E 5AE
Telephone: 020 7410 0330, e.mail info@kklf.org.uk

96557R

THE KAY KENDALL LEUKAEMIA FUND
INTERMEDIATE RESEARCH FELLOWSHIP

The Kay Kendall Leukaemia Fund invites applications from outstanding biomedical scientists for a four-year intermediate research fellowship to study any aspect of leukaemia. The research will typically address one or more questions relating to the epidemiology, aetiology, pathogenesis, diagnosis or treatment of leukaemia or a closely allied malignancy. Applicants may be of any nationality and should intend to work for at least part of the fellowship in an appropriate institution in the UK. The appointment will be made on either clinical or non-clinical payscales as appropriate, and will normally be taken up within 6 months of the award. The fellowship will cover the cost of salaries for four years for the fellow and may support one assistant together with costs of laboratory consumables but will not contribute to departmental overheads.

The application (by electronic mail as well as one hard copy) should be received on or before 4 May 2007. It must include a scientific proposal of up to 6 single-spaced pages (excluding references, costings and CV), and a statement from the departmental chairman or laboratory director that he/she is prepared to make available all appropriate facilities if the applicant is successful.

Further information can be obtained from the website www.kklf.org.uk or contact

THE KAY KENDALL LEUKAEMIA FUND
Allington House (1st Floor), 150 Victoria Street
London SW1E 5AE
Telephone: 020 7410 0330, e.mail info@kklf.org.uk

96558R

University of Dundee

The Translational Medicine Research Collaboration Laboratory

The TMRC is a unique partnership between Wyeth, four leading Scottish Universities, the NHS and Scottish Enterprise, to establish a pan-Scotland innovative research infrastructure focused on Translational Medicine. The TMRC central facility in The University of Dundee is a laboratory devoted to innovative biomarker identification and development in areas of Cardiovascular & Metabolic Disease, Inflammation, Musculoskeletal Biology, Neuroscience, Oncology and Reproductive Health. We are seeking outstanding scientists to establish the laboratory and drive the future of Translational Medicine. This is an exceptional opportunity to join a world-class organisation dedicated to the application of cutting-edge science for the treatment of significant unmet medical needs.

CLINICAL STUDIES MANAGER – LS/1677

(£41,544 – £46,758)

This position will be responsible for the planning and coordination of clinical trials conducted in multiple therapeutic areas. This position will ensure that clinical activities adhere to GCP/ICH, local laws and Wyeth standard processes and will extensively interact with Scotland clinical sites and Wyeth in the US and Europe. This role will entail coordination of protocol objectives and timelines.

Candidates must have at least a BSc. and at least 7-10 years clinical experience including experience working in the UK and/or Scottish regulatory environment. Excellent verbal and written communication skills, project management and organizational skills are required.

BIOINFORMATICS ANALYST – LS/1678

BIOSTATISTICS/BIOINFORMATICS GROUP

(£32,795 – £39,160)

You will support research using various genomic platforms for RNA expression (Affymetrix), proteomic and SNP analyses of samples from human and animal model studies. You will work with statisticians to analyse project data and assist in the integration of genomic data with clinical information. You will have a PhD or equivalent in molecular biology, bioinformatics, pharmacology, systems biology or a related discipline with at least 3 years of broad experience in informatics, preferably with experience in RNA profiling analysis and/or the use of genomic technologies for clinical disease applications. A proven ability to work collaboratively is necessary.

COMPUTER PROGRAMMER AND IT SPECIALIST – LS/1679

BIOSTATISTICS/BIOINFORMATICS GROUP

(£32,795 – £39,160)

You will customise or develop systems and programs that manage, analyze and report a variety of data types including clinical data, research assay data and genomic data. A senior programmer with a BSc. or MSc. in Computer Science, Biology, Statistics or other scientific discipline with at least 5 years application development experience you are proficient with Java and Java IDE tools, Perl or C++. You will have excellent communication and project management skills. Experience of software development in the life-science area and of software lifecycle management would be advantageous.

All contracts are available up to first half 2011 in the first instance.

Further details and an application pack are available from our website: www.jobs.dundee.ac.uk Alternatively, contact Human Resources, College of Life Sciences, JBC/MSI/WTB Complex, University of Dundee DD1 5EH, tel: (01382) 388969 or email: y.murray@dundee.ac.uk quoting the appropriate reference number.

Candidates will only be contacted if invited for interview.

Closing date: 29 March 2007.

As part of the recruitment process, the University requires that a Disclosure Scotland check is undertaken for this position.

The University of Dundee is committed to equal opportunities and welcomes applications from all sections of the community.

UNIVERSITY OF DUNDEE

97780R

www.dundee.ac.uk/jobs

Barts and The London
Queen Mary's School of Medicine and Dentistry

Institute Of Dentistry
Centre for Oral Growth & Development

Chair in Physical Sciences in Relation to Dentistry

From £55k per annum inclusive **Ref: 07081/LH**

Applications are invited from a suitably qualified individual for the position of Chair in Physical Sciences in Relation to Dentistry based within the 5-rated Institute of Dentistry, Barts and The London, Queen Mary's School of Medicine and Dentistry, Queen Mary, University of London.

We are seeking a researcher with an international reputation, and the successful candidate will develop an independent research programme focusing on aspects of research in biomaterials, biophysics or engineering relevant to dentistry which will enhance, complement and be synergistic with the Institute's overall research strategy and expertise within Queen Mary as a whole.

You will be expected to plan and direct the implementation of dental research activities and programmes of outstanding quality, international repute and innovation based on the Physical Sciences and advance the reputation of the Institute and the College. Duties of this post include both research and teaching and experience in teaching at undergraduate and postgraduate levels is required.

This is a full-time, permanent post and is available immediately. Salary will be on the Academic and Education Grade, with a professorial salary from £55k per annum inclusive.

Applicants are encouraged to discuss this position with: Professor Paul Wright, Dental Dean (p.s.wright@qmul.ac.uk) or Professor Mark Hector, Centre Lead for Oral Growth and Development and Deputy Director -Teaching (m.p.hector@qmul.ac.uk). Further details of the Institute's research activities may be found at http://www.smd.qmul.ac.uk/dental/

Candidates must be able to demonstrate their eligibility to work in the UK in accordance with the Asylum and Immigration Act 1999.

For an application form and further information contact our 24 hour recruitment line on 020 7882 6109 or email wch-recruit@qmul.ac.uk quoting reference number 07081/LH or alternatively please visit our website on http://www.hr.qmul.ac.uk/vacancies/

Completed application forms along with a copy of your curriculum vitae should be returned to Whitechapel Recruitment, Barts and The London, Queen Mary's School of Medicine & Dentistry, c/o SMD Management Offices, The Lodge House, Charterhouse Square, London EC1M 6BQ.

Closing date for completed applications is 12 noon (BST) on 14 March 2007.

Promoting excellence in teaching and research
Working towards equal opportunities

97782R

MRC National Institute for Medical Research

UCL

GENETIC DISSECTION OF A MURINE MODEL OF DOWN SYNDROME

TWO POSTDOCTORAL RESEARCHERS

We are offering Career Development Fellowships for postdoctoral researchers to work on a mouse model of human Down Syndrome that we recently generated (Science (2005) 309, 2033-7). This strain, termed Tc1, carries almost all of human chromosome 21 (HSA21), and recapitulates many of the features of the human syndrome, including alterations in brain, cardiac and craniofacial development, synaptic plasticity and behaviour. The purpose of this project will be to identify dosage-sensitive genes on HSA21 contributing to these phenotypes by using chromosome engineering to generate a series of novel mouse strains bearing deletions within mouse chromosomes of regions syntenic to HSA21. These will be crossed to the Tc1 strain to map the location of dosage-sensitive genes, and eventually to identify them. The project is vital for a number of other research laboratories with whom we collaborate. Applicants should have a background in molecular biology or mouse genetics.

The work is a collaborative project between Prof Elizabeth Fisher (Institute of Neurology, UCL) and Dr Victor Tybulewicz (MRC National Institute for Medical Research, London). The posts are funded by grants from the Wellcome Trust and the EU, will be based in the laboratory of Dr Victor Tybulewicz in the Division of Immune Cell Biology at NIMR, and are for 3 years in the first instance, potentially extendable for a fourth year.

Informal enquiries can be made to: Dr Victor Tybulewicz, Tel: +44 (0)20 8816 2184; email: vtybule@nimr.mrc.ac.uk http://www.nimr.mrc.ac.uk/immcellbiol/tybulewicz or Prof Elizabeth Fisher, Tel: +44 (0)20 7676 2037; email: e.fisher@prion.ucl.ac.uk

Based in north west London NIMR is the largest MRC Institute, supporting some 70 research groups and 500 bench scientists. The Institute provides excellent training for researchers in a multi-disciplinary environment and is equipped with state of the art facilities, including genetic modification of mice, imaging, histology, and sequencing.

Salary is from £26,405 to £32,357 per annum (inclusive of Location Allowance). Final Salary Pension Scheme available.

A recruitment information pack can be downloaded from the Institute website http://www.nimr.mrc.ac.uk/jobs/. This can also be obtained by contacting Stacey Saunders on 01793 301157 or emailing nimr.recruitment@ssc.mrc.ac.uk

Formal applications, which should include a full CV and the names and addresses of two referees, should be sent to Stacey Saunders, HR Recruitment Assistant, MRC Shared Service Centre, North Star House, North Star Avenue, Swindon SN2 1FF, alternatively email to nimr.recruitment@ssc.mrc.ac.uk quoting the appropriate reference number.

The closing date for completed applications is 30th March 2007.

The MRC is an Equal Opportunities Employer 97781R

University Hospital Zurich

GROUP LEADER POSITION IN TUMOR IMMUNOLOGY

The Division of Oncology at the University Hospital Zurich (USZ) (http://www.onkologie.usz.ch) invites applications for a group leader position (non-tenure track). Research programs should concern tumor immunology with a view to translational research. Potential topics include, but are not limited to, the role of regulatory T cells in tumor immunoediting, analysis of anti-tumor cellular responses and the potential of cancer 'stem cell-like' cells as targets for immune therapies. The successful candidate is expected to lead an independent and expanding, internationally competitive research group that attracts external funding, and to forge and strengthen local and international collaborations. In addition, he/she will actively contribute to the research environment at the institute, and participate in the teaching and supervision of graduate students. The Department is affiliated with the Ludwig Institute for Cancer Research (http://www.licr.org) and offers an interactive, well equipped research environment at the USZ site, located in the heart of Zürich.

Applicants should send (electronically if possible) a full CV, a list of research publications, and a short summary of their research objectives, together with the names and phone numbers of three references to:

Prof. Alexander Knuth
UniversitätsSpital Zürich, Departement Innere Medizin
Klinik für Onkologie, Rämistrasse 100, CH-8091 Zürich
Email: alexander.knuth@usz.ch

W97470R

College of Medicine, Dentistry and Nursing

Division of Medicine and Therapeutics

POSTDOCTORAL RESEARCH FELLOW IN BIOMARKER IDENTIFICATION

Salary Scale, Grade 7 (£28,290 per annum)

Full time, fixed term appointment

Location of post: Ninewells Hospital and Medical School

Applications are invited for a post-doctoral position funded by Lifescan Scotland to work on identification of biomarkers relevant to the pathophysiology and management of diabetes. The post will involve: a) screening human blood samples using Ciphergen protein chip arrays and Surface-Enhanced Laser Desorption/Ionization Time-of-Flight Mass Spectrometry (SELDI-TOF); b) analysing data generated for protein expression profiles and/or peaks of interest which may be suitable for formal identification; and c) establishing validation protocols for outcomes. Samples are available from a specific study performed as part of the contract, as well as from an established cohort (European Group for the Study of Insulin Resistance).

This is an opportunity to work in a multidisciplinary and translational group, involving interaction between both clinicians and scientists. There are opportunities for training in novel techniques developed within the University of Dundee.

The successful candidate will join the Diabetes Section within the Division of Medicine and Therapeutics, working with Dr John Petrie. He or she will collaborate closely in joint space with staff in Dr Calum Sutherland's group within the Neuroscience Research Institute. Dr Sutherland is a Diabetes UK Senior Fellow and an associate member of the Division of Signal Transduction and Therapy which is part of the internationally-acclaimed School of Life Sciences at the University of Dundee. Experience in bio-informatics/biostatistics is likely to be a significant advantage and experience in Ciphergen protein expression profiling would be beneficial but not essential.

The post is available for one year in the first instance (starting after 1st April 2007). Informal enquiries should be made to Dr John Petrie +44 (0)1382 632436 or j.r.petrie@dundee.ac.uk

Application packs are available from our website www.jobs.dundee.ac.uk Alternatively, contact Personnel Services, University of Dundee, Dundee DD1 4HN, tel: (01382) 344817 (answering machine). Please quote reference number: MD/1671/N. Closing date: 16 March 2007.

Applicants will only be contacted if invited for interview.

The University of Dundee is committed to equal opportunities and welcomes applications from all sections of the community.

97791R

www.dundee.ac.uk/jobs

UNIVERSITY OF DUNDEE

MRC | Laboratory of Molecular Biology

MRC Laboratory of Molecular Biology, Cambridge

Career Development Fellowship

Applications are invited for a Career Development Fellowship to carry out post-doctoral research on endocytosis and membrane ultrastructure in mammalian cells, within the group of Dr. B Nichols. This position provides an excellent opportunity to carry out fundamental research on the mechanism and function of different clathrin-independent endocytic pathways, and to learn a range of techniques.

You should have a PhD in a related field, with extensive practical experience of research applying cell biology, molecular biology and electron microscopy techniques. A desire to integrate electron microscopy with other approaches would be ideal. Further information may be obtained from Dr. Ben Nichols, email: ben@mrc-lmb.cam.ac.uk

This is a three year appointment with a likely starting salary in the range of £24,993 per annum, depending upon qualifications and experience. This is supported by a flexible pay and reward policy, 30 days annual leave entitlement, an optional MRC final salary pension scheme, and excellent on site sports and social facilities. Further information about the laboratory can be seen at: http://www.mrc-lmb.cam.ac.uk

For further information and an application pack please contact the Recruitment team: cambridge.recruitment@ssc.mrc.ac.uk or telephone 01793 301154 quoting reference CAM 2007-118.

Closing date: 29th March 2007

For further information about MRC visit www.mrc.ac.uk
The Medical Research Council is an Equal Opportunities Employer.
'Leading Science for Better Health'

97783R

Naturejobs gives an explosive start to your career!

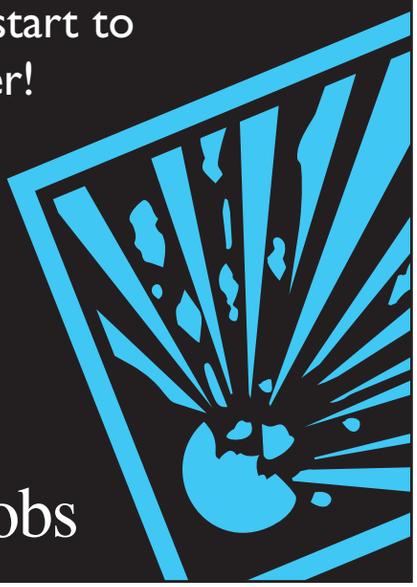

naturejobs

EMBO
Laboratory Management Courses 2007

THE ART OF
Leadership
FEWER CONFLICTS
MORE RESULTS

- → **Recruit the right staff**
- → **Develop your team**
- → **Communicate effectively**
- → **Delegate successfully**
- → **Solve problems**
- → **Manage conflicts**

2007 COURSE DATES
9–12 July
8–11 October
5–8 November

REGISTRATION FEE
€1500 *(including full-board accommodation)*

VENUE
Heidelberg, Germany

EMBO

www.embo.org
/yip/lab_mgm.html

W97653E

National Institute of Dental and Craniofacial Research

Division of Intramural Research

Research and Training at the NIDCR

The NIDCR intramural division pursues seminal problems in biomedical research that are difficult to tackle in university or industrial settings. To do so, a team of 35 senior and tenure track investigators, 125 postdoctoral fellows, and 75 staff scientists and technicians conducts basic, translational and clinical research in cell, molecular and developmental biology; microbiology and immunology; and neurobiology. A sampling of advances by NIDCR intramural investigators and their collaborators in the past few years includes:

•Discovered many genes involved in craniofacial development and growth.

•Discovered mechanisms that mediate branching morphogenesis of organs, including salivary glands, and identified roles for FGFs, extracellular matrix, and matrix receptors.

•Identified key proteins and physiological processes involved in regulating salivary gland fluid secretion, such as ion transporters, Ca2+ channels, and water channels.

•Demonstrated that macrophages are an important source of HIV during opportunistic infections, and that a Kaposi's sarcoma virus-encoded receptor plays a central role in AIDS-associated malignancies.

•Identified a TGF- dependent pathway for induction of Foxp3+ regulatory T cells.

•Identified receptors for sweet, sour, bitter and umami tastants, demonstrating that, at the periphery, taste perception is hard-wired into separate subsets of cells.

•Elucidated the signaling pathways by which small GTPases of the Rho family regulate gene expression in the nucleus.

•Identified and characterized post-natal stem cells from bone marrow and dental tissue, which re-form skeletal tissues and participate in repair of other damaged tissues.

NIDCR intramural researchers work in recently renovated, well-equipped laboratories on the NIH campus in Bethesda, Maryland. They are part of a larger scientific community at NIH comprising more than 1200 senior and tenure track investigators, 3800 postdoctoral fellows and 420 graduate students. As members of this community, they contribute to and benefit from an environment rich in intellectual and physical resources.

The intramural division at NIDCR is organized into six thematic research groups:

Cell and Developmental Biology Laboratory
Craniofacial and Skeletal Biology Branch
Gene Therapy and Therapeutics Branch
Oral Infection and Immunity Branch
Oral and Pharyngeal Cancer Branch
Sensory Biology Laboratory

The interests and expertise of scientists in these groups overlap significantly, leading to collaborations that are facilitated by the physical proximity of the laboratories. Collaborative initiatives are currently being developed to address the skeleton and associated structures, craniofacial tissue remodeling and salivary gland biology.

The NIDCR intramural division is committed to training the next generation of researchers and clinicians, and provides training opportunities on campus for recent college graduates, graduate students and postdoctoral fellows.

Postdocs receive an initial 2-year appointment, with possible extension up to 5 years. A variety of programs provide summer support to undergraduates and dental and medical students. Information about NIDCR intramural training opportunities is available at http://www.nidcr.nih.gov/Funding/Training/TrainingOpps.htm or by contacting the director of education, Dr. Deborah Philp, (dphilp@dir.nidcr.nih.gov).

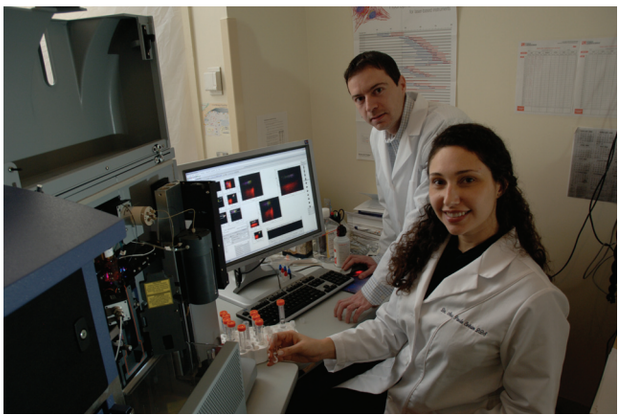

Additional information about NIDCR intramural research can be found at http://www.nidcr.nih.gov/Research/Intramural.htm.

DIRECTOR, PSI STRUCTURAL GENOMICS KNOWLEDGEBASE
National Institute of General Medical Sciences (NIGMS)

NIGMS is seeking an individual to serve as the Director of the PSI Structural Genomics Knowledgebase (SG-KB), a key component of the Protein Structure Initiative (PSI). The PSI is a national research program in the emerging field of structural genomics. The long-range goal of the PSI is to make the three-dimensional atomic-level structures of most proteins easily obtainable from knowledge of their corresponding DNA sequences. The PSI SG-KB will serve as a headquarters for scientific data and knowledge generated by the PSI-funded centers, so that they may be widely available to the scientific community. Information about the PSI may be found at: http://www.nigms.nih.gov/Initiatives/PSI.htm.

Requirements: The position will be a part-time temporary assignment for up to two years, with the possibility of an extension for up to two additional years. Individuals at an accredited U.S. public or private college or university, or technical institution of higher learning are eligible to apply. Students and employees from foreign universities are not eligible for consideration. Individuals detailed to the NIGMS remain employees of the outside organization, and may only serve in an advisory or consultative capacity.

Candidates must have a Ph.D. or equivalent degree in a field relevant to the position. The ideal candidate will have scientific knowledge and research experience in one or more of the following fields: molecular biophysics, structural biology, genomics, bioinformatics, and computational biology. In addition, candidates should possess experience in broad networking interactions and collaborations in the above research fields, a proven track record in directing and/or managing a large scientific database or large research project, as well as strong leadership ability and effective communication skills.

How to Apply: To be considered for this position, send to the e-mail address below a CV, bibliography, and a vision statement (not to exceed three pages) that presents your views on how to maximize the usefulness and impact of the Knowledgebase for the greater biological community.

NIGMSCV@mail.nih.gov

Applications must be received by the closing date: **March 30, 2007**. The National Institutes of Health inspires public confidence in our science by maintaining high ethical principles. Individuals detailed to NIH are subject to Federal government-wide regulations and statutes, as well as agency-specific regulations described at http://ethics.od.nih.gov. We encourage you to review this information. You may contact Kimberly Allen with questions regarding this announcement on 301-594-2755.

Advancing Science by

Seeking Your Input

NIH Center for Scientific Review

2007

Peer Review

Open House Workshops

Learn more at http://www.csr.nih.gov/Openhouse

Department of Health and Human Services
National Institutes of Health
National Cancer Institute

The Center for Cancer Research (CCR), National Cancer Institute (NCI), National Institutes of Health (NIH), is seeking applicants for an available Staff Scientist position.

The selected individual will provide senior scientific support for Drs. Carol Clayberger and Alan Krensky on studies related to the regulation of expression of the chemokine RANTES (Mol Cell Biol. 2007; 27:253-66; J Clin Invest. 2002;110:119-26; J Biol Chem. 2002;277:30055-65; Immunity. 1999;10:93-103). The successful candidate will have a doctoral degree with at least five years experience post degree. Candidate must have a strong background in molecular biology with training in transcriptional regulation and epigenetics. Experience with animal models and/or immunology is preferred. All applicants should submit a letter indicating their interest; a statement of research interests; current curriculum vitae and complete bibliography; and the names and addresses of five references (include email addresses) by **March 30, 2007**.

Applications should be sent to: **nciccrjobs@mail.nih.gov**. Please indicate **"Clayberger Staff Scientist"** in the subject line.

NW97609R

OPPORTUNITIES @ NIH THE NATIONAL INSTITUTES OF HEALTH

THE NIH IS DEDICATED TO BUILDING A DIVERSE COMMUNITY IN ITS TRAINING AND EMPLOYMENT PROGRAMS